Evaluation of a radiochemical method to estimate the rate of solute diffusion within a dual porosity Chalk aquifer

Simon Alexander Quinn

Department of Earth Sciences
UCL

A thesis submitted to University College London
in the Faculty of Mathematics and Physical Sciences
for the degree of Doctor of Philosophy (PhD)

June 2012

Declaration

I, Simon Alexander Quinn confirm that the work presented in this thesis is my own. Where information has been derived from other sources, I confirm that this has been indicated in the thesis.

Signed:

Date:

The real purpose of the scientific method is to make sure nature hasn't misled you into thinking you know something you actually don't know.

Robert Pirsig
Zen and the Art of Motorcycle Maintenance

Abstract

This thesis investigates a potential radiochemical method for estimating the capacity of the dual porosity Chalk aquifer to attenuate solutes.

Solutes are advected by groundwater flow through fractures, but are slowed and attenuated by molecular diffusion into immobile water in the Chalk matrix. Fracture apertures are a key factor controlling rates of both advection and diffusion.

The radiochemical model suggests that apertures may be estimated by comparing radon activity in groundwater with uranium-series isotope activities in the matrix. This estimate would be of great value if both radon release and solute attenuation are dominated by molecular diffusion.

The thesis tests the assumptions made in the radiochemical method through a series of laboratory experiments and field observations. This has been achieved by use of

- liquid-liquid extraction and luminescence spectrometry to assay Chalk core for uranium; and,
- energy-discriminated liquid scintillation to determine both the radium activity of Chalk core and the radon activity in springs and pumped groundwater.

The data demonstrate that

- the Chalk does not possess a homogeneous distribution of radon precursors, which are dependent on both lithology and disequilibrium within the decay chain;
- radon activity of pumped groundwater is highly variable and dependent on both the rate and duration of pumping; and,
- spring sources demonstrate variation in radon activity which are not readily explained by the prevailing hydrogeological conditions.

At a research site in Berkshire, double-porosity behaviour is shown to dominate solute transport, which can be characterised by an effective diffusion time. However, there is a clear disparity between diffusion times calculated from artificial tracer testing and estimated by the radiochemical method. This suggests that the radiochemical diffusion model is not appropriate in its current form to estimate rates of solute diffusion between fractures and the surrounding Chalk matrix.

Acknowledgements

At **University College London** Prof Tim Atkinson (who provided project supervision as well as guidance on the development of experimental methods and the treatment of errors), Dr Willy Burgess (for supervision and much assistance with the planning, arrangement and assistance with fieldwork, as well as proof reading), Prof John Barker (who provided many radon modelling suggestions and solutions), Tony Osborn (for much appreciated lab assistance, as well as help with completing IC analysis of all water samples), Danuta Kaminsky (computer issues), Celine Ahmed and Jennifer Wilgress (finance, assistance with couriering and car rental), Field Assistants Simon Cook (who also kindly provided me with his log interpretation of the Trumpletts Farm core), Ciara Fitzpatrick and Mohammad Hoque.

At the **British Geological Survey** Dr Ann Williams (for the arrangement of additional packer testing at the Trumpletts Farm site, for permission to sample groundwater for radon during other tracer test carried out by the BGS), Louise Maurice (who helped me to acquire additional field datasets, and also for her help with site access), Kate Griffiths and Mike Cheetham (packer testing), Dr Daren Gooddy (for the use of his bromide selective ion probe, and who also encouraged submissions to present at conference) and Dr Chris Milne (for Chalk pore water data collected under a separate project). At the **Centre for Ecology and Hydrology** Ned Hewitt (for field access) and Tabitha Sudworth, Renata Moraes and Rose Hargreaves (for making sense of LOCAR data).

At **Lancaster University** Dr Jackie Pates (who provided additional guidance with analytical techniques, in particular for radon sampling). At **Royal Holloway, University of London** Jacqui Duffett and Dr Emma Tomlinson (for ICP-AES analysis). At the **Environment Agency** Pete Orton (for agreeing to unrestricted site access), Jenny Reddaway (who provided Anglian borehole geophysical data) and Dr Rob Ward (for his permission to quote his radon data from pumped boreholes, assayed as part of his PhD thesis).

Other individuals include Dr Rob Low (for permission to quote spring and borehole radon data from his PhD thesis), Tony at Jannaways (for site access) and Rupert Cresswell (for help with computer illustrations).

Contents

Figures

Tables

Definitions

Notes: All mineral definitions are based on typical representations by Deer, Howie and Zussman (1992)

Allochthonous	Consisting of or formed from transported material; not formed *in situ*. (opp. "autochthonous")
Apatite	$Ca_5(PO_4)_3(OH,F,Cl)$
Carbonate-apatite	$Ca_5(PO_4,CO_3,OH)_3(F,OH)$
Authigenic	"Originating where found" This term is applied to minerals which have formed *in situ* within the host rock. (opp. "allogenic")
Calcite	$CaCO_3$, the principal component of Cretaceous Chalk
Glauconite	$(K,Ca,Na)_{\sim 1.6}(Fe^{3+},Al,Mg,Fe^{2+})_{4.0}Si_{7.3}Al_{0.7}O_{20}(OH)_4$
	Mica, though similar in structure to clay (illite). Typically formed by marine diagenesis in shallow waters. Associated with reducing environments and the presence of organic material.
Intraclast	A particle, typically composed of calcite, that is produced from erosion of the floor of a sedimentary basin.
Kaolinite	$Al_4[Si_4O_{10}](OH)_8$
Kaolinite – Illite – Smectite - Vermiculite	Clays (i.e. sheet silicates, hydrous), built from layers of tetrahedrally and octahedrally coordinated cations. Each member differs according to layer spacing, degree of cation exchange permitted and the degree of expandability through variation in water content.
Montmorillonite	A type of smectite clay, with a high cation exchange capacity (typically between 0.8 to 1.5 $meq.g^{-1}$).
Uranyl (ion)	$[UO_2]^{2+}$, with uranium present in its (oxidized) +6 valence state.

Notation

Symbol	*Units*	*Description*
a		Fracture aperture
b	[L]	Chalk block half thickness
$B(x)$	-	Block Geometry Function (BGF)
c_0	[M L^{-3}]	Initial concentration
c_f	[M L^{-3}]	Volume concentration of solute in the fracture
c_m	[M L^{-3}]	Volume concentration of solute in the matrix
c_∞	[M L^{-3}]	Equilibrium concentration of radon far from any void.
D_A	[L^2 T^{-1}]	"Apparent" diffusion coefficient. Can be expressed as $D_A = D_E/\phi_e$, and hence is larger than D_E
D_E	[L^2 T^{-1}]	"Effective" or "intrinsic" diffusion coefficient, which takes account of flowpath tortuosity. Hence smaller than D_T
D_L	[L^2 T^{-1}]	Longitudinal hydrodynamic dispersion coefficient. Can also be expressed as $D_L = \alpha_L.\bar{v} + D_E$
D_T	[L^2 T^{-1}]	Free water diffusion coefficient
i		Hydraulic gradient
K		Hydraulic conductivity
K_d	-	Partition coefficient
P_m	[M^{-1}T^{-1}]	Radon production rate (per unit dry mass of chalk)
P_w	[L^{-3-1}T^{-1}]	Radon production rate (per unit volume of water)
q	[L T^{-1}]	Darcian velocity $q=Ki$. Less than the average linear velocity, $\bar{v}$
t	[T]	Time variable
t_{cb}	[T]	Characteristic time for diffusion through a block
t_{cf}	[T]	Characteristic time for diffusion from a sheet channel "fracture"
t_{cs}	[T]	Characteristic time for diffusion from a fracture surface skin, of thickness b_s
$\bar{v}$	[L T^{-1}]	Average linear velocity. Equivalent to $\bar{v} = q/\phi_e$
x	[L]	Space coordinate along the flow direction in the fracture plane
z	[L]	Space coordinate in the direction normal to a planar fracture

Notation (cont.)

Symbol	*Units*	*Description*
α_L	[L]	Longitudinal dynamic dispersivity
λ	[T^{-1}]	Radioactive decay constant.
ϕ_e	-	"Effective" porosity, can be less than the total porosity, ϕ
ρ	[M L^{-3}]	Dry density of chalk
σ	-	Ratio of matrix to fracture porosity

1 Introduction

This thesis investigates and tests the viability of a new hypothesis that measurements of radon gas concentrations within the Chalk aquifer groundwater system, combined with knowledge of the concentration of uranium series radionuclides contained within the rock matrix, may be used to characterize aquifer contaminant transport properties.

This stems from a programme of works initiated by the UK's Natural Environment Research Council (NERC) to research and characterize the hydrological and ecological responses of low lying water catchments. The aim of this work was primarily to understand how rainfall, and the material it carries, recharges groundwater stores and runs off land into rivers and wetlands. The Lowland Catchment Research Programme (LOCAR) ran from 2000 until 2006 and provided thematic funding for a series of academic research teams and PhD studentships.

Included within the remit of LOCAR was a proposal to investigate the fate and transport of groundwater contaminants and to make predictions about how the natural attenuation properties of groundwater bodies may vary throughout a catchment. Normally, such research would require the extensive use of artificial tracer testing to directly evaluate contaminant transport in aquifers, but these are typically considered as technically difficult and prohibitively expensive to undertake on a large scale. An alternative radiochemical approach has been proposed that has the potential to build upon the results of such tracer tests, and to characterize aquifer transport properties over much wider areas.

1.1 Background to this thesis

The Chalk aquifer is the single most important source of public water supply in the south-east of England, supplying over 60% of the region's demand (MacDonald and Allen, 2001). In addition, the aquifer also has a important role to play on the river systems that it underlies, with many protected natural surface features, such fens and wetland, dependent on water supplied through either springs or river bed accretion (Wheater et al., 2006).

However, it is still considered difficult to assess with any confidence the vulnerability to pollution of surface waters and public water supply wells fed by Chalk groundwater . This is due in part to the sensitivity of Chalk groundwater quality to the rock fracture porosity and also by a lack of knowledge of its spatial distribution. The difficulty is reflected in recent guidelines developed by the Environment Agency for the management of land that

overlies unconfined Chalk, where changes in risk due to variation in fracture porosity and possible solution enhancement have yet to be addressed fully (Edmonds, 2008).

Many tests, such as tracer tests, have been conducted to try to establish the risk of contamination of the Chalk aquifer from pollution incidents, both from point sources (e.g. landfill sites, leaks from chemical manufacturers and related industries) and from those distributed widely (e.g. as pesticide and fertilizer application on agricultural land). These tests are normally undertaken to assess the likelihood of change in groundwater quality and to predict how that change may vary over time. In addition to the understanding gained about how the aquifer system behaves, this work may be required also as part of a more formal regulatory process (i.e. in the protection of potable waters for human consumption, or of vulnerable habitats that are fed by groundwater).

Hence, it is regarded as important to not only to be able to characterize the aquifer in terms of water resources, but also to be able to make predictions about how contamination may be stored and transported.

1.2 Development of the double porosity hypothesis

From a hydrogeological viewpoint, the Cretaceous Chalk is characterized as an aquifer in which water is stored in small pores within the fabric of the rock matrix but which, if advected, moves through a range of small connected fractures and larger fissures. Typically, such features represent only a very small component of the available volume, between 0.01% to 0.5% of the total porosity (Downing et al., 1979; Price, 1987; Younger and Elliot, 1995).

However, in large scale regional groundwater resource modelling it is commonplace to represent a saturated Chalk aquifer as a single porosity medium, where explicit representation of matrix and fracture hydraulic properties is removed (e.g. Rushton et al., 1989). In such examples, flow models are populated with values of storage coefficient and hydraulic conductivity that are derived from field evidence, such as borehole pump tests. In general these models are able to perform satisfactorily in relation to the reproduction of groundwater levels and river baseflows, but struggle to predict with accuracy the movement of particles. One reason for this can be understood simply from observations of water movement in boreholes during pumping – although the Chalk matrix is highly porous (values of total porosity can range up to 40%), most of the water stored within the matrix is relatively immobile compared to that contained within the fractures. The mean fracture water velocity is therefore much greater than the averaged Darcian water flux and the

individual pathways available to each particle may be more limited than when compared to a homogeneous aquifer.

Transport models often fail to reproduce the observed distribution of not only particles but also of dissolved species. Typically, the modelling of solute movement is based on an advection-dispersion analytical type solution which assumes a degree of both longitudinal and lateral dispersion within the saturated aquifer as a result of both variations in water velocity within individual flowpaths and also in the distribution in length of such routes from source to monitoring location (Fetter, 1999). Even in cases where groundwater velocities are close to zero, a solute will spread over time through the process of molecular diffusion rather than through mechanical dispersion.

However, evidence from both natural and artificial tracer test studies suggests that additional process may affect the mobility of groundwater solutes in fractured aquifers – namely sorption of the solute to fracture walls and diffusional exchange between the fractured system and a highly porous matrix (e.g. Foster, 1975; Ivanovich and Smith, 1978). In an attempt to explain the distribution of tritium in the unsaturated zone of the Chalk aquifer, Foster (1975) postulated that contaminant solutes are advected by groundwater flow through fractures, but may be slowed and attenuated by molecular diffusion into immobile water in the pores of the Chalk. In subsequent work by Barker and Foster (1981), it became clear that it was the fracture apertures that were the key factor controlling both advection and diffusion effects.

More recently, the results from some historical tracer tests undertaken in the Chalk aquifer that were originally modelled using pure advection-dispersion solutions have now been reinterpreted successfully in terms of a double porosity transport (e.g. Maloszewski and Zuber, 1993; Atkinson et al., 2000; Mathias et al., 2006a).

1.2.1 Field evidence of double porosity diffusion effects in Chalk

Since the work of Foster (1975), the study of matrix diffusion within fractured rocks has attracted considerable interest. Some examples from studies undertaken in the Chalk of southern and eastern provinces of England that demonstrate such behaviour are now briefly described.

The Tilmanstone Chloride "plume"

The Tilmanstone site is located in East Kent and was once the source of significant coal production in the UK. Saline groundwater encountered during operation was disposed either directly into near-by streams or into unlined chalk lagoons, over a period of nearly

seventy years. Eventually, the contamination of a local public water supply well forced the implementation of a pipeline to dispose of mine water by pumping it directly out to sea. Estimations for the total mass of chloride disposed directly onto the Chalk range from 270,000 to 320,000 tonnes with the total surface area affected by raised levels of chloride concentration estimated between 25-27 km^2 (Headworth et al., 1980; Watson et al., 2000).

The dual porosity nature of the Chalk has been used to explain the residence time of the saline contamination produced at the site. Although the source of saline rich water has now been removed, large concentrations of chloride contamination are still observed within the matrix pores. This contamination movement and evolution has been modelled by Bibby (1981) and more recently by Peedell (1994), who employed semi-analytical solutions employing Fickian diffusion of solutes between Chalk fractures and matrix.

The Chalk matrix is now considered to be a "persistent secondary [contaminant] source" (Burgess et al., 2005) and predictions for a return to background levels of chloride are estimated not to occur until at least 2020 (Carneiro, 1996).

Nitrate distribution within the Chalk unsaturated zone

The presence of elevated levels of dissolved nitrate (NO_3^-) in groundwaters is routinely reported in the literature. Generally considered a function of the excessive application of artificial fertilizers, high levels of nitrate are often associated with more rural agricultural catchments (Rivett et al., 2007). The evaluation of the presence of statistically significant trends in dissolved nitrate of groundwater sources has been undertaken by Stuart (Stuart et al., 2007). Included as part of this study were 74 Chalk boreholes, located mainly in the east of England. The analysis revealed an average annual increase of approximately 0.38 mg NO_3 l^{-1} a^{-1}, albeit with a large standard deviation (0.78 mg NO_3 l^{-1} a^{-1}).

Although these data indicate a long term trend, it is clear that there is also significant seasonal variation present at some monitoring sites. This effect has been attributed partly to the diffusional exchange of nitrate held with the matrix of the seasonally unsaturated zone as groundwater levels rise during periods of groundwater recharge. This hypothesis is also similar to that of Fretwell et al (2005), who modelled the vertical distribution and temporal evolution of chloride and chlorinated hydrocarbons contained within the matrix pore space of the unsaturated zone, using a semi-analytical form of a double porosity transport model developed by Barker et al (2000).

Mathias et al (2006b; 2007a) also suggested that nitrate migration throughout the unsaturated zone may be modelled successfully by assuming solute diffusion between the

fractures and the unsaturated matrix, but that the small degree of solute front dispersion within the matrix observed in some Chalk cores can only be explained if vertical matrix flow is permitted. This is in contrast to Fretwell (2005), who assumes that the matrix pore water is essentially immobile.

The South Farm tracer test

The South Farm tracer test was conducted by Ward (1989), and had a radial, forced gradient configuration. Located near to the town of Thetford in East Anglia, the aquifer is locally confined, overlain with approximately 20-25 m of superficial glacial deposits. During the test, water was pumped at a rate of 38.5 $l.s^{-1}$ (~3.3 $Ml.day^{-1}$) for 500 hours from a borehole that penetrated 60 m of uncased Chalk.

A fluorescein tracer was injected uniformly into another borehole located 199 m from the abstraction borehole. The first recording of tracer breakthrough occurred after 32 h of pumping, with the peak concentration recorded after 93 h. A subsequent long tail in the tracer concentration was recorded for the remainder of the pump test.

The tracer breakthrough has been modelled by several authors using many solutions, for example by 1-D advection-dispersion, 1-D advection-dispersion with radial flow and 1-D radial flow in a double porosity medium (Atkinson et al., 2000; Coy, 2001; Mathias et al., 2006a). The results demonstrated that the Chalk in the study area behaved in a manner most similar to that predicted by a double-porosity medium model over timescales of approximately 500 hours, with good matches to both leading edge and the tail of the breakthrough curve. Estimates of fracture porosity and dispersivity were calculated at 0.5 % and 12 m respectively (Atkinson et al., 2000).

Aquifer Storage and Recovery in Chalk

An aquifer storage and recovery test was undertaken during 1997-1998 within the Chalk aquifer at a borehole located at Lytchett Minster, near Poole in Dorset. Periods of water injection, no pumping and water abstraction were repeated over nine cycles and solute concentrations were measured throughout. Typically, in such tests no tracer is injected in to the aquifer; rather, fresh water is pumped into the ground. The change in solute concentrations observed during pumping are then considered to be controlled by the mixing of the new and pre-existing formation water and the diffusional exchange of solute from the matrix into the fractures.

Barker et al (2000) successfully recreated the evolution of pumped water chloride concentrations by employing a double-porosity solute transport model. Gaus et al (2002) reanalyzed the data from the Lytchett Minster site and model the results using SWIFT, a

3D groundwater model code which can incorporate radial flow, dual porosity diffusion and the representation of discrete fractures. Their main conclusion supports the hypothesis that diffusional processes have a significant impact on composition of the recovered water.

1.3 A comparison between advection-dispersion and double porosity solute transport models.

Figure 1—1 illustrates some of the alternative ways that are used to model the movement of solutes within a saturated aquifer. These models are all based on partial differential equations for dispersion and diffusion that have been developed for homogenous media.

1.3.1 Formulation of an advection dispersion model (ADE)

This type of model assumes that the transport of solutes or particles takes place in a single medium, be it fractures in the case of limestone aquifers or a porous matrix for those of sandstone or unconsolidated aquifers. The ability for solutes to diffuse into another media that is not part of the transport mechanism, such as an immobile pore space, is not modelled explicitly.

At its simplest a pure advection-only model for a fractured aquifer can be represented by

$$\frac{\partial \mathrm{c}}{\partial \mathrm{t}} + \mathrm{v_f}\frac{\partial \mathrm{c}}{\partial \mathrm{x}} = 0 \qquad (1\text{-}1)$$

where v_f = fracture flow velocity, c = solute concentration, t = time and x = distance.

This model does not permit the spatial spreading of the solute in any way. As illustrated in Figure 1—1, the movement of a tracer within a saturated aquifer is transported in exactly the same form as it was originally introduced.

In a fractured rock, the movement of solutes is unlikely to follow such a simple mechanism as pure advection or "plug flow". Rather, solutes will become dispersed both on a molecular level (by Fickian diffusion) and also mechanically as the path length and flow velocity for any individual molecule will vary as water moves through the aquifer.

The extent to which these two methods of solute spreading are important in solute transport is normally considered a function of both the flow velocity and the timescales and distance involved. But together, these processes are often referred to as "hydrodynamic dispersion" and their effects can be observed in many (single porosity) aquifers. It can be characterized in its simplest one dimensional form by the equation:

$$\frac{\partial c}{\partial t} + v_f \frac{\partial c}{\partial x} = D_L \frac{\partial^2 c}{\partial x^2} \qquad (1\text{-}2)$$

where D_L = the 'longitudinal hydrodynamic dispersion coefficient', normally defined to include the effects of both mechanical dispersion and molecular diffusion parallel to the principle flow direction (e.g. Fetter, 1999). In most productive fractured aquifer systems, the effects of molecular diffusion are far outweighed by the dispersion caused by the variations in flow path and flow velocities (Barker, 1991) within a fracture network. In such cases D_L is often approximated to:

$$D_L = \alpha_L |\bar{v}_x| \qquad (1\text{-}3)$$

where α_L is termed the longitudinal dispersivity (with units of length) and $|\bar{v}_x|$ is the absolute average linear velocity in the x direction.

By ignoring longitudinal molecular diffusion, a type solution for the above differential equation, and assuming instantaneous injection of tracer, will take the form

$$c(x,t) \propto \frac{1}{\sqrt{4\pi D_L t}} \cdot \exp\left[\frac{-(x-\bar{v}t)^2}{4D_L t}\right] \qquad (1\text{-}4)$$

Source: (Fetter, 1999 , Ch.2)

According to this solution, the tracer pulse will change in form, as illustrated schematically in Figure 1—1. The peak concentration will be less with respect to the input and the overall shape will be smoothed. Characteristic of such dispersion is the presence of a distinct "tailing" to the breakthrough curve, which in reality reflects the distribution of flow velocities within the fracture network.

By making suitable substitutions, it is possible to reformulate Equation *(1-4)* to present the solution in terms of a set of characteristic "travel times" which will be useful for subsequent comparisons. Hence:

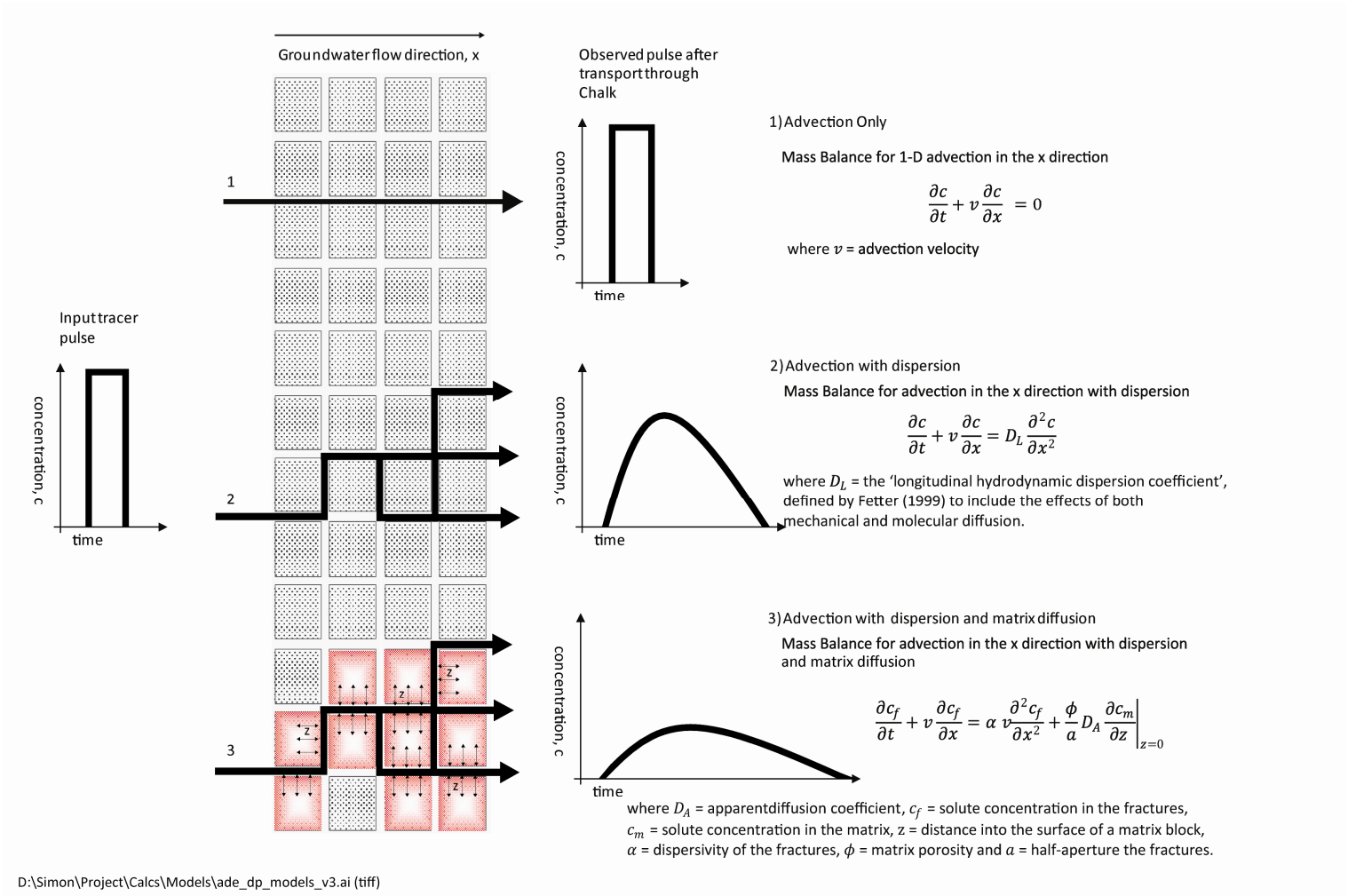

Figure 1—1 Examples of modes of contaminant transport in Chalk

$$t_a = \frac{x}{v_f} \qquad \text{an "advection time"} \qquad (1\text{-}5)$$

$$t_D = \frac{\alpha_L}{v_f} \qquad \text{a "hydrodynamic dispersion time"} \qquad (1\text{-}6)$$

the resulting solution takes the form:

$$c(t, t_a, t_D) \propto \frac{1}{v_f\sqrt{4\pi t_D t}} \cdot \exp\left[\frac{-(t-t_a)^2}{4t_D t}\right] \qquad (1\text{-}7)$$

In this example, it would be possible to attempt to fit a concentration versus time tracer breakthrough curve at a known distance away from the tracer injection point to obtain values of the parameters t_a and t_D, and from which v_f and α_L could be calculated.

1.3.2 Formulation of a contaminant transport model in a double porosity aquifer

Figure 1—1 also sketches double porosity effects. In this case, groundwater flow in fractures advects the tracer across the diagram while the solute is strongly attenuated by molecular diffusion into and out of immobile pore water in the blocks of chalk between the fractures.

Transport models can include the movement of water and solutes between the rapidly transported fracture water and the matrix pore space. These models normally attempt to represent solute behaviour using measureable parameters such as dispersivity, rock porosity, a solute diffusion coefficient and known fracture spacing (e.g. Mathias et al., 2006a). For example, for a non-sorbing conservative tracer (i.e. one that does not decay) the partial differential equation governing transport within a single planar fracture is described by Atkinson et al (2001) as follows:

$$\frac{\partial c_f}{\partial t} + v_f \frac{\partial c_f}{\partial x} = \alpha_L v_f \frac{\partial^2 c_f}{\partial x^2} + \frac{\phi_e}{a} D_A \left.\frac{\partial c_m}{\partial z}\right|_{z=0} \qquad (1\text{-}8)$$

where in addition to the terms described previously ϕ_e = 'effective' matrix porosity, a = fracture width, D_A= 'apparent' diffusion coefficient of the solute in the matrix[1], c_m = solute concentration in the matrix, and z = distance into the surface of a matrix block.

[1] Note: The 'apparent' diffusion coefficient D_A is defined throughout as the 'effective' diffusion coefficient divided by the matrix porosity i.e. D_E/ϕ_e. The 'effective' diffusion coefficient D_E is defined as the 'free water'

For the matrix, the governing equation is simplified by the assumption that the interstitial water is effectively immobile when compared to the fracture water and that only molecular diffusion can occur. Hence:

$$\frac{\partial c_m}{\partial t} = D_A \frac{\partial^2 c_m}{\partial z^2} \qquad (1\text{-}9)$$

An example of a solution to Equation *(1-8)*, for the case where the effects of hydrodynamic dispersion are regarded as negligible when compared to that of double porosity diffusion, is provided by Maloszewski and Zuber (1985). By expressing their solution in terms of representative travel times, analogous to that presented in Equation *(1-7)*, the solution for an instantaneous injection of tracer takes the form (J.A. Barker, *pers. comm.*):

$$c_f(t, t_a, t_{cf}) \propto \frac{t_a}{v_f\sqrt{4\pi t_{cf}(t-t_a)^3}} \cdot \exp\left[\frac{-{t_a}^2}{4t_{cf}(t-t_a)}\right] \qquad (1\text{-}10)$$

for $t > t_a$, where

$$t_{cf} = \frac{(a/2\phi_e)^2}{D_A}$$

a = fracture width

In this solution, a new characteristic "diffusion time" has been introduced, t_{cf}, which for a non-sorbing, conservative solute travelling through a set of planar fractures is defined by Barker et al (2000) as the timescale on which a diffusing solute penetrates a volume of matrix water equal to that in the adjacent fracture. Barker et al (2000) calculated that for transit times greater than approximately $3t_{cf}$ (typically between several hours to several days for the Chalk), double-porosity diffusion predominates over hydrodynamic dispersion. A further exploration of this claim is discussed in Chapter 7.

In theory therefore, an estimation of the value of t_{cf}, combined with knowledge of the apparent diffusion coefficient D_A for any given solute, should also make it possible to calculate the 'effective' width of the fractures that are present within the aquifer.

diffusion coefficient D_T multiplied by a tortuosity factor, to account for the longer pathways that solutes must take in a porous medium.

1.4 Formulation of a radon diffusion model in a double porosity aquifer

The presence of radon gas dissolved within the Chalk groundwaters is well documented, and evidence from the literature is discussed in detail in Chapter 2. Assuming no external source, it is proposed that some of the radon produced within the matrix must recoil or diffuse into adjacent fractures where, unsupported, it will eventually decay.

One hypothesis is that the distribution of radon between the matrix and the fractures is controlled in a similar way to the methods of solute diffusion described above. This assumption was developed by Atkinson et al (2001) into the form of a simple mathematical model for predicting the radon content of fracture water, in terms of the parent concentration in the matrix. They begin by expressing the source of radon production within the solid matrix as:

$$P_w = 2.53 \times 10^{24}\, E\, \frac{\rho_m}{\phi} \lambda_{238} U \left[\frac{^{226}Ra}{^{238}U}\right] \qquad (1\text{-}11)$$

(Note: modified to correct a typing error in the original paper)

where P_w = the production rate of radon per unit volume of pore water, as a result of emanation from within the matrix (atoms.m^{-3}.s^{-1}), $0 \leq E \leq 1$ = the efficiency of the emanation of radon from solid grains into the pores, ϕ = the matrix porosity, ρ_m = the bulk density of the rock (kg.m^{-3}), λ_{238} = the decay constant of the uranium isotope ^{238}U (seconds^{-1}), U = the uranium concentration of the solid matrix (kg.kg^{-1}), and $\left[^{226}Ra/^{238}U\right]$ is the isotope activity ratio between the two isotopes of radium and uranium. *(Note that a further explanation of the relevant radioisotopes and decay constants cited in this introduction is provided in Chapter 2.)*

Radon atoms that are ejected into the saturated pore space will dissolve and diffuse from the matrix to the adjacent fractures. In the fractures, the radon concentration is determined therefore by the balance of the rate of supply from the adjacent matrix and the radioactive decay that will occur within the fractures themselves.

Atkinson et al (2001) assumed that the movement of radon can be modelled by Fickian diffusion within the matrix and by advection within the (planar) fractures. A schematic diagram is presented in Figure 1—2 to highlight the geometry assumed, and which is labelled with axes directions used in the formulation of subsequent equations.

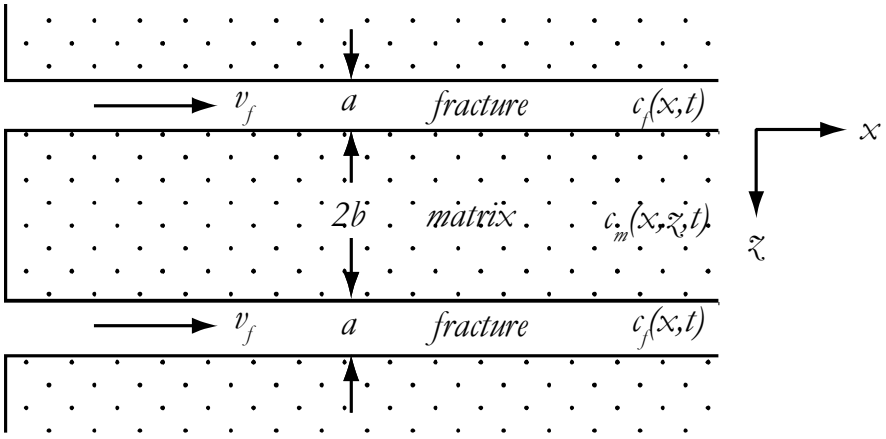

d:\simon\project\docs\thesis\figures\chalk_model_block.ai

Figure 1—2 Double porosity model geometry

By converting the production rate, P_w, into an equivalent equilibrium radon concentration, i.e.,

$$c_\infty = \frac{P_w}{\lambda_{222}} \qquad (1\text{-}12)$$

the governing equations can be expressed as follows:

a) for the matrix block, assuming it can be treated as effectively infinite when compared to the half-life of radon and the time it would take radon to diffuse across the block's width:

$$\frac{\partial c_m}{\partial t} = D_A \frac{\partial^2 c_m}{\partial z^2} + \lambda_{222}(c_\infty - c_m) \qquad (1\text{-}13)$$

where c_m = solute concentration in the matrix, all other parameters being the same as expressed previously for Equation *(1-8)*, and,

b) for the fractures:

$$\frac{\partial c_f}{\partial t} = -v_f \frac{\partial c_f}{\partial x} + \frac{\phi_e}{a} D_A \left.\frac{\partial c_m}{\partial z}\right|_{z=0} - \lambda_{222} c_f \qquad (1\text{-}14)$$

where c_f = solute concentration in the (well mixed) fracture.

Atkinson et al (2001) provide a steady state solution to the governing equations in the cases of both zero and non-zero fracture flow. However, a subsequently corrected reformulation by Barker (*pers comm*) expressing the solution in terms of c_∞ instead of P_w, is stated here:

$$c_f(x) = c_f(\infty) + \left(c_f(0) - c_f(\infty)\right) \cdot \exp[-\xi t_a] \quad (1\text{-}15)$$

$$c_m(x,z) = c_\infty + \left(c_f(x) - c_\infty\right) \cdot \exp\left[-z\sqrt{\frac{\lambda_{222}}{D_A}}\right] \quad (1\text{-}16)$$

where

$$\xi = \lambda_{222} + \frac{2\phi_e D_A}{a}\sqrt{\frac{\lambda_{222}}{D_A}} = \lambda_{222}\left(1 + \frac{1}{\sqrt{\lambda_{222} t_{cf}}}\right) \quad (1\text{-}17)$$

$$c_f(\infty) = \frac{c_\infty}{1 + \sqrt{\lambda_{222} t_{cf}}} \quad (1\text{-}18)$$

$$t_{cf} = \frac{(a/2\phi_e)^2}{D_A} \quad (1\text{-}19)$$

Because the variable t_{cf} has the same form as the parameter in Barker et al's (2000) double-porosity model of solute transport, Atkinson et al (2001) suggest that by making paired measurements of uranium concentration in solid chalk and radon activity in pumped groundwater it could, in principle, be possible to estimate and map t_{cf} and hence to predict transport and attenuation of hypothetical contaminants.

Using the emanation model - preliminary assumptions

The powerfulness of this simple result makes the radiochemical method a potentially attractive tool in the area of groundwater source protection. It could be envisaged that groundwater radon measurements, made over an entire catchment, combined with uranium analysis of core material in the laboratory, may be made much more readily than the instigation of a large tracer test programme. Moreover, the uranium analysis could be limited to selected boreholes if it could be shown that its distribution was generally uniform throughout the Chalk.

Atkinson et al (2001) continued their work by making predictions of the likely values of t_{cf} that result from using the radon emanation model with field parameters. To do this, they used a range of sources that include uranium-series studies on Chalk material, groundwater radon sampling and breakthrough results from traditional radial flow tracer tests for comparison and validation. However, it is accepted that the amount of data originating from the same locality is sparse and the authors are required to make a range of

assumptions to populate the model parameters. These assumptions are stated below and their limitations are highlighted:

i. The system is at equilibrium with regards to the balance between radon diffusion from the matrix and the decay within the fractures. This suggests that the fracture flow paths are sufficiently long to allow equilibrium to be achieved and that neither the source term strength, nor the radon diffusion coefficient for Chalk, varies along them. If equilibrium has not been achieved, it is clear from Equation *(1-18)* that values of t_{cf} will be overestimated, and as a consequence will lead to an overestimate of effective aperture size. Atkinson el al (2001) calculated that such equilibrium will have occurred after approximately 25 days.

ii. The radon measured in fracture waters is supported by transfer from the matrix alone and that this process can be represented by an effective (Fickian) diffusion coefficient. Implicit therefore to this assumption is that radon contained within fracture waters is entirely unsupported by other sources, either within the fracture water itself or external to the Chalk aquifer system as a whole.

iii. The distribution of uranium and radium, the immediate parent of radon, can be assumed to be uniform throughout the matrix. Clearly if radium is concentrated within the fracture walls, either by sorption or by the process of isotopic fractionation (Chapter 2), then the boundary conditions of the diffusion model will change substantially and bulk determinations of radium will tend to lead to an underestimate of the actual radon mass transfer rate from matrix to fractures.

iv. The isotopic ratio between uranium-238 and radium-226 is known and does not vary, and hence allows uranium to act as a proxy for the source term. This assumption is beneficial in terms of laboratory analysis (Chapter 4), but as is clear from the combination of Equations *(1-11)*, *(1-12)* and *(1-18)* uncertainty in this term will lead to a strong (second order) effect on estimates of t_{cf}. Atkinson et al (2001) cite data from studies on Chalk samples from Lincolnshire (Cuttell et al., 1986) to justify this assumption , but it is accepted that the data are few in number.

v. Finally, from the study of radon emanation from limestones and theoretical calculations of emanation efficiency as a function of particle size (Andrews and Wood, 1972), Atkinson et al (2001) assume that 100% of radon produced within solid Chalk is ejected into the surrounding pore space and is able to diffuse towards larger fractures. If in reality the source term is not as strong as this, values of t_{cf} will be overestimated further.

1.5 Research Proposal and Objectives

Given the similarity in the mathematical solutions to both the attenuation of solutes by double porosity diffusion and the emanation of radon from the Chalk matrix outlined in the previous section, a set of project aims can now be developed. These are namely, to test the radon emanation and transport model developed by Atkinson et al (2001) and to determine if there is a strong correlation between the natural radiochemistry of groundwater and the diffusion processes that govern contaminant attenuation.

Hence, the overall aims of the thesis can be summarized as follows:

i. To test the validity of the assumptions that have been made in deriving the radiochemical model, by undertaking a series of field and laboratory measurements of uranium series radionuclides within the Chalk and associated groundwaters and to make predictions of the magnitude and variation in transport parameters such as t_{cf} and apparent fracture aperture size,
ii. To test the agreement of the model with independent tracer test data, ideally from the same locality as the data collected above, in order to be make comparisons between the estimates of transport properties, and if necessary to explain why differences may occur, and,
iii. To evaluate the usefulness of the radiochemical model as a means of estimating values of t_{cf}, which can be employed to predict the likelihood of contaminant attenuation by double-porosity diffusion.

1.5.1 Objectives

The stated aims have been broken down further into a series of identifiable objectives that help to focus the areas for investigation and which are used to form the body of the work that supports this thesis. These are namely:

a) To develop an understanding of the source, production, variation and transport of the uranium-238 series radionuclides in the Chalk (Chapter 2)

This objective will be met be undertaking a literature review of uranium series studies in carbonate rock systems and to summarize the important processes that are thought to control the radon activity in both the aquifer substrate and groundwaters. Therefore, it will be necessary to describe the mathematics of the decay processes involved, the physical and chemical properties of the daughter products and to explain the theoretical ingrowth of these products over time. These areas will be the key to understanding the methods by which radon escapes physically from its source area and is then transported through the

matrix. Previous work from similar studies of radon in the Chalk aquifer by other authors will also be examined.

b) To chose a field area in which to undertake field measurements and to collect other relevant hydrological data for comparison (Chapter 3)

It is apparent that, although data exist on the distribution of uranium series nuclides in the Chalk in the UK as well as radon activity in groundwaters, there are few studies that combine measurements in the same location. In addition, the lack of independent tracer test results at the same sites makes it difficult to compare directly the predictions made by the proposed radiochemical diffusion model.

To be able to test the radon diffusion model as formulated by Atkinson et al (2001), it is desirable to measure the bulk uranium content of the Chalk matrix at the same location as that where groundwater is sampled for radon. As this thesis is supported by a studentship awarded under NERC's LOCAR programme, it is proposed that work is undertaken at the same locations as selected by other co-workers for the purposes of efficiency and to minimise the risk of obtaining inappropriate datasets for later comparison. In particular, three projects, all funded under the LOCAR programme, complement the work undertaken as part of this thesis:

i. Results from a series of tracer tests undertaken at a research site with the Pang catchment, Berkshire, reported under Mathias et al (2007b), and studies on borehole geophysics and groundwater flow heterogeneity at the same site reported by Williams et al (2006),
ii. The identification of groundwater springs, results from a series of single borehole dilution tests and a catchment scale tracer tests reported in part by Maurice et al (2006), which provide an opportunity to make observations of groundwater radon content at sites that have been studied intensively over a period of three years, and,
iii. Complementary studies investigating the presence of radon and other dissolved species in the river systems of the same catchment reported by Mullinger et al (2007), which are useful for making general comparisons and which may help to identify and quantify the possible surface influences on spring radon activity.

c) To develop appropriate analytical methods for the assay of uranium series nuclides (Chapter 4)

A quick and simple laboratory method of uranium assay for dissolved Chalk samples is desired if large numbers of Chalk samples are to analysed without the need to outsource such work to other more specialized groups. From an initial review of the literature, analytical methods based on the phosphorescence of the UO_2^{2+} ion species in solution

seem appropriate, although it is envisaged that pre-concentration and selective extraction may be required to achieve acceptable detectability and repeatability.

Methods for the determination of radon gas dissolved in groundwaters have often focused on the method of "gas and trap", which requires large volumes of water to be taken at each location (typically 20 l) and require extensive laboratory time to analyse each sample. Other more rapid measurements that also require less water (typically 500 ml) may be possible by solvent extraction and liquid scintillation counting, but it is likely that new experimental procedures may be required to ensure adequate levels of detection.

Liquid scintillation may also been employed for radium-226 assay by exploiting the natural ingrowth of radon produced in sealed samples. Although the detection limits are high relative to other methods and the throughput rather slow, the procedure could enable a profile of radium distribution to be made for Chalk core material without requiring the purchase of additional analytical equipment.

It will be necessary to demonstrate that all of the techniques suggested are sufficiently reliable and repeatable at the levels of activity anticipated in Chalk sediments and groundwaters.

d) To assay important radon precursors in Chalk core (Chapter 5)

To test the assumption that radon precursors are uniformly distributed throughout the Chalk sequence, it will be necessary to assay material from the same location that groundwater radon samples are taken. Chalk core has been obtained from boreholes under the LOCAR programme and it is proposed that this be sampled at the meter scale, paying attention to changes in lithology and the location of known flowing water horizons.

It is proposed that these same samples may be reanalyzed further for radium content. By doing so, this will permit an estimate of the isotopic activity ratio $^{238}U/^{226}R$ to be made for each sample. From this work, it should then be possible to test the hypothesis that these isotopic ratios do not vary throughout the core.

e) To perform a radon assay of Chalk groundwaters (Chapter 6)

An original incentive of the radon diffusion model was the potential development of a method for mapping spatially the parameter t_{cf}, i.e. effectively an evaluation and prediction of the contaminant transport properties of the aquifer across a catchment area. Given the original model assumptions, any variation in groundwater radon content would be therefore a reflection of a change in this parameter.

In order to test this assumption, a temporal and spatial survey of groundwater sources (both springs and boreholes) is proposed where observations may be compared with other hydrological data obtained for the same localities, e.g. precipitation, groundwater levels and thickness of the unsaturated zone.

f) To determine the emanation efficiency of radon gas from saturated Chalk core (Chapter 6)

The radon diffusion model is also dependent on knowledge of the efficiency that radon produced within matrix material can move initially into the matrix pore space (either though recoil or by diffusion) and then by diffusion to fracture surfaces.

As previous work suggests that rates of emanation in Chalk will be very high, due to the small diameters of the base coccolithoporoids shell fragments that make up over 95% of bulk Chalk material, it is proposed that this assumption should be tested using a series of laboratory scale experiments that determine the emanation efficiency of a range of Chalk samples which have different particle sizes. Savings could be made in analysis time if the results from the previous radium survey were employed and the results compared with the theoretical maximum radon activity possible through secular equilibrium.

g) To investigate the suitability of the radon emanation and diffusion model (Chapter 7)

Finally, for the model to be validated as a method to predict rates of contaminant transport in the Chalk aquifer, it is necessary to test the following hypotheses:

i. That double-porosity behaviour dominates for solute transport and can be characterised by an effective t_{cf} value, despite the potential heterogeneity of the fracture flow; and that
ii. The data obtained from the uranium, radium and radon assay on Chalk core and groundwaters can be used to prediction the same transport parameters.

The first hypothesis can be tested by a critical evaluation of the application of existing double porosity models to previous tracer test experiments and from new tracer tests undertaken as part of the LOCAR programme. An appropriate way to test the second hypothesis would be to compare the predictions made by the radiochemical diffusion model to those types of tracer tests undertaken at the same location.

h) To draw conclusions about the validity of the model to predict transport properties (Chapter 8)

Finally, according to the outcomes of the above, recommendations are made to the applicability and suitability of the radon diffusion model to map transport parameters in the Chalk.

2 Uranium Series elements in the hydrological environment

To be able to test the model outlined in Chapter 1, it is regarded as important to develop an understanding of the source, production, variation, and transport of the uranium-238 series radionuclides in the natural environment and in particular within the Cretaceous Chalk aquifer.

Firstly, the background theory of radioactivity is described, which includes a description of the different modes of decay that are observed within the uranium series decay chain. This is followed by an exploration of the mathematics of radioactive decay and the prediction of the growth of daughter products, to highlight the time scales required to achieve radioactive equilibria. Such calculations are subsequently carried forward to assist in the development of robust methodologies for the sampling and measuring of both radium and radon content of groundwater (Chapter 4), as well as to understand the observations of uranium series disequilibrium in the Chalk matrix (Chapter 5) and in helping to explain the spatial and temporal variation in radon content measured at different spring locations across the study area (Chapter 6).

Secondly, the theoretical cause of uranium series disequilibrium is discussed, which includes a review of radon emanation models developed by previous authors as well as an assessment of the applicability of such models in the Chalk aquifer (which may act in a different way to that of other more cemented limestones). In particular the factors affecting both the radon content of Chalk matrix pore waters and the surrounding fractures are reviewed.

Thirdly, previous work from similar studies of uranium, radium and radon concentrations in carbonate aquifers in the UK by other authors is summarised, including a description of some of the key findings.

Finally, a review of radon chemistry is made to judge whether is it appropriate to assume that it is a non-sorbing gas.

2.1 Background

2.1.1 Radioactive decay and the growth of daughter products – generalized equations

The empirical law of radioactive decay is widely regarded to have been first postulated by Rutherford and Soddy in a series of joint publications during 1902 and 1903, culminating in the now classic paper "Radioactive Change" (*Phil. Mag.*, 5 (1903), 576-591). With this publication and the development of a generalized disintegration theory and associated constant, λ, it was possible to describe mathematically the observed processes of radioactive decay (i.e. such as the production of helium gas from the decay of thorium). With the refinement by von Schweidler in 1905 of the definition of λ as a probabilistic atomic constant (see Trenn (1977) for a reproduction of the original German paper), it was possible to apply the theory universally to all radioactive nuclides.

The theory may be quoted as follows (e.g. Trenn, 1977):

> *"Radioactive decay is a purely random process and the probability of a given radioactive nucleus disintegrating is fixed and is independent of the presence or absence of other radioactive nuclei. Thus, the rate at which these radioactive nuclei disintegrate is dependent simply on the number present at any time and is expressed by the relationship*
>
> $$\frac{dN}{dt} = -\lambda N \qquad (2\text{-}1)$$
>
> *where N is the number of radioactive atoms at any time t [and] λ is the radioactive disintegration constant."*

Taking this result and assuming that N_0 is the initial number of radioactive atoms at t=0 and that the decay constant λ is time independent., the solution of eq (2-1) can be expressed as:

$$N = N_0 e^{-\lambda t} \qquad (2\text{-}2)$$

where N is the number of radioactive particles remaining at time t.

However, the rate of disintegration of a radioactive source is more commonly referred to in the literature as its activity, A. By multiplying both sides of Equation (2-2) by λ, it is possible to express this equation in terms of activities (i.e. 'λN'):

$$A = A_0 e^{-\lambda t} \qquad (2\text{-}3)$$

where A_0 is the initial activity of the sample and A is the activity after time t.

The decay constant λ is considered independent of all physical and chemical conditions such as temperature, pressure, concentration and age of the radioactive atoms (Ivanovich and Harmon, 1992).

Half Life

The half life $t_{½}$ can be defined as the time taken for the activity of a radioactive source to decrease to half of its initial value, i.e. when $A = 0.5A_0$. Substituting this value into Equation (2-3) yields the result:

$$t_{1/2} = ln(2)/\lambda \qquad (2\text{-}4)$$

Values for the half life of radionuclides can range over many orders of magnitude. For example uranium-238 has a half life of 4.5×10^9 years, whereas that of polonium-214 is only 1.6×10^{-4} seconds.

Growth of daughter products

When a radioactive element disintegrates, the decay products that are formed may be stable, such as is the case when carbon-14 decays by beta particle emission to form the stable isotope nitrogen-14. However, in many cases radioactive elements do not decay directly to a stable state but rather, undergo a series of decays, until a stable isotope is obtained. The uranium-238 decay series is an example of such a chain.

The rate of decay of a daughter product may be derived by calculating the difference in rates of production (i.e. by the decay of its parent) and the rate of loss (i.e. by decay). For example:

$$\frac{dN_1}{dt} = -\lambda_1 N_1 \quad ; \quad \frac{dN_2}{dt} = +\lambda_1 N_1 - \lambda_2 N_2 \qquad (2\text{-}5)$$

where $N1$ and $N2$ are the number of atoms of parent and daughter, and λ_1 and λ_2 are their associated decay constants.

When there are many decay products in an chain, each with its own decay constant, the solution for the activity of each radionuclide becomes more difficult. Bateman (1910) provided a generalized solution to the problem that involves the calculation of a series of dimensionless functions of the individual decay constants.

If only the parent radionuclide is present initially the amount of any subsequent decay product can be calculated from a series of differential equations with the form:

$$\frac{dN_N}{dt} = +\lambda_M N_M - \lambda_N N_N \qquad (2\text{-}6)$$

where N_N represents the number of atoms of the decay product of interest and N_M is the number of atoms of the immediate parent. N_M is evaluated by using a recursive procedure upon all the decay products further up the chain.

The solution yields an expression for N_N of the form:

$$N_N = N_1^0(C_1 e^{-\lambda_1 t} + C_2 e^{-\lambda_2 t} + \cdots + C_M e^{-\lambda_M t} + C_N e^{-\lambda_N t}) \qquad (2\text{-}7)$$

where N_1^0 represents the number of parent atoms present at $t = 0$, and the coefficients of the form C_x are calculated as follows:

$$C_1 = \frac{\lambda_1}{\lambda_N - \lambda_1} \cdot \frac{\lambda_2}{\lambda_2 - \lambda_1} \cdot \frac{\lambda_3}{\lambda_3 - \lambda_1} \cdot \cdots \cdot \frac{\lambda_M}{\lambda_M - \lambda_1}$$

$$C_2 = \frac{\lambda_1}{\lambda_1 - \lambda_2} \cdot \frac{\lambda_2}{\lambda_N - \lambda_2} \cdot \frac{\lambda_3}{\lambda_3 - \lambda_2} \cdot \cdots \cdot \frac{\lambda_M}{\lambda_M - \lambda_2}$$

$$C_M = \frac{\lambda_1}{\lambda_1 - \lambda_M} \cdot \frac{\lambda_2}{\lambda_2 - \lambda_M} \cdot \frac{\lambda_3}{\lambda_3 - \lambda_M} \cdot \cdots \cdot \frac{\lambda_M}{\lambda_N - \lambda_M}$$

$$C_N = \frac{\lambda_1}{\lambda_1 - \lambda_N} \cdot \frac{\lambda_2}{\lambda_2 - \lambda_N} \cdot \frac{\lambda_3}{\lambda_3 - \lambda_N} \cdot \cdots \cdot \frac{\lambda_M}{\lambda_M - \lambda_N}$$

(2-8)

A numerical code that uses this solution to calculate the amount of decay product in a chain given any initial boundary condition has been kindly provided for use in this thesis by John Barker (*pers comm*).

2.1.2 Modes of disintegration

The process of radioactive decay is based on the concept that unstable nuclei attain greater stability by emitting energy (losing mass). The physical process of decay may manifest itself through the emission of several types of particle from an atom's nucleus – alpha particles (which consist of 2 neutrons and 2 protons, i.e. a helium nucleus), and beta particles (electrons). Associated with the emission of these particles, additional electromagnetic radiation in the form of γ-rays (i.e. 'gamma' radiation) may also be emitted. As described mathematically above, one or more separate decay events may be required before the nucleus achieves a more stable nuclear arrangement, dependent on the originating parent atom.

The emission of each particle will affect the atomic nucleus in a different way (see Table 2—1). Alpha particles are positively charged with a relative atomic mass of 4. As the

ejection from the nucleus results in a loss of 2 protons, the element *transmutes* into one with a lower atomic number An example of this is present during the production of radon-222 (^{222}Rn) from radium-226 (^{226}Ra).

$$^{226}_{88}Ra \rightarrow {}^{222}_{86}Rn + {}^{4}_{2}He \qquad (2\text{-}9)$$

As beta particles are electrons, there is no significant change in atomic mass following ejection. However, as electrons carry a negative charge, there will be a necessary change in the atomic charge as well. In effect, the nucleus has gained a positive charge with no change in mass – hence its atomic number increases by one but its total mass remains the same. An example of this is present during the production of proactinium-234 (^{234}Pa) from the decay of thorium-234 (^{234}Th).

$$^{234}_{90}Th \rightarrow {}^{234}_{91}Pa + e^{-} \qquad (2\text{-}10)$$

Finally, another form of beta emission may occur when a positron (i.e. a positively charged electron) is emitted instead of an electron. In this case, the daughter nucleus has gained a negative charge with no change in mass, hence the atomic number decreases by one.

Gamma radiation results in neither a change in mass nor charge and on its own does not result in the transmutation of an element.

Table 2—1 Modes of nucleus disintegration

		Radiation		*Effect on nuclide*	
Process	*Type*	*Charge*	*Mass*	*Charge Z*	*Mass A*
Alpha emission	alpha particle	+2	4	-2	-4
Beta emission	β^- particle	-1	0	+1	0
	β^+ particle	+1	0	-1	0
Gamma emission	gamma ray	0	0	0	0

Source: Abridged from Faires and Boswell (1981)

2.1.3 Uranium-238 decay series

The uranium-238 decay series is the longest natural decay sequence of any known radioisotope. As summarised by Ivanovitch and Harmon (1992) the sequence begins with the heaviest naturally occurring nuclide ^{238}U and through a sequence of both alpha and beta emissions terminates at the lightest of the radiogenic lead isotopes, ^{206}Pb.

The sequence is represented schematically in Figure 2—1. In this figure atomic number is plotted on the x-axis and relative atomic mass on the y-axis. Uranium-238 is located in the top right hand corner of the plot, with all subsequent decay products connected to each box by lines. On such plots, diagonal lines indicate alpha decay (i.e. both atomic mass and atomic number are reduced by 2), whereas horizontal lines indicate beta emission (i.e. where mass remains constant but atomic number increases by 1). The figure also indicates the half life for each nuclide and, for each particle emission, the amount of energy released (which in some case may be more than one) and the probability that each decay path will occur. For example, the decay of uranium-238 to uranium-234 involves three separate decay events, producing one alpha particle and two beta particles in total:

$$^{238}_{92}U \xrightarrow[\alpha\ 4.15\ \text{MeV}\ (23\%)]{\alpha\ 4.20\ \text{MeV}\ (77\%)} {}^{234}_{90}Th \xrightarrow{\beta} {}^{234}_{91}Pa \xrightarrow{\beta} {}^{234}_{92}U \qquad (2\text{-}11)$$

In this example, the energy of the single alpha particle emitted may have two discrete values, each with an observed probability of being produced. In other cases, there may be a 'branching' of the decay sequence where there is potential for either an alpha or beta particle to be emitted. For example, the decay of polonium-218 (the immediate daughter of radon-222):

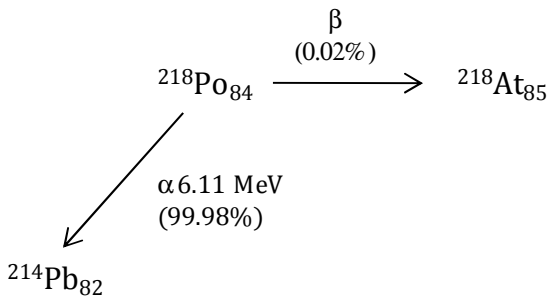

(2-12)

Of particular interest to this study is radon-222, which emits only alpha particles - the predominant group being at 5.486 MeV (~100% of the total decay) and a much weaker one at 4.983 MeV (~8×10^{-2}). As indicated in the figure radon-222 has a half life of *c.*3.825 days although its immediate daughter products (^{218}Po, ^{214}Pb, ^{214}Bi, ^{214}Po and ^{210}Ti) all have half lives much shorter than this. Consequently, and as will be described in the following

section, radon and its immediate decays products are observed to rapidly reach a state of equilibrium with each other resulting in a single radon decay event being characterised by observing the rapid successive emission of a three alpha and two beta particles.

Figure 2—1 The uranium-238 decay series, reproduced from Ivanovich and Harmon (1992)

2.1.4 Radon-222

Radon-222 is the dominant isotope of radon present in the natural environment. Other natural isotopes exist, for example radon-220 and radon-210 (produced through the thorium-232 and uranium-235 decay series respectively), but both have much shorter half lives and hence are difficult to sample and measure in the field. The physical properties of radon are presented in Table 2—2, with an additional plot of variable solubility in water illustrated in Figure 2—2. Of particular note is that it exists as a gas at room temperature, in contrast to all other elements within the decay sequence, and that it is soluble in water.

In most studies, radon is considered to be an inert gas that does not enter into chemical reactions (Ivanovich and Harmon, 1992). However, weak Van der Waals bonding may be present, for example in radon clathrates such as Rn-$6H_20$ in which a lattice of six water molecules encloses a single radon atom. The production of both simple and complex radon fluorides has also been reported in the literature (e.g. Stein, 1983), which suggests that radon can also exist in a cationic form, albeit for a short time (Stein, 1985).

Table 2—2 Physical and Chemical Properties of radon-222

	Property	*Comment*
Relative Atomic Mass	222.02	(^{12}C=12.000)
Boiling Point[1]	-61.8°C	
Melting Point[1]	-71.0°C	
Density[1]	9.96 $kg.m^{-3}$	At standard temperature and pressure
Molar Volume[3]	50.5 $cm^3.mol^{-1}$	
Physical State	Gas	At standard temperature and pressure
Solubility[2]	See Figure 2—2	Expressed by the Oswald coefficient, k, representing the equilibrium between the gas concentration in the liquid phase ($[Rn]_l$) and the gas concentration in the gas phase ($[Rn]_g$)
Half Life[1]	3.825 days	Equates to a decay constant of 0.18121 $days^{-1}$
Recoil Energy[4]	85.0 keV	Upon production from the decay of 226Ra (alpha recoil)
Recoil Range[4]	64 .0μm (air), 0.050 μm (water), 0.036 μm (glass)	

Source: 1) Cothern (1987) , 2) Clever (1979) 3) http://EnvironmentalChemistry.com/yogi/periodic/Rn.html Accessed on-line: 29/10/2004) Andrews and Wood (1972)

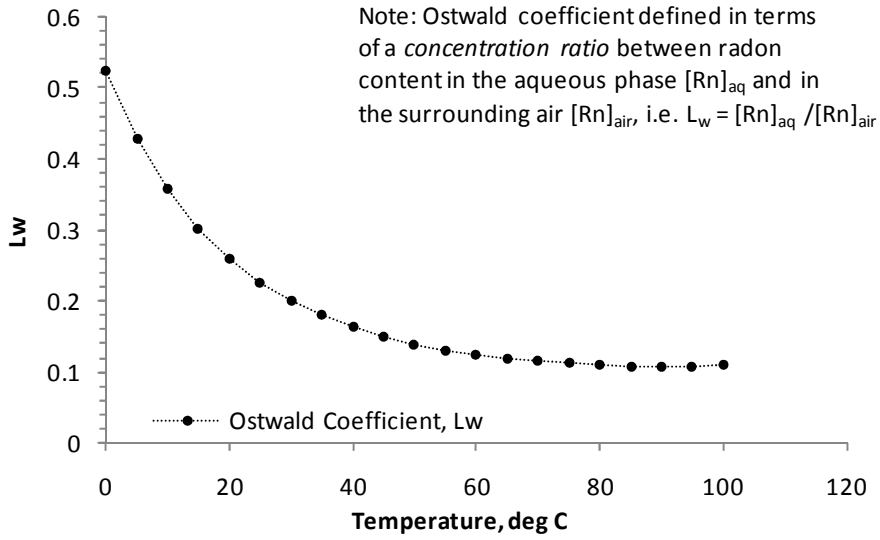

d:\simon\project\calcs\radon\[solubility_clever_1979.xlsx]battino

Figure 2—2 The solubility of radon in water expressed as an Ostwald coefficient, dervied from experimental work by Battino, reported in Clever (1979).

2.1.5 Radioactive equilibria

As stated previously, the activity of a radionuclide (i.e. the rate of disintegration) is equal to the number of atoms present multiplied by its decay constant. By using Bateman's (1910) solution (Section 2.1.1), it can be demonstrated that differences in the individual decay constants of each nuclide within the chain can result in three distinct states of equilibrium.

Secular Equilibrium

If the decay constant of the parent radionuclide is much less than that of its daughter product (i.e. its half life is much longer) and in addition the system under investigation can be considered "closed", i.e. no daughter products are removed from the chain, then it is possible for all members of the chain will attain the same activity given enough time. In this scenario, the system is said to be in a state of "secular" equilibrium. Examples of this phenomenon are found throughout the uranium-238 decay chain and include the production of radon-222 (and all subsequent decay products) from the decay of radium-226. A graphical representation of the build-up of activity for a typical radium standard solution is presented in Figure 2—3. After 30 days of ingrowth, within a sealed radium standard solution, the radon activity (and that of all other daughter products until lead-210) will have reached 99.6% of that of the radium activity.

Transient Equilibrium

If the decay constant of the parent nuclide is only slightly less or about the same as that of the decay product, the total activity will initially rise. This results from the combined decay of all radionuclides. Each parent's activity will peak slightly before the activity of its decay

product but eventually a balance is reached. The total activity then decays at about the same rate as the original radionuclide. The system is then said to be in a state of 'transient' equilibrium. An example of this can be illustrated by plotting the theoretical build up of the decay products of a pure sample of radon-222, as presented in Figure 2—4. Equilibrium between all decay products is reached within approximately three hours, but the overall activity will then decline, with less than 0.5% of the initial radon activity remaining after thirty days.

Entire Series Disequilibrium

If the decay constant of the parent is much greater than that of its daughter products (i.e. its half life is smaller), then the total activity will build up to a maximum and then decline. As the original radionuclide eventually decays away, at no point will the activity of each radionuclide reach equilibrium with its parent. In such situations, the system is said to be in a state of 'continuous disequilibrium'.

Isotope Activity Ratios

At any point, the activity of two isotopes may be compared with each other by calculating their isotopic activity ratio (IAR). In the cases of secular and transient equilibrium described above, IAR values equal to unity indicate that this state have been achieved. Some examples of the time required in a closed system for isotope pairs within the uranium-238 decay series to achieve an IAR of unity are presented in Table 2—3, calculated on the assumption that the entire system may be regarded as closed and that all of the daughter isotopes have been produced during the period of decay (i.e. they are not present initially). Of particular note is that for the case of the $^{226}Ra/^{238}U$ a period of *c.*2.6 Ma is required for secular equilibrium to be achieved. If field evidence shows that this is the case (one of the assumptions made by Atkinson et al (2001), outlined in Chapter 1), such a result would suggest that the Cretaceous Chalk must have exhibited 'closed' behaviour with respect to the radionuclides between ^{238}U and ^{226}Rn for at least the same period of time.

Table 2—3 Time to an Isotope Activity Ratio of ~1 (99.9%) for relevant radionuclide pairs

Radionuclide Pair	*Time to reach an Isotope Activity Ratio of 0.999 between pairs*
$^{234}U/^{238}U$	~2.5 Ma
$^{226}Ra/^{238}U$	~2.6 Ma
$^{226}Ra/^{234}U$	~186,700 yr
$^{222}Rn/^{226}Ra$	~39 days

Calculation: Based on coding supplied by J.A. Barker (pers comm)

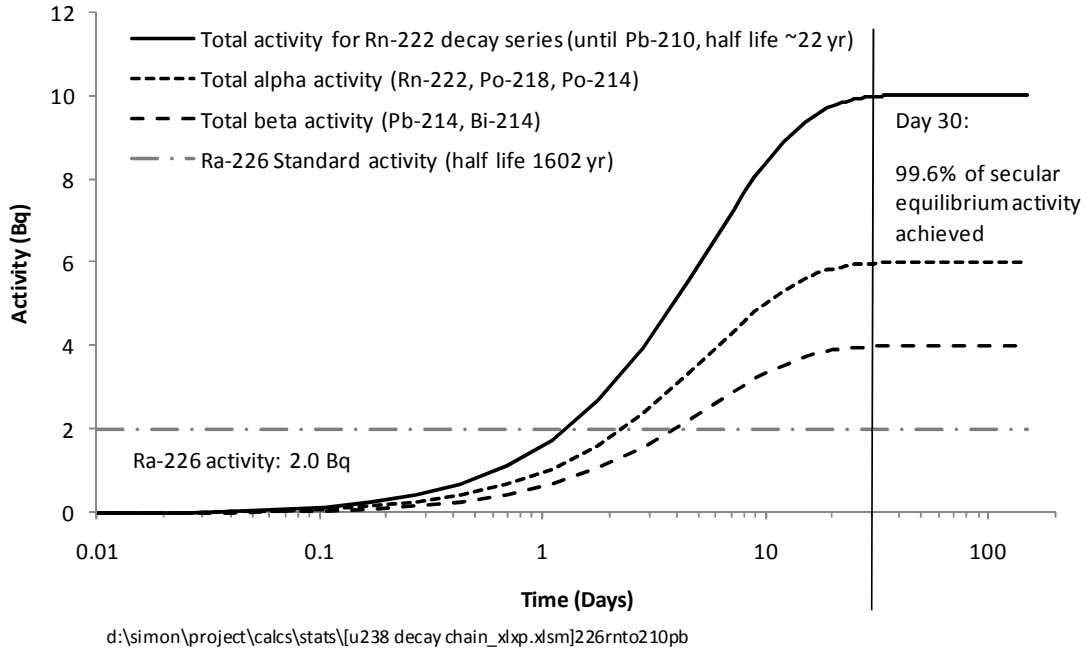

Figure 2—3 Theoretical growth of all daughter products produced from the decay of a Radium-226 standard solution (until Pb-210).

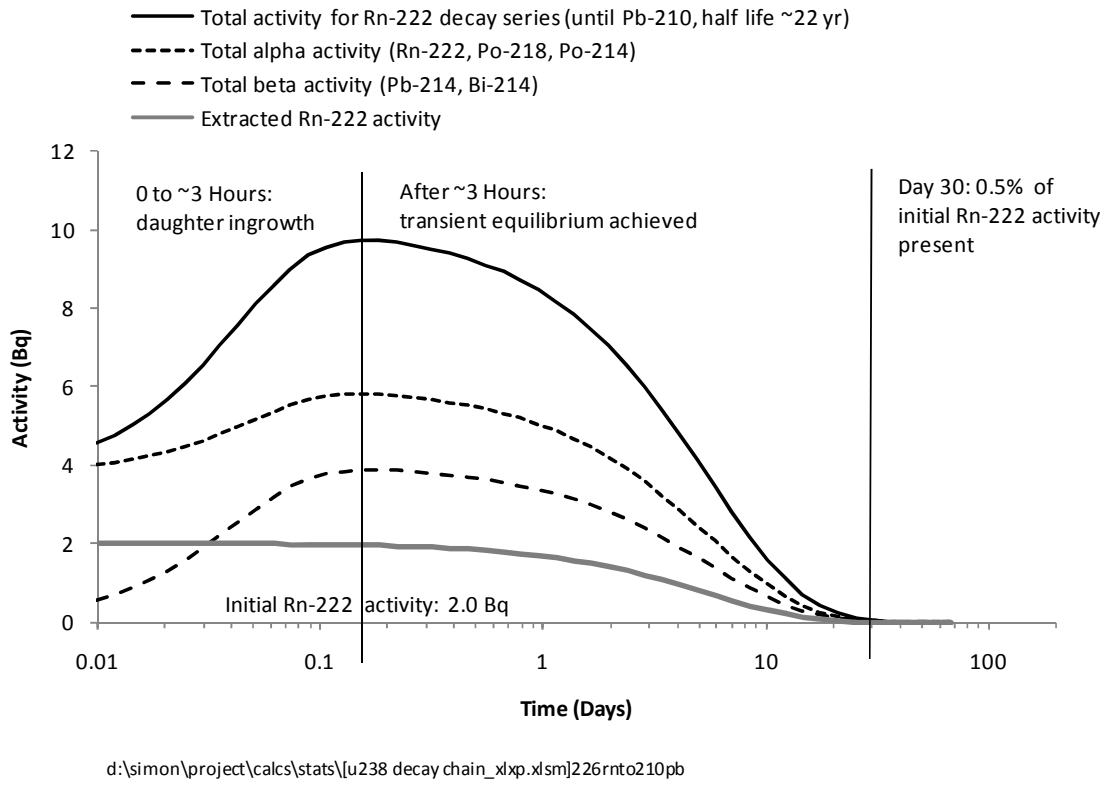

Figure 2—4 Theoretical growth of all daughter products produced from the decay of an extracted Radon-222 sample and indication of the subsequent time to decay.

2.1.6 Causes of uranium series disequilibrium in aquifers

As noted by many authors (e.g. Asikainen, 1981; Ivanovich and Harmon, 1992; Bonotto et al., 2001; Suksi et al., 2006), the presence of true secular equilibrium of uranium series nuclides within the geological timescale is often not achieved. This is typically due to both the varying physical and chemical properties of each daughter product, which may respond in different ways to the prevailing geological conditions. For example, uranium and thorium are both members of the actinide series of elements in which the '5f' orbitals are progressively filled by electrons, and the similarity in their electron configuration results in both elements exhibiting similar chemical properties. Both can exist in a tetravalent state (i.e. U^{4+}, Th^{4+}), and they are often found to substitute for each other in many compounds, which may explain their close association with each other (Faure, 1986). However, uranium can also more readily exist in the hexavalent (U^{6+}) form in oxidising environments and the resulting uranyl ions (UO_2^{2+}) are readily soluble in water. As a consequence, in 'open' geological systems, uranium is observed to be much more mobile than thorium, leading to an increase in U/Th disequilibrium over time. For example, uranium is often enriched with respect to thorium in marine sediments and this is particularly true in carbonates where uranium can co-precipitate with calcium carbonate (Ivanovich and Harmon, 1992), thorium remaining effectively insoluble throughout. Uranium may be also incorporated in carbonate-fluor-apatite and other phosphorites as either a separate uranite phase, as an adsorbed or structurally incorporated uranyl ion, or as direct substitution of Ca^{2+} for U^{4+} in the crystal lattice structure (Panczer et al., 1998).

In isotopic terms, groundwaters may often exhibit excess ^{234}U compared to ^{238}U due to the former's increased ability to be leached from sediments. Although chemically identical, it is often considered that the site within crystalline structure may become damaged though alpha particle emission during the decay of ^{238}U, resulting in preferentially favourable routes for ^{234}U to migrate to the surrounding pore space.

Finally, extreme $^{222}Rn/^{226}Ra$ disequilibrium is often encountered in groundwaters, suggesting that the radon activity is unsupported by an associated dissolved radium source. Krisnaswami et al (1982) demonstrated that sorption effects are likely to remove radium from solutions when compared to radon. They also concluded that the adsorption of radium in oxidising groundwaters is rapid and that radium isotopes do not migrate far from their source even in the presence of an active groundwater flow system.

2.2 Radon Emanation

Radon emanation studies in the literature may be grouped according to three main areas of research:

i) Theoretical mathematical representations of the emanation of radon gas from a simplified representation of individual rock substrates or grains, which are generally difficult to measure experimentally;

ii) The development of macro-scale models, correlated to field data, that encapsulate many different physical attributes and processes present at the pore space level, but which do not attempt to represent them explicitly;

iii) Combined emanation plus transport studies that seek to explain variations in radon content within different geological formations, both spatially and temporally, and which may include other transport processes such as sorption and diffusion.

In this regard the model of Atkinson et al (2001) outlined in Section 1 is an example of the third type of approach – i.e. a) the emanation factor E (Equation. *(1-11)*) representing a composite effect of many individual emanation processes and b) emanation coupled with an advection-diffusion model for the Chalk groundwater flow system. A similar approach was used by Wanty et al (1992), who developed a macroscopic model of radon emanation from rock to groundwater, accepting that such up-scaling techniques necessarily introduced a degree of empiricism to the approach.

In assessing the suitability of such an approach, the individual methods of emanation which may contribute the overall effect are now briefly outlined. For reference, a schematic illustration of a idealised single grain and the processes involved is provided in Figure 2—5.

Direct Recoil

Radon may be released by direct recoil, namely that radon atoms (and possibly the associated alpha particle) are physically ejected from pore walls upon production from the decay of a radium atom. The distance that an ejected radon atom can travel can be a function of the surrounding medium – distances being several orders of magnitude less if the pores are saturated with water than with air. For example, in a series of experiments designed to understand why radioactive disequilibrium may exist between ^{238}U and ^{234}U in sea waters, Kigoshi (1971) measured the concentration of both ^{234}Th and ^{234}U present in the aqueous phase of a suspension of finely ground zircon sand (particles being of the

order of 1 to 10 μm in diameter). He demonstrated that the presence of ^{234}Th in solution could be

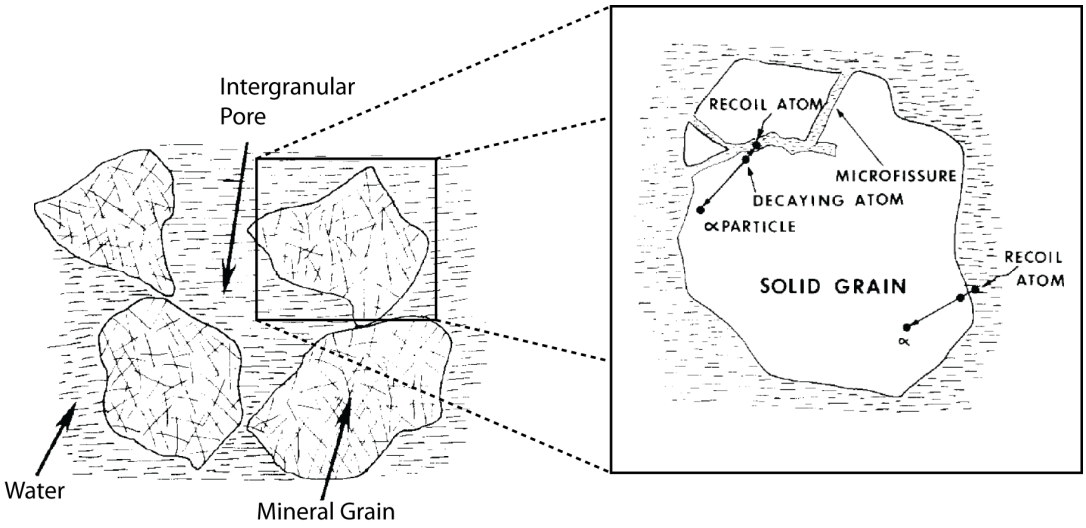

Figure 2—5 Schematic diagram illustrating the conceptual model of radon emanation through alpha recoil and diffusion within and external to a solid grain into the surrounding pore water (after Rama and Moore, 1984).

predicted in terms of zircon density and initial uranium content alone, and that a simple 'ejection through recoil' model was sufficient to explain this effect. The experiments also confirmed an excess of ^{234}U present in solution compared with ^{238}U, but from the rate of leeching it was suggested that ^{234}U atoms may also move along 'fossil tracks', created at the surface of the solid silicate as a consequence of alpha recoil. Kigoshi (1971) demonstrated that the recoil distance inferred from emanation experiments is likely to be affected by the presence of water within the pore space, citing previous column experiments that demonstrated that dry sediments released much less ^{234}Th from the solid phase than a saturated sediment. Such work suggests that higher emanating efficiencies are to be expected in saturated media – due to the dissipation of the kinetic energy of the recoiled radon atoms, limiting their ability to be re-embedded in the surrounding pore walls.

In a detailed mathematical representation, Semkow (1990) outlined alpha-recoil emanation theory, derived using theoretical shapes with variable thicknesses of radon producing material. This work was extended through the development of an emanation model for single grains, to determine if a relationship between emanating power and the size of grain and radium distribution within it could be determined. The model took account of processes such as pore wall embedding, the role of overlapping pores and the impact of water saturated void space (where recoil distances are much smaller than in air). Semkow (1990) noted that, although it was theoretically possible to calculate the emanating

power for a grain if the specific surface areas was known, in reality such a property is difficult to determine for non-uniformly spherical shapes, such as grains. It was further noted that, in comparison with measured data, the model performed poorly where particles had a high specific surface area and where the radium source term was distributed throughout the grain.

Diffusion along crystal boundaries

Andrews and Wood (1972) suggested however that the mechanism of direct recoil was not sufficient in itself to explain elevated radon concentrations in groundwater. Assuming that the recoil range for ^{222}Rn in rock matrices is likely to be in the same order as that for silicate glass (0.036 μm), Andrews and Wood (1972) noted that only those atoms located very close to the surface of rock particles are ever likely to be ejected. They demonstrated that the theoretical escape probability, for all radon atoms produced within a particle, is inversely proportional to the particle diameter. Applying their model to the Chalk, where individual crystals of calcite present may have a diameter of the order of 1 μm (see Chapter 3 for more details of Chalk composition), would yield a maximum emanation efficiency of only *c.*4.9%.

Andrews and Wood (1972) considered further that the efficiency of both the direct recoil method, combined with potential diffusion through crystal lattices into the surrounding pore space should be a function of the particle's specific surface area, which is similarly inversely proportional to the particle diameter (i.e. $E \propto 1/d$). However, their analysis of radon emanation from a selection of particles sizes from Carboniferous Limestone and Midford Sand (a marine Upper Lias sediment) demonstrated that emanation was proportional to $1/\sqrt{d}$, suggesting that other processes must enhance the rate of diffusion from within the particle. They argued that radon may diffuse more rapidly than predicted due to the presence of individual crystal boundaries (which may provide preferential routes to the particle surface) and that intersections of such pathways for uniform grains are also shown to be proportional to $1/\sqrt{d}$.

The ^{222}Rn diffusion coefficient in Carboniferous Limestone was shown by Zereshki (1981)to be much greater (*c.*10^{-7} cm^2 sec^{-1}) than could be accounted for by lattice diffusion alone (estimated at less than 10^{-20} cm^2 sec^{-1}), and was also attributed to intergranular diffusion. Similarly Cuttell *et al* (1986) used radon estimates in the Lincolnshire Chalk to estimate the specific surface area of rock in contact with groundwater and to estimate an equivalent radon emanation factor by pure recoil.

However, the emanation efficiency estimated by this method (62%) was considered too large to be explained by recoil alone and it was recognised that other factors such as the role of intra-granular diffusion and the location of the radium source in relation to fracture walls must also be considered.

Diffusion along micro-fractures or 'nano-pores'

Rama and Moore (1984) demonstrated through laboratory studies that radon emanation from single particles was much greater than would be expected from the geometry alone and also concluded that preferential paths (or 'nano-pores') for radon diffusion must exist within individual grains. In contrast, Krishnaswami and Seidemann (1988) demonstrated that radon diffusion along crystal boundaries was negligible for certain silicate materials, due to the low rate of argon isotope release from the same samples produced by neutron irradiation. They concluded that such minerals are not in fact permeated by nano-pores that may provide rapid diffusion paths along the particle surfaces but rather, that radium was preferentially distributed on grain surfaces or within surrounding accessory minerals. In the rock samples analysed, additional minerals included allanite (part of the epidote group), uranium bearing zircon and apatite.

Location of the source term

Andrews and Wood (1972) demonstrated, that for larger cemented particles of Old Red Sandstone, emanation may be enhanced further by the presence of secondary phases in the rock, and suggested in such examples that the source of radon may well be preferentially located within the cement rather that the sand particles themselves. Combining all such processes, Andrews and Wood (1972) calculated that for the limestone and sandstone particles measured total release of radon from within a particle could be obtained from particles of the order of 1-2 μm in diameter.

Sasaki et al (2004) demonstrated that small water saturated pores (of the order of 10 nm in width) could also result in high emanation factors, but these alone could not explain emanation factors greater than *c.*0.2, and that grain size and shape must also be considered. They also noted that emanation values (expressed as a percentage of total radon produced) will be less if radium is uniformly distributed throughout the grain. Sasaki et al (2005) furthered this work to explain large emanation factors (>*c.*0.6) observed in some materials and considered two different grain type models – two components mixed together (large radium free grains surrounded by fine radium rich material), and a second type with one grain type with radium. In both cases, much higher rates of emanation were achieved (up

to 0.75), in both cases due to selecting very small grain sizes for the radium bearing medium.

2.2.1 Radon Sorption

Although regarded as chemically inert, the sorption of radon to sediments with high organic content has been reported in the literature. For example, Wong et al. (1992) determined sediment-water radon partition coefficients for a series of unconsolidated sands with organic content ranging from *c.*19 to *c.*124 mg C/g. They demonstrated that radon exhibited absorptive behaviour that increased with organic fraction, that the sorption isotherms fitted a linear-type model and that the sorption was readily reversible. They concluded that the observations were consistent with their original hypothesis that radon was readily sorbed to organic matter, which is consistent with the observed high partition coefficients observed for radon in non-polar organic solvents (see Chapter 4 for a further discussion on radon partition).

Radon is also observed to be readily sorbed to activated carbon at standard temperature and pressure, a phenomenon exploited for the purposes of health protection in areas of high natural background radon production (Goh et al., 1992).

2.3 Uranium series measurements in Chalk aquifers

Although many authors have previously reported on levels of radon activity in chalk or other carbonate aquifers, relatively few published studies exist that report both radon activity in groundwater and uranium and radium activity in host rock from the same locality. Normally, data on solid geology U series content are few in number and averages from other localities are often employed (e.g. Younger and Elliot, 1995).

However, there are a few studies that do report U series content specifically. Ward (1989) measured radon activities of groundwaters pumped from three abstraction wells in East Anglia (discussed in greater detail in Chapter 6), but in addition assayed several Chalk samples using neutron activity analysis for uranium and radium content sourced from local quarries. Ward also measured the $^{234}U/^{238}U$ and $^{226}Ra/^{238}U$ isotopic activity ratios of the same samples and found in particular that the iron stained walls of flowing fractures in the saturated zone of the Chalk contained proportionally higher levels of radium than the surrounding Chalk matrix. The IARs for the different types of Chalk were also shown to vary, dependent on whether the sample was taken from the bulk matrix or highly lithified sections. Ward (1989) suggested that the variation in these data can be explained through either

i) a degree of preferential diffusion of daughter products;
ii) adsorption from another source further up the groundwater flow path; or
iii) an affinity of radium for iron/manganese hydroxides (located on some fracture walls)

Low (1996a; 1996b) sampled Chalk groundwater for radon content (both boreholes and springs), also in East Anglia. His data showed both spatial and temporal variation over the 15 months that samples were taken. Analysis of three Chalk samples from a borehole core for uranium and thorium assay was undertaken by means of both alpha-spectrometry and solid state nuclear track detection. Low's (1996a) analysis demonstrated ^{238}U concentrations of the order of 0.3-0.4 $\mu g.g^{-1}$ in the carbonate fraction of the Chalk, but with higher concentrations in the acid insoluble phase (2.4-8.0 $\mu g\ g^{-1}$, using 0.1 M HNO_3 as the dissolving acid).

Cuttell et al. (1986) measured the uranium, thorium, radium and radon isotope content of water samples in the Chalk groundwaters in Lincolnshire, where the aquifer was subdivided into a series of zones according to the major ion chemistry. These zones represented a range of groundwater ages, from very recent groundwater occurring at outcrop, through to much older (up to 30,000 years BP) groundwater at depth, with low levels of nitrate and enrichment of minor ions (e.g. strontium and iodide) and with low or slightly negative Eh. High salinity groundwater along the coast was also identified. Measurements were also made of the uranium, thorium and radium content of solid samples from 3 locations and showed ^{238}U content in the order 0.05 to 0.18 $\mu g\ g^{-1}$ for white Chalks with elevated content (1.34 $\mu g\ g^{-1}$) in one marl band. Estimates of the $^{226}Ra/^{238}U$ isotopic activity ratio for each sample revealed a range from 0.7 to 1.1, with an average value of 0.94 ± 0.13 indicating that most samples were slightly depleted in radium compared to uranium. Cuttell et al. (1986) also compared $^{234}U/^{238}U$ ratios in groundwater to total uranium content and demonstrated that the there was a clear difference in signature between the oxidised groundwater system and one where reducing conditions prevailed. They noted that Eh dominated the control of uranium in solution, oxidising conditions promoting the formation of soluble carbonate and phosphate uranyl complexes. These data are discussed in more detail in Chapter 5 where a comparison with this study's results is made.

Zereshki (1981) investigated radon and radium concentrations in cave system percolation water, springs and tap samples in UK Carboniferous Limestone, as well as a spectrometric

determination of the ^{238}U and ^{232}Th and ^{40}K content and ^{222}Rn release from overlying soils, with the average ^{238}U content calculated to be 5.4 $\mu g.g^{-1}$. By comparing the radon content of water of a fully saturated soil and assuming an isotopic activity ratio for $^{238}U/^{226}Ra$ of unity, Zereshki estimated a radon emanation efficiency of 0.187. Applying a similar method to the Carboniferous Limestone rock matrix yielded a value of 0.125, which was attributed to a lower specific surface area compared to that for disaggregated soil.

Finally, although no measurements of radon activity were recorded, Hubert et al (2006) undertook an extensive series of measurements of uranium series disequilibria in Chalk core samples and associated groundwaters in northern France, for the purposes of assessing the potential mechanisms of U-series migration within the aquifer. In particular, Hubert et al (2006) observed variations in $^{234}U/^{238}U$ isotopic activity ratios that correlated with the location of the sample within the core, with values greater than unity typically found within the zone of local water table fluctuation. This result was attributed to the mobilisation of ^{234}U from the overlying unsaturated zone (from chemical weathering), combined with calcite precipitation near the water table. All but one water sample analysed within the study (i.e. groundwater, spring and river samples) showed enrichment in ^{234}U (as reported by others such as Bonotto et al., 2001 for a granite aquifer).

3 Study Area

This chapter describes two adjacent Chalk catchments in Berkshire, from which hydrological and radiological data relevant to the study have been obtained. These data are used subsequently to test the radiochemical method which was outlined in Chapter 1 and which is explored further in Chapter 7. The catchments were selected primarily on the basis of the large amount of data that were readily available, both through recent data collation and collection as part of the LOCAR programme, but also from the many historic litho-stratigraphic and groundwater related studies undertaken in this area.

Firstly, the geological setting is examined, and the potential links between lithology and the source of radon gas. Data from both mapped outcrop and borehole records are used to construct cross sections that illustrate the relationship between the Chalk, Palaeogene and other superficial deposits.

Secondly, all geographical and hydrological data collated is presented in a series of integrated plots. The data demonstrate that the selected catchments are typical examples of Chalk catchments in the south of England, although there are differences between the two in terms of the generation of runoff and the sources of river flow.

Thirdly, the hydrogeological data available are described and an attempt has been made to identify the most import characteristics of the Chalk in the storage and transport of groundwater. This includes providing evidence of the fractured nature of the rock well as presenting evidence that suggests that near surface processes may generate more karst-like solution features which may affect contaminant transport velocities.

Fourthly, the individual sites selected for radon assay are described, where activity has been recorded at regular intervals over 24 months. These data provide a basis to test a) the applicability of the procedures developed in Chapter 4 and b) the transport model as developed so far in Chapter 7. In particular, a description is made of the Trumpletts Farm research site in the River Pang catchment. This site was used for a variety of exercises, including two open hole pumping tests, a series of packer tests, radon sampling and from where core was obtained to undertake assays of both uranium content and radium activity.

Finally, the data are integrated and summarized in a series of cross sections that are used to highlight key aspects of both catchments.

3.1 Catchment Overview

The Pang and Lambourn catchments are located to the west of the town of Newbury, approximately 60 km west of London and form part of the Berkshire Downs. Adjacent to each other, both catchments are predominantly rural and agricultural with little heavy industry or major conurbations. Situated on the north-western side of the London Basin they are also considered representative for most of the Chalk outcrop in southern England, especially the areas where overlying Tertiary deposits are present (Wheater et al., 2006), though less representative of the formally glacial areas, i.e. north of Ivinghoe Beacon, in the Chiltern Hills (as illustrated by Boulton, 1992). The location of each catchment is indicated in Figure 3—1 and the individual site locations that are discussed throughout the text are plotted on Figure 3—2.

Figure 3—1 includes boundaries marking the surface water divides. These have been determined previously by applying a surface drainage algorithm to output from a 50 m horizontal resolution digital terrain model (DTM), supplied by the LOCAR data centre. As will be discussed in Section 3.3, these boundaries do not necessarily reflect the extent of the subsurface groundwater divides, which are known to vary in extent through time. (DTM derived topography, included on this figure as 25 m contours, is also used in Figure 3—3 and Figure 3—4 as shaded relief, superimposed with major and superficial geology, and in Figure 3—12 with contours of aquifer transmissivity.)

Both catchments are low lying, with the ground height ranging from approximately 40 mAOD in the south-east where the Pang outflows to the River Thames, rising to 260 mAOD in the north-west at the top of the Chalk escarpment As will be discussed in Section 3.2 the topography broadly reflects the underlying geological structure, albeit with subsequent modification by episodes of erosion.

The main Lambourn drainage channel trends approximately south-east. A number of dry valleys are also apparent – examples of these include Great Shefford (that drains from the north-east), Maidencourt Farm (from the west), and from both sides of the channel immediately south of Weston.

In contrast, the main Pang drainage channel changes direction several times form its source. Initially south flowing, the river turns east in its lower reaches before finally flowing north towards the River Thames. Again, in contrast with the Lambourn catchment only a few, poorly defined, valleys are present.

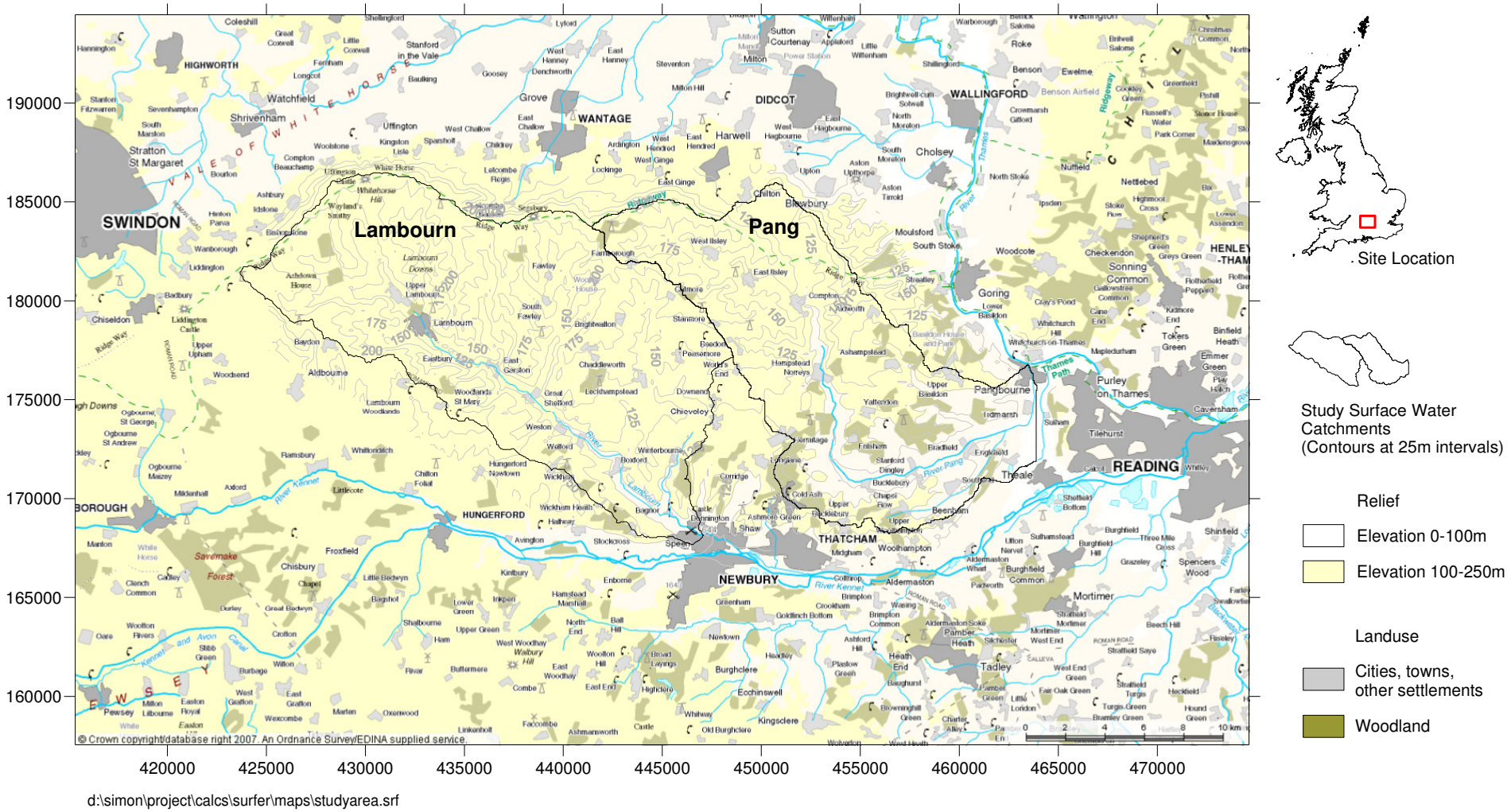

Figure 3—1 Field Study Area - Pang and Lambourn River Catchments, West Berkshire. 1:300000

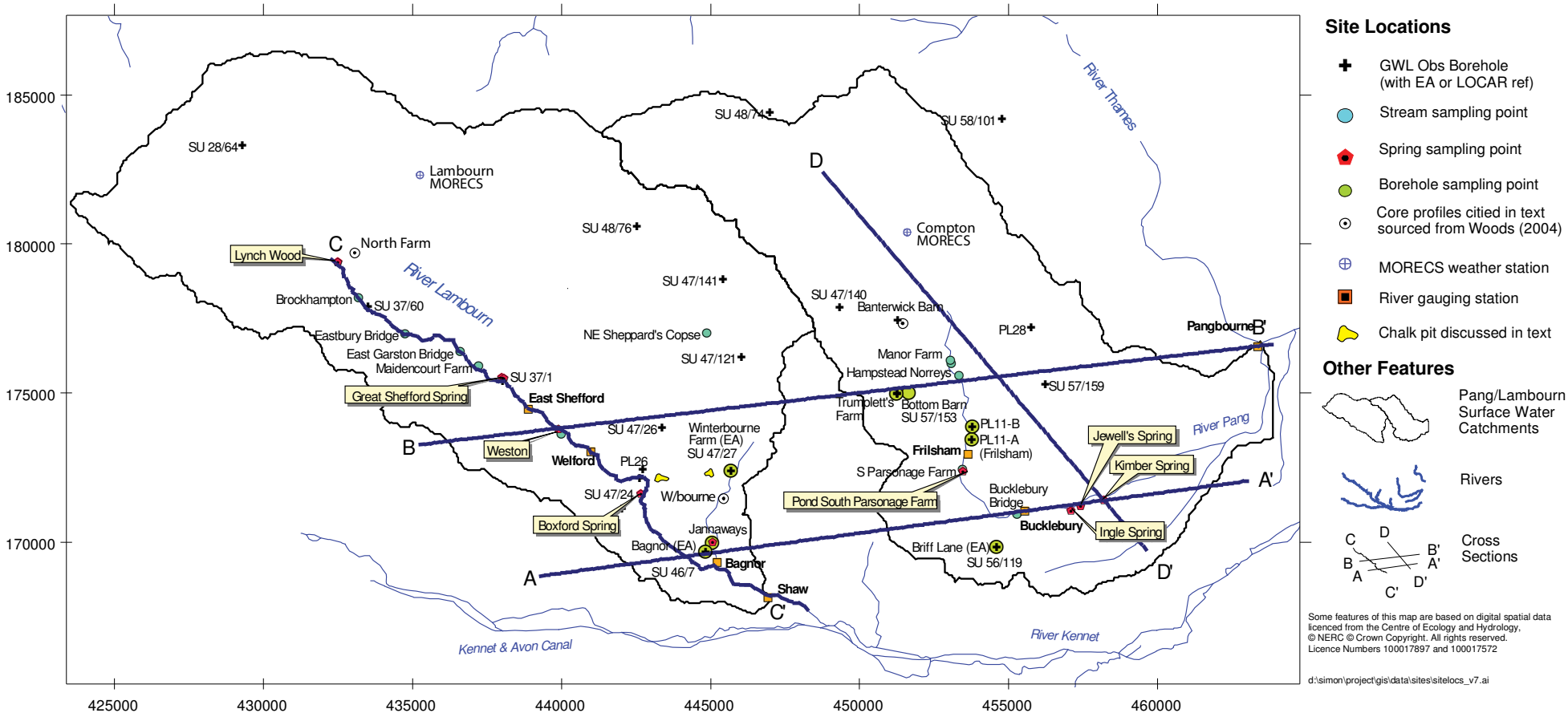

Figure 3—2 Field Study Area – Site Location Map

3.2 Geology

Both catchments are situated within the Southern Chalk Province, at the western edge of the northern limb of the London Basin. They both lie principally on the Cretaceous Chalk, the main aquifer of the region, with an overall regional dip of less than two degrees, trending to the south-east or south. Although minor faulting and variations in dip and strike are present, no major structures have been identified in the Chalk within this area (Bradford, 2002).

The geology of the catchments is presented in Figure 3—3 (Solid) and Figure 3—4 (Quaternary only). The dominant geological sequences within each catchment are post-Cenomanian Chalk sequences, underlain by the Upper Greensand and Gault Formations that outcrop to the northwest of both catchments. The Chalk is overlain by Tertiary deposits in the south-east. Superficial deposits are present in the valley bottoms, and separately cover some of the upper parts of the interfluves and valley slopes.

3.2.1 Gault Formation

The Gault Formation is of Albian Age (i.e. Lower Cretaceous) and crops out to the north and north-west of the study area. It consists variably of calcareous mudstones and silty mudstones, stiff to very stiff, dark grey or blue grey silty clay with pale mottling. Discrete bands of phosphatic, pyritic and calcareous nodules also often occur (Rawson, 1992). Its thickness varies between 30-70 m and it thickens from the west to the east. Dipping gently beneath the Upper Greensand and Chalk the Gault formation is normally considered to be an aquiclude (Rushton et al., 1989), and hence is regarded as the hydrological base to both catchments.

3.2.2 Upper Greensand

The Upper Greensand Formation consists mainly of bedded pale yellow-brown, pale grey and greenish grey bioturbated siltstones and very fine silty sandstones, indicative of formation in more shallow seas c.f. the Gault Clay (Rawson, 1992). Characteristically, the beds also contain significant amounts of the mica group mineral glauconite which, although a mica, is similar in structure to clay (illite). Glauconite, typically formed by marine diagenesis in shallow waters, is normally associated with reducing environments and the presence of organic material. The thickness of the Upper Greensand in the study area varies between 15-30 m (Rushton et al., 1989).

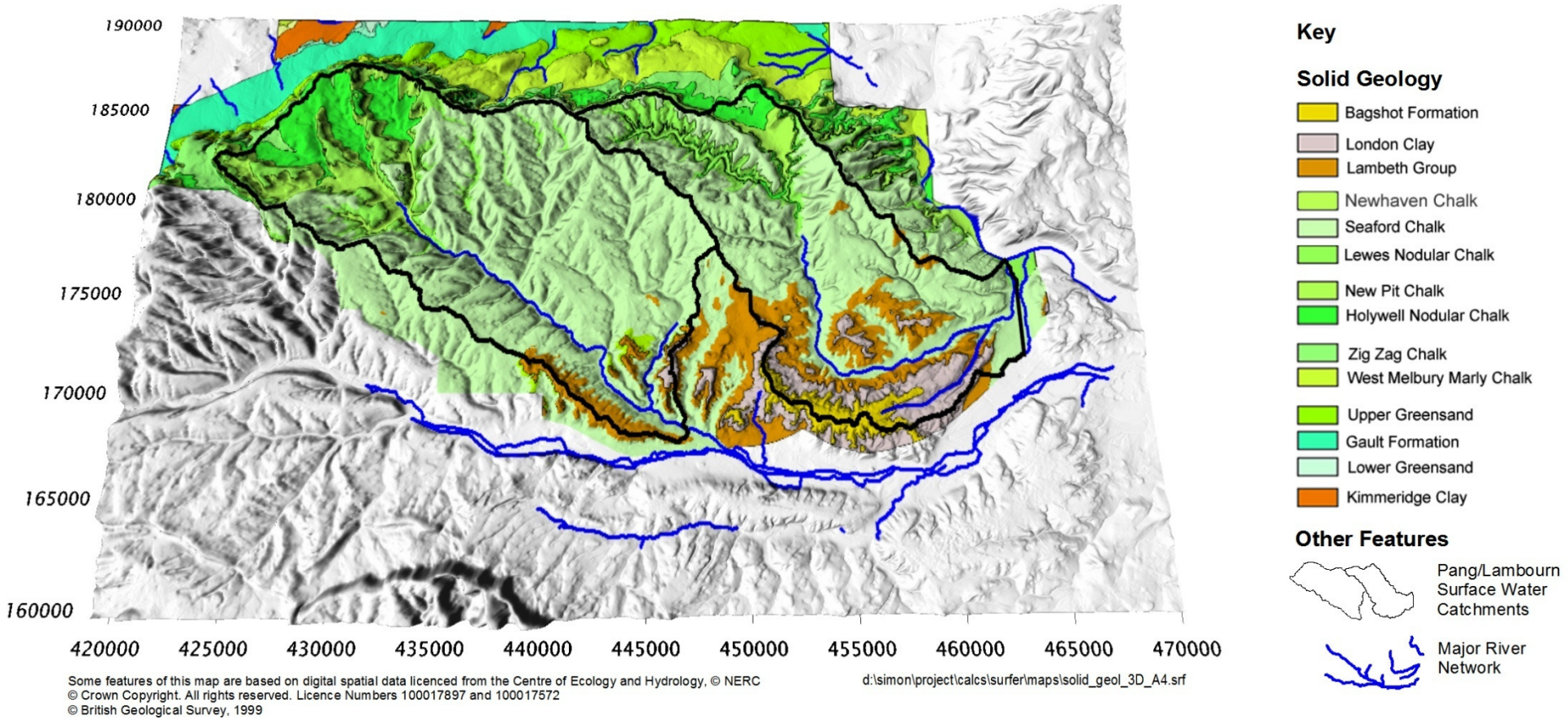

Figure 3—3 Digital Terrain Model (DTM) of Pang and Lambourn catchments, draped with Solid geology. 1:300000 (vertical exaggeration x10)

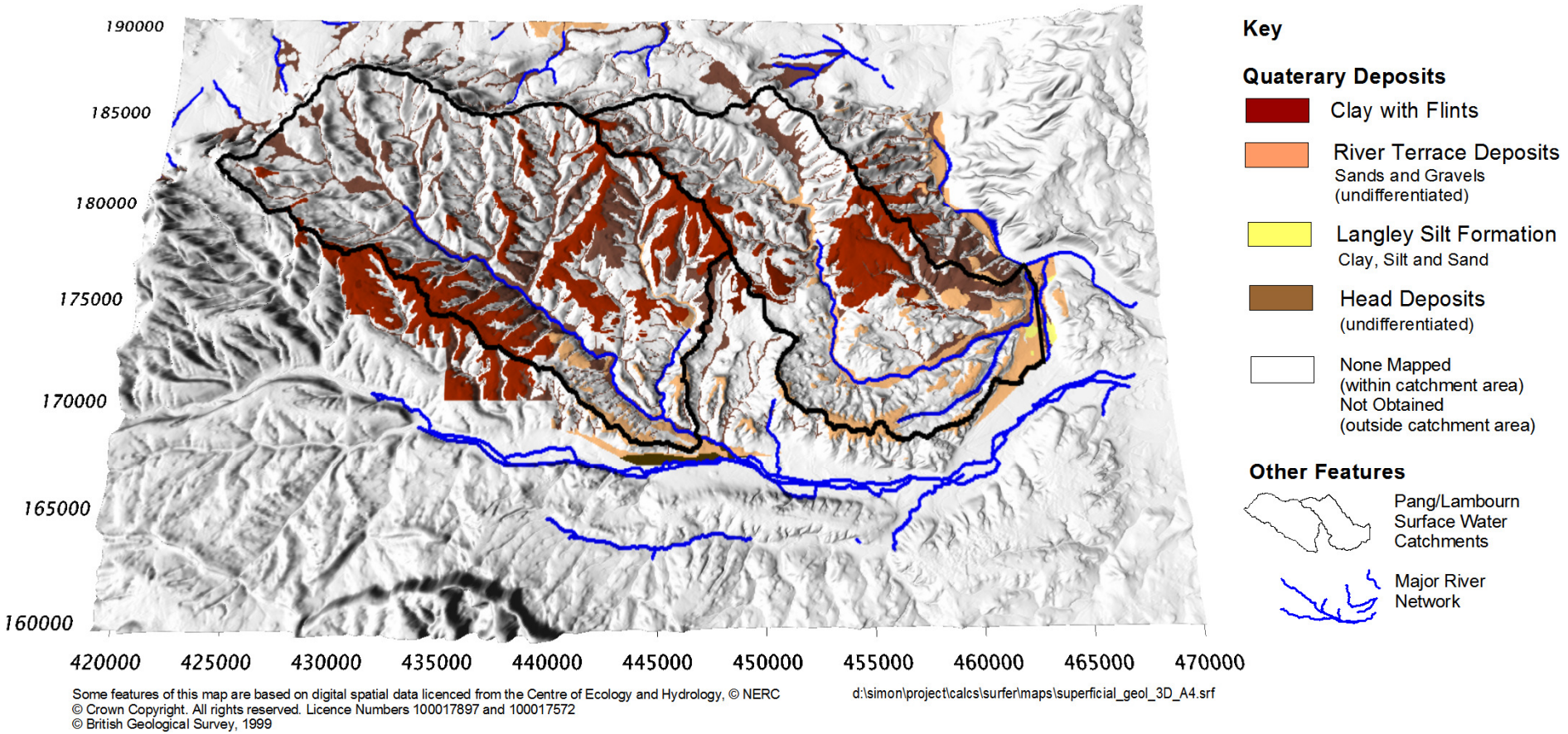

Figure 3—4 Digital Terrain Model (DTM) of Pang and Lambourn catchments, draped with Quaternary geology. 1:300000 (vertical exaggeration x10)

3.2.3 Chalk – Lithology

The Chalk is predominantly a very fine grained soft white micritic low-magnesium limestone (c.98% $CaCO_3$,) but which, dependent on its depositional environment and subsequent diagenesis, also contains other secondary features such as thin marl bands, flint seams and hardgrounds.

The primary sediment is considered pelagic in origin, i.e. having accumulated on the sea bed, rather than having been transported by mechanical forces. Typically between eighty and ninety-two percent of the biogenic components of the sediment consists of the skeletal remains of a single marine phytoplankton, *Haptophyta*. Built from individual calcite laths, the alga exoskeleton is constructed in stages; firstly into individual dish-like plates ("coccoliths") and then by accumulation into a three dimensional spherical structure ("coccosphere"). Although the overall structure resembles a form of protection, its exact function remains unknown. Hancock (1993) suggested that the skeleton may provide a way for the organism to limit its rate of photosynthesis, as there is a strong correlation between the number of coccoliths produced (per alga) and the depth below the ocean surface at which they are found.

In the case of the purest white chalks, the rate of deposition of the debris (produced either as algae shed their outer plates or upon their death) is considered sufficiently high that dissolution of the calcite material does not take place. Examples of preserved coccolith structure, determined by the use of scanning electron microscopy, are illustrated in Figure 3—5(A). Although complete plates are present (c.3 to 4 μm across), it is common to observe individual laths, which can be as small as 0.5 to 1 μm in diameter (e.g. Price, 1987). In this example, the image reveals the open structure of the rock, with good preservation of the shell fragments and little in the way of mineral infill or recrystallization. As a consequence, the porosity of such sediments remains high, typically between 30 and 40% of the bulk volume (Price et al., 1993). In addition, calculations of the distribution of pore throat sizes within blocks of competent Chalk made by mercury injection reveal a median value of between 0.8-1.0 μm, in line with the scale of the component laths (Price et al., 2000). The remainder of the biogenic components of the sediment (between 5 and 10%) consists of a mixture of shell fragments from either foraminifera, bivalve molluscs or ostracods. In areas of moderate post depositional diagenesis, sparry calcite may line the external moulds of such fossils. The resulting increase in void space (on the scale of 10-100 μm in diameter) is illustrated in Figure 3—5(B).

Figure 3—5 Scanning Electron Microscope (SEM) images of Seaford Chalk

A) **High magnification image of Seaford Chalk from Lulworth, Dorset. Individual laths consist of crystals of calcite that form larger amalgamated structures (coccoliths). Pore spaces are of the order of one micron. Reproduced from BGS Baseline Report Series 4 (Edmunds et al., 2002)**

B) **Sample from Chalk exposure at Birling Gap, East Sussex. The fine calcium carbonate matrix is interspersed with larger voids, due to the recystallization of foraminifera or bivalve shells. Reproduced from Betson et al (2004).**

Electron microprobe analysis of single coccoliths specimens from the Cretaceous Chalk by Burki et al (1982) suggests that they may be coated by secondary phase minerals such as clay, quartz or apatite, $[Ca_5(PO_4)_3(OH,F,Cl)]$. By gentle dissolution of the calcite component of the shell, Burki et al (1982) demonstrated the presence of a skin of generally amorphous material, but with an elemental composition suggestive of smectite. More recent work using X-ray spectrometry by Balogh (2008) indicated the presence of amorphous iron and manganese oxides as major coatings, but could not confirm the presence of clay from the analysis of the crystal form of the sample residue. However, the presence of aluminium and silicon in the samples suggested that clay coatings may be present, albeit as a minor component and with a thickness of only a few nanometres.

Other diagenetic process may alter the sediment structure either during deposition or subsequent to compaction. Hancock (1993) differentiates between penecontemporaneous and late stage diagenesis. The primary diagenesis of the coccolith ooze that deposited on the sea bed is thought to have included very high rates of bioturbation by both surface feeding and shallow burrowing animals. Evidence of fossilized *Thallassinoides* burrows also indicates that some organisms could bury up to about one metre below the sea bed. Deeper than this, physical compaction, without significant calcite solution, would reduce the porosity, initially around 75-80% at the surface , to between 30-40%.

Secondary types of diagenesis, such as the formation of nodular chalk and lithified hardgrounds, are believed to have been formed during a break in normal pelagic sedimentation and are discussed below. Much later types of diagenesis such as thermal and tectonic effects are not considered here, due to the lack of support for their presence in the study area.

Nodular Chalk and Hardgrounds

Episodes of a low coccolith production have been ascribed to periods of sea level fall, diapiric uplift or rejuvenation of uplift along an earlier tectonic axis (Hancock, 1993). If the rate of coccolith supply slows down (or stops completely) sufficient organic material may be entrained into the sediment to promote the activity of sulphate-reducing bacteria within the anoxic environment found below the actively bioturbated surface.

Through oxidation of the organic material, the production of H_2S and free carbonate ions is promoted. Given the abundance of calcium present in solution, it is likely that new crystals of calcite may precipitate. Such lithification may also result in the simultaneous depletion of strontium and the enrichment of iron, manganese and magnesium (Rawson, 1992). The effect of recrystallization is to the reduce the open pore space and to increase

the hardness of the surrounding sediment. With time, such nodules of chalk may grow laterally and the beginnings of an extensive hardground may form.

Many of the hardgrounds present in the Chalk show evidence of scouring, abrasion and bioerosion. Evidence of extensive mineralization by glauconite and phosphate has also been found in the burrows and borings of surface dwelling organisms, in mineralized intraclasts and fecal pellets. According to Jarvis (1992), this suggests that lithification took place on the sea floor at or close to the interface between the sediment and the seawater, at depths of between 70-100 m below sea level.

Examples of hardgrounds within the study area include the sequence of up to five episodes of lithification represented by the Chalk Rock group found near the base of the Lewis Nodular Chalk Formation. This sequence contains large quantities of "collophane" or hydroxyl-apatite (Morgan Jones, 1977). A description of the formation is provided under in Section 3.2.4.

Phosphatic chalks

By convention, phosphatic chalks are defined as those facies which contain a P_2O_5 content greater than 5% (Jarvis, 1992). Greyish in colour, sometimes gritty chalk in blocky masses, the mineralogy of phosphatic chalks consists of low-Mg calcite, carbonate-fluorapatite, quartz, glauconite and iron oxides. In general they contain higher concentrations of Na, P, and Sr, but less Ca than white chalks and hardground chalks (Jarvis, 1980). They are normally associated with a high levels of biological activity, where matter decaying in an anoxic environment provides dissolved PO_4. Where the pH of the sediment has been lowered, calcite may be dissolved and replaced by microcrystalline francolite (i.e. apatite that contains appreciable CO_2 and more than 1% F).

The phosphate may also be pelletal consisting of a combination of small fecal pellets (produced by detrital feeders), foram tests and fish teeth. Normally light brown colour, these fossils can make up between 10-30% of the entire bulk rock in localized horizons (Morgan Jones, 1977; Pacey, 1985).

An investigation of the natural gamma activity of Chalk boreholes demonstrated a correlation between the presence of a non-carbonate fraction and elevated levels radioactivity when compared to the surrounding white Chalk (Pacey, 1984b). By the use of gamma spectral data Pacey (1984b) showed that the bulk of the signal was not produced from the decay of ^{40}K as previously assumed and that, in fact, less than 5% could be explained by this process. Although he did not measure the uranium content directly,

Pacey (1984b) infers that when the contributions from ^{40}K and ^{232}Th are subtracted from the total gamma count, over 70% of the radioactivity must be produced as a result of decay from the ^{238}U decay series.

Pacey (1984b) also noted that the acid insoluble fractions from the Chalk matrix and marl bands may contain "considerable amounts" of apatite and compared these to the phosphatic Chalks in other locations. In a subsequent investigation of the trace element chemistry of phosphatic chalks, it was found that they could contain "up to 20 times" more uranium than the average shale, with levels of total uranium content ranging between 35 to 55 ppm (Pacey, 1985).

Examples of phosphatic chalks have been found within the study area, in particular at Boxford and Winterbourne Chalk pits. A description of both these sites is provided in Section 3.2.4.

Marl bands

An increase in the relative supply of clay or silt particles during sedimentation can produce a visible change in chalk facies from pure white chalk to that of "chalk marl". The increase may be due to an overall change in clastic input or simply as a result of greater rates of calcite dissolution at greater depths (Rawson, 1992). The resulting marl may be often several centimetres thick and may also be laterally continuous. Examples of this include the Southerham Marls at the base of the Lewes Nodular Chalk Formation, which have been identified within boreholes across the study area (Woods and Aldiss, 2004).

Other less well defined wispy "flasers" of marly chalk are also found within otherwise white chalk. These are not generally laterally continuous, but tend to surround small depositional features within in the chalk matrix. Hancock (1993) suggested that they may be formed after local dissolution of calcite and the resulting concentration of the non-carbonate fraction. In terms of mineralogy, the smectite group of clays usually dominates within all formations, and has been determined by X-ray diffraction analysis to consist mainly of calcium-montmorillonite (Morgan Jones, 1977). Other clays such as chlorites may be present in trace amounts throughout much of the chalk.

Pacey (1984a) noted the presence of Mg rich clays in chalk-marl samples from Lincolnshire and with further identification of pyroclastic particles ascribes their presence to "in situ alteration of an aeolian transported volcanic ash". Smectites are examples of clays that have a high degree of expandability and a high cation exchange coefficient. Exchange may happen with both monovalent and divalent cations (such as radium). In addition, there is

evidence of both barium and radium adsorption in other types of clay species such as illites and kaolinites (e.g. Komarneni et al., 2001; Hidaka et al., 2007).

Marls and beds with higher clay contents generally have a lower porosity than whiter chalks. However, larger marl bands may also act as a focus for flow in the saturated zone and cause perched water tables to develop in the unsaturated zone.

Flints

Silica (quartz or cristobalite forms) is present as an accessory mineral in the complete chalk sequence (Morgan Jones, 1977) and may be present as both a detrital (typically as iron stained grains) and authigenic forms (e.g. foraminiferal pseudomorphs). Within the chalk sequence it can also exist in the form of more laterally continuous beds of flint nodules (aka "chert", irregular or lumpy in appearance) or in tabular form (flat and sheet-like). The beds are so extensive that they have been be used to define elements of Chalk stratigraphy across the English Chalk (e.g. Woods and Aldiss, 2004; Woods, 2006).

Although there is uncertainty regarding the timing of its production in relation to sedimentation, the source is considered to be biogenic, i.e. from diatoms, radiolaria and sponges, and it is thought that as the material underwent a series of diagenetic changes it became concentrated into nodules. Murphy (1998) postulated that sulphate reducing bacteria, present in the anoxic zone of the sea-bed, altered the local pH of the surrounding pore waters to cause the dissolution of carbonate and the precipitation of dissolved silica.

Examples of flint beds occur throughout the study area and are discussed further under the Section 3.2.4.

Other Mineralogical Features

In a study of the non-carbonate fraction of chalk core from boreholes within the study area, Morgan-Jones (1977) identified nodular marcasite (a dimorph of pyrite, FeS_2) widely distributed throughout all lithologies. Samples from the Chalk Rock hardgrounds also contained pyrite, associated with phosphate concretions and which was thought to have been precipitated *in situ* within an anoxic environment. Estimates of iron and phosphorus content from the Chalk Rock were made also at Banterwick Barn, with values ranging up to 2.5% Fe_2O_3 and 6.5% P_2O_5 (Murphy, 1998)

Non-clay framework silicates, such as the zeolite heulandite, were present mainly in marl rich seams, but also occurred in much purer chalks in core from a borehole at Winterbourne. The core form this site also included trace amounts of fluorite (CaF_2), needles of rutile (TiO_2) and limonite ($FeO.OH.nH_2O$).

3.2.4 Chalk – Stratigraphy of the Berkshire Downs

The study area has been recently remapped by the British Geological Survey using a new lithostratigraphic classification for the Chalk, as proposed by Bristow et al (1997), Rawson et al (2001) and based also in part on the work of Mortimore (2001). A more recent detailed synthesis of this work is also provided by Woods and Aldiss (2004). In this work, the traditional lithostratigraphic zones of Upper, Middle and Lower Chalk are replaced by a series of further differentiated units employing lithological, biostratigraphic and geophysical marker beds. A summary of the relationship between the old and new classification was prepared by Woods and Aldiss (2004) and is presented in Figure 3—6.

Although the Grey Chalk Group is present beneath both catchments, this unit is too deep to have been penetrated by most borehole drilling. Rather, the boreholes used in this thesis are all in within the White Chalk Subgroup (as defined by Bristow), with the clay and sand content decreasing higher up the stratigraphic sequence; from the soft, medium grey, marly West Melbury Chalk Formation to the massive, white Seaford Chalk Formation. Individual formation members are described further below, based on the descriptions by Woods and Aldiss (2004).

Figure 3—6 The stratigraphy of the Late Cretaceous Chalk of the Berkshire Downs proposed by various workers, with transitional zonal scheme for comparison (reproduced from Woods and Aldiss, 2004).

Holywell Nodular Chalk

The Plenus Marls mark the base of the White Chalk Subgroup, which is characterized at its base by hard, nodular chalk and in higher levels by the presence of shell fragments of the bivalve *Mytiloides*. This formation also contains the hard nodular Melbourn Rock (up to 5 m thick), which is was more traditionally defined as the base of the classically recognized Middle Chalk. Towards the top of the sequence, nodular marly horizons are inter-bedded with more shelly layers. Analysis of cores taken from boreholes with the study area (at Winterbourne and Banterwick) shows a variation of formation thickness between 11.3 m and 16.9 m.

New Pit Chalk Formation

Typically softer than underlying formations, the New Pit Chalk is predominantly smooth-textured with numerous marly chalk horizons. From correlation of borehole records across the Berkshire Downs, it is considered the most laterally variable in thickness, measured between 34.5 m to 47.5 m across the Pang and Lambourn catchments.

Lewes Nodular Chalk Formation

The Lewes Nodular Chalk is described by Woods and Aldiss (2004) as consisting of "hard, nodular, gritty chalk, with common flints, marl seams and hardgrounds". There are mineralized hardgrounds towards the base, which are commonly referred to as the "Chalk Rock", and which were formally used to define the base of the traditional Upper Chalk sequence in the Berkshire Downs. These hardgrounds can be easy recognized in borehole geophysics profiles by a large natural gamma peak, thought to be caused by a high concentration of the mineral glauconite. Above the Chalk Rock, the succession grades from a mix of hard nodular flinty chalk to "sporadically nodular".

From core obtained from the Trumpletts Farm borehole (LOCAR), the thickness of this formation is estimated at 26.5 m within the Pang catchment.

Seaford Chalk Formation

The Seaford Chalk is the dominant solid rock unit present at outcrop. The formation grades from a hard nodular gritty chalk at its base into a more soft through to smooth-textured chalk with occasional weak marl bands. The lower basal sequence is difficult to demarcate from the Lewes Nodular Chalk at outcrop, but changes in resistivity mean that it is possible to locate in boreholes. The total thickness in the Pang catchment is estimated at *c.* 89 m for the formation (Woods and Aldiss, 2004), although only the lower 65.5 m has been recovered from core at Trumpletts Farm (see Section 3.5.2).

Newhaven Chalk Formation

The youngest of the Cretaceous Chalk formations present in the study area, the Newhaven Chalk crops out in small areas to the south and east of the River Lambourn, in area triangulated roughly by the villages of Boxford, Winterbourne and Bagnor (see Figure 3—3). It is generally characterised as having numerous flint seams with some nodular chalks (Rawson, 1992), and some evidence of this can be found within pit exposures at both Boxford and Winterbourne (see below). No known recovery of this formation from core is recorded in this area, although a possible uncertain classification of the top of LOCAR PL26 (Boxford) is acknowledged (unpublished driller's logs, supplied by Tabitha Sudworth, CEH, *pers comm*).

3.2.5 Chalk – Examples of Chalk exposure and core

Boxford Chalk Pit (SU431719)

This disused pit is located approximately 500 m SE of the Boxford borehole array drilled as part of the LOCAR programme (see Figure 3—2) and a description of the biostratigraphy has been collated by Mortimore et al (2001).

This pit exposes Chalk of Lower Santonian and Upper Coniacian age, effectively the upper most part of the Seaford Chalk Formation present in the study area. The exposure has been classified in term of three distinct units –

a) a lower, competent block of soft white chalk with two "poorly lithified, glauconitized" hardgrounds and other minor hardgrounds throughout, one with a "shiny phosphate veneer",

b) an upper more disturbed unit with a complex structure including folded and inverted hardgrounds (probably related to a local slump structure), and finally

c) a phosphatic chalk at the upper surface, highly fossiliferous, concentrated in "poorly defined burrows within a less strongly phosphatic chalk matrix".

Uncertainly over the interpretation of these units in terms of relative age and the potential structural controls are evident in this account. However, it is clear that heavy phosphatization is present in this section, which may suggest that high concentrations of uranium series nuclides are potentially present within this horizon (Pacey, 1984b).

Winterbourne Chalk Pit (SU448722)

The chalk sequences exposed in this locality are slightly younger than those at Boxford, and have been classified as Upper Santonian to Lower Campanian in age (Mortimore et al., 2001). Hence, the section presents some of the few exposures of the Newhaven Chalk

Formation that lies above the Seaford Chalk. The section presents a "flintless phosphatic chalk lithofacies", with common pelletal phosphate observed within the white chalk sections towards the base of the pit. The four major hardgrounds present are all weakly glauconitized, although some are also iron stained.

Detailed Borehole Cores – Banterwick Barn No 2, Winterbourne OBH and North Farm

Banterwick Barn No. 2 (SU513775) is located in the upper reaches of the Pang catchment, 2.5 km N of the Trumpletts Farm borehole array and comprises of Coniacian and Turonian chalk sequences, terminating in the Ballard Cliff Chalk immediately above the Plenus Marls (Figure 3—6) High density geochemical measurements of the recovered core were made by Murphy (1998). This demonstrated that major-elements correlate well with sedimentological features and that Fe, Mg, P and S are all generally higher in the marls and hardgrounds than white chalks. Detailed sampling from the Chalk Rock confirmed the presence of mineralized (glauconitized and phosphatised), nodular, lithified surfaces.

Winterbourne OBH (SU454716) lies close to the course of the Winterbourne stream approximately 800 m SSE from the Winterbourne (EA) observation borehole and 2 km NNE from the Bagnor (EA) observation borehole. The stratigraphy is similar to that at Banterwick Barn, although some marl horizons have been cut out by Chalk Rock and the Holywell Nodular Chalk is approximately 5 m thinner at this locality.

North Farm (SU332797) is located at the top of the Lambourn catchment 800 m E of Lynch Wood. The core obtained is predominantly from the Grey Chalk Subgroup, with base of the West Melbury Marly Chalk being richly glauconitic with common phosphatic clasts. Woods and Aldiss (2004) describe the base of the Zig-Zag Chalk as being marked at this site by a "tough, medium grey silty bed" with 6 m of "alternations of marl and limestone" located directly above. The remainder of the formation is characterized by "smooth-textured, creamy-grey chalk, with marls and marly chalk horizons".

The correlation of the stratigraphy of these three boreholes undertaken by Woods and Aldiss (2004) is reproduced in Figure 3—7.

Figure 3—7 The lithostratigraphy and correlation of three cored boreholes in the Pang and Lambourn catchments (reproduced from Woods and Aldiss, 2004).

3.2.6 Palaeogene Sediments

In both river catchments, the Upper Chalk is overlain in part by Palaeogene sediments deposited unconformably on an eroded upper surface. The Reading and Woolwich Formations, also referred to as the Lambeth Group, lie unconformably over the Chalk sequence and form the oldest of the Palaeogene sequences in the area. Both formations are mainly argillaceous, but sand and silt horizons have been mapped towards upper sections of the Reading Beds. These structures are predominantly in the form of channel deposits (McDowell et al., 2008). Other sandy layers are often found at the boundary between the Reading Formation and the Chalk.

Since recent BGS re-mapping, it is apparent that the formation is more extensive than previously thought, although uncertainty remains as to its exact distribution due to the inaccuracy with which these veneers can be distinguished from the Quaternary deposits that occur in similar topographical positions. The common occurrence of small glauconitic pebbles on the surface of nearly all the deposits of clay-with-flints suggests that clay-with-flints either incorporates much material from the Reading Beds or overlies unmapped deposits of the latter formation (Curry, 1992).

Lying above a generally sandy and glauconitic contact with the Lambeth Group, the London Clay Formation comprises of uniform, stiff, blue-grey marine clay with occasional alternations of more silty beds. The thickness of this unit is highly variable but can be up to 90 m thick (Rushton et al., 1989). Capping the London Clay Formation in the Pang catchment, the Bagshot Sands consist of a highly variable series of un-fossiliferous sands, clays and silts.

3.2.7 Quaternary Sediments

The distribution of superficial deposits (comprising principally Clay-with-flints, Head and Alluvial sediments and valley gravels) is mapped in Figure 3—4.

Clay-with-flints

These are stiff orange brown to reddish brown clay deposits containing unworn flint nodules and pebbles, and occasional local silty and sandy deposits. These deposits can generally be up to 10 m thick (Owen, 1981) and overlie the Chalk on the higher interfluves over extensive areas in both catchments. There is debate to their origin, but they are generally considered to be deposits created by both modification of the original Palaeogene cover and the solution of the underlying chalk (e.g. Catt and Hodgson, 1976). Circular dissolution pipes, often up to 10 m in diameter, and 15 m deep may occur beneath or have been noted close to the margins of Clay-with-Flint deposits. These are formed by

preferential dissolution of the Chalk and, although such features occur widely in the area, they may be particularly significant for recharge processes around the edge of less permeable cover.

Head Deposits

The BGS identifies two main types of head deposits – 1) those that are generally gravelly and found on the upper and intermediate slopes of Chalk valleys, and which may contain Clay-with-flints debris; and 2) variable deposits of clay, silt, sand and gravel found in the upper reaches (many dry valley sections) of Chalk valleys. The latter deposits are a common feature of both catchments.

River Terrace Deposits

The thickness and nature of River Terrace deposits vary across the study area and are mapped by the BGS as a range of undifferentiated sand and gravels. Grapes et al (2006) determined the alluvial gravels of the River Lambourn at West Shefford to consist of c. 4 m of gravels, overlain by thin calcareous peaty soil. More extensive floodplain wetlands may act as a local alluvial gravel aquifer.

Alluvial Deposits

Deposits of clay, silt, sand, gravel and peat occur in variable thicknesses in the intermediate and lower reaches of the valley bottoms. The potential increase in thickness down valley is concordant with the down-valley increase in valley bottom width. The general distribution of these superficial deposits is given on the BGS maps, but the lithological and thickness distributions are not known.

3.3 Hydrological Data

3.3.1 Rainfall and Groundwater Recharge

The main period of fieldwork that took place as part of this thesis began in January 2005 and ran for two years until January 2007. For most of this time, the south of England experienced atypical drought conditions and in particular included a reduction in rainfall over two successive winter seasons (i.e. November to April), the critical period for groundwater recharge. The lower than average rainfall may be observed from a comparison between the long term average monthly rainfall (1961-90) and actual recorded rainfall at the Met Office weather station at Oxford, approximately 30 km to the north of the study area (Figure 3—8). Seasonal variations from weather stations at Wallingford (10 km from Pangbourne) and at Frilsham (within the study area) are presented in Table 3—1 and demonstrate a similar pattern.

In addition, 2005 and 2006 constituted the "warmest two-year sequence ever recorded in the 337 year Central England Temperature series", (CEH, 2008). Evaporation from meteorological stations at Lambourn and Compton have been used to calculate the effective rainfall for a series of different crop types and Figure 3—13 and Figure 3—14 illustrate the effective rainfall (for grassland) within each catchment. The calculation, based on the MORECS 2.0 methodology, uses daily climatic data as well as simplified classifications of soil and land use type to estimate actual evaporation and soil moisture deficit and "excess" or effective rainfall (Hough and Jones, 1999).

The combination of higher than average evaporation and lower than average rainfall has resulted in a reduction in the water available for groundwater recharge. The Centre for Ecology and Hydrology have estimated the effective winter recharge at Sheepdrove Farm (near the village of Lambourn) and conclude that during 2004 and 2005 values were approximately half of that calculated in the subsequent year (CEH, 2008). These data are tabulated in Table 3—1, and allow actual and net rainfall (i.e. rainfall minus actual evaporation) during the study period to be compared.

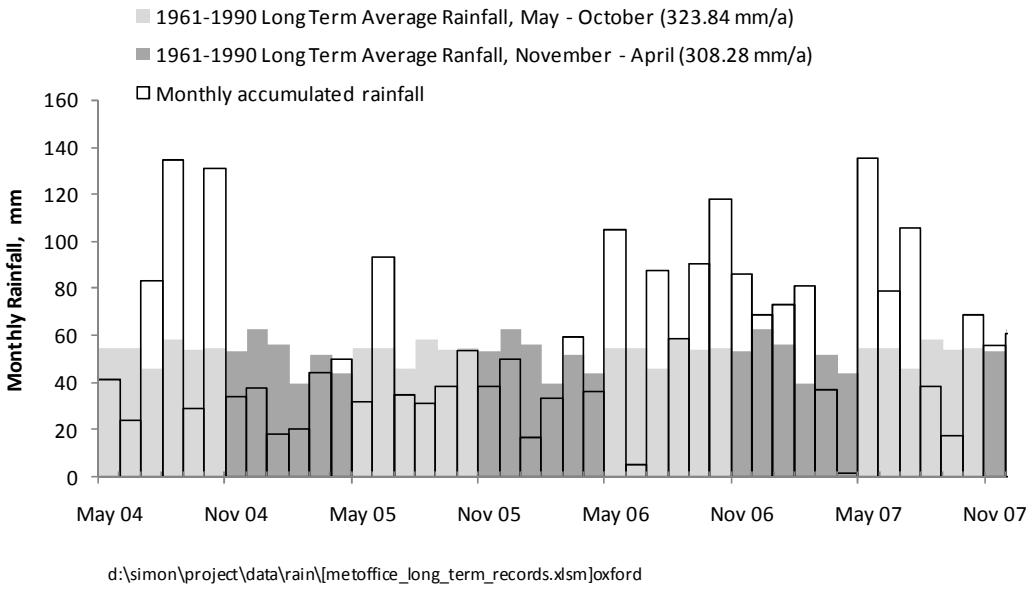

Figure 3—8 Comparison of monthly accumulated rainfall recorded at Oxford between October 2004 and April 2007, compared with 1961 to 1990 Long Term Average.

Table 3—1 Comparison between seasonal variations in actual and net rainfall for weather stations close to the study area.

Period	*Met Office Weather Station, Oxford*[1]		*Weather station, CEH Wallingford, Oxfordshire*[2]		*LOCAR weather station, Frilsham*[3] *(PL11)*		*Rainfall minus AE, Sheepdrove Farm (Lambourn)*[5]
LTA Annual Rainfall (mm)	632.1 (1961-1990)		598.0 (1972-2001)		703.0[4] (1961-1990)		-
LTA Winter Rainfall (Nov–Apr)	308.3	*(100%)*	295.4	*(100%)*	-	-	-
Winter 2004/05	204.8	*-27.8%*	185.9	*-37.1%*	259.0	-	141
Winter 2005/06	234.0	*-36.3%*	224.4	*-24.0%*	224.4	-	156
Winter 2006/07	348.1	*+17.0%*	306.5	*+3.8%*	-	-	307

Notes: (1) Weather station data from Oxford obtained from Met Office Historical Records Service, http://www.metoffice.gov.uk/climate/uk/stationdata/oxforddata.txt, accessed 11 November 2008. (2) Data sourced from West Berkshire Water Watch Report May 2006, CEH, http://www.nwl.ac.uk/ih/nrfa/water_watch/locar/2006/05/, accessed 11 November 2008. (3) Hourly weather station data for Frilsham 2002 to 2007 obtained under agreement from the LOCAR data centre, http://www.nwl.ac.uk/locar/main.htm, received August 2005, updated November 2008. (4) LTA data for Frilsham estimated from an adjacent raingauge at the river (Source: National Flow Archive http://www.nerc-wallingford.ac.uk/ih/nrfa/station_summaries/039/114.html, accessed 10 June 2006). (5) Data calculated manually by adding net monthly rainfall between November to April (inclusive) from Figure 3, sourced from ref (2).

3.3.2 Rivers

River Pang

The River Pang is a small tributary of the River Thames, whose perennial head is estimated to rise near the village of Hampstead Norreys, but which may flow further upstream (from the village of Compton) during periods of high groundwater levels. The river proceeds to flow south to the hamlet of Bucklebury, strikes east towards Bradfield, before finally flowing northwards to join the Thames at Pangbourne. The Pang has been classified as a "bourne" river, where the head of the river is controlled by local groundwater piezometry and where flow is heavily influenced by baseflow accretion (Bradford, 2002; Wheater et al., 2007).

Daily flows recorded at Frilsham, Bucklebury and Pangbourne from January 2005 to April 2007 are included within the integrated plot Figure 3—13. Until the rapid increase during the wet winter of 2006-7, the flows recorded at each gauge are well below their long term average values (cf. Table 3—2). For example, the average daily flow for the river at Pangbourne calculated between January 2005 to October 2006 (inclusive) is 0.31 m^3s^{-1} (26.8 $Ml.day^{-1}$), less than half of its long term value (0.66 m^3s^{-1} or 57.0 $Ml.day^{-1}$).

The hydrograph also illustrates the general lack of flow within the upper reaches during the summer, albeit with occasional peaks during intense rainfall events. This same clear rapid response to rainfall is observed at Pangbourne, the furthest downstream gauge, just upstream of the confluence with the River Thames. This suggests that, in its lower reaches, the river may be receiving water as rapid runoff from the less permeable Tertiary deposits that are present in the lower catchment (see Figure 3—3). The influence of surface runoff is also reflected in the calculated base flow index at the Pangbourne river gauge (which ranges from 0.61 - 0.89, depending on the calculation assumptions, see Table 3—2).

A detailed accretion survey of the River Pang was undertaken by Grapes et al (2006) between October 2002 and November 2005. Their data are presented in Figure 3—9, the plots having been modified slightly to illustrate sampling point locations of relevance to this study and the distances upstream from known gauging locations. By defining periods of high and low flow based on the presence of "continuous flow throughout the catchment", they were able to demonstrate the change in accretion rate as a function of both flow rate and reach location. During high flows, it is apparent that the river accretes at a fairly constant rate between its source at Compton downstream to Jewell's, averaging between 0.01 to 0.03 $m^3s^{-1}km^{-1}$. This rates rises between Jewell's and Frogmore Farm,

which is associated with the Blue Pool spring complex. It is also clear that during periods of low flow the Pang is supported primarily from this location alone.

Blue Pool

The Blue Pool spring complex is estimated by Grapes et al (2006) to contribute between 0.1 m^3s^{-1} (8.6 $Ml.day^{-1}$) and 0.2 m^3s^{-1} (17.3 $Ml.day^{-1}$) of groundwater to the River Pang, which represents the majority of the river flow recorded at Pangbourne in the summer months and between 50-75% of the total accretion in its lower reaches in the winter (Bradford, 2002). The complex consists of a series of actively flowing springs spread over area of *c.*0.03km^2, artificially enlarged in the recent past to provide a reliable water source for commercial cress growing (see Figure 3—17 later in this chapter for a map of the springs in the lower Pang which have been sampled for radon).

The water within the Blue Pool is thought to be sourced predominantly from groundwater from the Chalk, although rapid increases in flow and turbidity due to rainfall events have been recorded by several authors. Banks et al (1995) confirmed the presence of high groundwater velocities by conducting a tracer test from surface swallow holes c.4.7 km east of the feature (Holly Lane and Tylers Lane). They reported an initial breakthrough within 16.5 hours after injection, with the peak arriving within 19.5 hours, which equated to travel velocities of 6.84 $km.day^{-1}$ and 5.78 $km.day^{-1}$ respectively. They attributed the fast response time to the presence of laterally extensive "micro-karst features" (e.g. solution enhanced fractures of the order of several millimetres present near the ground surface).

Maurice et al (2006) undertook a similar series of tracer tests during the winter of 2005 from a swallow hole, close to those used by Banks et al (Smithcroft Copse), to the Blue Pool and demonstrated similar travel velocities (time to peak *c.*24 hours after injection indicating a travel velocity of 5.12 $km.day^{-1}$). By continuous monitoring of the tracer breakthrough over time they were also able to estimate the total tracer recovery after first arrival (*c.*26%). Maurice et al (2006) attributed this low recovery to the influence of "multiple pathways, with dispersion from the main conduit into smaller fissures and fractures". By assuming a fixed fracture aperture, calculated by estimating the local hydraulic gradient and measurement of flows, they concluded that there was not sufficient time for the effects of double porosity diffusion within the Chalk to dominate the tracer arrival time or the shape of the breakthrough tailing.

Other spring locations in the vicinity of the Blue Pool, such as Jewells and Ingle Spring were also sampled as part of this work. From the lack of any tracer recovery at these sites

Maurice et al also postulate that some sections of the fast flow paths may be discrete and isolated from other groundwater sources.

River Lambourn

The River Lambourn follows a south-easterly course for approximately 20 km, rising in wet years from its seasonal head at Lynch Wood near the village of Lambourn, and joining the River Kennet at Newbury. During low flows, the head of the river may move downstream by up to 6 km to Maidencourt Farm (Griffiths et al., 2006). The daily mean flows recorded at permanent gauging stations on the main channel, and on its small tributary the Winterbourne Stream (which joins at Bagnor), are plotted on Figure 3—14.

As with the River Pang, the river flows recorded during the study period represent low flow conditions. Between January 2005 and October 2006 the mean daily flow recorded at the Shaw gauging station was 0.98 $m^3.s^{-1}$ (84.7 $Ml.day^{-1}$), which equates to only 56% of the long term average flow recorded between 1962 and 2005 (1.74 m^3s^{-1} (150.3 $Ml.day^{-1}$), see Table 3—2).

The baseflow indices for all gauges on the Lambourn are greater than for those on the River Pang. At Shaw, the furthest downstream gauge, estimates of BFI range from 0.84 to 0.97, indicating that the river is predominantly groundwater fed. The flow records also indicate that it is only during intense winter rainfall events that other sources of water such as surface runoff or lateral interflow are observed. One possible reason for this may be the lack of low permeability Tertiary deposits or significant Clay-with-Flints close to the river that would promote such rapid surface flows.

The survey undertaken Griffiths et al (2006) indicated that, although the river accretes steadily throughout its course, there are also a number of discrete springs and seepages that provide water during periods of high flow, which are associated with dry valley topographic features intersecting the main channel. This is particularly noticeable between Maidencourt Farm and the village of Welford (Figure 3—9), where a large dry valley to the north east meets the river at right angles (i.e. at Great Shefford, as illustrated on Figure 3—1). Griffiths et al (2006) calculated that the rates of flow accretion in these locations is more variable in winter and spring and ascribe this effect to when "riparian areas are close to saturation and the river becomes more responsive to heavy rainfall events".

Table 3—2 River Gauging Station Flow Summary

Catchment	*Gauging Station*	*Catchment Area (km^2)*	*Q10 (m^3s^{-1}) (1)*	*Mean Flow (m^3s^{-1})(1)*	*Q95 (m^3s^{-1}) (1)*	*Data Range*	*Base Flow Index (BFI)(2)*		
							(Gustard et al, 1992)(3)	*(Peters et al, 2005)*	*(Griffiths et al, 2006)*
Pang	Frilsham	89.8	0.579	0.230	0.000	1991 to 2003	0.94	0.88 – 0.98	0.87
	Bucklebury	109.0	0.685	0.280	0.001	1991 to 2003	-	-	0.87
	Pangbourne	170.9	1.190	0.660	0.194	1968 to 2003	0.89	0.67 – 0.77	0.61
Winterbourne	Bagnor	49.2	0.320	0.170	0.052	1962 to 2003	0.96	-	-
Lambourn	East Shefford	154.0	1.570	0.760	0.113	1966 to 1983	-	-	0.97
	Welford	176.0	1.670	1.020	0.414	1962 to 1983	0.98	-	0.98
	Shaw	234.1	2.890	1.740	0.767	1962 to 2005	0.97	-	0.84

Notes: (1) Source: UK National River Flow Archive (http://www.ceh.ac.uk/data/nrfa/) Accessed August 2006. (2) Base Flow Index data sourced from Institute of Hydrology Report 108 (Gustard et al., 1992), Peters et al (2005) and Griffiths et al (2006). (3) The baseflow index calculated by Gustard et al includes an component of "interflow". Hence their calculation may overestimate the groundwater component sensu stricto by incorporating lateral seepage through soils etc.

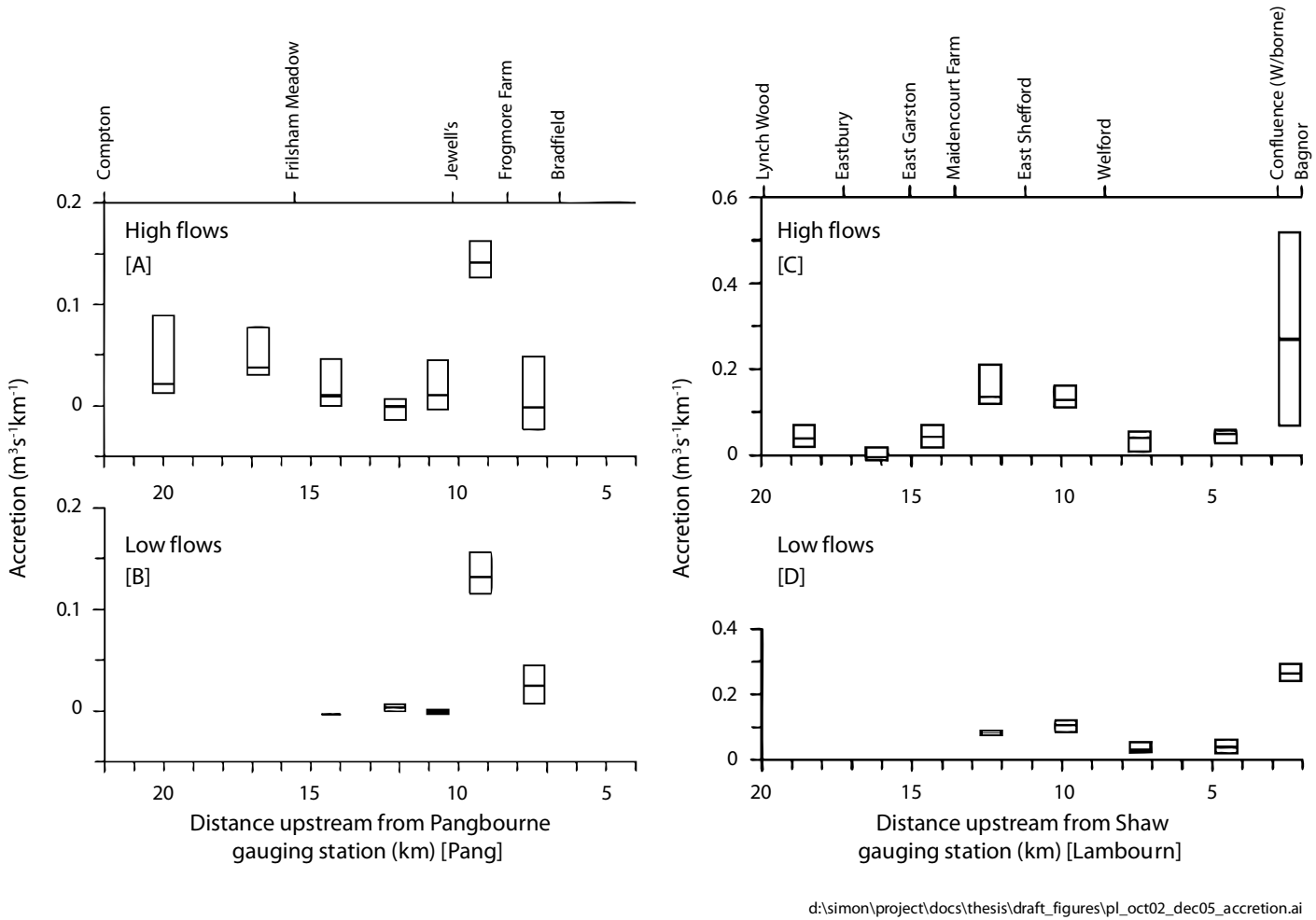

Figure 3—9 Comparison of median accretion rates between the River Pang and Lambourn in periods of high (A,C) and low (B,D) flow conditions between October 2002 and November 2005. Q25 and Q75 accretion rates also indicated. [Modified from source (Griffiths et al., 2006)]

3.4 Hydrogeology

3.4.1 Overview

Although the Chalk matrix has a high porosity, its permeability is extremely low due to the size of the interconnecting pore throats. Estimates of intrinsic matrix permeability range from 10^{-9} to 10^{-8} m.s^{-1} (Price et al., 1993). Rather, it is the fractured nature of the Chalk that results in the aquifer being one of the most productive aquifers in the UK. Figure 3—10 demonstrates this effect by comparing the matrix porosity (determined in the laboratory by drying and re-saturating selected core samples) and the hydraulic conductivity (determined by packer testing) of borehole PL10A at Trumpletts Farm. Although the matrix porosity does increase slightly towards the top of the bore (from *c.*30 to *c.*40%), the hydraulic conductivity does so at a much greater rate than would be expected from theory. In this example, the increase in permeability (approximately linear in log-normal space) is due to the greater degree of fracturing that occurs towards the top of the borehole (Williams et al., 2006). It is also clear from such work that, during pumping, the majority of groundwater movement in the Chalk takes place in the largest and most well connected fracture sets.

3.4.2 General Hydraulic Properties

Chalk Matrix

The porosity of the Cretaceous Chalk matrix is high compared with other more extensively lithified carbonates, such as the Carboniferous Limestone. This is due mainly to the preservation of the open void spaces present during deposition, and which may persist even after bioturbation and reworking of the original sediment. Bloomfield et al (1995) undertook a study of the regional variation in porosity and dry density of the Chalk in south east England. In general, an increase in porosity in younger sediments was observed, which typically contained less marl and other non-carbonate material than the pre-Turonian formations. In particular, analysis of core from the Thames region revealed a mean porosity of 38.8% (± 5.8%) for post-Turonian sediments (including the Lewes Nodular and Seaford Chalk Formations), although there was considerable variation between stratigraphic units (range 5.6% to 48.9%).

The specific yield of the matrix is not as high as the porosity would suggest. This is due to the very small pore throat diameters typical of the Chalk. The resulting high pore-water suctions means that only *c.*3% of the actual porosity (or *c.*1% of the bulk volume) will be drained under natural gravity conditions. However, Price (1987) argues that given the specific yield for unconfined Chalk is between 1-3%, this volume represents a significant part of the total yield. (See Table 3—3 for a summary of hydraulic properties.)

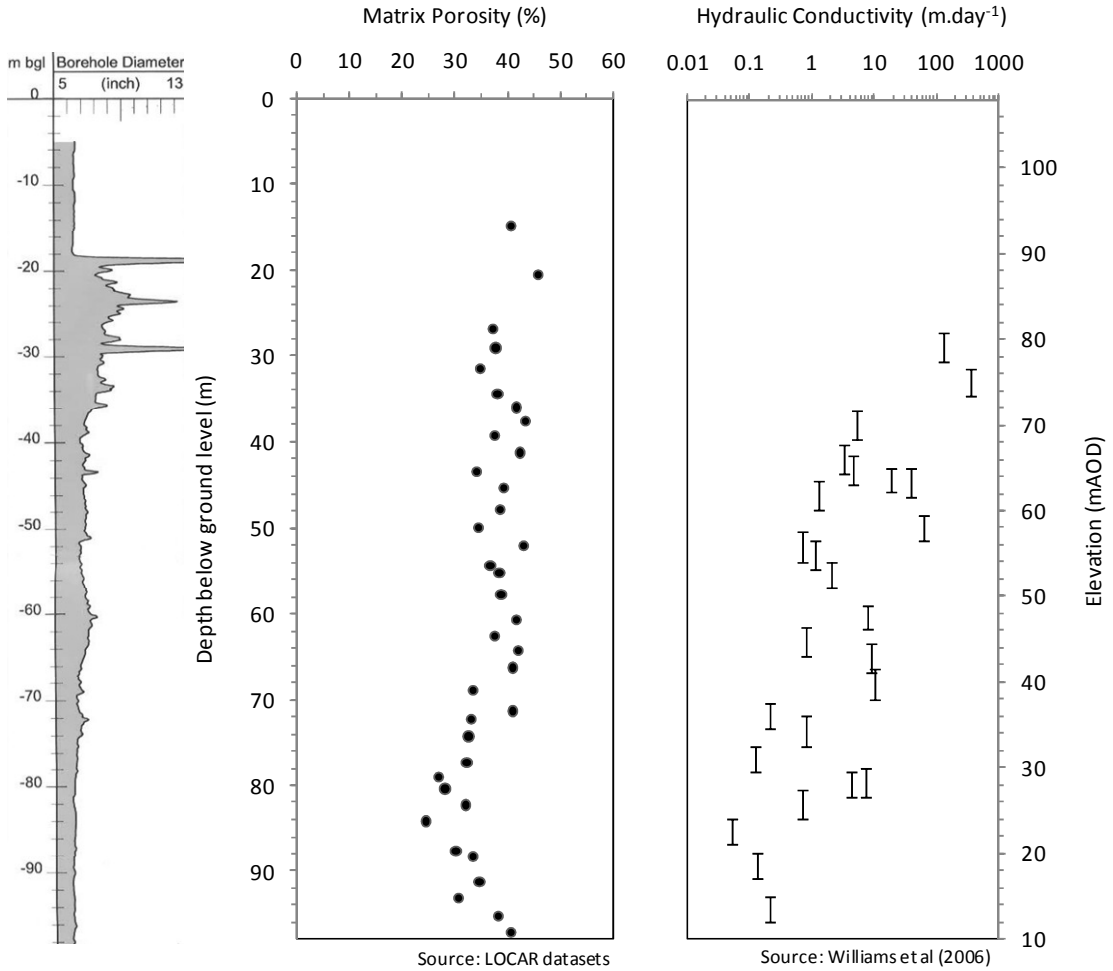

Figure 3—10 Vertical variation in matrix porosity and hydraulic conductivity at Trumpletts Farm borehole A (PL10A).

Table 3—3 General hydraulic properties of the Chalk aquifer

Property	*Chalk matrix*	*"Primary" Fractures (no solution enhancement)*	*"Secondary" Fractures (individual)*[1]
Porosity	0.2 – 0.4	?0.001 – 0.01	~1.0
Horizontal hydraulic conductivity ($m.day^{-1}$)	*c.*0.001	0.1	25,000
Specific Yield	~0.03 (of total porosity) or ~0.01 (of bulk volume)		?1.0
Transmissivity ($m^2.day^{-1}$)[2]	0.2	20	500

Notes: (1) Equivalent transmissivity for a 200 m thick aquifer, (2) assuming a width of 0.02 m for an individual fracture
Source: (Price, 1987)

Fractures

The Chalk possesses fractures on a range of scales that reflect their mode of production. Price (1987) referred to both "primary" and "secondary" fractures to differentiate between those formed initially through sedimentological or tectonic events with those have been enhanced or enlarged in some way by solution of calcite along its pathway. Others, such as Younger (1989), classified the pathways as either fractures of fissures depending on their size, but does not take into account the mode of formation.

Bloomfield (1996) undertook a detailed analysis of fracture length, orientation, spacing and aperture size of an exposed section of Seaford Chalk at the Play Hatch Quarry, *c.*10 km east of Pangbourne. Three principal orthogonal fractures sets were identified at this site – those parallel to bedding, as well as two high angle cross cutting fault or joint sets. Interestingly however, Bloomfield (1996) did not agree that the Chalk can be represented by these sets for the purposes of solute transport modelling as this simple representation does not reflect the inherent heterogeneity of the natural fracture aperture sizes which will affect the distribution of flow rates and flowpaths. Rather, a conceptual model of the Chalk was developed that consisted of "scale-invariant fault-bounded segments, within which are laterally continuous bedding plane features with heterogeneous apertures and a pervasive array of orthogonal interconnected joints".

In this study, the orientation of the dominant joint sets had a NW-SE strike that has been observed in other locations within the London Basin. Bevan and Hancock (1986) noted that this fracture orientation is present throughout the Upper Cretaceous and Palaeogene rocks in southern England and in northern France. They also observed that in southern England in particular other E-W trending fractures are often superimposed upon this structure thought to be due to a period of convergence and uplift during the Oligocene and early Miocene.

Fracture Permeability

Although permeability is observed to decrease with depth (e.g. Rushton et al., 1989), large increases in flow are observed at discrete horizons well below the surface. The Chalk Rock in particular is one of the most productive units with the Upper Chalk (MacDonald and Allen, 2001). It is thought that the higher degree of lithification associated with such hardgrounds results in fractures that tend to break cleanly, have a more even aperture and have a high degree of connectivity (Bloomfield, 1996).

Bloomfield (1996) demonstrated that there is a difference between the spacing distributions of mapped fractures at the Play Hatch quarry exposure and the inferred flow spacing (from

temperature log and flow impeller data) in an adjacent pumping well. From this study, Bloomfield (1996) estimated that "only *c.*10-20% of any bedding plane feature will flow at rates sufficient to be recorded by the flow logs".

Zimmerman et al (1992) developed stochastic models to illustrate that the "effective" fracture aperture may be much less than that mapped at outcrop, due to the presence of natural asperities, i.e. where two surfaces of the fracture are in contact. They demonstrated that the effective permeability of the fracture is less than that assuming a parallel plate model, and that the reduction is a function not only of the degree of contact between the fracture walls but also on the obstruction geometry. Indeed, for a more realistic irregularly spaced distribution of asperities, they illustrated that the fracture permeability may be reduced by over half (compared to a planar fracture) if the contact area between fracture walls is *c.*20% of the total wall area.

Karst

In hydrogeological terms, the word 'karst' is normally ascribed to aquifers in which the initial granular or fracture conditions have been modified by some form of dissolution (Maurice, 2008). As such, the term is most often applied in the UK to carbonate aquifers, such as the Magnesian, Jurassic and Carboniferous limestones. However, increasingly the same terminology is now being used to describe surface features observed within the Cretaceous Chalk (Maurice et al., 2006)[2].

Although the Chalk is generally regarded as having low mechanical strength, small scale features such as dolines (or 'sinkholes', surface depressions indicating local dissolution or the collapse of the underlying rock strata), stream sinks (where there may be significant loss of stream flow to the aquifer) and dry valleys (indicative of areas of periglacial solution enhancement, when groundwater levels were elevated) are often present, although the formation of large cavities is considered to be quite a rare occurrence compared to other limestone aquifers. The high groundwater flow velocities, observed in the tracer tests conducted form lower Pang stream sinks to Blue Pool (see above), support the hypothesis that the development of a highly permeable and well connected network of solution

[2] However, the exact application and meaning of the term is open to different interpretations – for example Price and Banks (1996) argue that, although solution enhancement is locally important in terms of water transport, the Chalk behaves in a very different way hydrogeologically to other more cemented limestones, (where all water transport and storage is within fractures with effectively none within the rock matrix). Subsequently, to avoid direct comparison to such aquifers the use of the word 'karst' has sometimes been resisted.

enhanced fractures and fissures is indeed possible. However, what is less clear is the extent to which these feature may be regarded as laterally contiguous at the catchment scale. Tracer recoveries at the Blue Pool, reported by Maurice et al (2006), averaged c.23% indicating a substantial loss of mass – which may suggest either rapid diffusion of tracer into fracture walls or more likely, given the inferred residence time, that sections of the fracture network are better characterized as multiple pathways where there is potential for flow into many smaller fissures and fractures.

In addition to the work within the Pang catchment, other tracer tests have confirmed the presence of fast flowing conduits within the Chalk. For example, Atkinson and Smith (1974) injected Rhodamine WT dye into swallow holes within the Hampshire Chalk and monitored for breakthrough at two well known spring sites. Traces of dye were found at both locations, a distance of 5.75 km away from the injection site, and peak concentrations were recorded between 62.5 and 67.0 hours after injection. This equated to a straight line travel velocity of 2.21 km.day^{-1}. Atkinson and Smith suggested that turbulent flow in an open system of solution enhanced fissures would be required to achieve this velocity, given the observed hydraulic gradient with the Chalk. Such work supports the theory of McDowell et al (2008) that solution enhanced (and hence higher permeability) Chalk is often formed at the fringes of overlying Tertiary strata, where rainfall runoff is focused into surface channels and where the acidity of the water is generally greater than that of Chalk groundwaters.

This view is supported by Maurice et al (2006) who, from extensive mapping of surface features, characterized the Pang and Lambourn catchment in three distinct karstic zones (see Figure 3—11):

i) Extensive surface karst in the lower reaches of the catchments, where the Chalk is overlain by Palaeogene deposits (Zone 1);;
ii) Middle reaches of the catchments where Palaeogene cover has been removed through erosion, but with the presence of many doline features close to the edge of low permeability superficial deposits such as Clay-with-Flints (Zone 2);
iii) Upper reaches, where there is a lack of superficial deposits and the Chalk is exposed at surface with little evidence of surface karst (Zone 3).

Figure 3—11 Conceptual zones of karstification in the Pang and Lambourn catchments as delineated by Maurice et al (2006) (Figure reproduced from the same citation)

Hydraulic Conductivity

Although the matrix is relatively impermeable, it still presents a very large volume available for water storage. Fractures provide a distribution system for water; but given their low porosity (expressed in term of the bulk rock) they are thought to gain water from the matrix when fluid pressures are lowered within them by, for example, the pumping from wells.

Price (1987) states that geophysical evidence suggests that hydraulic conductivity may be enhanced around particular elevations in the Chalk, possibly associated with a past or present groundwater table. The reduction in the rate of groundwater level recession usually observed suggests a general reduction in fissure related sub-horizontal hydraulic conductivity with depth, although it could also be related in part to an increase in specific yield with depth, or delayed yield related to drainage from the partially saturated zone.

Development of transmissivity with the Pang and Lambourn catchment area

Owen (1981) summarized the drilling of boreholes both close to the river and on the interfluves within the Pang and Lambourn catchments as part of the Thames Groundwater Scheme. These were chosen deliberately to cover a wide range of locations, including those areas were yields were expected to be low. The work indicated that highly fractured and brecciaed Chalk produces high values of transmissivity in the main river valley bottoms

(between 500 and 1000 $m^2.day^{-1}$). Less transmissive areas were located typically in the valley margins and in some dry valleys (<100 $m^2.day^{-1}$). Owen makes the observation that there is a correlation between topography and contoured values of transmissivity and suggests that this is due to the solution enhancement of rock fractures, where there is a concentration of flow. He also noted that the yield in boreholes was delivered through a limited number of fractures, parallel to bedding. The bulk of these fractures lay above 50 m depth, with the remaining between 50 and 75 m depth (in valley areas, and presumably indicative of the elevation of the Chalk Rock horizon). These observations are in agreement with Price (1987) who concluded that the upper 50 m of the saturated zone generally has a much greater permeability than the deeper aquifer. However, at depth the more brittle chalk of the various rock bands, such as the Chalk Rock, may also represent discrete and important contributory flow horizons.

Subsequent to this work, Rushton et al (1989) included the variation of permeability with depth into a regional groundwater resource model for the Kennet Valley, that included the Pang and Lambourn catchments. The spatial distribution as presented by Owen (1981), and used by Rushton et al (1989) for the purposes of groundwater modelling, is illustrated in Figure 3—12.

Some authors have suggested that the phenomenon of high valley transmissivity is due to the coincidence of areas of pre-existing structural weakness within the Chalk (e.g. as discussed in Younger, 1989). By this hypothesis, aquifer transmissivity would be expected to be high in areas that were more highly brecciated and fractures as a result of tectonic disturbance However, others suggest that the enhanced fractures and pathways are due to the concentration of flows from the surrounding catchment, a mixing of waters from different locations and the subsequent dissolution of calcite. Younger (1989) suggested that during the Devensian (the last glacial maximum) enhanced carbonate dissolution in "taliks" (i.e. unfrozen volumes of near surface Chalk underneath the main river channels) may have increased permeability and concentrated flows even further in valley bottoms and that once formed these areas would act as a local sink for groundwater.

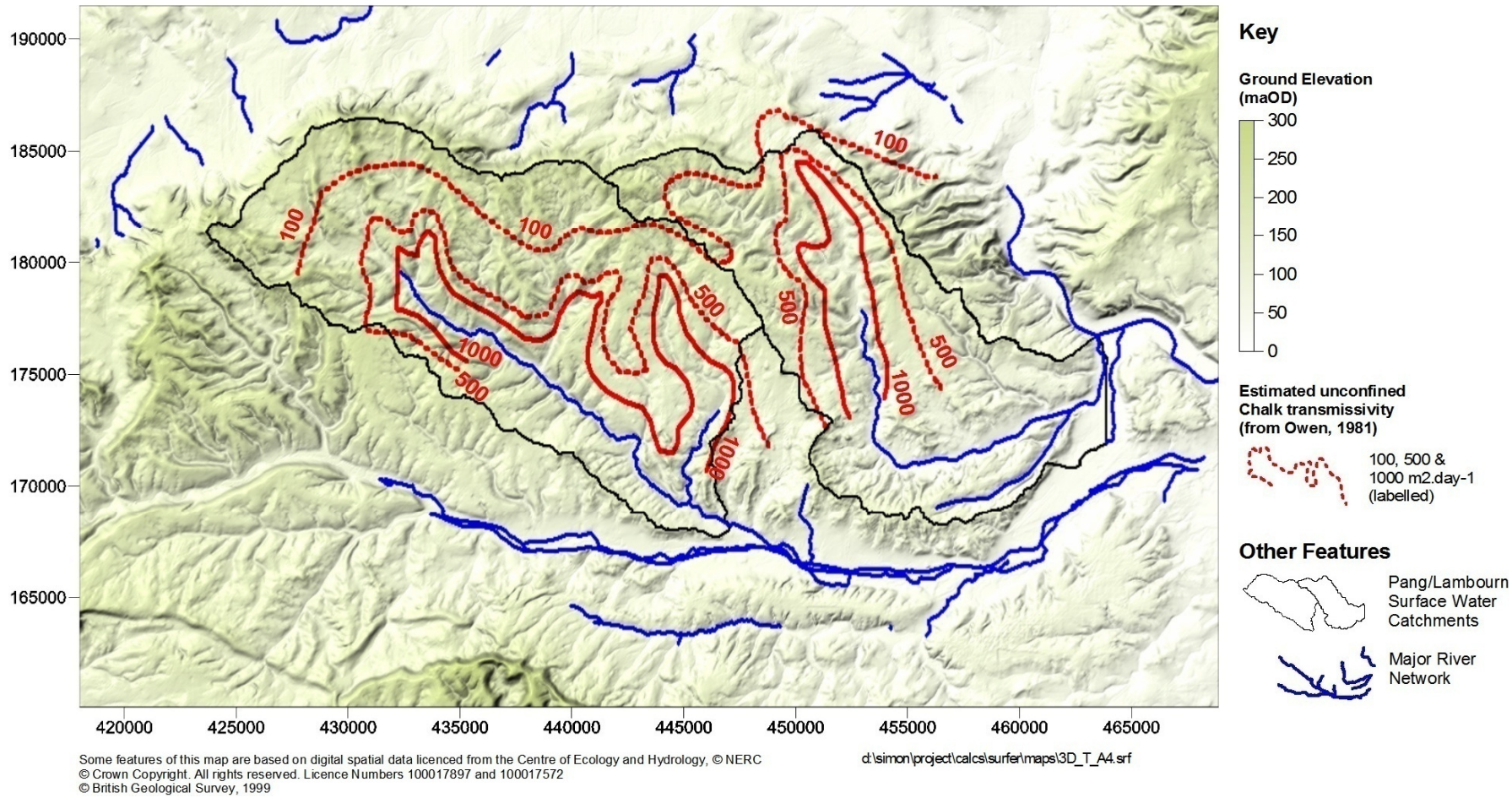

Figure 3—12 Estimation of spatial variation in unconfined Chalk transmissivity (as interpreted by Owen, 1981)

3.4.3 Groundwater Levels

Integrated catchment plots

A selection of borehole records from each catchment, chosen on the basis of their long term record and location (i.e. near to river, on interfluve, drift covered etc), are presented in Figure 3—13 and Figure 3—14. To aid interpretation, these figures also include all available river flow and meteorological data as well as an indication of when field sampling was undertaken. With the exception of the data from Frilsham, the vertical scale of the plots has been kept constant, so that a direct comparison of groundwater level fluctuations between boreholes may be made.

Of note is the general decline in water levels between October 2004 until December 2006, for boreholes located in the Pang catchment that are more than a few kilometres away from the river, e.g. at SU47/140 (Ashridge Wood) and PL28 (Beche Park Wood). At these localities, recharge events during the winter of 05/06 are not sufficient to return groundwater levels to their elevation in the previous year. It is also apparent that the degree of fluctuation is greater on the interfluves, than closer to the main river channel. This is also reflected in the contoured change in groundwater level across the catchments discussed in the following section (c.f. Figure 3—16).

Multilevel piezometer data from the Frilsham borehole array on the Pang indicates that, close to the river, there is a vertical hydraulic gradient that drives groundwater from the near surface to depth (the data plotted are readings from taken from 10 and 37 mbgl respectively). This suggests that, during the period of measurement, the river should lose water to the ground rather than gaining baseflow. This hypothesis is supported from the overall flow recession observed at the Frilsham gauge and the lack of accretion calculated by Griffiths et al (2006) during low flow periods (c.f. Figure 3—9).

Groundwater levels within the Lambourn catchment do not recede to the same extent as those of the Pang, although most of the plots presented are for boreholes located near winter flowing stream sections. The water table at borehole SU48/76 (Brightwalton Common) does show some sign of an annual decrease, but not to the same extent as SU47/140 (Ashridge Wood) located on an interfluve within the Pang catchment. This subdued change may be a reflection of the greater Clay-with-Flints cover at this location, which may smooth the delivery of recharge throughout the year.

All the boreholes plotted are located within the unconfined Chalk, with the exception of SU56/119 (Briff Lane). This location, *c.* 1 km to the south of the River Pang, is overlain by

both London Clay and Lambeth Group deposits. The recorded groundwater level change over time is small (less than 0.5 m).

Contour plots of groundwater levels

Groundwater level data from boreholes that penetrated the Chalk were used to generate water table contours across the study area. The contours were calculated by the kriging method at a 200 m resolution and then processed further to reduce to ground level any interpolated elevations that exceeded the local topography. An estimate of the distributed groundwater table for October 2005, calculated on the basis of 15 borehole locations, is presented as 5 m interval contours in Figure 3—15(A). This figure also plots the site locations of the boreholes used and the major spring and borehole sampling points for radon. Further details of these sites are presented in Section 3.5.

The general distribution compares well in the lower river reaches with the 5-year mean spring groundwater level contours calculated by Griffiths et al (2006) who used a more comprehensive dataset. However, it is noticeable that all levels are lower as a consequence of the extensive groundwater level recession experienced during the summer of 2005.

The contours suggest that the River Lambourn acts as a focus for groundwater flow throughout its course. Even at the end of the summer months, groundwater converges to the river and will provide baseflow in the perennial reaches. Hence, the river is likely to gain baseflow steadily as it flows towards the River Kennet and this is confirmed by the accretion rate profiles undertaken by Griffiths et al (2006), plotted on Figure 3—9, and in previous studies (Grapes et al., 2005; Grapes et al., 2006).

The same cannot be said of the River Pang, where it seems that groundwater passes beneath the main channel and flows instead to the River Thames to the east of the catchment. Only in the lower reaches of the Pang do groundwater levels seem to be controlled by elevation of the river course. It may be inferred therefore, that upper reaches of the river may only intercept groundwater at high groundwater levels and may be considered as a high level drain feature. It is also clear that the inferred groundwater catchment area of the Pang is different to that for surface waters. The contours suggest that, at low groundwater level conditions (such as is represented by data from October 2005), the baseflow component of the river in its lower reaches may be sourced from up to 10 km to the west and north-west of the topographic catchment. Estimates of the groundwater catchment size, presented by Wheater et al (2007), also demonstrated the spatial extent is subject to change on a seasonal basis and they concluded that an effective groundwater catchment is difficult to define.

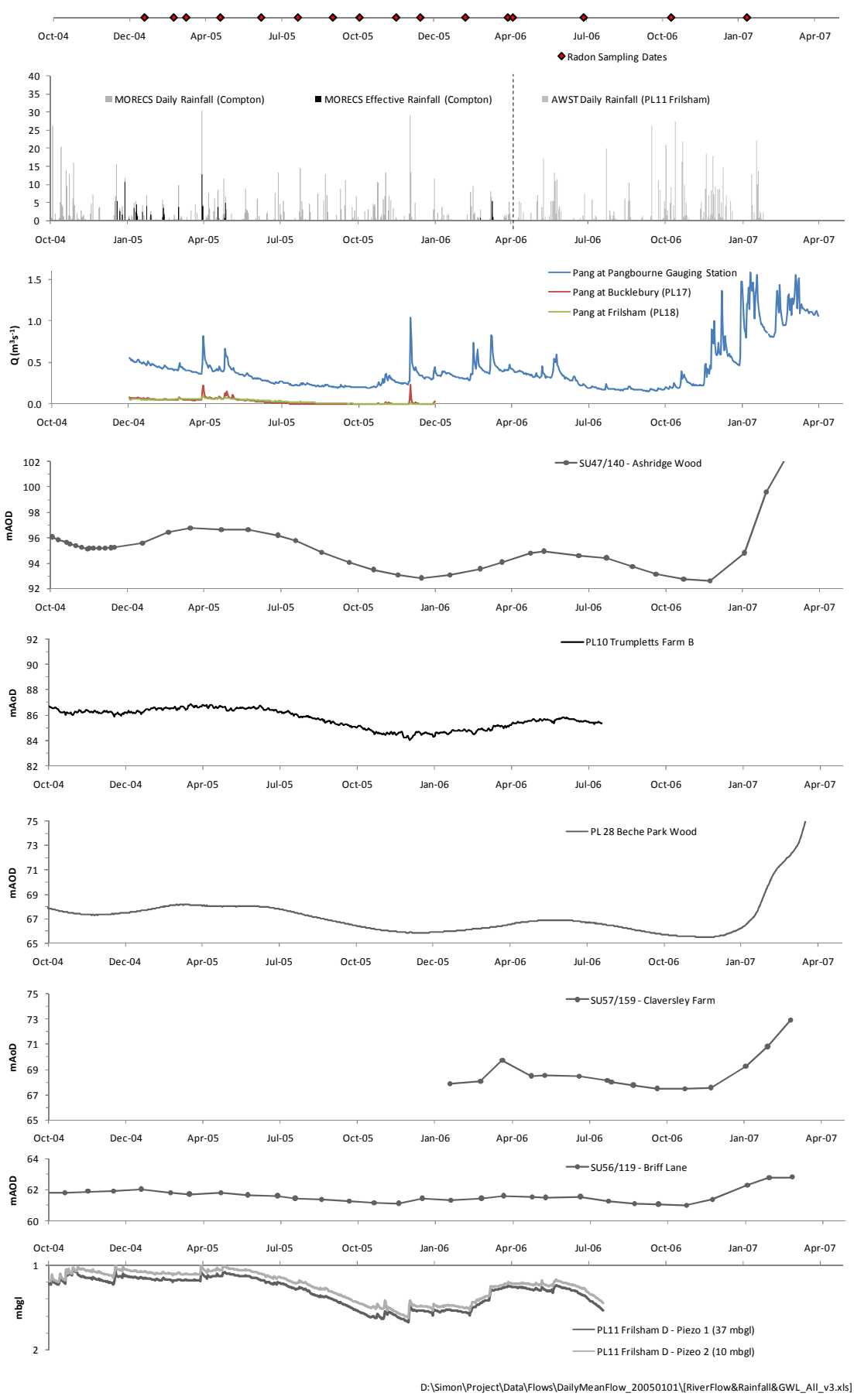

Figure 3—13 Groundwater Level Hydrographs – Pang catchment (Oct 2004 to May 2007)

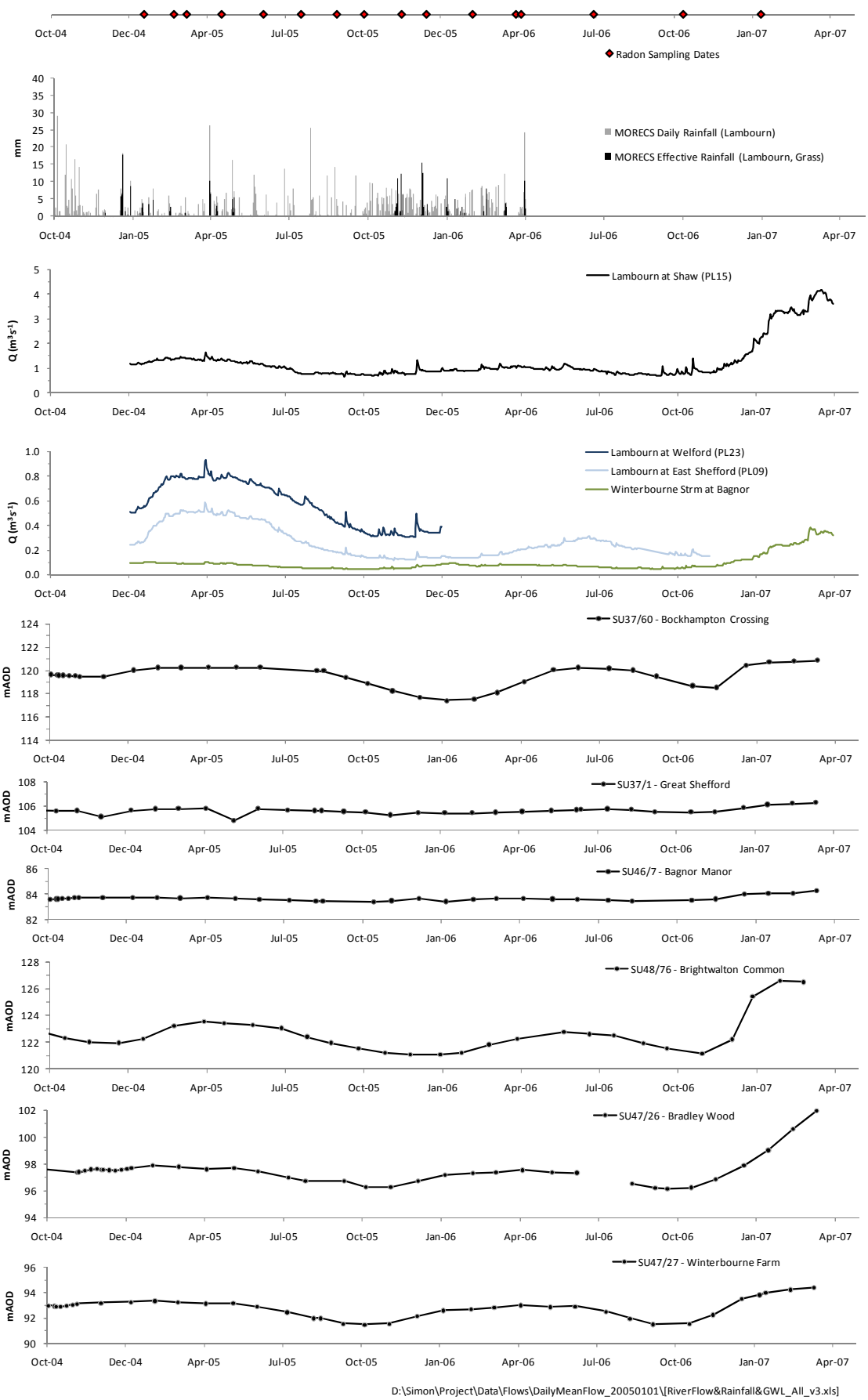

Figure 3—14 Groundwater Level Hydrographs – Lambourn catchment (Oct 2004 to May 2007)

The magnitude and orientation of the local horizontal hydraulic gradient inferred by the distances between contours is presented in Figure 3—15(B). It should be noted that these vectors do not indicate groundwater flow direction *per se*, due to the heterogeneity of the chalk aquifer and the possible presence of preferential flow paths. However, at the regional scale, these vectors may be regarded as a qualitative indication of the likely flow regime and the contrast between the two catchments is apparent. Hydraulic gradients tend to align themselves sub-parallel to the River Lambourn water course, which suggests that the river is acting as a groundwater flow boundary and hence may accrete along its length. In contrast, flow direction is at right angles to the River Pang in its upper reaches and only in periods of high groundwater levels does the river intercepting groundwater. This can be inferred from the estimates of accretion rates presented previously in Figure 3—9.

Depth to Water Table

By subtracting contoured groundwater elevation from measured surface topography, it is possible to estimate the spatial distribution of the depth to the Chalk water table. This has been calculated for October 2005 and is presented as a coloured raster image in Figure 3—16(A), with a spatial resolution of 200 m. For the Lambourn catchment, the depth to water table ranges from zero at the main river channel (over its entire length) to over 140 m at the top of the catchment close to the Chalk escarpment. Shallow depths are also inferred in the small feeder channels to the east and west of the main water course.

For the Pang, the water table intersects ground level approximately half way down the catchment from the surface-water divide to the north. This indicates that, above this position in the catchment, the river does act as a boundary to flow and that groundwater continues to flow eastwards towards the River Thames. It is also apparent that the river has a more laterally extensive saturated valley bottom in its lower reach, when compared to the Lambourn.

Groundwater Level Change

An estimate of the change in groundwater level over the summer of 2005 has been made by comparing the difference in contoured values between October and April, and is plotted in Figure 3—16. As would be expected, the maximum groundwater level change (c.5 m) is observed within the upper reaches of each catchment.

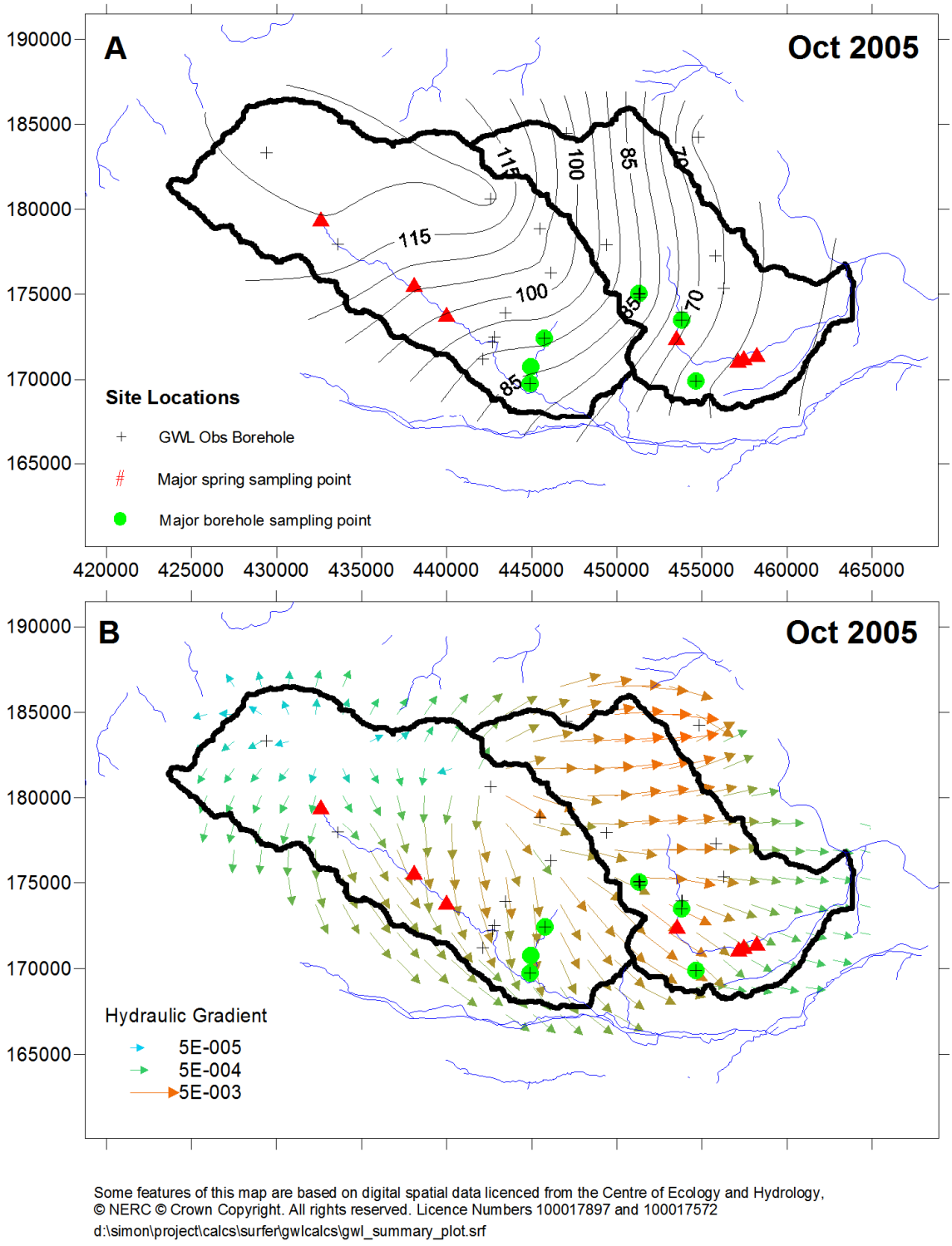

d:\simon\project\calcs\surfer\gwlcalcs\gwl_summary_plot.srf

Figure 3—15 Chalk Groundwater Level Contour Maps, October 2005

A) Groundwater level contours based on available Environment Agency and LOCAR datasets.
B) Groundwater flow lines annotated with inferred hydraulic gradient, assuming rock isotropy at the catchment scale.

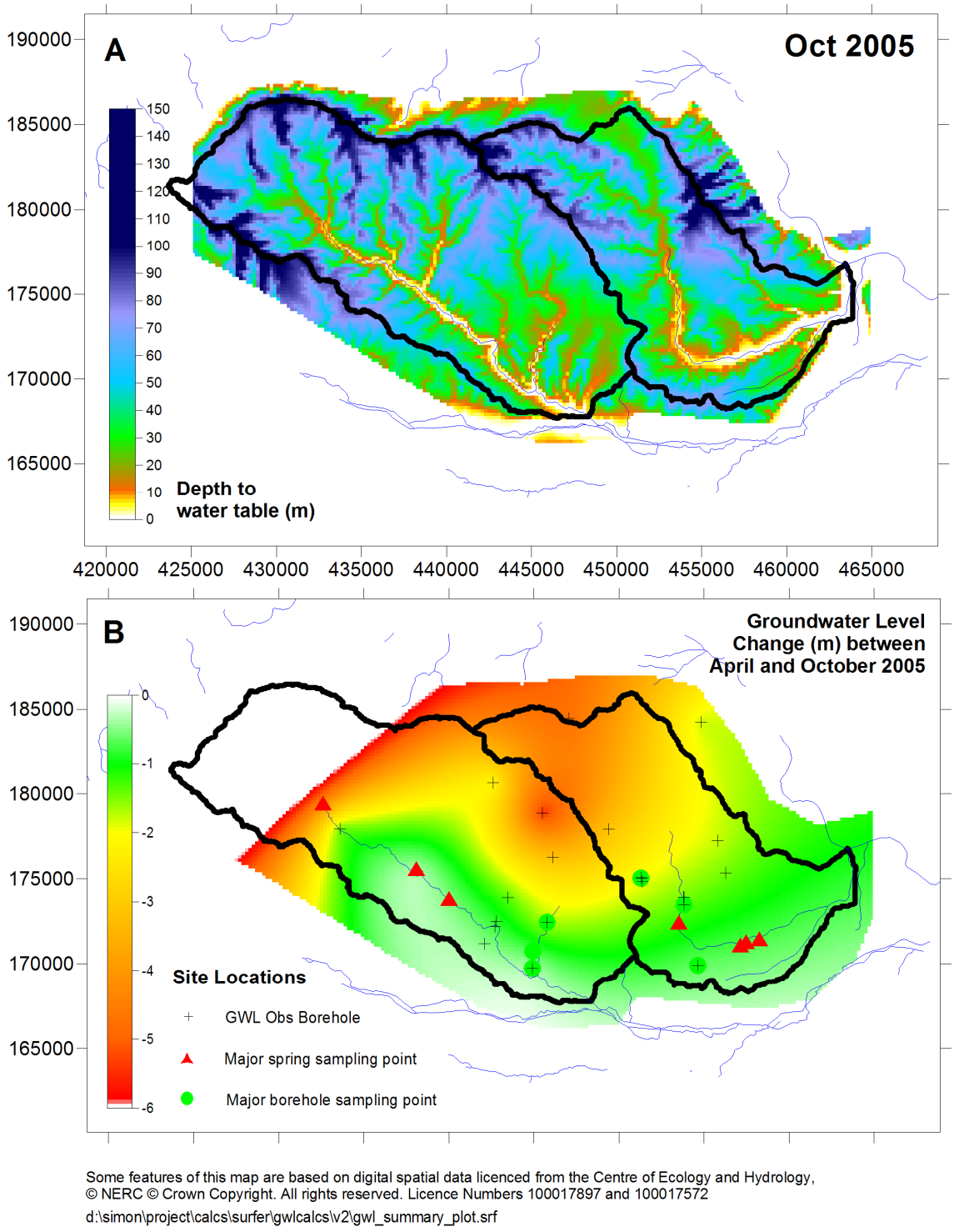

Figure 3—16 Groundwater Level Difference Contour Maps

A) Depth to water table October 2005, based on difference between Chalk groundwater levels and DTM data (200m resolution).

B) Groundwater level change between April and October 2005 using calculated groundwater contours.

3.5 Radon Sampling Locations

3.5.1 Springs – Pang

Three of the most prominent spring locations in the lower Pang were sampled at regular intervals throughout the monitoring period, typically between 4-6 weeks apart. Kimber Spring, which forms part of the Blue Pool spring complex, is located at its most western point (see Figure 3—17). It consists of a *c.*1 m deep pool of water where active groundwater inflow is observed from the continuous reworking of silt grade bed material. This phenomenon was observed over the entire sampling period, even during the summer months.

Further west, the spring at Jewell's Farm consists of groundwater seepages along a small reach adjacent to a road (Figure 3—17). Although the reach was generally flowing, the point of groundwater emanation moved downstream slightly by a few metres during the summer months. Small excavations were made into sandy sediment to enable water samples to be taken beneath the water-air interface and to minimise the loss of radon to air.

The spring at Ingle Farm feeds groundwater to an adjacent pond. The location has been modified to include a brick surround and glass cover, which protects the source from surface runoff and transported sediment from a nearby bank. The spring is thought to have flowed continuously throughout the monitoring period, on the basis of observed discharge from the pond to the River Pang. However, no quantitative flow measurements of this were made.

In addition, a pond south of Parsonage Farm was included in the sampling round (Figure 3—2). From the water temperature and subsequent analysis of the aqueous chemistry data this site was not considered to be a spring; however its water level was considered to reflect the local groundwater table. As groundwater levels fell during the drought period, the pond dried until a small patch of Chalk was exposed at its base. The remaining pond was covered in a thick (several metres) of soil and clay.

3.5.2 Boreholes – Pang

LOCAR site PL10 (Trumpletts Farm) consists of three 100 m open boreholes and three 40 m deep holes which were completed with multi-level piezometers. The boreholes were drilled in the vicinity of an Environment Agency abstraction bore (known as Bottom Barn), which forms part of the West Berkshire Groundwater Scheme. The 100 m boreholes at Trumpletts Farm are cased to approximately 20 mbgl, at which competent Chalk is encountered. Analysis of the recovered core suggests that, in this location, the Seaford and

Lewis Nodular Chalk are *c* 65.5 m and *c.*26.5 m thick respectively, with the Chalk Rock encountered between 81.0 to 82.5 mbgl (Adams et al., 2004). Preserved core from borehole "A" was selected for uranium and radium analysis, based on the logging records supplied by BGS. Rock samples were chosen throughout the sequence, particular and attention was paid to any differences in fracturing and lithology. The results of these analyses are described in Chapter 5. The EA abstraction borehole was also used in a series of pump tests and radon samples were obtained throughout the duration of two tests undertaken in the spring of 2005. These results are described in Chapter 6.

Frilsham Meadow is a LOCAR research site located close to the River Pang, where it flows underneath the M4 motorway. It consists of eleven boreholes of varying depth and completion status, of which two were selected for radon sampling. Borehole "B", located 30 m from the main river channel and drilled to c.40 m bgl, was sampled by a small submersible pump. Following a collapse of the borehole wall, subsequent samples were taken from borehole "A", located somewhat closer to the river (20 m) but which was also drilled to a similar depth. Meteorological data from the adjacent weather station data were also obtained.

Briff Lane is *c.*1 km south of the Pang, at the boundary to a small sewage treatment works. It is a confined Chalk borehole, 57 m in depth, overlain by London Clay and Lambeth Group deposits. Evidence from field chemistry suggests that the water is deoxygenated (see Chapter 6 for a discussion of the evolution of groundwater chemistry with pumping). It is also clear from the results of single borehole dilution testing that groundwater movement with the borehole is very slow, with tracer still detectable within the borehole several months after injection (L.D. Maurice, *pers comm*).

3.5.3 Springs – Lambourn

Weston Springs are located at the bottom of a small hill, to the north of the main Lambourn channel, where seepages feed a small pond. A location was chosen closest to the river, where the pond bed was relatively clear of debris and where, on occasion, small bubbles indicated possible upward movement of groundwater. A flexible hose was used to sample water from the base of the pond by use of a peristaltic pump.

In contrast, the seepages at Great Shefford Springs are much more diffuse, the land consisting of a marsh with a large amount of plant and soil debris. During the winter months, small ponds of water appeared towards the centre of the marsh and it was possible to sample water directly from these. During dryer months it was necessary to excavate

some of the debris and to allow water to seep into the hole, then sampling as normal. For several months the marshes were completely dry and it was not possible to sample at this location.

Lynch Wood is located just to the north of the village of Lambourn and during wetter months the springs here are considered the main source of the river. Consisting of a series of large interconnected ponds, a sample location was chosen towards the top of the system where water could be observed flowing from sediment at the base of a small feeder channel. In dryer months, and for the most of 2005, the springs at Lynch Wood were dry and it was not possible to sample.

The springs at the Jannaways property have been used to feed a series of connected recreational ponds. Although the ponds were thought to receive groundwater from their bed a small additional pump was used to augment flows from a shallow borehole to the west of the main pond. It was possible to sample the outflow pipe from this pumped source and to collect un-aerated samples suitable for radon measurement.

3.5.4 Boreholes – Lambourn

The EA monitoring borehole at Bagnor Manor is located c.100 m south west of the western pond at Jannaways. It lies to the south of a small hill (*c.*35 m of elevation difference) and is bounded on three sides by river courses – the Winterbourne Stream to the east and the Lambourn to the south and west. Available groundwater level data are included within Figure 3—14 and show very low variation over the two year record; maintaining a water elevation of *c.*84 mAOD (which equates to *c.*12 mbgl). Water samples were pumped from this borehole using an MP1 submersible pump from a depth of 26 mbgl, to coincide with a flow horizon identified from single borehole dilution testing (L.D. Maurice, *pers comm*)

Winterbourne Farm, which also forms part of the EA's groundwater monitoring network, is located *c.*3 km NNE of Bagnor Manor. It has been drilled close to the ephemeral reaches of the upper Winterbourne Stream and as such the groundwater levels are close to the ground surface (dip *c.*3 m bgl). In a similar approach to Bagnor, water samples were pumped from this borehole using a pump from a depth of 12.5 mbgl, to coincide with a flow horizon identified from single borehole dilution testing.

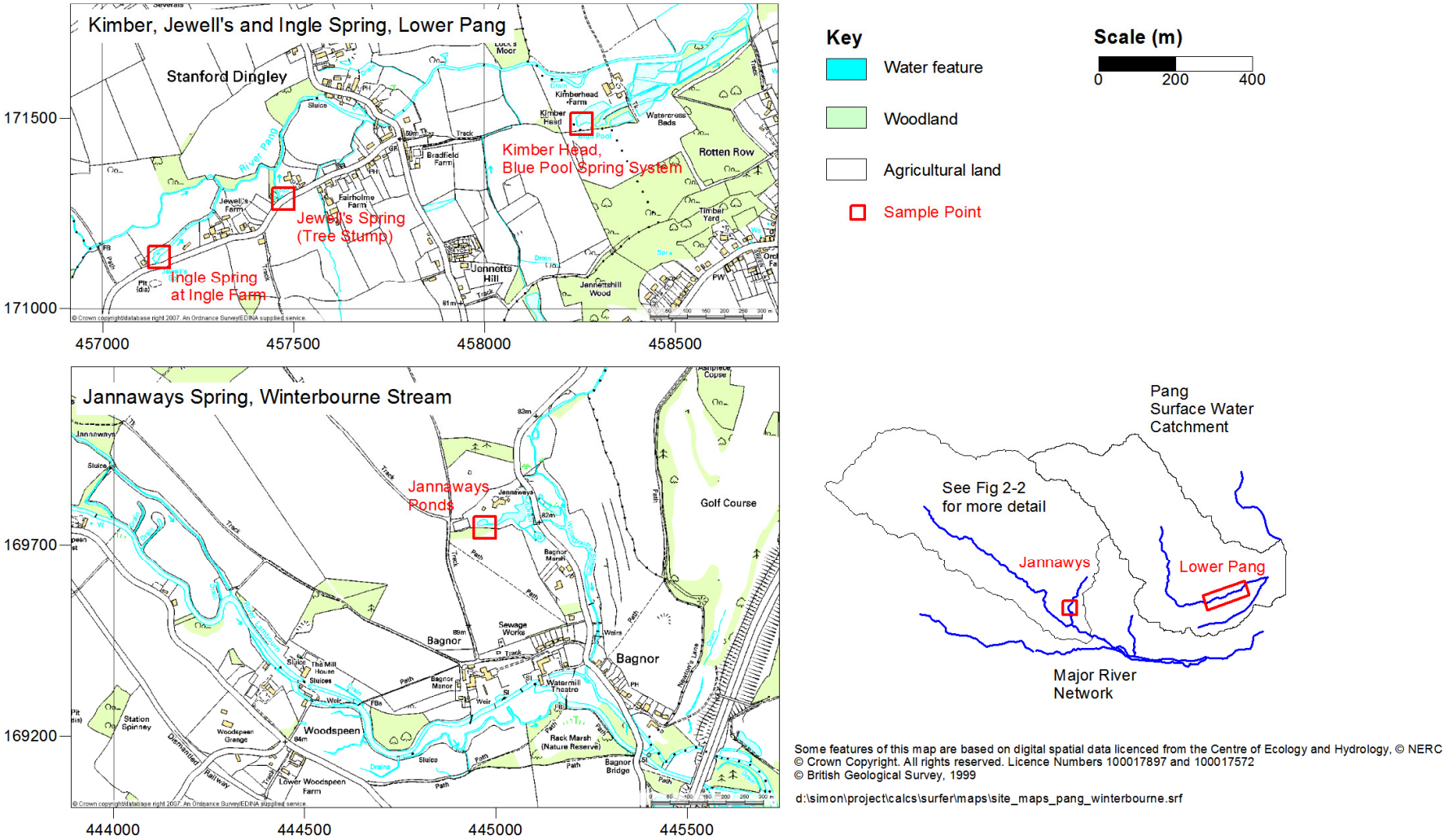

Figure 3—17 Major Spring Sampling Locations – River Pang and Winterbourne Stream

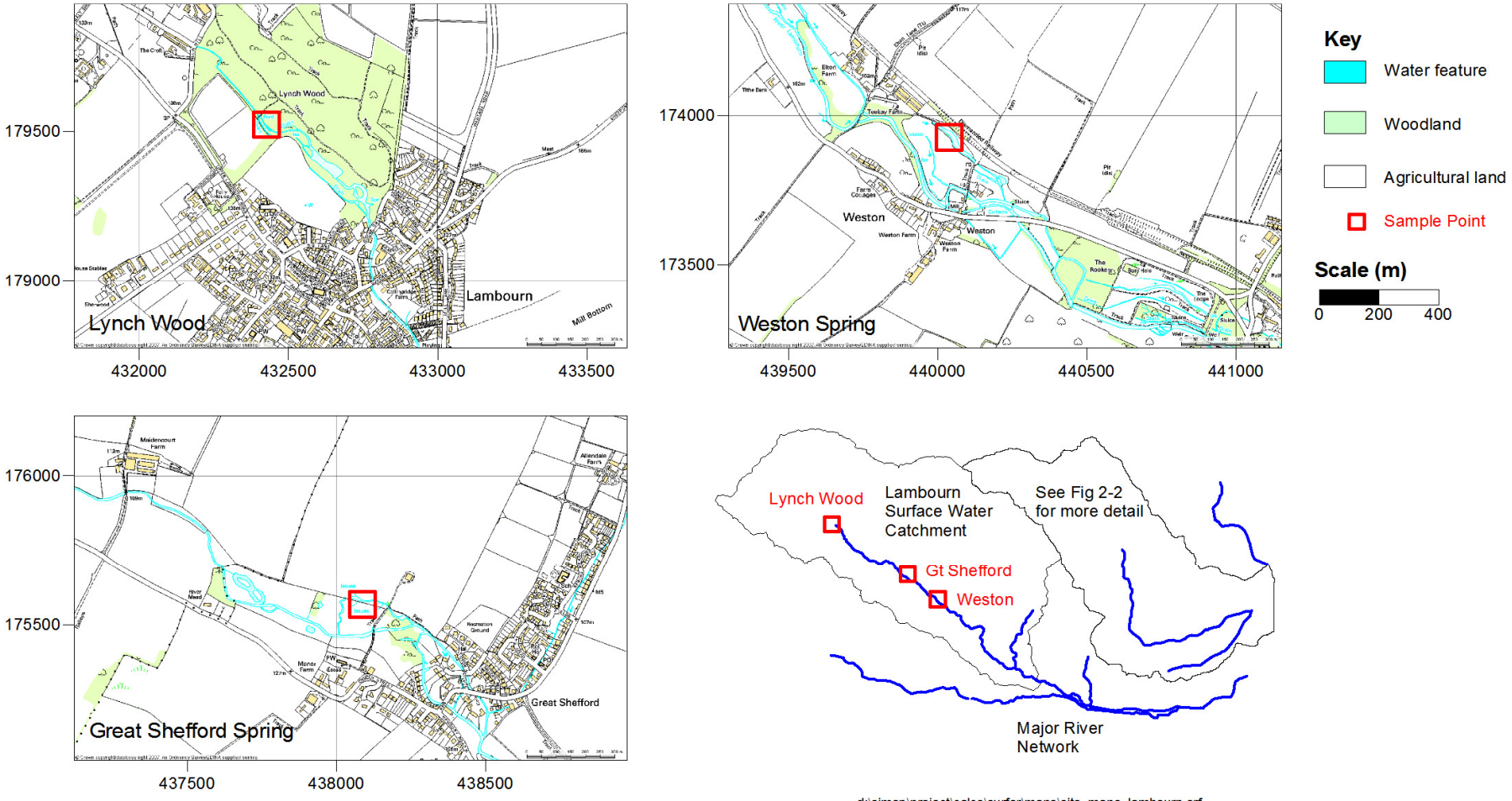

Figure 3—18 Major Spring Sampling Locations – River Lambourn

3.6 Integrated cross sections

Four cross section of the study area, (indicated on Figure 3—2) are presented in Figures 3—19 to 3—22. These sections include:

i. representation of the surface topography, based on 200m resolution DTM data;
ii. an interpreted geological section, using stratigraphic evidence from boreholes and from knowledge of the surface outcrop from GIS;
iii. groundwater levels for both April and October 2005, based on the intersection of the line of cross section with the regional groundwater contours calculated previously (e.g. Figure 3—15);
iv. an indication of the main rivers where they intersect the section, (with the exception of the section AA' which represents the downstream profile of the Lambourn river course; and,
v. the monitored spring sites.

These sections are useful to highlight that:

i. the dip of the chalk is *c.*2° to the south east, and that no major faulting or deformation of the unit is apparent;
ii. the depth to water table increases in the interfluves and can be up to 50 m below ground level at higher elevations;
iii. the ephemeral nature of the groundwater fed sections of the upper Pang, groundwater levels being *c.*10 m below its bed during 2005; and,
iv. that Clay-with-Flints deposits are present mainly on the interfluves and range in thicknesses up to *c.*10 m.

The four sections have been combined into a 3D fence diagram, to illustrate the spatial arrangement between them, and is presented in Figure 3—23.

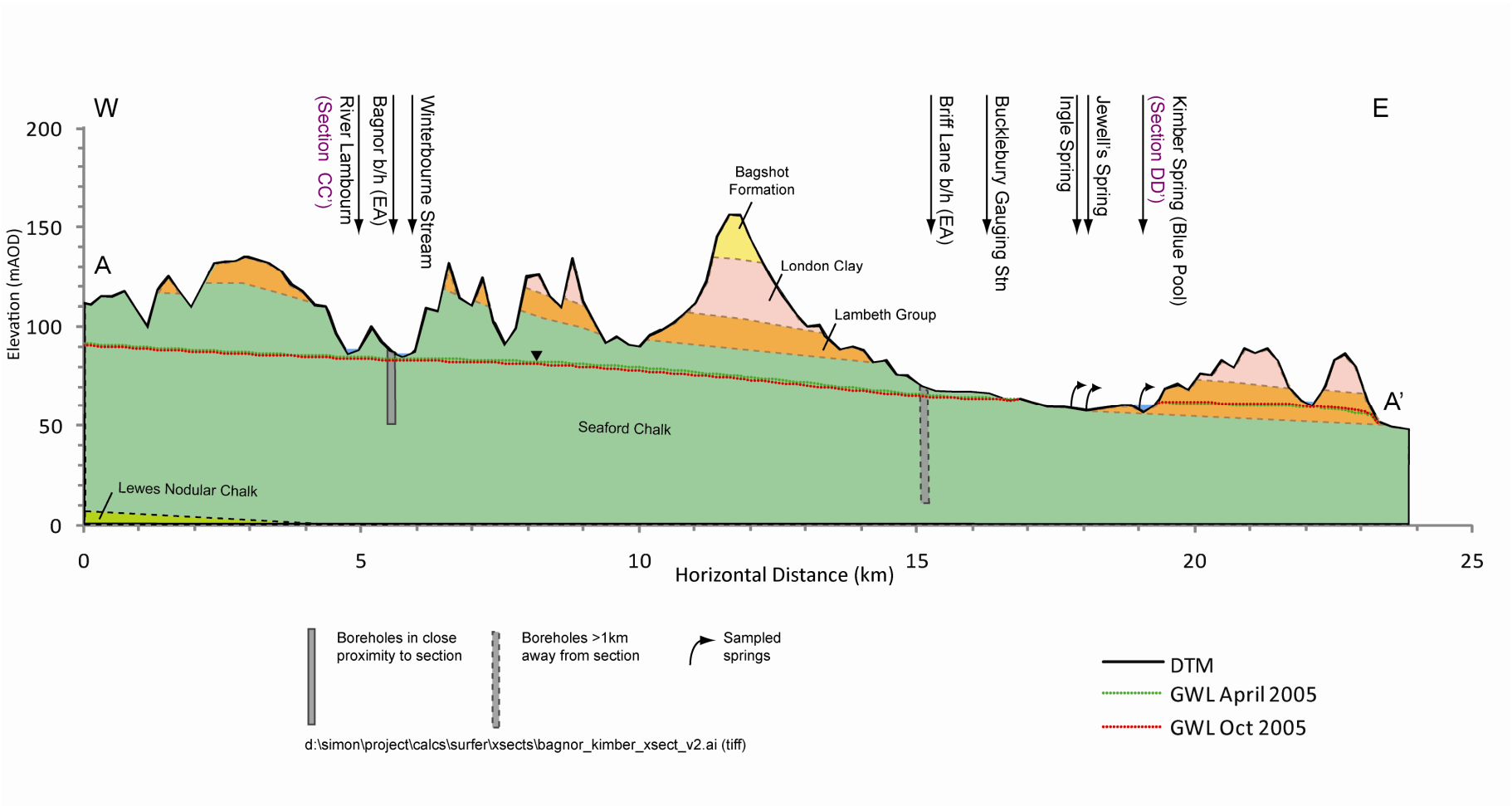

Figure 3—19 Cross Section AA' - River Lambourn at Bagnor to River Pang at Blue Pool Spring system

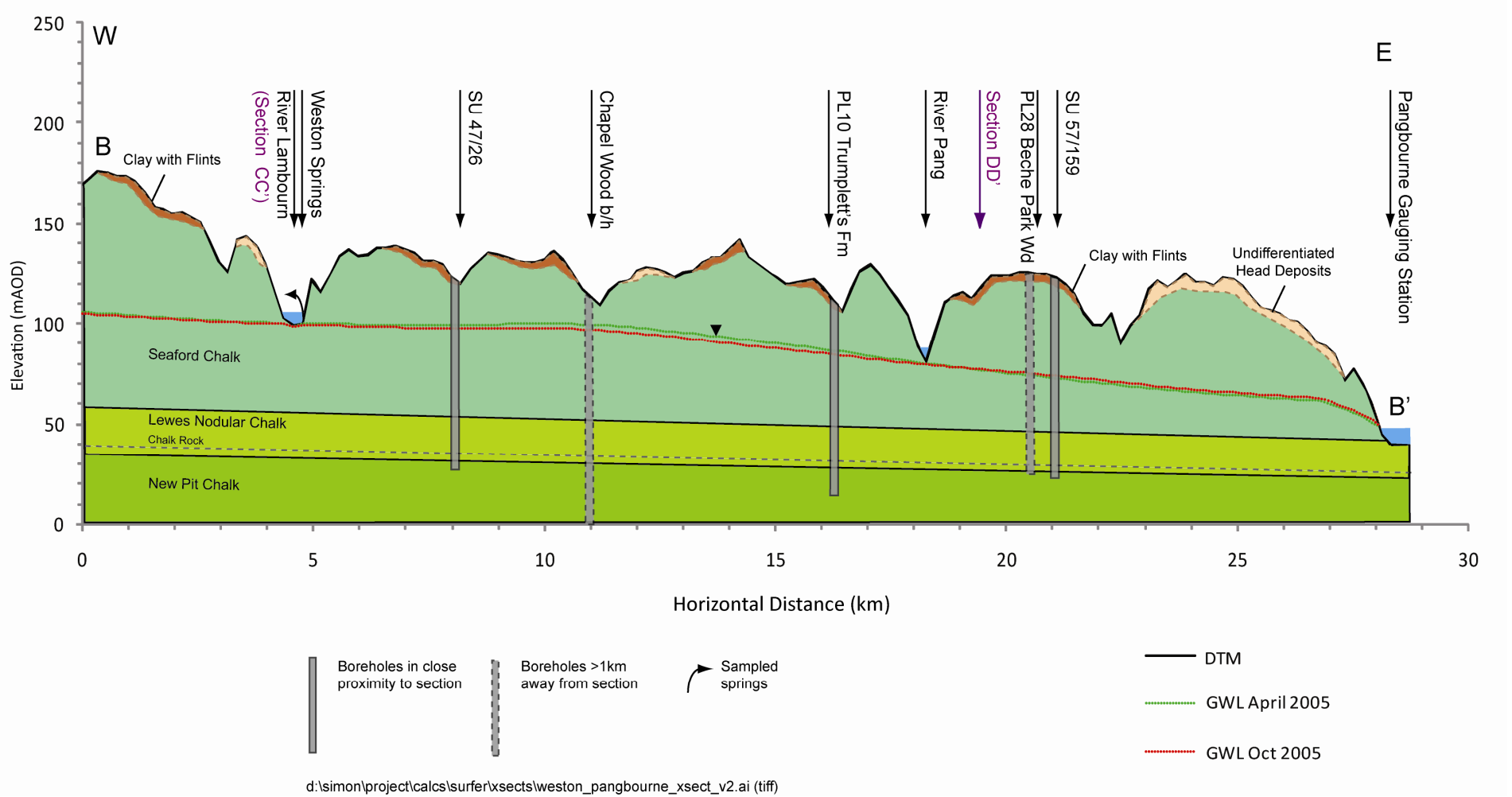

Figure 3—20 Cross Section BB' - Weston Springs to River Pang at Pangbourne

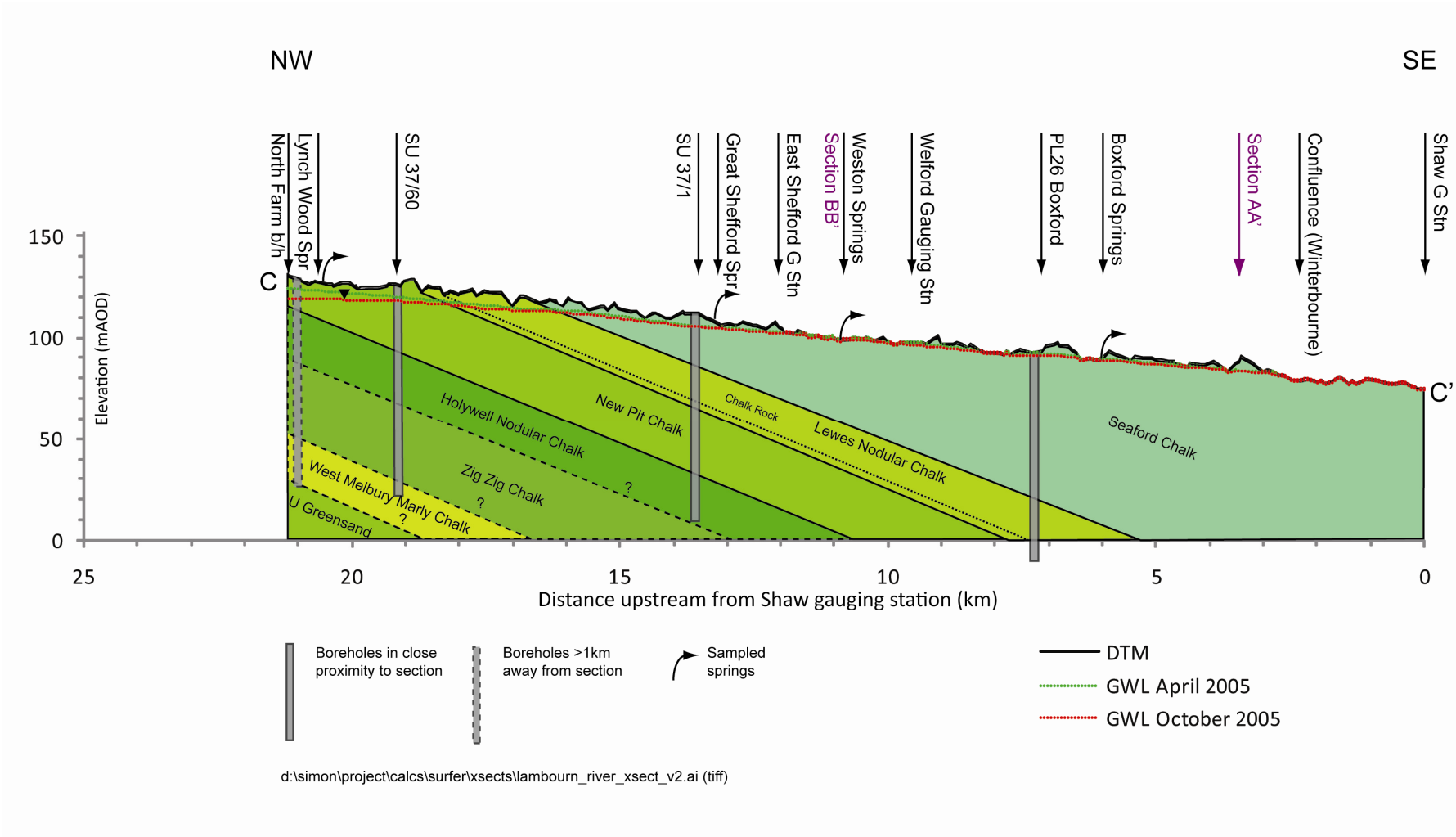

Figure 3—21 Cross Section CC' - River Lambourn upstream from Shaw gauging station

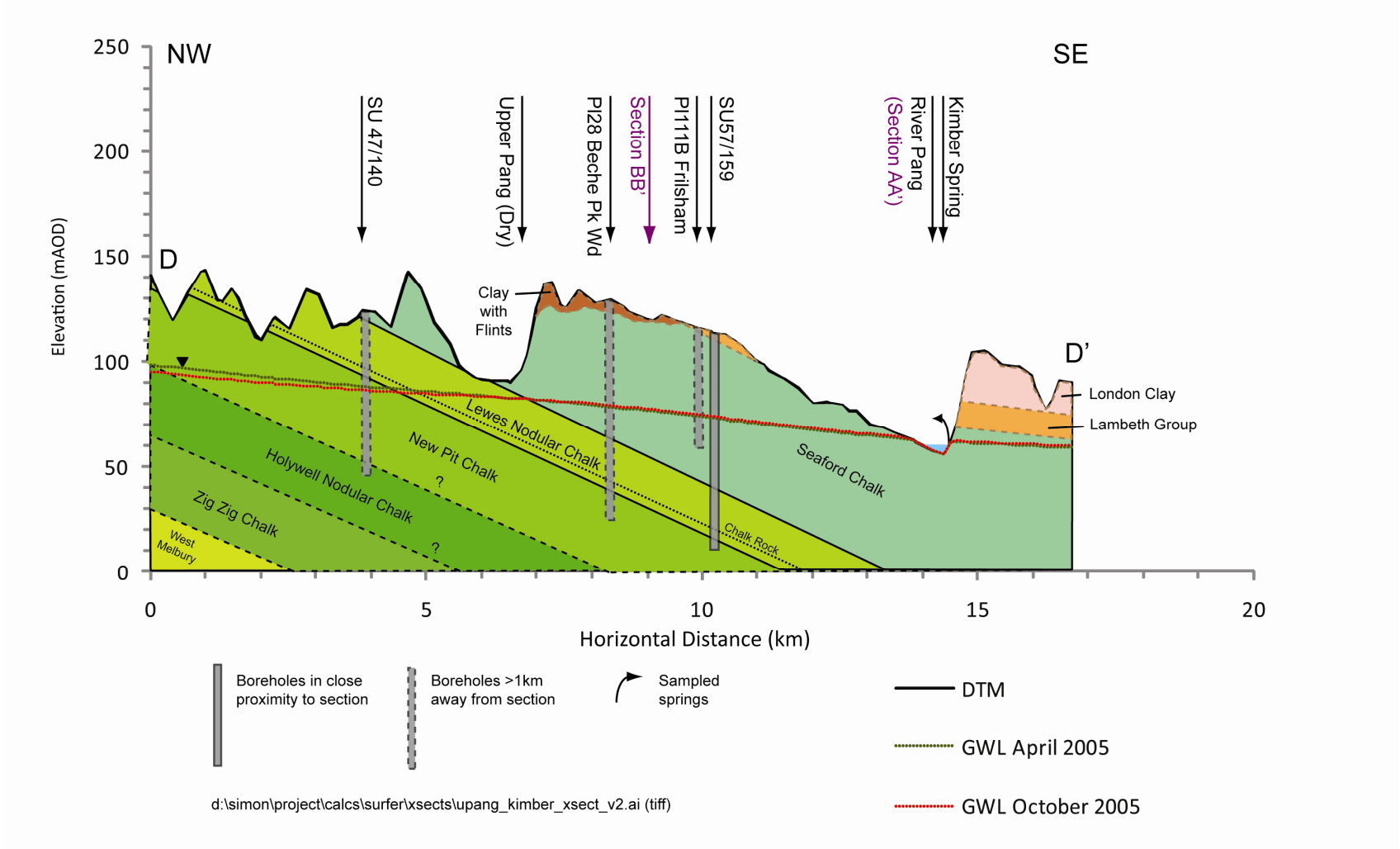

Figure 3—22 Cross Section DD' – Upper Pang Catchment to Kimber Spring (Blue Pool)

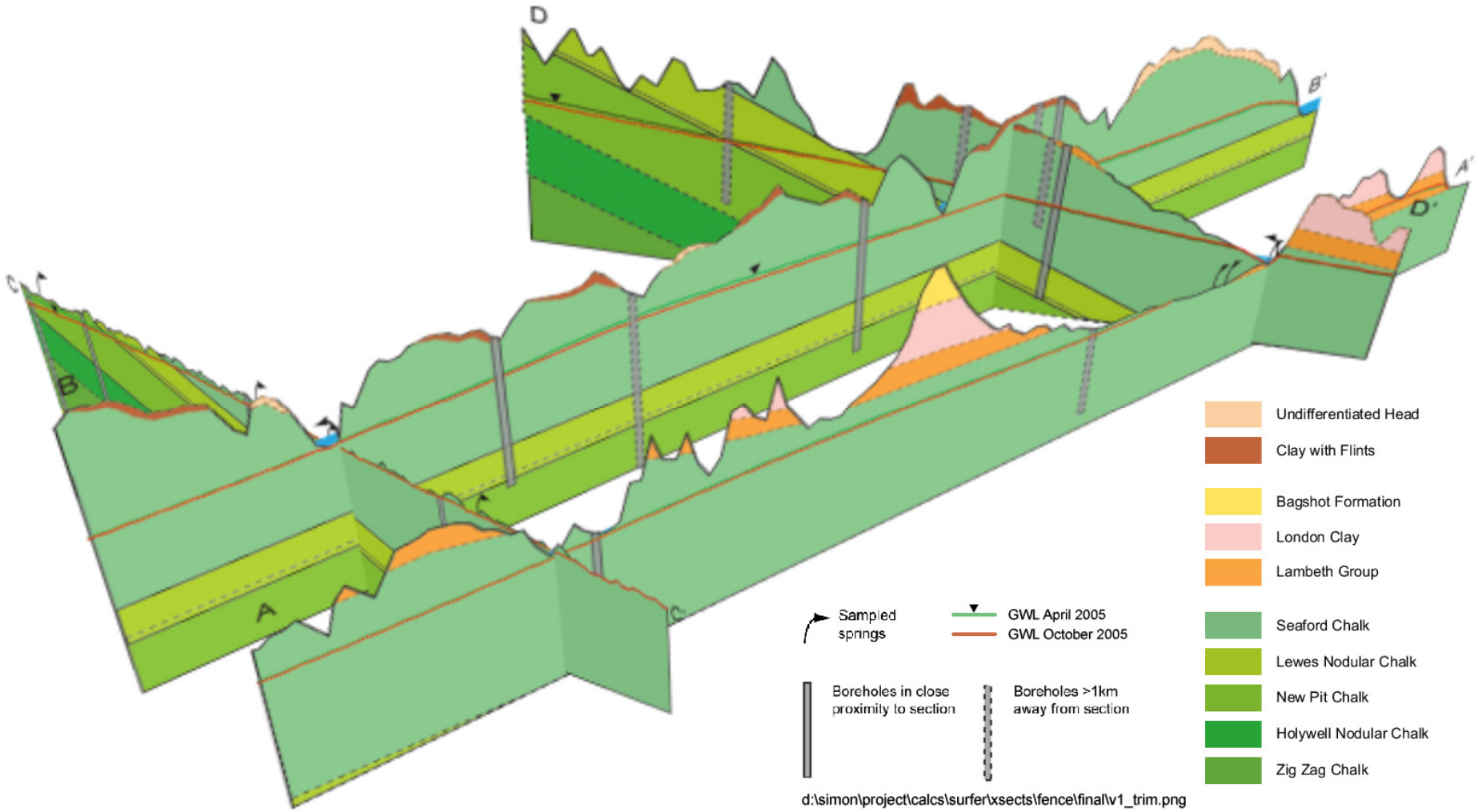

Figure 3—23 Geological Fence Diagram combining cross Sections AA', BB', CC' and DD'

4 Experimental Methods

This chapter describes the methods developed as part of this thesis for the analysis of uranium and radium in solid core material and dissolved radon gas in groundwaters. A description of other more standard methods, in both water chemistry analysis and for the collection of field data, is also provided for reference.

Firstly, the preparation of Chalk core material is described, which involves the use of strong acids to attempt complete dissolution of both the carbonate and clay components. The presence of acid insoluble mineral phases is observed, but is shown by XRF analysis to consist mainly of quartz material which is not regarded to be the primary source of uranium. Bulk uranium is determined from the dissolved fraction by a multi stage process that involves a) the selective extraction of the uranyl ion from a strong acid solution into an organic solvent through the formation of a soluble complex using tri-n-butyl phosphate, b) by back-extraction into a weak phosphoric acid solution and c) by spectrometric analysis of the resulting uranyl phosphate complex by exploiting its natural phosphorescence. The method is shown to work well over three orders of magnitude in uranium concentration, although its lower limit of detection is shown to be rather high in comparison to other procedures.

Secondly, the determination of radon by use of liquid scintillation analysis is described. By use of a selective extraction and pre-concentration stage, small volumes of environmental water samples water may be analysed, minimising both natural background and interference from other radionuclides. By use of alpha-beta separation, it has been possible to reduce natural background counts and to increase the sensitivity of the procedure to a level appropriate for natural Chalk groundwaters.

It has also been shown possible to determine bulk radium activity by monitoring the natural ingrowth of radon in sealed solutions of dissolved rock matrix. Furthermore, by making assumptions about the uranium activity of the same samples (using the previously determined mass) it has been possible to estimate the isotopic activity ratio $^{226}Ra/^{238}U$ for a selected number of samples.

Finally, the emanation of radon from solid material is measured for a range of particle sizes and Chalk types. Through knowledge of the radium activity is has been possible to determine the degree of relative emanation from each sample.

4.1 Bulk Uranium Assay

Total uranium concentration has been determined using a method that combines the research of Francois (1958), Kaminski et al (1981), and Williams and Miller (1983) and is based on the selective extraction of dissolved uranium from solution by liquid-liquid solvent extraction followed by analysis using luminescence spectroscopy. Other suitable methods for uranium assay also exist; these include inductively coupled plasma – mass spectrometry (ICP-MS) (e.g. Henry et al., 2001; Demidova and Saprykin, 2004), alpha spectrometry (e.g. as employed by Kigoshi, 1971 in the study of alpha recoil distances), photometric determination using Arsenzo III reagent (e.g. Khan et al., 2001), and the use of highly accurate laser-induced fluorescence spectroscopic techniques (e.g. as outlined by Meinrath et al., 1999). However, the first method was chosen in preference to these other options given the relatively simple methods of sample preparation, the ease of use of a luminescence spectrometer and the potential for rapid sample throughput.

4.1.1 Sampling

Chalk core sub samples from the LOCAR boreholes drilled at the Trumpletts Farm research site were obtained by agreement from the BGS core store at Keyworth, and material from borehole PL10A was chosen in preference to others due to generally competent recovery from *c.*4.4m to 91.7m bgl. As this borehole was also chosen for the purposes of groundwater sampling and tracer testing (Chapter 3), the location proved to be a suitable choice for direct comparisons to be made between bulk uranium content and groundwater radon activity.

In total, 84 small blocks of Chalk were sampled, distributed at approximately 1 m intervals throughout the core material. (See Chapter 5 for an indication of the positions within the core; and Appendix F for further sampling and preparation details).

The samples were chosen to cover a range of potential Chalk units, as well as where evidence suggested interaction with moving groundwaters, e.g. the presence of iron/manganese hydroxide staining on fracture surfaces (Spink, 2002). Fully competent blocks were taken to represent the Chalk matrix and other blocks were chosen on the basis that they were bounded both at the top and bottom by fracture surfaces.

For one block (with upper and lower *in situ* surface elevations of 34.40 m and 34.59 m bgl respectively), small sub-samples were prepared in the laboratory after drying of between *c.*5-10 mm thickness, using a fine saw (60 teeth/cm).

4.1.2 Sample Preparation

For assay by luminescence spectrometry, it was necessary to dissolve all Chalk samples in advance of analysis. A process chart, presented in Figure 4—1, illustrates the stages of sample preparation that were employed. Small blocks (*c.*8-12 g) of Chalk were dried in an oven for at least 24 hours at 105 °C. After cooling, the blocks were then crushed using an agate pestle and mortar and stored in air tight plastic bags.

An initial dissolution method was based upon a simplification of US EPA Method 3051A (EPA, 2009), a standard microwave digestion approach which employs "inverse Aqua Regia". However, in preliminary experiments and in consultation with laboratory staff it was apparent that microwave digestion did not provide any significant benefit to the dissolution process (either in the time to dissolve a batch of samples or in the degree of dissolution of non-carbonate fraction). Hence, samples were eventually dissolved using a simple hot-plate and refluxing method, albeit with the same acids and relative volumes as recommended in the initial method.

Approximately 0.5 g of chalk sediment were accurately weighed into small 25 ml conical flasks. To this, 9 ml conc HNO_3 were added, initially drop-wise to prevent excessive effervescence and accidental loss of sample. To this 3 ml conc HCL were added and the resulting solution covered with a watch glass and refluxed at 90 °C for *c.*3 hours, until the orange fumes of volatile nitrosyl chloride (NOCl) and chlorine (Cl_2) had disappeared. The flasks were then removed from the heat and allowed to cool to room temperature.

The solution was suction-filtered using 0.2 μm cellulose nitrate filter papers to remove any remaining solid material. The filtrate was then reheated on a hot plate and the solution evaporated down to incipient dryness. Additional conc HNO_3 was added at this point and the solution re-evaporated, with the procedure repeated for a third time to ensure that all HCl had been driven off. Finally, the dry sample was re-dissolved in 2% v/v HNO_3 and the solution stored in sealed volumetric flask for later analysis.

The used filter papers were dried in a oven at 50 °C for one hour and reweighed after cooling to determine the mass of original chalk sample that had not been dissolved. Some of the papers were also kept for the investigation of potential radium analysis by radon ingrowth (see Section 4.3).

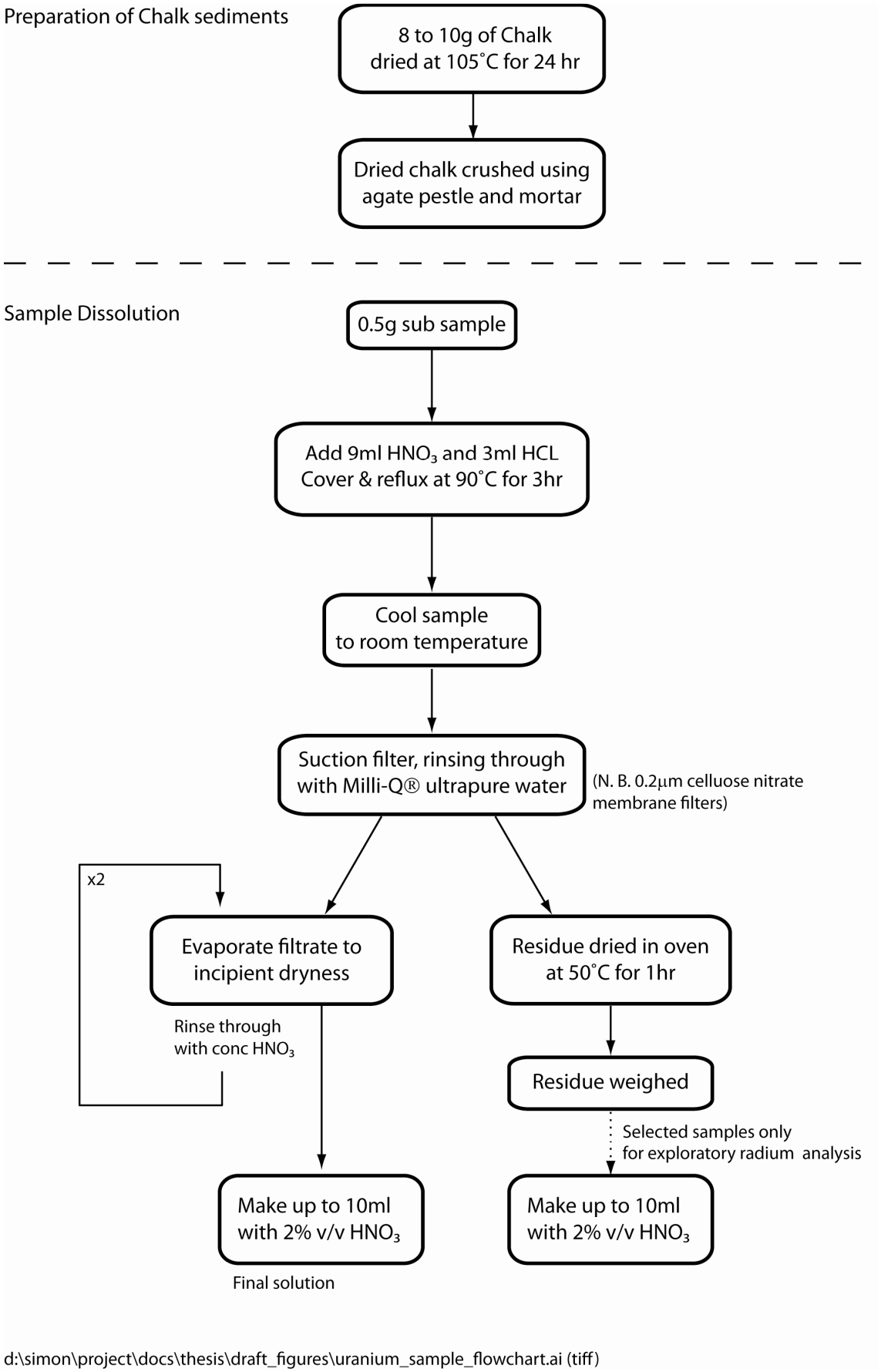

d:\simon\project\docs\thesis\draft_figures\uranium_sample_flowchart.ai (tiff)

Figure 4—1 Chalk sample dissolution process chart

Acid insoluble fraction

From preliminary work, one concern of using a method based on a combination of hydrochloric and nitric acids is that it may not provide total sample dissolution and that subsequent assay may potentially under-represent the total bulk uranium content of the Chalk (EPA, 2007).

As a case in point, Low (1996) illustrated the potentially significant variation between different components of the Chalk through a separate analysis of soluble and acid insoluble fraction of two samples from the Trunch borehole in Norfolk. In this case, samples were dissolved by the slow addition of 0.1 M HNO_3, and adjusting the pH of the solution to a value of 1.0. Any remaining solids were separated and dissolved by treatment with perchloric ($HClO_4$) and hydrofluoric (HF) acids in an pressurized container. Analysis of the uranium content in both the soluble and insoluble fractions is presented in Table 4—1. It is clear that in both cases the uranium concentration is greater in the acid insoluble phase by approximately one order of magnitude. Expressing the insoluble phase uranium content as a proportion of the total sample mass suggests that for these Chalk samples up to c.9% of the mass may be not brought into solution through treatment by HNO_3 alone.

However, the degree to which these conclusions can be applied to the preparation method adopted is limited. Low (1996) used a weak form of nitric acid to remove essentially the readily dissolvable carbonate fraction, followed by the use of strong acids to dissolve reamaining clays and other silicate structures. This method differs considerably from the use of a combination of concentrated nitric and hydrochloric acids, which would be expected to dissolve most Chalk components with the exception of quartz and other silicates (EPA, 2007). In addition, Tessier et al (1979) noted that treatment by concentrated HNO_3 and HCl would also be expected to destroy all organic matter, with better performance than the standard treatment of HNO_3 and H_2O_2.

Table 4—1 Example uranium content in acid insoluble fractions, after treatment with 0.1M HNO_3 only (reproduced from Low, 1996)

Sample	*Uranium, mg.kg^{-1} (soluble fraction)*	*Uranium, mg.kg^{-1} (insoluble fraction)*	*Insoluble mass fraction*	*Uranium in insoluble fraction*
Trunch 49.6m Maastrichtian Chalk	0.4488 (± 0.0023)	8.0374 (± 0.1332)	0.52%	8.6%
Trunch 300m Santonian Chalk	0.3124 (± 0.0017)	2.4284 (± 0.0465)	0.52%	3.9%

d:\simon\project\data\uranium\[upreviouswork.xlsm]low_digestion

Analysis of the insoluble components from two Chalk samples dissolved using conc HNO_3 and HCl was undertaken by X-Ray Diffraction, one sample from the Seaford Chalk, the other of Chalk Marl. The results indicate that (Figure 4—2),

i. for the sample with low marl content all crystalline strucures are dissolved with the exception of quartz, but,
ii. that some clay material may remain undissolved where the marl content is high.

In summary therefore, it is apparent that there are potential sources of error in the preparation method if total dissolution was assumed. However, it is considered that the method can still be justified on the basis that:

i. in Chalk most uranium (by mass) is associated with
    a. 3-4um thin coatings of smectite precipitated on carbonate grains (Marcos et al., 2000), and
    b. pelletal phosphates (Pacey, 1984b),

    both of which are readily dissolved by nitric acid, providing that the grains are free of refractory mineral inclusions (Evans et al., 2005),
ii. that radium produced as the decay products of uranium incorporated within the crystalline structure of quartz and framework silicates such as muscovite is unlikely to contribute radon to the pore space, given the small recoil distances in such structures (Andrews and Wood, 1972) (also see Section 2.1)

Of interest in this study is a estimation of a source term that is most readably accessible to transient groundwater conditions, that is to say on a timescale of days to weeks. All uranium that may act as is primary source is considered to be present in solution, and that incorporated within the crystalline structure of resistate material would not be expected to act as a primary source of radium.

In order to confirm that radon was not being generated from the insoluble Chalk fractions, the resistate material was retained from the filtering stage of sample preparation and subsequently analyzed for radium content by radon ingrowth (Section 4.3).

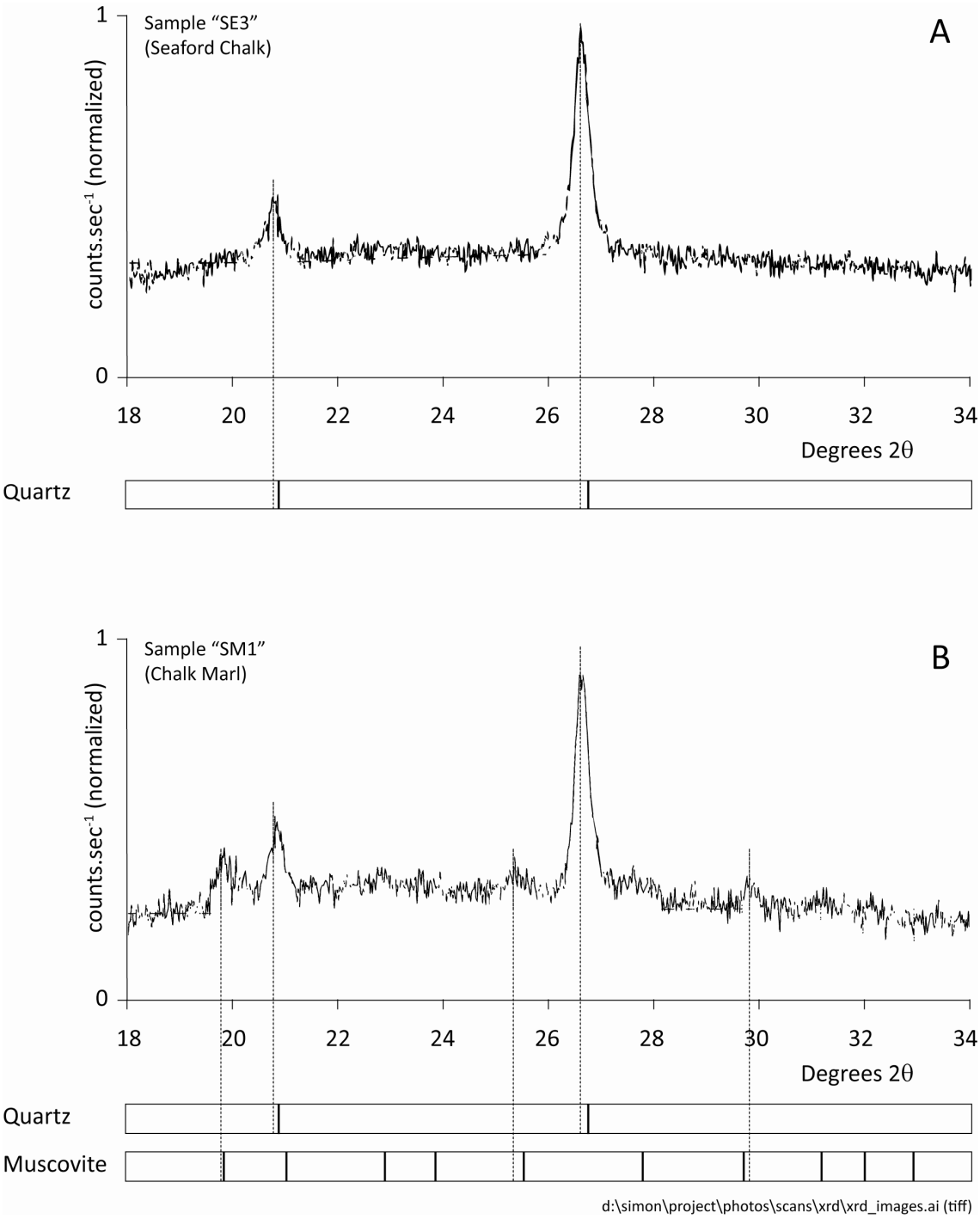

Figure 4—2 X-ray diffraction analysis of residue after dissolution of samples using HCl and HNO_3

A) SE3 – Sample of Seaford Chalk from unit directly above Seven Sisters Flint Band sourced from Birling Gap, East Sussex.

B) SM1 – Sample from marl band within the Holywell Nodular Chalk Formation sourced from Pinnacle Steps, East Sussex

Extraction and Concentration

To minimise the interference from potential chemical quenchers (in particular Fe^{3+}), a selective extraction and pre-concentration procedure is used before measurement. Similar to the UREX procedure used in the nuclear reprocessing industry (the development of which is discussed in Ivanovich and Harmon, 1992, Chapter 4) this is a liquid-liquid extraction process which employs tri-butyl-phosphate (TBP) in hexane as the extractant. The method also requires the use of a salting out reagent (aluminium nitrate) to increase the nitrate concentration in the aqueous phase to obtain a high distribution ratio (Rasmussen (1996) provides an historical overview of the development of this technology). A back extraction procedure is then used to bring the concentrated $[UO_2]^{2+}$ species into an aqueous phosphoric acid medium, which can be analyzed directly by a luminescence spectrometer.

The initial complexing and extraction may be summarized as follows -

$$UO_2{}^{2+}(aq) + 2NO_3{}^{-}(aq) + 2TBP\ (org) \longrightarrow \qquad (4\text{-}1)$$

$$UO_2(NO_3)_2(TBP)_2(org)$$

where TBP represents $(C_4H_9O)_3PO$.

Originally, Francois (1958) demonstrated that the uranyl ion $[UO_2]^{2+}$ may be preferentially extracted from a solution by use of tri-butyl phosphate (TBP) dissolved within an organic solvent such as iso-octane. A high uranyl partition coefficient between the two phases was maintained through the addition of a concentrated solution of aluminium nitrate, which enabled a >99% removal of the ion with a single extraction. In addition, through analysis by fluorometry, Francois (1958) estimated that *c.*99% of uranium was transferred to the iso-octane phase when the pH of the aqueous phase was "in the range of 3 to 6", compared with *c.*86% extraction from "an aqueous phase 3M in nitric acid".

For the extractant phase, Francois (1958) maintained a ratio of solvent to TBP of 10:1 (lower than that adopted by previous authors) to minimize the degree of co-extraction of other ions, in particular Bi^{3+}, Fe^{3+}, Ce^{4+} and Th^{4+}. More recently, Williams and Miller (1983) investigated the co-extraction of Fe^{3+}, Mn^{2+} and Cl^{-} using a concentration of only 1% (v/v) TBP in hexane and demonstrated "adequate separation" when considering the potential quenching effects of such ions. They also demonstrated that such a reduction in the concentration of TBP improved the detection efficiency of the overall preparation method (discussed further in the next section).

Isolation and enhancement of uranium phosphorescence

Kaminski et al (1981) demonstrated that the rather weak phosphorescence of uranyl ions in solution can be often masked by the fluorescence of other phenolic and carboxylic compounds present in environmental samples (e.g. humic acid). Such samples, when excited by ultra violet radiation, emit photons that span a wide range in wavelengths, often masking the presence of uranyl ions. However, it is possible to measure uranyl phosphorescence in isolation by reducing the interfering fluorescence signal using two dominant methods –

i. by delaying the period of measurement until after all fluorescence has decayed (times of the order of *c.*10^{-9}s, c.f. *c.*10^{-5}s for that of phosphorescence), and
ii. by maximizing uranyl phosphorescence through the prevention of signal quenching, typically produced in aqueous samples by the interaction of the excited ion with water molecules.

Such precision in time discretization (in the order of μs) is possible with modern luminescence spectrometers. Williams and Miller (1983) illustrated the advantage of using a time delay between sample excitation and the start of measurement by comparing the signal to noise ratio for the same sample under different machine configurations. By selecting an initial delay of 0.30 μs and a gate count time of 250 μs, Williams and Miller (1983) were able to achieve a 5-fold increase in detectability compared to when no time delay was used. They also demonstrated that a concentration of 1% TBP in hexane produced the greatest intensity of signal in the final aqueous phase and that a 10% solution of phosphoric acid produced the longest lifetime for uranyl phosphorescence.

These results are supported by previous work by Sill and Peterson (1947), who investigated the enhancement of uranyl phosphorescence through the addition of concentrated phosphoric and hydrofluoric acids. They observed a ten-fold increase in phosphorescence intensity by adding 5 to 10% solution of phosphoric acid to aqueous samples of previously digested sediments. This phenomenon was confirmed by Kaminski et al (1981), who presented a positive correlation between phosphoric acid concentration and signal intensity, up to a maximum limit at a volume ratio of 1:10, acid:sample.

Therefore, to maximise the detectability of the uranium in solution, it was desirable to perform a further back extraction from the organic phase into an aqueous phase of a phosphorescence enhancer, such as phosphoric acid. In line with the results previously cited, an enhancer concentration of 10% H_3PO_4 was chosen to perform the back

extraction. 2 ml of the hexane phase were carefully pipetted and mixed with 3ml of acid. The solution was then shaken continuously for two minutes and then left for a further ten minutes to allow the phases to separate fully. At this stage, 2 ml of the aqueous phase were then extracted from the sample bottle and pipetted into a clean quartz cuvette.

Note on reagent impurity

Phosphoric acid is known to have high level of uranium, often due to the production process (e.g. Khorfan et al., 2001). In an attempt to minimize the introduction of other sources of uranium during the extraction phase both the aluminium nitrate and phosphoric acid solutions were pre-washed with a solution of 1% (v/v) TBP/hexane.

Blank samples were also measured routinely to assess the degree of this potential effect and to ensure that the background signal was well known.

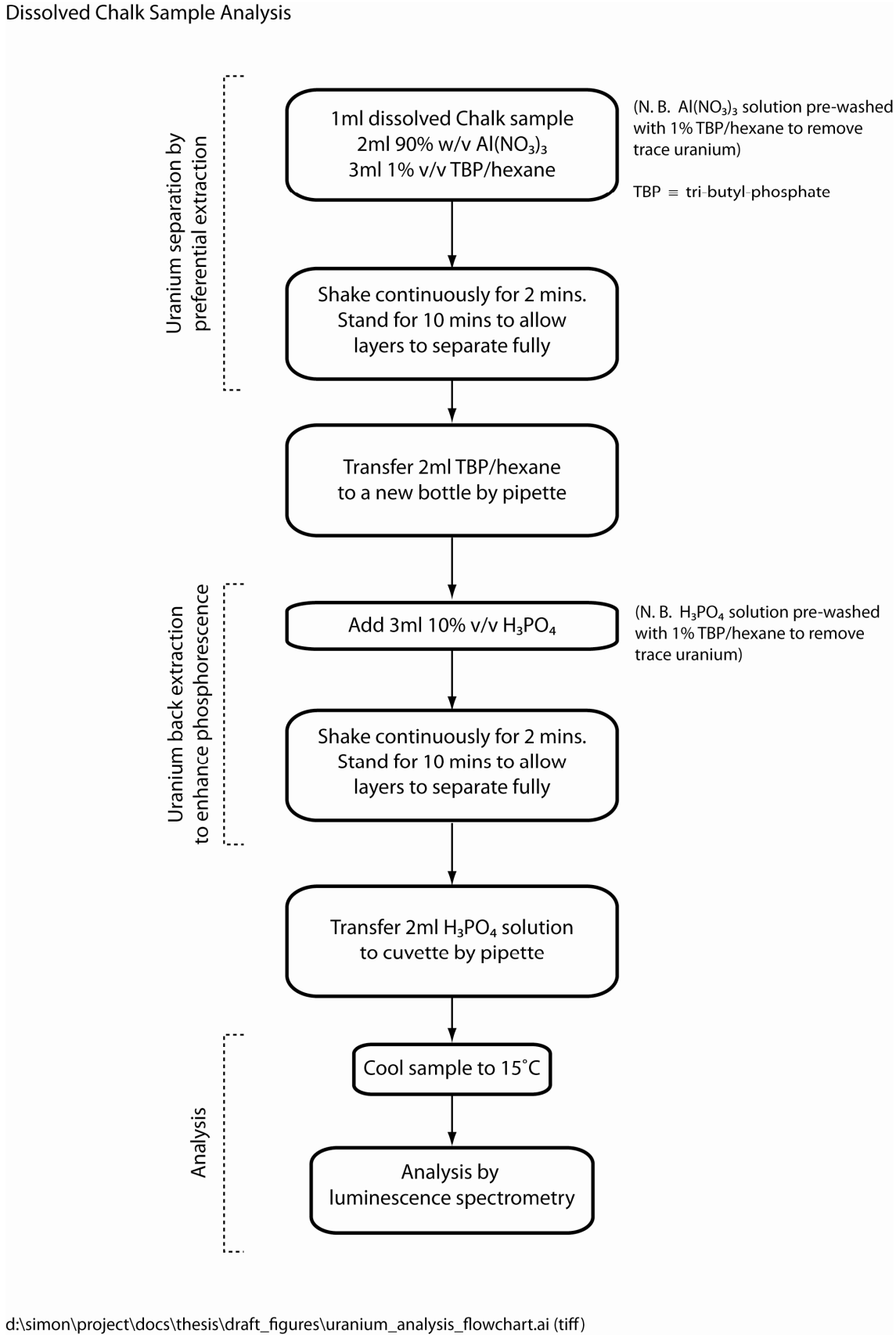

Figure 4—3 Chalk sample uranium analysis process chart

4.1.3 Analysis by Luminescence Spectrometer

Theory of Uranium phosphorescence

The first systematic observation of the phosphorescence of uranyl salts and uranium glass were made by Becquerel (1867). Later, Nichols and Howes (1917) extended this work to study the decay rate of various uranyl salt solutions, including uranyl nitrate – typically by subjecting solid samples to ultra-violet light (i.e. a wavelength of *c.*245 nm), and recording the decay of the visible yellowish-green light that was emitted by the sample. Such phenomena can be described in terms of energy absorption and release by electrons that surround a molecule. Energy in the form of electromagnetic radiation (such as ultra-violet light), can be released through an excited electron returning to a "ground state" in several different ways.

These processes are best illustrated by a Jabłoński diagram (Lakowicz, 1999) and a generic example is presented in Figure 4—4. On the vertical axis, the diagram represents distinct energy levels at which electrons may exist when surrounding a nucleus or a larger molecule. Through the absorption and release of energy electrons may make a transition between these levels. Set adjacent to each other on the horizontal axis are two particular "spin states", i.e. particular arrangements of electrons each with their own values of "spin" or angular momentum. Singlet states are defined as where electron pairs have a combined spin of zero, a triplet state where the total spin is equal to one. Further detailed discussion of quantum mechanics is beyond the scope of this thesis, but it should be noted that as an excited electron "relaxes", i.e. when it loses excess energy, photon emission can occur either (a) between states of the same spin state (e.g. S1 to S0), termed "fluorescence" or (b) between different spin states (e.g. T1 to S0), termed "phosphorescence".

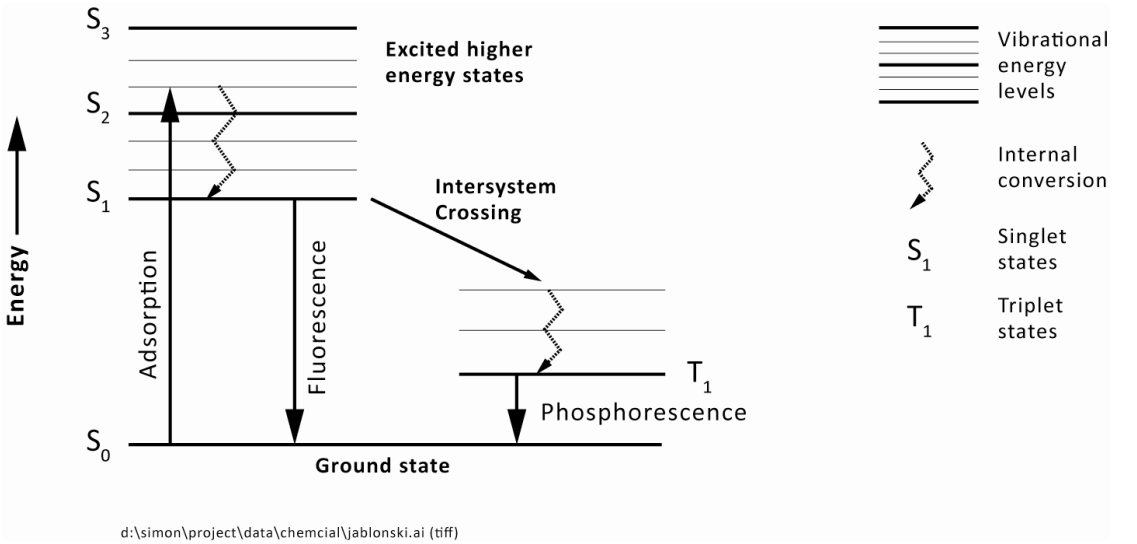

Figure 4—4 Example of a Jabłoński diagram, modified from Lakowicz (1999)

The two processes may be identified by analysis of the rate of emission decay – as noted by Williams and Miller (1983) fluorescence decay occurs on the order of nanoseconds (10^{-9} s), whereas phosphorescence exhibit much longer lived signals (of the order of 10^{-5} s).

In addition, there are other non-radiative relaxation processes that can occur such as "internal conversion", which is a transition between energy states of the same spin state, and "intersystem crossing" is a transition between different spin states. Other non-radiative routes not represented on the diagram but important in the detection of uranium species include the quenching by water molecules which can occur if the uranyl ions are not "shielded" by other species such as hydrofluoric or phosphoric acid (Kaminski et al., 1981). The net effect of non-radiative deactivation of an excited molecule is decreased detectability of the species in solution when using method such as luminescence spectrometry.

Spectroscopy

Sample analysis was undertaken by use of an Perkin Elmer LS55 Fluorescence Spectrometer – a simplified schematic of the main components is illustrated in Figure 4—5. A pulsed xenon lamp provides a continuous emission spectrum of light over a range of *c.*200-700 nm, however light emitted from the source may be filtered as it passes through an excitation monochromator, consisting of a 'tuneable' diffraction grating. As a secondary monochromator is located in front of the sample photomultiplier, it is also possible to filter the wavelength of emitted light from the sample. In such a way, particular excitation wavelengths and emission peaks may be chosen that provide an optimum configuration for uranyl phosphorescence. Any variations in the intensity of the lamp that may provide erroneous signal strength are corrected for by splitting the excitation beam at source and by measuring the difference between the sample signal with that from a reference photomultiplier.

The LS55 permits the user to select a slit width (or 'band pass') for both monochromators that limits the range of wavelengths that may pass though the grating. In practice the choice of slit width is a compromise between desired *selectivity* (e.g. more than one fluor may be present, each with slightly different excitation wavelengths) and in the *sensitivity* of the machine (e.g. sample emission spectra may consist of more than one peak, but which may not contribute to the total signal count if the slit width is too narrow).

In the specific case of the analysis of uranyl ions, machine settings similar to those stated by Williams and Miller (1983) were adopted (Table 4—2).

Table 4—2 Perkin Elmer LS55 – monochromator and gate settings for uranyl analysis

Parameter	*Value*	*Unit*	*Comments*
Excitation wavelength	258.0	nm	Excitation wavelength of uranyl ion in phosphoric acid medium
Excitation slit width	5.0	nm	Narrow width limits excitation to uranyl species only
Emission wavelength	497.0	nm	Set at the first major peak of the uranyl emission spectrum
Emission slit width	15.0	nm	Wider slit width ensures that signal peak maximum is measured, even if its wavelength varies slightly.
Lamp flashes	5	-	Rapid repeated pulses of light used to enhance uranyl phosphorescence prior to measurement.
Count delay	0.03	ms	Based on Kaminski et al (1981) and Williams and Miller (1983).
Count time	0.25	ms	Slightly greater than the maximum lifetime of uranyl ions in solution in 10% H_3PO_4, as recorded by Williams and Miller (1983).
Cycle time	200.0	ms	Total length of time taken for one measurement – much longer than phosphorescence relaxation time.
Integration time	10	s	All individual measurements collated and averaged.

An example of a complete emission spectrum (corrected for background) between 440 and 610 nm for a standard uranium solution excited at 258 nm is illustrated in Figure 4—6. Four main intensity maxima are observed, which correspond to dominant energy transfers between excited and ground states (Meinrath, 1997). For both calibration and routine measurement of samples, the intensity of only the first peak (i.e. at 497 nm) was chosen, due to the stability in both wavelength and intensity of the peak during repeat measurements of the same sample. Furthermore, the LS55 was observed to generate less variation in signal intensity when the emission monochromator was set at a fixed wavelength.

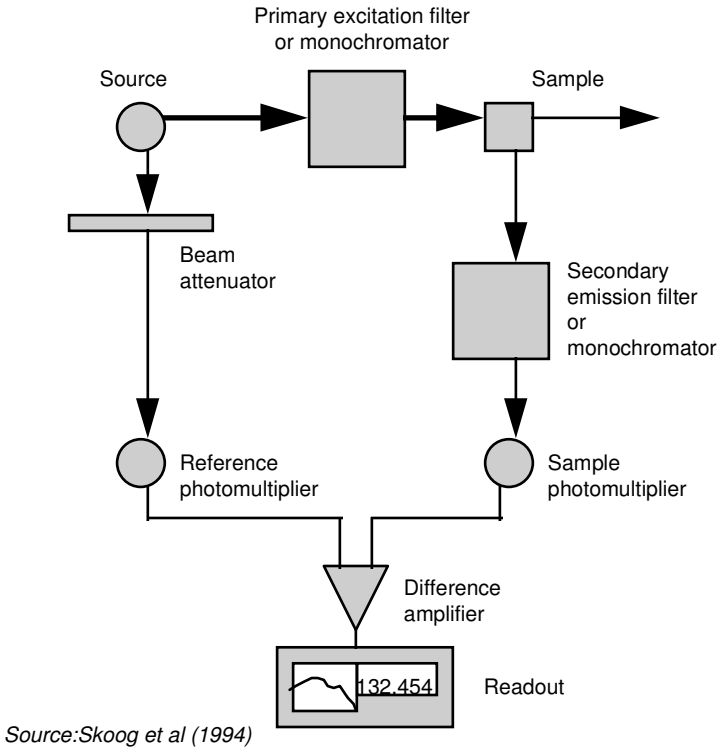

Source:Skoog et al (1994)

Figure 4—5 Schematic diagram highlighting key components of a standard spectrofluorometer.

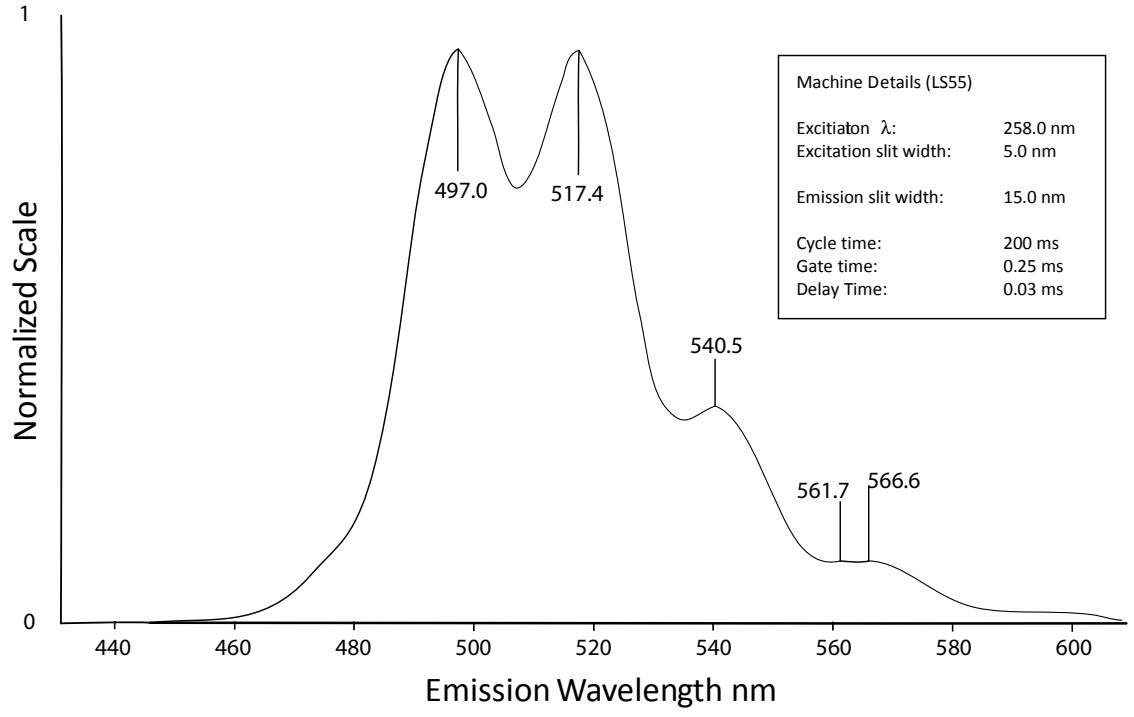

d:\simon\project\data\ls55\images\ls55_spectra.ai

Figure 4—6 Emission spectra produced by the Perkin Elmer LS55 luminescence spectrometer (in phosphorescence mode)

Sensitivity analysis

The sensitivity of the machine response to a series of both sample properties and environmental conditions is presented in Figure 4—7.

Giridhar et al (2005) demonstrated a positive correlation between nitric acid concentration (between the range 0.1M to 8M) and the U(VI) distribution ratio between 1.1M TBP/n-dodecane and the aqueous phase. Alibrahim and Shlewit (2007) also observed an increased extraction efficiency of uranium (by tri-butyl phosphate in hexane) as a function of nitric acid concentration (0.1M to 5M). Therefore, it was considered appropriate to check the potential variation in final sample signal intensity with small variations in sample pH that may result during sample preparation. The pH of a series of samples was varied by mixing a 1.0 ppm ($mg.l^{-1}$) uranium standard with different concentrations of HNO_3 and the resulting solutions prepared for analysis using the standard approach as previously developed. The results indicate however that, for a pH range between *c.*0.01 and 4.1 (equivalent to a concentration between *c.*1 M and 8×10^{-5} M), no significant trend in extraction efficiency is observed. These results suggest that it is only with much greater acid strengths that those used with the present method that may produce changes in the overall extraction efficiency.

Iron (III) is a well known quencher of the uranyl phosphoresce at concentrations which may be considered common in dissolved environmental samples (e.g. Sill and Peterson, 1947; Veselsky et al., 1988). Meinrath et al (1999) demonstrated that the uranium recovery by fluorescence spectrometry in the presence of Fe^{3+} at a concentration of 10 $mg.l^{-1}$ was *c.*2.5% without extraction compared with *c.*94% with initial extraction using TBP/hexane and subsequent back extraction using 9% phosphoric acid. Hence, Meinrath et al (1999) concluded that separation of uranium from such quenchers is usually compulsory.

In the analysis of the Banterwick Barn borehole in the Pang catchment Murphy (1998) determined the iron content of solid Coniacian and Turonian Chalk samples. Values of *c.*0.09 to 0.3 wt % were typical throughout the profile with the exception of the Chalk Rock hardground where values as high as 1.5 wt% (3 samples) 2.5 wt% (1 sample) were recorded. High Fe/Ca ratios found in the hardgrounds also reflected the increased clay mineral, pyrite and iron oxide components of the facies.

To test that the selective extraction procedure adopted prevented the co-extraction of iron in this expected range, known concentrations of Analar grade iron (III) nitrate were made by dissolving the salt in deionized water and added to uranium standard, in each case adjusting to a final uranium concentration to 1.0 ppm.

The results for iron concentrations from 0 to 1500 ppm analysed in duplicate are presented in Figure 4—7. They indicate that, although there may be a slight decrease in the final extracted uranyl phosphorescence at iron concentration of 1500 ppm, the duplicate inter-sample variation is still large in comparison. Hence, it is considered that for the majority of Chalk samples to be analysed (where the typical iron concentration is of the order of 200 ppm) iron is not co-extracted with uranium in sufficient quantities to interfere with the final signal intensity.

Finally, the phosphorescence of the uranyl complex has been observed to be highly dependent on sample temperature (e.g. Benson et al., 1975) – a reflection of "collisional quenching" that is considered due to increases in the vibrational energy of the surrounding water molecules (Lakowicz, 1999). Variation of the sample cuvette temperature, achieved by use of a holder cooled by the recirculation of water supplied from a regulated water bath, demonstrated a *c.*17% increase in signal intensity when the temperature was decreased by 10 °C (i.e. from 20 to 10 °C). However, the benefits of increased signal intensity on sample detectability was limited due to the production of atmospheric condensation on the outside of the cuvette at lower temperatures. In practice, the temperature of the cuvette was regulated at *c.*15 °C to ensure that a enhanced signal could be stabilized without risk of such interference.

Standards and Calibration

In dilute samples, it can normally be assumed that emission intensity is directly proportional to species concentration. In contrast, when species concentrations become high enough that the absorbance of radiation is greater than *c.*5%, direct proportionality with concentration is typically lost and the rate of emission lags behind the increase in concentration (Skoog et al., 1994). To understand this relationship, suitable standards are made to calibrate the spectrofluorometer before and during the analysis of samples.

Uranium standards of 0.005, 0.01, 0.05 and 0.1 $mg.l^{-1}$ were prepared from a standard atomic absorption solution of 1 $mg.l^{-1}$ U in 1 wt.% HNO_3 (Sigma-Aldrich). 1 ml of each standard was prepared in the same manner as regular samples, i.e. by liquid-liquid extraction. 2 ml of the final phosphoric acid solution were added to a quartz cuvette which was then sealed with a plastic stopper. Each standard was measured before and repeated during the analysis of the dissolved Chalk samples. From this work, is was possible to validate the linear response of the spectrometer, which is presented in Figure 4—8. This figure also includes a 95% confidence belt which demonstrates the observed variation in

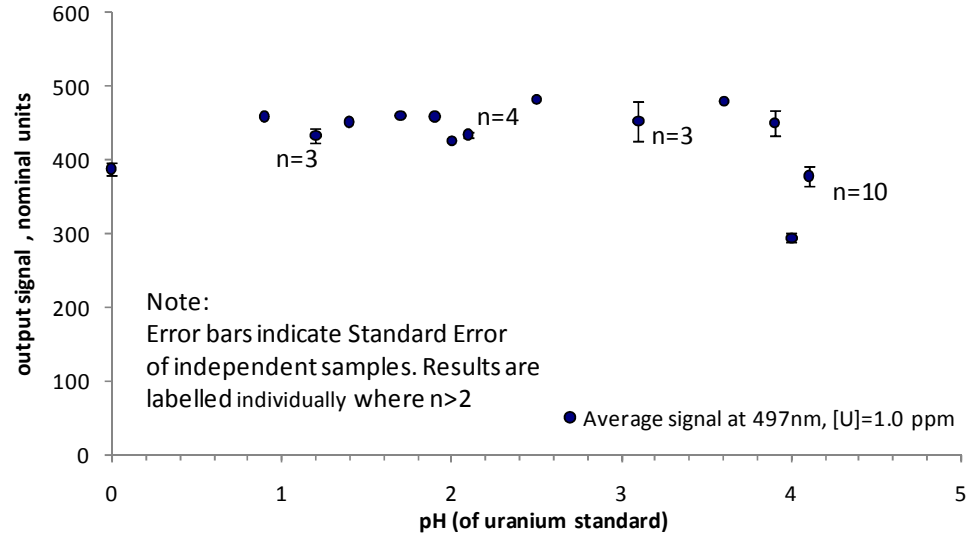

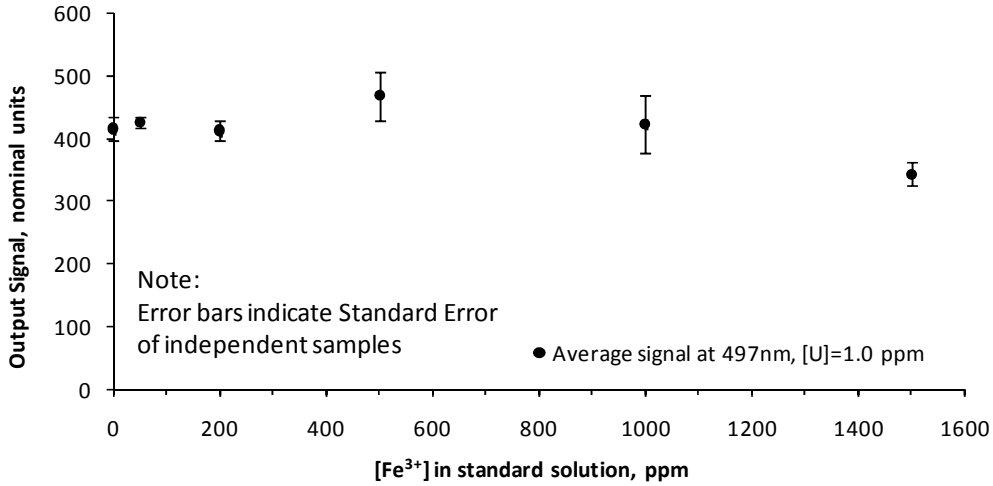

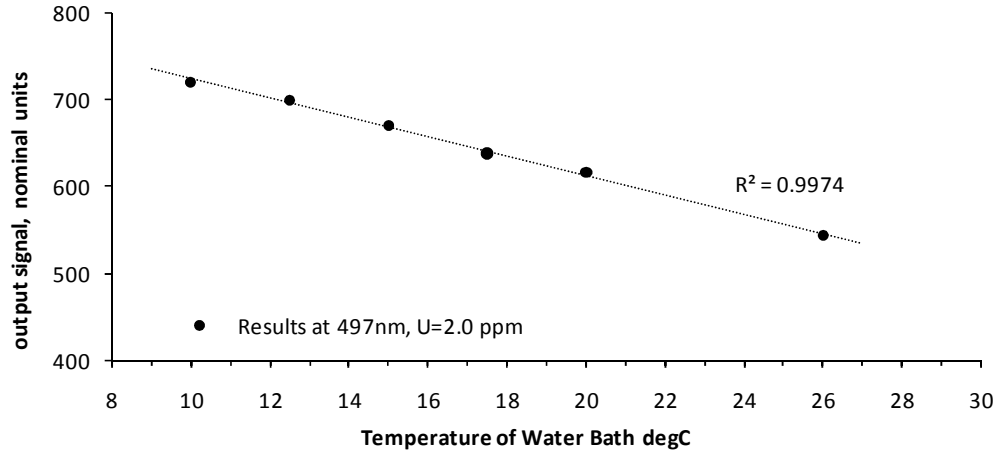

d:\simon\project\calcs\uranium\[uconc&phwork.xlsm]output

Figure 4—7 Variation of signal as function of sample temperature, standard pH and dissolved Fe^{3+} concentration in solution.

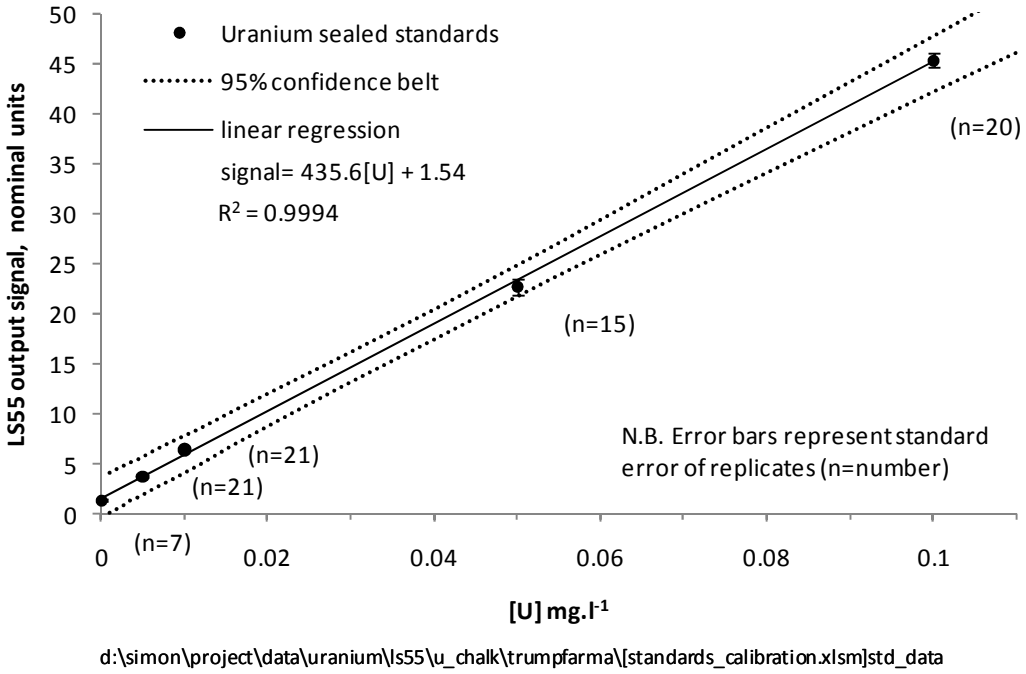

d:\simon\project\data\uranium\ls55\u_chalk\trumpfarma\[standards_calibration.xlsm]std_data

Figure 4—8 Uranium standards calibration curve, using LS55 luminescence spectrometer.

Table 4—3 Uranium standards – replicate error

Standard concentration (mg-l^{1})	*Machine Signal (arbitrary units)*	*Standard Deviation*	*Standard Error (n)*	*n*
Blank	1.39	0.20 (14%)	0.08 (5%)	7
0.005	3.72	0.28 (8%)	0.06 (2%)	21
0.010	6.46	0.40 (6%)	0.09 (1%)	21
0.050	22.73	2.88 (13%)	0.74 (3%)	15
0.100	45.35	3.26 (7%)	0.73 (2%)	20

Source: d:\simon\project\data\uranium\ls55\u_chalk\trumpfarma\[standards_calibration.xlsm]std_data

signal intensity. At 0.01 mg.l^{-1} the long term average signal was 6.46 (nominal units) with a standard deviation of 0.40 (*c.*6%) and standard error of 0.09 (n=21, *c.*1.4% of the signal). The goodness of fit of the regression (R^2 = 0.9994) confirms that both the extraction efficiency of the preparation procedure and the machine response may be assumed to be linear and well characterized over the concentration range tested.

Final uranium concentration calculation

Based on the linear regression calculation of the dissolved chalk sample has been calculated from:

$$[U] = \frac{sample\ conc\ (mg.l^{-1}) \times sample\ volume\ (l)}{sample\ mass\ dissovled\ (mg)} \qquad (4\text{-}2)$$

where the sample concentration is inferred from the linear regression presented in Figure 4—8.

Analysis of the replicate error (as presented in Table 4—3) demonstrates that the standard errors of individual standards are small in comparison to the sample signal. Hence, it was expected that most error would be introduced a result of uranium content variation between duplicated Chalk samples. However, these data may be used to estimate a value of detection limit for the analytical method. As described by Skoog et al (2004, Ch.8D-1), an estimate of the detection limit (DL) for analytical methods that employ a calibration curve may be defined as the analyte concentration that yields a response "of a confidence factor k higher than the standard deviation, s_b, of the blank" as given by:

$$DL = \frac{ks_b}{m} \qquad (4\text{-}3)$$

where

m is the calibration sensitivity (i.e. the slope of the calibration curve), and

k is chosen to be 2 (confidence level of 92.1%) or 3 (98.3%).

Employing this equation to the results presented in Figure 4—8 and Table 4—3 yields an lower detection limit of 0.0009 mg.l^{-1} (92.1% confidence) and 0.0014 mg.l^{-1} (98.3%), which is considered sufficient for Chalk uranium assay (where the mean uranium concentration is estimated initially at *c.*0.2 ppm (Younger and Elliot, 1995; Younger and Elliot, 1996).

4.1.4 Calculation of isotopic activity

Given the predominance of ^{238}U (which, as explained in Chapter 2, will comprise most of the uranium atoms present in any sample due to its long half life (c.f. ^{234}U), the activity and an estimate of ^{238}U activity can be estimated from the bulk uranium concentration (as determined in the previous section).

$$A\left[^{238}U\right] = 1000 \cdot \frac{[U]}{10^6} \cdot \frac{1}{238\ (g)} \cdot Av \cdot \lambda_{238} \qquad (4\text{-}4)$$

where

$A\left[^{238}U\right]$ is the uranuium activity assuming all uranium is present as ^{238}U (Bq.kg^{-1})

$[U]$ is the bulk uranium concentration (μg.g^{-1})

Av is Avagadro's number (6.022×10^{23}) and

λ_{238} is the decay constant for uranium-238 (4.881×10^{-18} s^{-1})

This approach may also be used to determine the activity error term.

4.2 Radon (^{222}Rn) activity in water

As outlined in Chapter 1, a primary objective of this thesis was to undertake a temporal and spatial radon survey of groundwater sources (both springs and boreholes) and to test the hypothesis that the radon signature is primarily a function of its source term. Given the potential variation in radon activity observed in the Chalk aquifers (e.g. Low, 1996a), repeated collection of samples from selected locations over time also allows for comparisons to be made with other hydrological data from the same area. As a result, a series of water samples was undertaken from the localities described in Chapter 3 over a period of approximately two years, from January 2005 until January 2007.

4.2.1 Sampling Methods

As radon is a gas, the non-aeration of samples is of critical importance, as waters exposed to air during sampling will naturally lose radon to the air phase. Such aeration may therefore result in an underestimation of the total radon content of the source, with no systematic method to correct for such error. For similar reasons, any significant increase in sample temperature during its collection is also undesirable, given the inverse relationship with radon gas solubility (Clever, 1979).

Hence, although the sampling methods may differ according to location the general protocol for collection and storage of the water samples remained the same in each case. The methods which are described below have been adapted from those developed previously by the BGS when sampling groundwaters for dissolved CFCs (D Gooddy, BGS, *pers comm*).

Springs

Water samples at surface water sites (i.e. at springs and rivers) were collected through sterile PVC tubing that was weighted and lowered beneath the water surface. A peristaltic pump was used to fill 540ml Winchester bottles, sterilized in the laboratory in advance. Each sample bottle was continuously flushed with sample water until at least three bottles volumes had passed through the apparatus. Any possible accidental aeration at this stage was prevented by containing the bottle within a larger bucket and by sealing the sample using an airtight cap. As each sample was collected, it was placed with a cool box to regulate the sample temperature (typically between 9-11 °C). A schematic diagram illustrating the configuration of the sampling components is presented in Figure 4—9.

Boreholes (Open Section)

Water samples from groundwater observation boreholes were initially collected using a small battery operated WaSP-P3B submersible pump. However, after initial trials a low

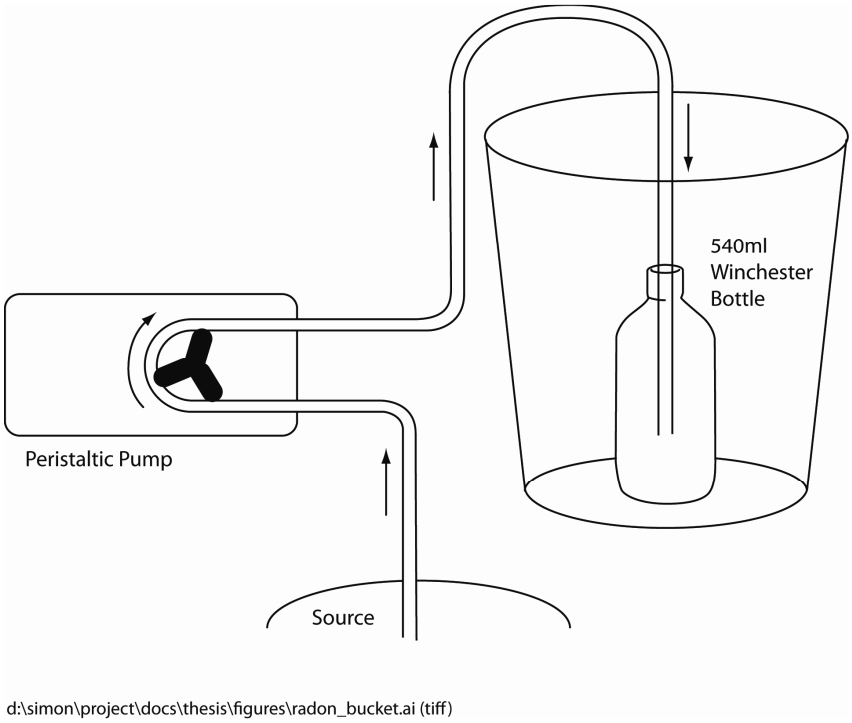

d:\simon\project\docs\thesis\figures\radon_bucket.ai (tiff)

Figure 4—9 Schematic sampling configuration at spring sites

pump rate (<0.1 $l.s^{-1}$) and poor battery performance in the field resulted in the system being replaced by a more powerful and reliable Grundfos MP1 submersible pump. Typical pump rates of 0.5 $l.s^{-1}$ (1.8 $m^3.hr^{-1}$) were achieved for all sites, which enabled several boreholes to be sampled during the course of a single sampling day. In a similar configuration to that used when spring sampling water was abstracted from the borehole without noticeable aeration and was routed by use of a section of nylon tubing into a standard Winchester bottle that was placed at the bottom of a larger container. The container was allowed to overflow continuously throughout pumping, ensuring that the sample bottle was completely submerged at all time.

Each borehole was pumped for approximately 40 minutes, during which time other field variables such as water temperature, conductivity and pH were also measured. Radon samples were taken throughout the pumping process to provide an additional check that samples had equilibrated and were representative of the surrounding formation waters. For larger production borehole pump tests, where the pump rate was too high to feed water through the "bottle and bucket" configuration directly, a sealed sampling tap unit was installed at the well head. An example of a dual sampling line that was used during the pumping of the Bottom Barn borehole at the same time as a fluorescent tracer test is illustrated in Figure 4—10. By adjusting the flow rate through the sampling valve, it was possible to use the "bucket" method to take a series of radon samples without interference with other monitoring equipment.

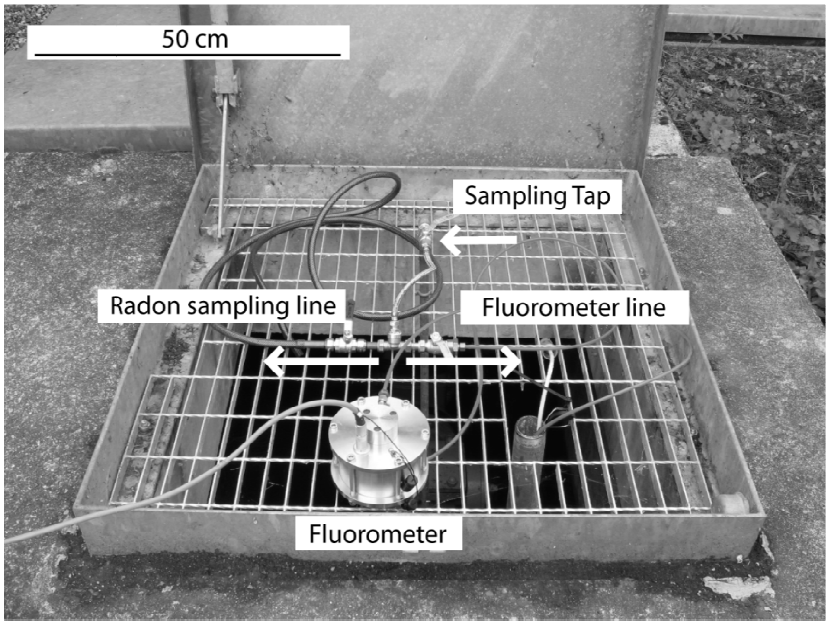

Figure 4—10 Sampling configuration at Bottom Barn abstraction borehole during tracer testing

Boreholes (Discrete Interval Sampling)

Although sampling using a submersible pump in an open borehole may be used to investigate the potential variation in groundwater chemistry with depth, the results may be highly ambiguous. From simply its construction within the aquifer or from the action of sustained pumping, vertical flows induced within the water column may mask any variation of formation waters that flow into the borehole at discrete horizons.

In contrast, packer testing permits the sampling of groundwater from well defined intervals within a borehole and is designed to minimize the mixing of other groundwater sources that may be present when depth sampling.

Packer Design

The development and use of a double packer system is described by the BGS (Williams and Price, 1988) and a schematic diagram of the design is presented in Figure 4—11. The test interval (i.e. the section from where water is pumped) is bounded both above and below by inflatable packers – lengths of reinforced rubber hose, with the ends sealed to short steel cylindrical blocks. A perforated steel pipe of fixed length connects the two packers together and ensures that the distance between them is held constant between tests.

Both packers are inflated using a pressurized gas supply (typically nitrogen) from the surface by means of an single supply line that is connected to both units. Inflation to *c.*8 bar is achieved slowly over a period of *c.*20 minutes; with deflation occurring more slowly (*c.*40 minutes) by simply disconnecting the supply line at ground surface.

To ensure a good seal between the packers and the borehole wall, all gas supply lines and other cables for additional monitoring equipment run inside the perforated pipe from the base of the test interval and up through the top packer. The lines are transferred to the outside of the rising main by use of a "cross over piece" as illustrated in Figure 4—11. This unit is also used to transfer cables from a pressure transmitter unit to within the packered interval, which also provides a means to monitor changes in hydraulic head within the section during pumping.

For ease of construction, the pump is also located somewhat above the test interval, mounted in an stainless steel housing. The pump is connected to the rest of the sealed pipe-work to ensure that all water pumped is taken from between the two packers.

Packer Deployment

As part of the LOCAR programme of works, this double-packer system was used to investigate the variation in hydraulic conductivity of the Chalk at the Trumpletts Farm research site (Williams et al., 2006). These data have been presented previously in this thesis under Section 3.4 (Catchment Hydrogeology).

As part of the radon data collection phase for this thesis, the packer system was re-commissioned from the BGS to investigate the variation in radon activity of formation waters with depth at borehole PL10A (i.e. at the same location as the previous hydraulic conductivity investigation). Four packered intervals of *c.*4 m were sampled between 28 and 45 mbgl, before failure of the equipment prevented further testing at this location. Water was pumped at a rate between 38 and 42 $l.min^{-1}$ (2.3 to 2.5 $m^3.hr^{-1}$) over a period of approximately 30 minutes per section. Given the volume of each test interval, calculated on the basis of caliper log data, this configuration ensured that at least 6 (and up to 14) interval volumes were pumped at each elevation.

Subsequent to packer failure, the equipment was reconfigured to pump continuously from a greater depth, where previously tracer testing had indicated an outflow of water during the pumping of the nearby Bottom Barn abstraction borehole and which was considered to be associated with the increased permeability of the Chalk Rock (Mathias et al., 2007b). Due to a restriction in the borehole, it was not possible to lower the pump casing to the same level of this inflow (i.e. at *c.*81 mbgl, or 26 mAOD). Rather, the base of the pump was located *c* 10 m above the blockage point (which equates to *c.*12 m above the Chalk Rock horizon). At this elevation, entrainment of suspended Chalk debris, presumably produced as a consequence of the partial borehole wall collapse, was considered to have reduced sufficiently to prevent possible damage to the pump equipment.

Groundwater was abstracted continuously for 7 hours at an average rate of 106 $l.min^{-1}$ (6.4 m^3 hr^{-1}), samples being obtained throughout the pumping period and assayed later for radon activity and major ion chemistry. Field measurements for pH, dissolved oxygen, temperature and conductivity were also made at regular intervals during the test.

The results of both the packered tests and open hole test are presented in Section 6.2.2.

Sampling from Packered Intervals - Caveat

Even though a double packer system minimizes the mixing of water from different flow horizons *during* pumping, there can be no knowledge of the mixing that has occurred *before* the test has begun. For example, it may be envisaged that the penetration of an open borehole, through an aquifer with a pre-existing natural vertical hydraulic gradient, may enhance flow between horizons due to the highly permeable conduit for water that now exists. Therefore, one consequence may be that groundwater samples taken from certain horizons may not be representative of the original formations waters.

However, in the case of radon sampling, this effect is suspected to be minimal. As the half life of ^{222}Rn is 3.8 days there can be no long term net effect on the radon content of individual fractured flow paths unless the source term (^{226}Ra) is also transported and subsequently re-precipitated during the lifetime of the borehole's construction. Demonstration of low ^{226}Ra activity within Chalk groundwater and sufficient pumping of each horizon are therefore considered sufficient prerequisites for obtaining representative radon samples from each horizon.

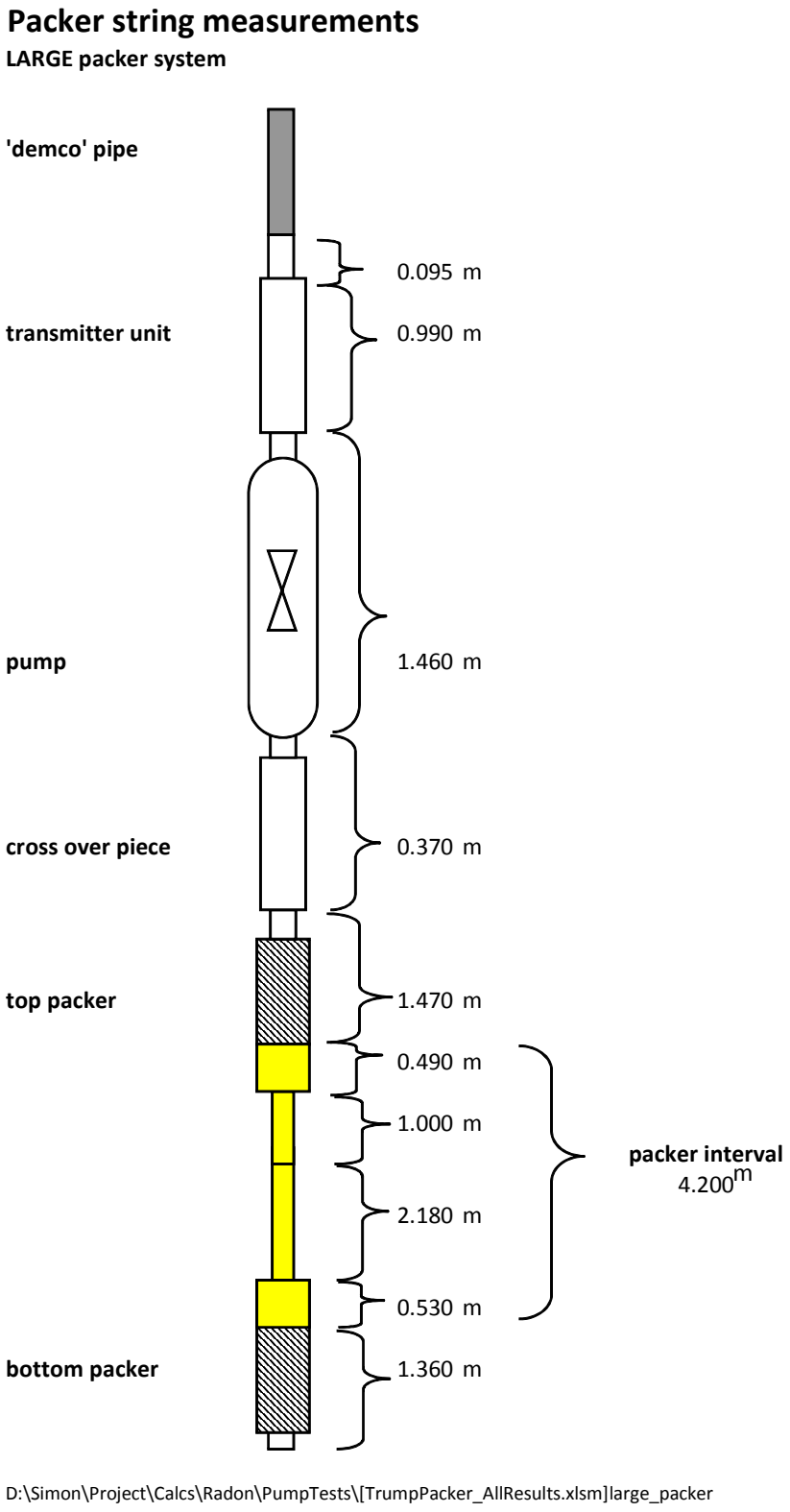

Figure 4—11 Large diameter packer equipment as configured for the discrete interval sampling of the Trumpletts Farm borehole (PL10A)

4.2.2 Radon Sample Extraction and Concentration

The measurement technique, derived from that described by Pates et al (2007) and previously employed by Gresswell (2004), consists of a series of pre-concentration and extraction procedures using toluene, an organic solvent with a known high radon partition coefficient. The concentrated solutions are then assayed by liquid scintillation analysis, the details of which described in Section 4.2.3.

Radon Partitioning

Radon has a greater solubility in many organic solvents such as toluene than compared to water (Clever, 1979), and this property may be used to preferentially extract and concentrate dissolved radon into a separate phase, which can then be used in subsequent analysis (e.g. Prichard and Gesell, 1977; Schubert et al., 2007).

The efficiency of extraction is a function of the partition coefficient (or "Ostwald" coefficient) of radon between toluene and water, and possibly also that of air and water of the sample if air has been entrained into the sample. As such coefficients are defined in terms of a *concentration ratio*, it is also appropriate to take into account the relative volumes in question to determine the distribution of actual mass (and hence activity) between the different phases.

For example in a three phase system (water-toluene-air):

$$\mathrm{A_{total}} = \mathrm{V_{air}}[\mathrm{Rn}]_{\mathrm{air}} + \mathrm{V_{tol}}[\mathrm{Rn}]_{\mathrm{tol}} + \mathrm{V_{aq}}[\mathrm{Rn}]_{\mathrm{aq}} \qquad (4\text{-}5)$$

where A is the activity, V is the volume and $[Rn]$ is the concentration of radon of each phase. Therefore, at equilibrium, the expected relative activity within the toluene phase can be expressed as:

$$\frac{\mathrm{A_{tol}}}{\mathrm{A_{total}}} = \frac{\mathrm{V_{tol}}[\mathrm{Rn}]_{\mathrm{tol}}}{\mathrm{V_{air}}[\mathrm{Rn}]_{\mathrm{air}} + \mathrm{V_{tol}}[\mathrm{Rn}]_{\mathrm{tol}} + \mathrm{V_{aq}}[\mathrm{Rn}]_{\mathrm{aq}}} \qquad (4\text{-}6)$$

By definition the Ostwald coefficients are represented by:

$$\mathrm{L_W} = \frac{[\mathrm{Rn}]_{\mathrm{aq}}}{[\mathrm{Rn}]_{\mathrm{air}}} \quad ; \quad \mathrm{L_T} = \frac{[\mathrm{Rn}]_{\mathrm{tol}}}{[\mathrm{Rn}]_{\mathrm{air}}} \qquad (4\text{-}7)$$

Hence, by substitution and simplification, the radon activity fraction in toluene can now be expressed in terms of volumes and partition coefficients only:

$$\frac{A_{tol}}{A_{total}} = \frac{V_{tol}L_T}{V_{air} + V_{tol}L_T + V_{aq}L_W} \qquad (4\text{-}8)$$

As radon is a gas its solubility will change as a function of temperature and hence the Ostwald coefficients for radon are not constant. Although the variation in the coefficient for radon in water as a function of temperature has been derived empirically and is reported extensively by Clever (1979), fewer data are available for that of toluene. However, more recent estimates of L_T at room temperatures have been made by Bem et al (1994), Theodorsson (1996) and also by Schubert et al (2007).

Assuming average values for Ostwald coefficients (L_T = 13.2, L_W = 0.25, both at 20 °C), the calculated effect of variation in the toluene extracted fraction as a function of the water/toluene volume ratio can be determined. Figure 4—12 illustrates an example where no air is present in the sample container. Calculation of the ratio L_T/L_W in this case (52.8) highlights the unequal distribution of radon gas between the water and toluene phases. For the example of a 540ml Winchester sample bottle, in which 30ml of the water has been removed and replaced with toluene, the extraction efficiency of the toluene phase is estimated at 75.6% of the total mass of radon in solution.

However, as is apparent from Equation *(4-6)*, there will be a reduction in the toluene extraction efficiency if air is also present in the sample bottle. The theoretical effects on the reduction in radon extracted into the toluene phase as a result of entrained air are tabulated in Table 4—4. These results have been calculated for air representing 1%, 5% and 10% of the total sample volume, with the assumption that the solutions are well mixed and have achieved partition equilibrium.

It is clear from this calculation that small amounts of trapped air in the sample bottle do not significantly alter the extraction efficiency of toluene. For an air bubble that is equivalent to 1% of the total sample volume (*c.*5ml for a standard 540 ml Winchester sample bottle with an internal polycone seal), and for a water to toluene volume ratio of 17:1 (the ratio chosen above), the net effect is a reduction in radon extraction of 0.7%. Comparisons with other potential sources of error is the sampling method are evaluated in Section 4.2.5.

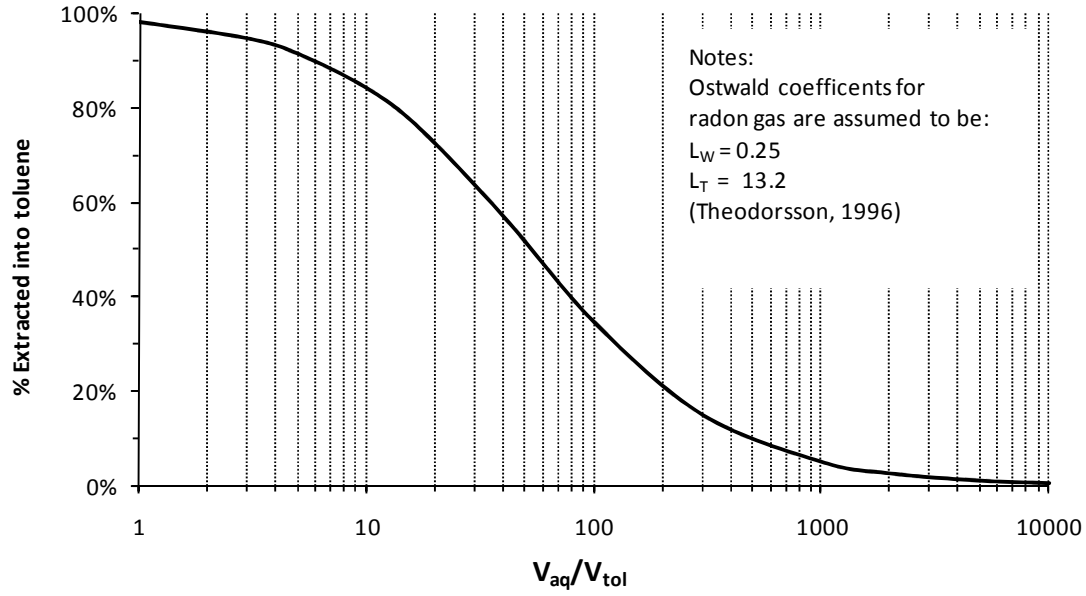

d:\simon\project\calcs\stats\[rn_analyticalmethods_xl97.xlsm]tricarb

Figure 4—12 Toluene radon extraction efficiency for a two phase system as a function of the ratio between the relative volumes of water and toluene (at equilibrium, 20 °C)

Table 4—4 Toluene radon extraction efficiency for a three phase system (toluene/water/air), as a function of air fraction for relative volumes of water and toluene.

V_{aq}/V_{tol}	*No air present*	V_{air} (1%)	V_{air} (5%)	V_{air} (10%)
1	98.1%	98.0%	97.4%	96.5%
3	94.6%	94.4%	93.2%	91.7%
5	91.3%	91.0%	89.4%	87.3%
10	84.1%	83.5%	81.1%	78.0%
17	**75.6%**	**74.9%**	**71.7%**	**67.9%**
40	56.9%	55.9%	52.1%	47.6%
100	34.6%	33.7%	30.3%	26.7%
300	15.0%	14.5%	12.7%	10.9%
1000	5.0%	4.8%	4.2%	3.5%

Note: Bold cells indicate the V_{aq}/V_{tol} ratio used in subsequent machine calibration and field sample extractions
Calculation source: d:\simon\project\calcs\stats\[rn_analyticalmethods_xl97.xlsm]partition

Procedure

Due to the short half life of radon, field samples were processed in the laboratory typically within 24 hours of sampling. Additionally, as each of the analyses was performed in series, the batch size was also limited to 20 at any one time to ensure that all samples were assayed within one ^{222}Rn half life since field collection, thus maximizing the potential for radon count detection above background. A schematic diagram indicating the procedure for sample analysis is presented in Figure 4—13.

In a fume cupboard, 30ml of water were carefully removed from each bottle and quickly replaced with an equivalent volume of Analar grade toluene. The bottles were resealed and shaken vigorously for a minimum of five minutes, before being allowed to settle. After approximately one hour, the bottles were inspected to ensure that the toluene and water phases had fully separated.

In preparation for analysis by liquid scintillation, 10 ml of Ultima Gold LLT scintillant were pipetted into a 20 ml Teflon coated low diffusion plastic vial, supplied by Perkin Elmer Inc. 10 ml of toluene extracted from each sample bottle were then pipetted slowly into the scintillation vial, ensuring that the pipette tip remained below the meniscus of the scintillant throughout to minimize the loss of radon to the atmosphere. The vial was sealed with a cap lined with aluminium foil and the contents were gently mixed. The vial was then left for a least four hours, to allow the radon daughter products to reach secular equilibrium (as discussed previously in Section 2.1.1).

Extension

For a sub-selection of sample bottles, the toluene removed was replaced by fresh stock, the bottle resealed and placed in an inverted position to prevent the accidental loss of toluene through the cap seal. After storage for at least 30 days (equivalent to *c.*8 half lives of ^{222}Rn), the sample was analyzed once more for radon. After this time the natural decay of any unsupported radon will have decreased to at least $1/2^8$ (0.0039) of that present at the time of field sampling and, in general, will be below the limit of detection (see Section 4.2.4 for a discussion on the calculated detection limit for this method).

Therefore, by inference, the continuing presence of radon in the sample indicates that it is supported from a dissolved source (i.e. ^{226}Ra). In addition, as secular equilibrium will have been achieved by this time (as explained in Section 2.1.5), the activity of radium can be inferred directly from that of its radon daughter product.

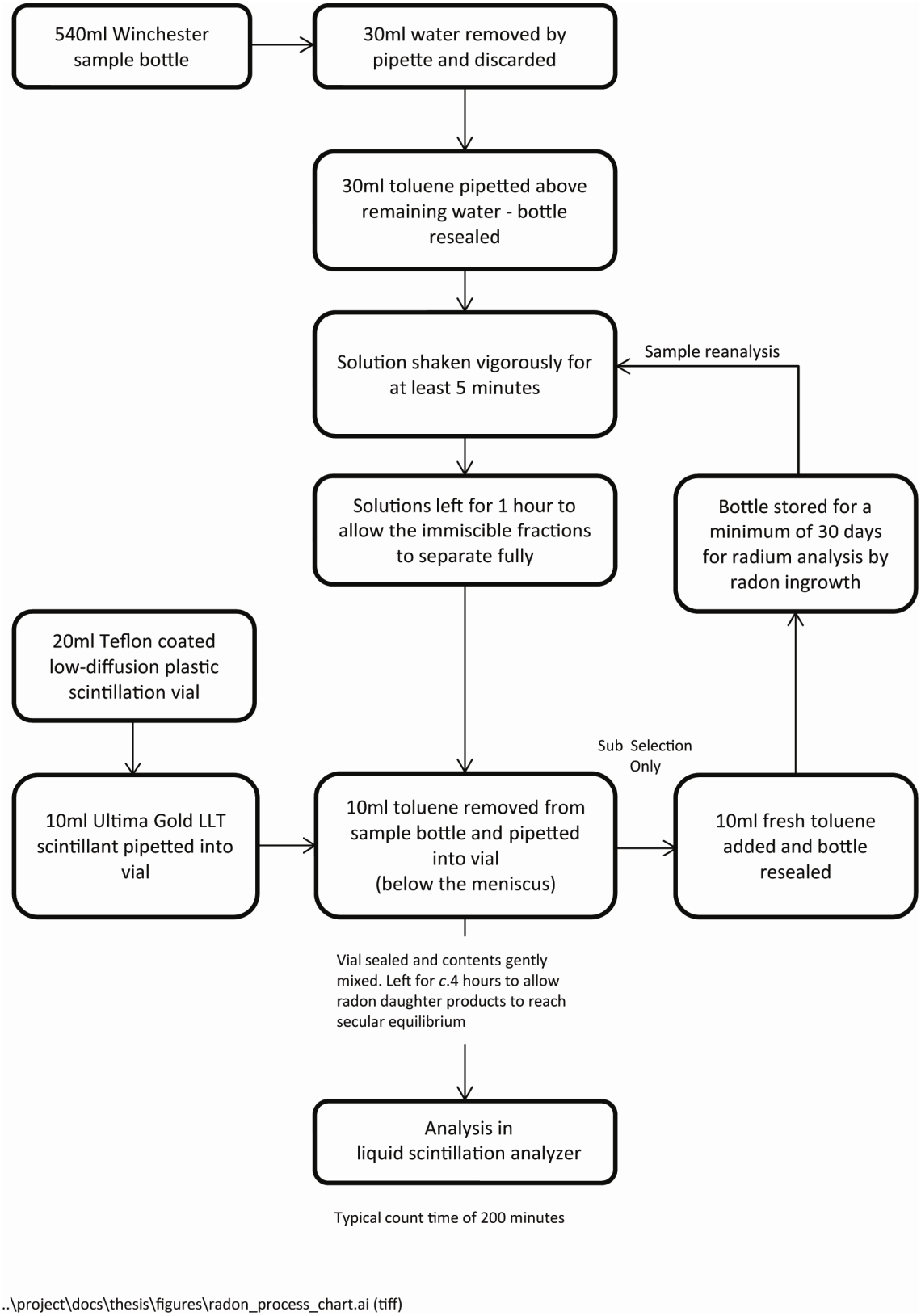

..\project\docs\thesis\figures\radon_process_chart.ai (tiff)

Figure 4—13 Radon analysis process chart

4.2.3 Liquid Scintillation Analysis

Scintillation is the term given to the method of detecting ionizing radiation by observation of energy loss through its interaction with a luminescent material. Liquid scintillation in particular allows such measurements to be made in solvents to which a "fluor" has been added (i.e. a fluorescent chemical which releases adsorbed energy as light). It is ideally suited to the detection of radiation types that have low penetrations, for example α and low energy β-particles. Such particles are easily prevented from penetrating the walls of most detectors by the presence of physical shielding (e.g. lead), leading to a low background noise within the sample chamber.

Historically, the technique was developed by Reynolds et al (1950), who constructed a detection device consisting of two diametrically opposed photomultiplier tubes and a accompanying coincidence circuit – a configuration which assures that genuine light pulses which reach both tubes are counted, whilst spurious electronic pulses, which are normally recorded by only one tube, can be ignored. In this way, the unit differentiates between actual photon emission from liquids and electromagnetic background interference. Moreover, it is also possible to infer the energy of the original particle through analysis of the pulse height recorded by the photomultiplier tubes (Prichard et al., 1992) and in this way liquid scintillation counters can also be used as a form of particle energy spectrometer.

Two liquid scintillation analyzers were used, both of which were able to measure alpha and beta activity in an energy window of between 0 and 2000 keV – initially a TriCarb 2260XL (Packard) that measured total activity and subsequently a TriCarb 2900TR (Perkin Elmer) which included the ability to perform α/β separation based on pulse shape discrimination (PSD). As will be described, the use of such signal separation permitted an increase in the number of groundwater samples that could be analysed in a single batch without severely affecting the overall counting statistics.

Scintillation Cocktail

Scintillation cocktails are designed to maximize the detection of emitted photons and are selected on the basis of the nuclide under investigation and the solvent in which it is being carried. In this study, Ultima Gold LLT (Perkin Elmer Inc.) was chosen – a proprietary di-isopropyl naphthalene (DIN) based cocktail that contains the primary scintillant 2,5-diphenyloxazole (PPO) and which is designed specifically for the assay of tritium, ^{3}H. However, its properties have also been demonstrated to be suitable for efficient α/β separation when mixed with solvents such as toluene, and has previously been used in other radon extraction studies (Pates and Mullinger, 2007).

The chemical structure of the major components are presented in Table 4—5. DIN based solvents, such as Ultima Gold, demonstrate a high efficiency in both absorbing radiative energy from the ionizing particles and transferring it to the scintillant (Pates et al., 1993). Such solvents also show a minimum of adsorption of the light emitted, which is important for maintaining high count efficiency (Thomson, 1991). The scintillant PPO has also been shown to have a high absorption of energy from solvent molecules and good chemical stability (Brooks, 1979).

Table 4—5 Chemical structure of major scintillation cocktail components (Ultima Gold LLT)

Chemical Name	*Formula*	*Structure*
Di-isopropyl naphthalene (solvent)	$(C_3H_7)_2C_{10}H_6$	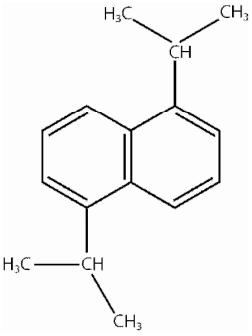
PPO [2,5-diphenyloxazole] (scintillant)	$C_{15}H_{11}NO$	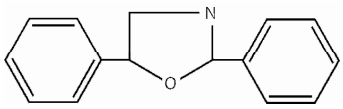

Quenching Effects

Quenching decreases the number of decay pulses observed by the photomultiplier tubes. It can be caused by either components with the scintillation cocktail that interfere with the transfer of energy from solvent to fluor (chemical quenching), or from the adsorption of the photons within the sample (colour quenching).

The degree of quench is calculated by both analyzers by use of a low energy external standard γ-ray source (^{133}Ba) and the calculation of a spectral index (often referred to in the literature as "tSIE", or the transformed Spectral Index of External standard). By recording the energy distribution of the recorded counts the index reflects both the maximum energy of the sample pulse height spectrum as well as the magnitude and shape of the spectrum (L'Annunziata and Kessler, 2003). Values of tSIE tend to decrease as the sample quench increases, reflecting a decrease in counting efficiency, a downward shift in the pulse height spectrum and a reduction in the value of the mean pulse height.

The majority of groundwater samples analyzed as part of this thesis had tSIE values that were approximately equal to that of the background vials analyzed at the same time. Similar observations have been previously by Pates and Mullinger (2007) when performing radon assay that included a pre-concentration stage. Hence, correcting for variable quench was not considered critical to this study, as the extraction method prevented major quenching agents being present in the vial.

Where samples did have a reduction in count efficiency, this was thought due to changes in colour from clear to light brown, possibly as a result of the extraction of organic material in to the toluene phase during radon extraction. However, this effect was observed in samples from only one location – the pond south of Parsonage Farm on the River Pang. Samples from this site had a high degree of sediment suspension and in extreme cases the toluene extraction method was abandoned, due to the poor separation of water and toluene in the sample bottle.

Alpha beta separation

The energies of alpha and beta particles produced as part of the radon decay series differ substantially. As explained previously in Section 2.1.3, the decay chain from ^{222}Rn to ^{214}Po releases three alpha particles of energies 5.49, 6.11 and 7.83 MeV (in relation to the decay of ^{222}Rn, ^{218}Po and ^{214}Po) whereas the two beta particles have an energy spread between 0.69 to 3.26 MeV (^{214}Pb and ^{214}Bi respectively). In methods with good peak resolution it should therefore be possible to indentify the three alpha particles, without interference from beta decay and the natural machine background (caused in part through cosmic ray interactions with the machine apparatus and natural radiation in its construction materials). However, this is not the case with liquid scintillation and the alpha particles cannot usually be differentiated from beta particles by light intensity, due to the differences in efficiency in which the particles interact with the scintillation cocktail.

In reality, the energies of the alpha particles recorded by liquid scintillation are approximately one tenth of their theoretical maximum (the actual and measured energies of the alpha particles produced as part of the radon decay series are summarized in Table 4—6). An unfortunate consequence of this effect is to make the energy distributions for alpha and beta particles (partially) overlap. With the addition of a naturally occurring beta background, it is therefore difficult to achieve the low detection thresholds that are associated with other methods of detection, such as alpha spectrometry.

Table 4—6 Comparison between actual and measured alpha particle emission energy for predominant decay products of the ^{222}Rn decay series.

Decaying Nuclide	*Alpha Particle Energy*[1] *(MeV)*	*Typical energy record by LSC using UGLLT scintillation cocktail (keV)*
^{222}Rn	5.49	390
^{218}Po	6.11	455
^{214}Po	7.83	675

[1]Ivanovich and Harmon (1992)

However, with appropriate signal processing it is possible to separate the two types of particle through analysis of their pulse decay shapes as recorded by the photomultiplier tubes (e.g. Pates et al., 1993). Depending on the form of the excitation of the scintillation cocktail, electrons can enter a number of different "states" as illustrated previously in Figure 4—4. As noted by Pates et al (1983), the higher ionization of alpha particles causes a greater number of electron triplet states to be formed by alpha particles; the physical consequences of which results in the observed pulse decay time being longer, due to a greater component of the pulse produced through the mechanism of phosphorescence rather than (singlet state) fluorescence. A simplified diagram illustrating the difference in pulse shape between alpha and beta particles with the same initial light intensity is shown in Figure 4—14.

Pulse Decay Discrimination (PDD)

Therefore, with suitable signal processing, the differences in the rate of pulse decay can be used to discriminate between the two particles types. However, the decay rate differences between alpha and beta particles may be a function of many parameters, including the nuclide of interest and also cocktail type (e.g. Prichard et al., 1992; Pates et al., 1993; Bem et al., 1994).

With the Tri Carb 2900TR, it is possible to vary a time-gate parameter called the "pulse decay discriminator" (PDD), to ensure that the maximum number of true alpha events can be recorded without misclassification. Setting the PDD too low can result in true beta events being recorded within the alpha channel. Conversely, setting of the value too high can result in true alpha events being recorded as beta and risk being discarded.

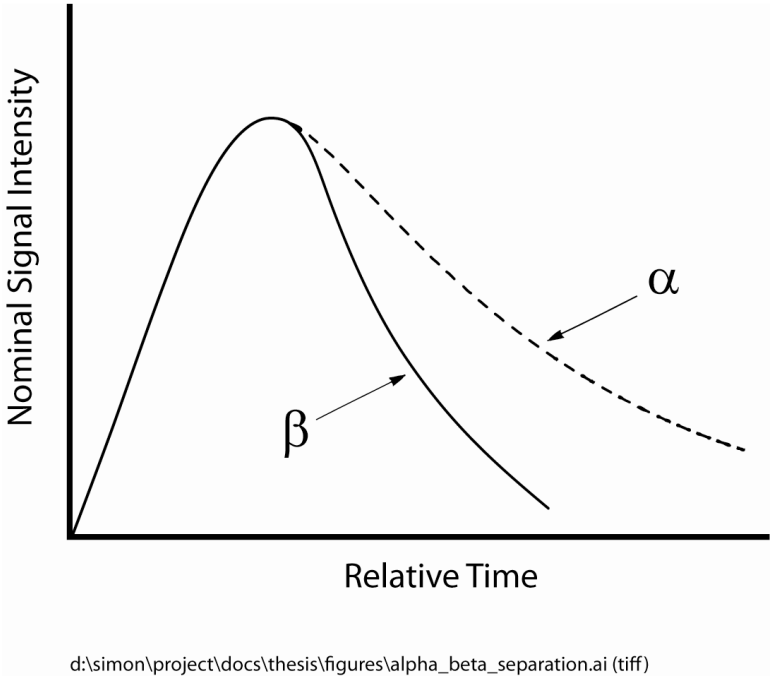

Figure 4—14 Representative light pulse shapes for alpha and beta particles recorded by a liquid scintillant (modified from Passo and Cook (1994))

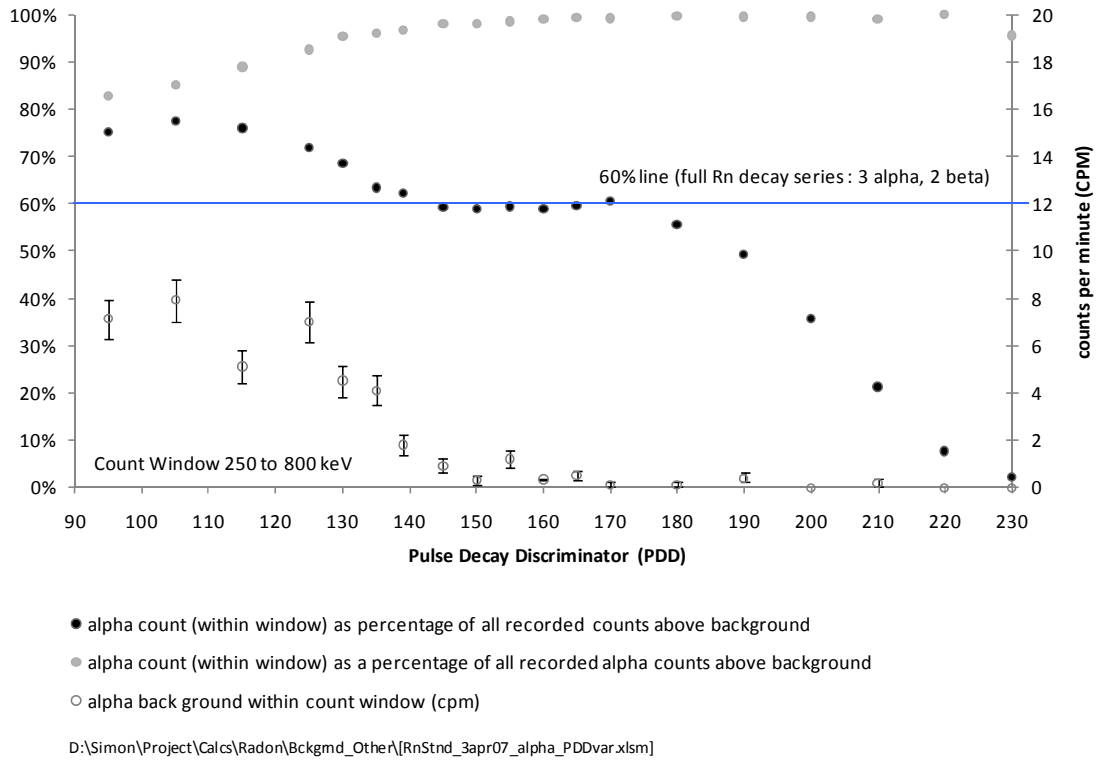

Figure 4—15 Relative counting efficiency for the alpha channel versus Pulse Decay Discriminator (PDD) setting with Ultima Gold LLT scintillant.

To set the value of PDD correctly a methodology similar to that described by Pates and Mullinger (2007) was adopted. Assuming that the counting efficiency of the counter is 100% (typical in such equipment, given the geometry of the vial and counting chamber), the optimum value for the discriminator should result in 60% of the counts measured for a radon standard that has reached secular equilibrium being classified as alpha decay (i.e. there are 3 alpha decays and 2 beta decays in the radon decay series).

To validate this method of calibration, a radon standard was repeatedly analysed over short count times (10 min) for a range of different discriminator settings. For each repeat analysis a separate blank vial was also measured to assess any change in the background count in the alpha channel. The result from this work are presented in Figure 4—15. For each PDD setting, the total number of counts recorded in the alpha channel is expressed in terms of a percentage of the total number of counts recorded (minus the background count). The form of the curve, similar to that presented by Pates and Mullinger (2007), shows a plateau of the alpha counts recorded at *c.*60% of the total counts recorded. Therefore, for a PDD setting of between c.140 to 170 the machine is able to differentiate well between alpha and beta events, i.e. without significant misclassification. Setting of the PDD for radon assay between these limits is therefore appropriate.

The variation in alpha background counts are also plotted on the same figure. As might be expected, the background count rate is high for low values of PDD, a consequence of too many natural background beta decays being misclassified as alpha decay. However, at a PDD of 165 the background count rate is reduced to *c.*0.5 cpm, whilst misclassification is remains at a minimum. This setting therefore represents the optimum setting for this sample configuration and cocktail choice.

An example of the distribution of discriminated counts for a high standard (10.1 $Bq.l^{-1}$) is presented in Figure 4—16. In the alpha channel, three overlapping peaks may be identified, which correspond to the three alpha particles emitted in the decay chain. Although the exact alpha particle energies are well known, each resulting spectrum is spread in liquid scintillation analysis over several hundred keV, considered due to alpha interactions with the solvent and the optical properties of the scintillation vial itself. Background counts are low in comparison to the signal, demonstrating the efficiency of pulse discrimination.

In the beta channel, a wide spectrum of energies is observed, reflecting the contribution from the decay of ^{214}Pb and ^{214}Bi. High background counts at lower energies are

considered due to cosmic ray interactions producing Cherenkov radiation, secondary electrons and gamma rays, all of which may be detected by the machine's photomultiplier tubes (Passo and Cook, 1994). Fortunately, few such background counts are misclassified by time-resolved discrimination as alpha events and so the background in this channel remains low.

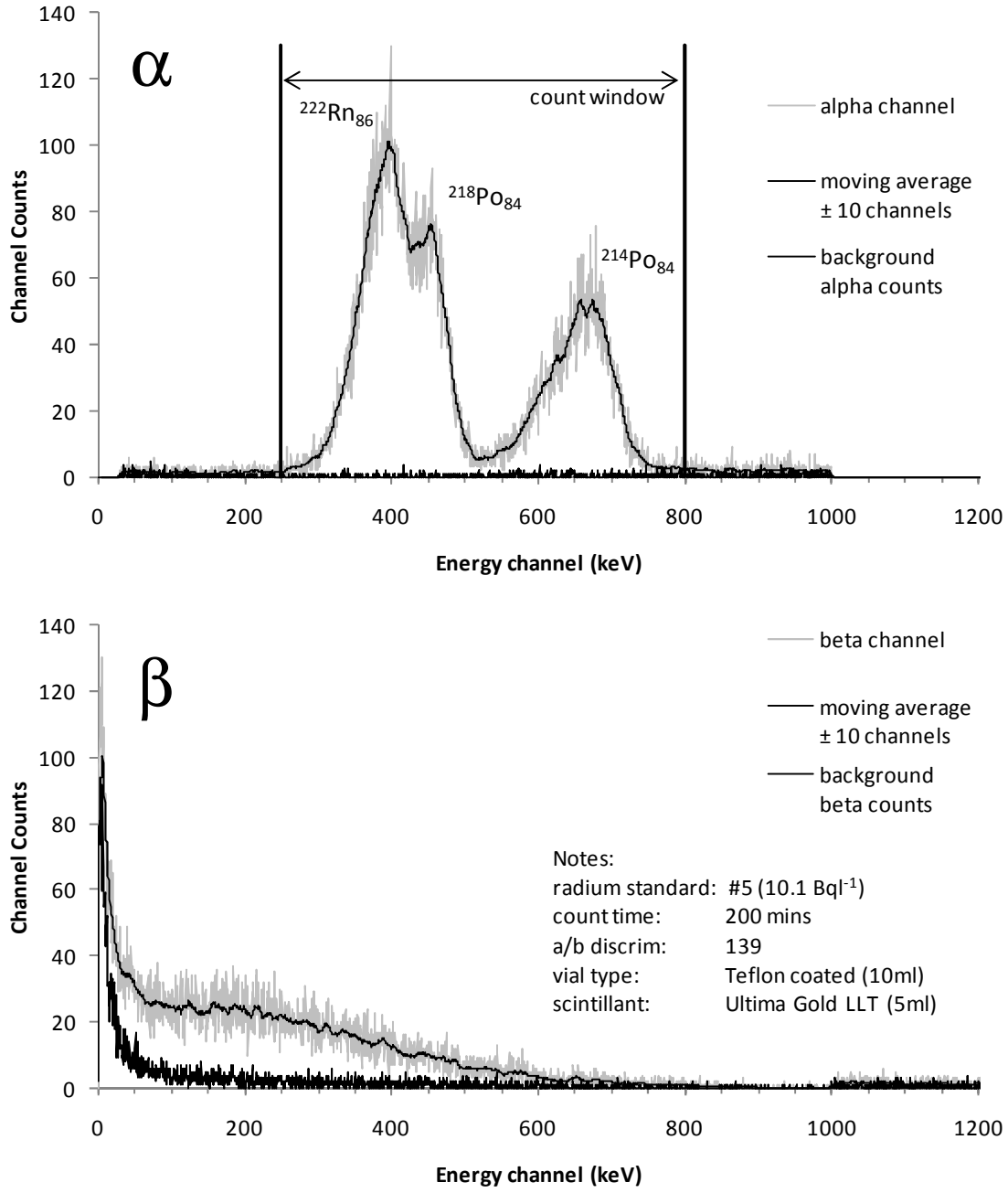

Figure 4—16 Example of the total counts recorded for an aqueous radium standard by a Perkin-Elmer TriCarb 2900TR liquid scintillation analyzer.

Vial selection

Teflon coated low diffusion plastic vials were used throughout the investigation. These were chosen initially on the basis that they have been specifically developed to provide better energy resolution and lower background beta counts, due to the absence of ^{40}K and reflective surfaces typical in standard glass vials (Perkin Elmer Inc, *pers comm*).

However, a known disadvantage of using plastic is for the potential for radon to sorb to and potentially diffuse through the material, reducing the activity within the vial. Although Escobar (1996) demonstrated that such effects were negligible even after one month, Passo and Cook (1994) noted that *c.*9 days after preparation the percentage of pulse misclassification (i.e. true alphas being recorded as betas and vice versa) increased from *c.*0.5% to 1% of the total activity. One potential impact of this effect would be to increase the alpha background count rate over time, as background counts may be included within the alpha channel with greater probability over the sampling time.

Analysis of the decay of the same radon standard, within both plastic and glass vials, confirmed in fact that both types were suitable for use. Estimates of the half-life and its standard error, calculated from regression analysis of the decay curve, indicate that both methods produce values that overlap with the true 222Rn half life value of 3.82 days (

Figure 4—17). However, given the limited analysis time adopted for the plastic vial the range of the standard error for the calculated radon half-life was slightly greater (3.77 days $< t_{½} <$ 3.90 days) when compared to that of glass (3.80 days $< t_{½} <$ 3.83 days).

An interesting observation in this experiment is the lower overall background in the alpha channel for the glass vial - a result seemingly contrary to the original decision to select plastic vials on the basis of their low levels of radioisotope impurity. As the total (i.e. non discriminated) background for glass vials was always greater than that from plastic, this result suggests that either a) the optimum setting for the pulse decay discriminator (PDD) varies according to the vial type or that b) in general there are fewer event misclassifications with glass vials. Further work would need to be undertaken to determine which of these processes dominate.

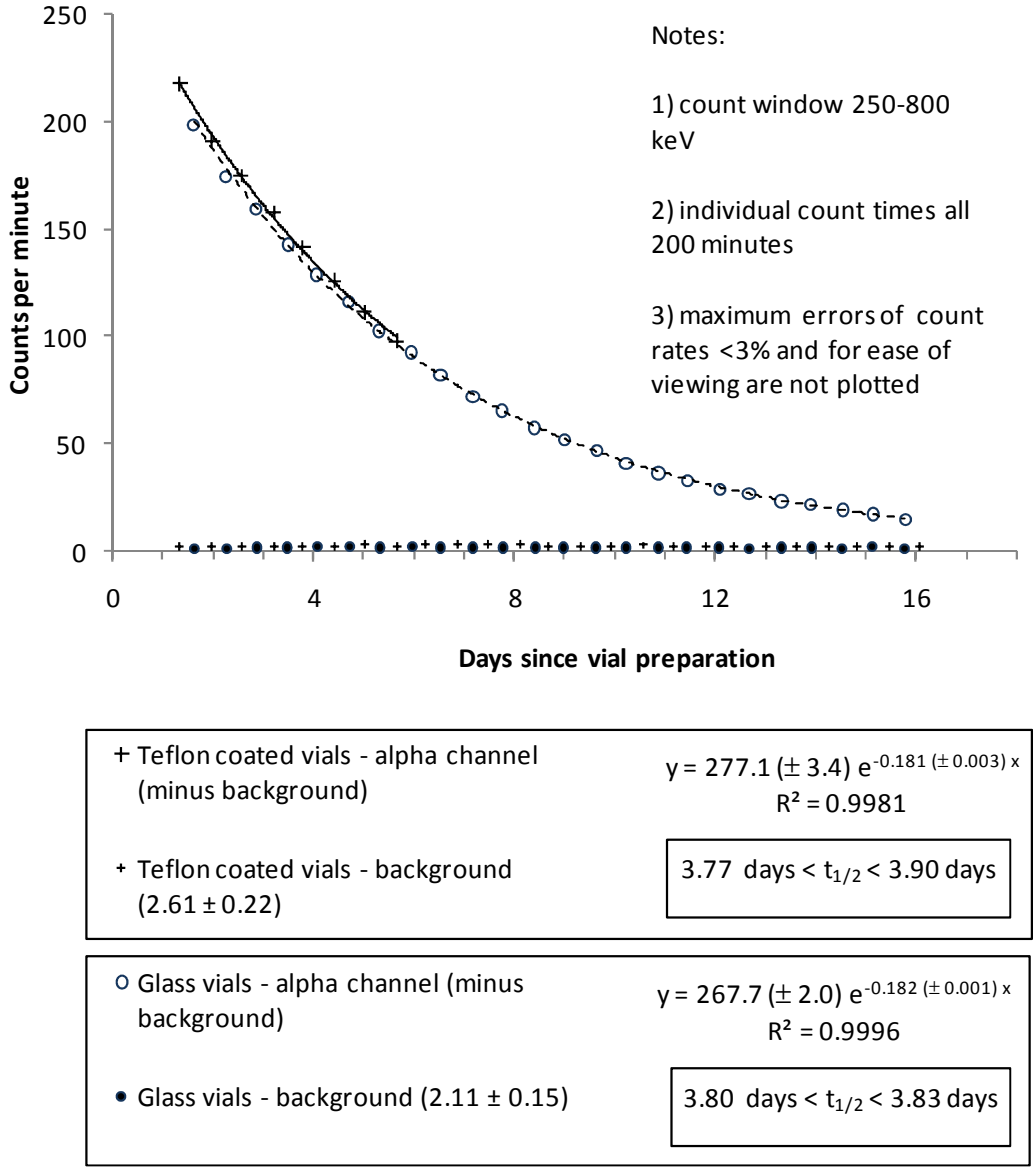

Figure 4—17 Comparison of radon standard decay curves between plastic and glass vials.

Count region

Although the TriCarb 2900TR records the total number of counts in each of the available 0.5 keV energy channels (i.e. from 0.5 to 2000 keV), the actual count window is often reduced to improve the signal-to-background ratio. In liquid scintillation studies it is typical to express this ratio as the square of the detection efficiency divided by the background and is termed the Figure of Merit (FOM) (e.g. Passo and Cook, 1994).

$$FOM = \frac{E^2}{B} \qquad (4\text{-}9)$$

where E is the count efficiency (%) and B is the background count rate (CPM)

The variation in this value for a typical radon analysis is illustrated in Figure 4—18. In this case, a known standard was prepared by the normal liquid-liquid extraction process. By careful weighing before toluene extraction (and again after refilling), it is possible to determine the water:toluene:air ratio within the sample bottle. From calculation of the theoretical partitioning of radon into the toluene phase, and knowledge of the volume removed for analysis, it is then possible to estimate the total alpha activity within the scintillation vial.

Through comparison between the theoretical and measured activity, it is possible therefore to estimate the count efficiency for any given window[3]. Additional measurement of a blank toluene/Ultima Gold LLT solution provides an estimate of the background count rate.

The results demonstrate that optimization of the count window can provide large gains in the Figure of Merit, which by implication will decrease the overall radon limit of detection.

[3] It should be noted however that by this method there is no independent measurement of the toluene extraction efficiency or measurement of any loss of radon that has occured during the transfer of toluene from the sample bottle into the scintillation vial. As a consequence it is likely that the count efficiency of the liquid scintillation anaylzer will be underestimated by the approach adopted, as these other losses will have been incorporated within the calculation. In a study focused on method development Pates and Mullinger (2007) used γ-spectrometry to determine true vial activity and hence were able to compare the observed radon extraction efficiency of toluene with its theoretical value, as well as assess the counting efficiency of their apparatus for a selected count window (specifically 200-800keV). However, as they also note, it is "not necessary to determine absolute counting efficiency and absolute extraction efficiency for routine applications". In this thesis the demonstration of a stable calibration curve using radium standards that cover over a degree of magnitude in activity is considered sufficient for the purposes of routine radon assay.

The chosen count window configuration for radon assay is also plotted on Figure 4—18. The discrepancy between this choice and the potential maximum value of FOM is clear – the window selected is much wider than the 'optimum' range. However, the more precautionary window has been adopted as the energy distribution of the counts recorded within the alpha channel tended to vary slightly from sample to sample (a phenomenon which was considered a function of small changes in sample quench). By increasing the window to cover the entire alpha signal, the impact of this variation on count efficiency was minimized. Such use of wide count window is apparent in other similar liquid scintillation studies (e.g. Prichard and Gesell, 1977; Freyer et al., 1997; Pates and Mullinger, 2007).

Calibration Curve

Fourteen standards were analyzed at regular intervals throughout the analysis period, to determine the count efficiency of the scintillation analyzer over the range of possible environmental radon concentrations. The standards consisted of radium solutions of

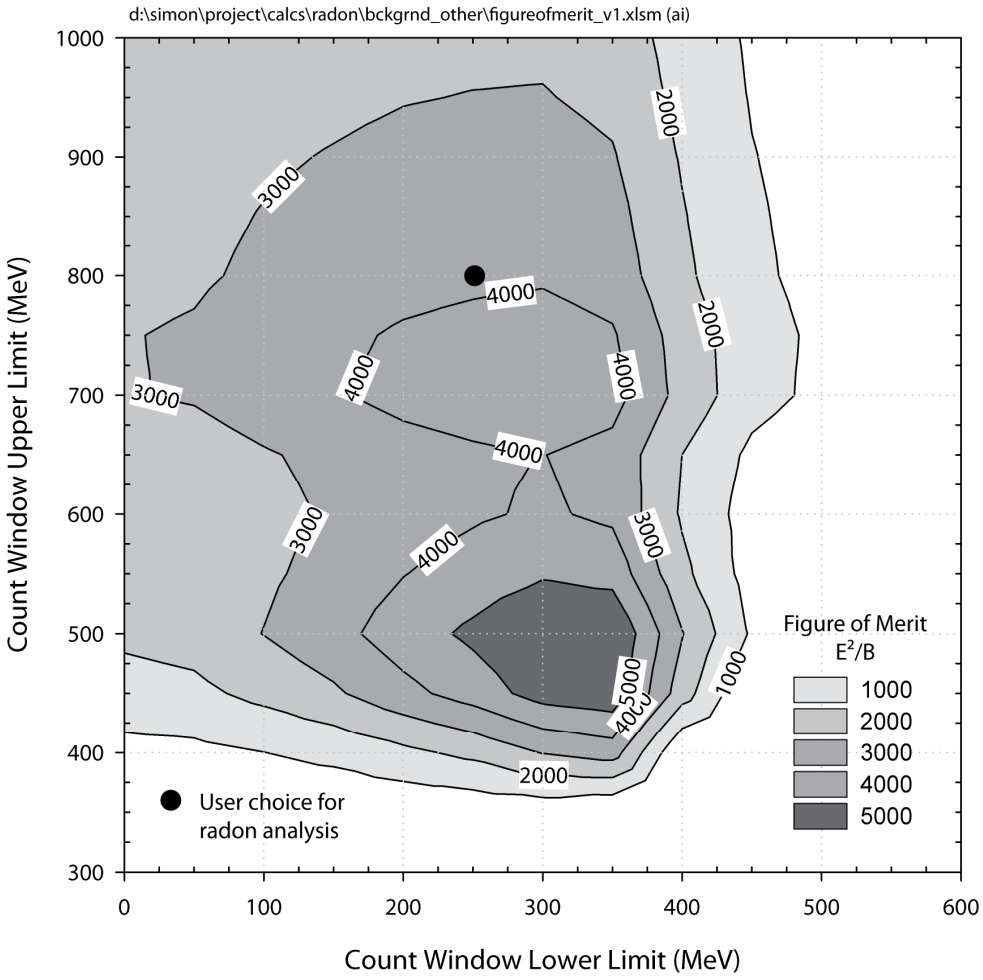

Figure 4—18 Contoured values of Figure of Merit (E^2/B) for radon standard #1A (1.56 $Bq.l^{-1}$), counted on a Perkin Elmer TriCarb 2900TR LSC for 200 minutes (alpha channel only)

known activity which had been prepared previously at the University of East Anglia and which were used by Low (1996b) for the calibration of a gas scintillation cell. The standards were subsequently decanted at University College London into 540ml Winchester bottles, which were identical to those used in during all subsequent field sampling (Gresswell, 2004).

To ensure that the measurement of standards was as similar as possible to field samples, 30ml of each standard was discarded and replaced with Analar grade toluene. The bottles were then stored for at least 40 days at a time, to allow for secular equilibrium between radium and its decay products to be achieved. As a further precaution, the bottles were stored in an inverted position to prevent accident loss of toluene through the bottle cap and seal. Each standard was weighed before and after toluene extraction, to determine if there had been a reduction in toluene volume during storage. If air was present, its volume was calculated from the difference in weight after refilling. The theoretical extraction efficiency was adjusted accordingly to take its presence into account (as discussed previously in Section 4.2.2).

As with field samples, all standards were shaken for at least 5 min by hand and allowed to settle for approximately one hour before toluene extraction. 10 ml of toluene was then removed and added to a low diffusion plastic vial prepared with 10 ml of Ultima Gold LLT scintillation cocktail. The vials were then loaded into the scintillation counter, stored for 4 hours to allow for secular equilibrium to be achieved and then counted for 200 minutes. Several vials of fresh toluene and scintillant were analyzed during each run to measure the background count rate. After the batch was completed, the count rates were time corrected to infer the activity present at the time of preparation, with the count standard deviation adjusted proportionally.

A comparison was made of the theoretical activity of the vial (given the known standard activity and the calculated toluene extraction efficiency) and that measured by the machine. The resulting calibration curve is presented in Figure 4—19, with each data point representing a single standard measurement. A coefficient of determination (R^2) value of 0.997 and narrow 95% confidence limits indicate that the relationship is strongly positively correlated.

The regression also suggests that the counting efficiency of the machine remains constant over the range of radium standards.

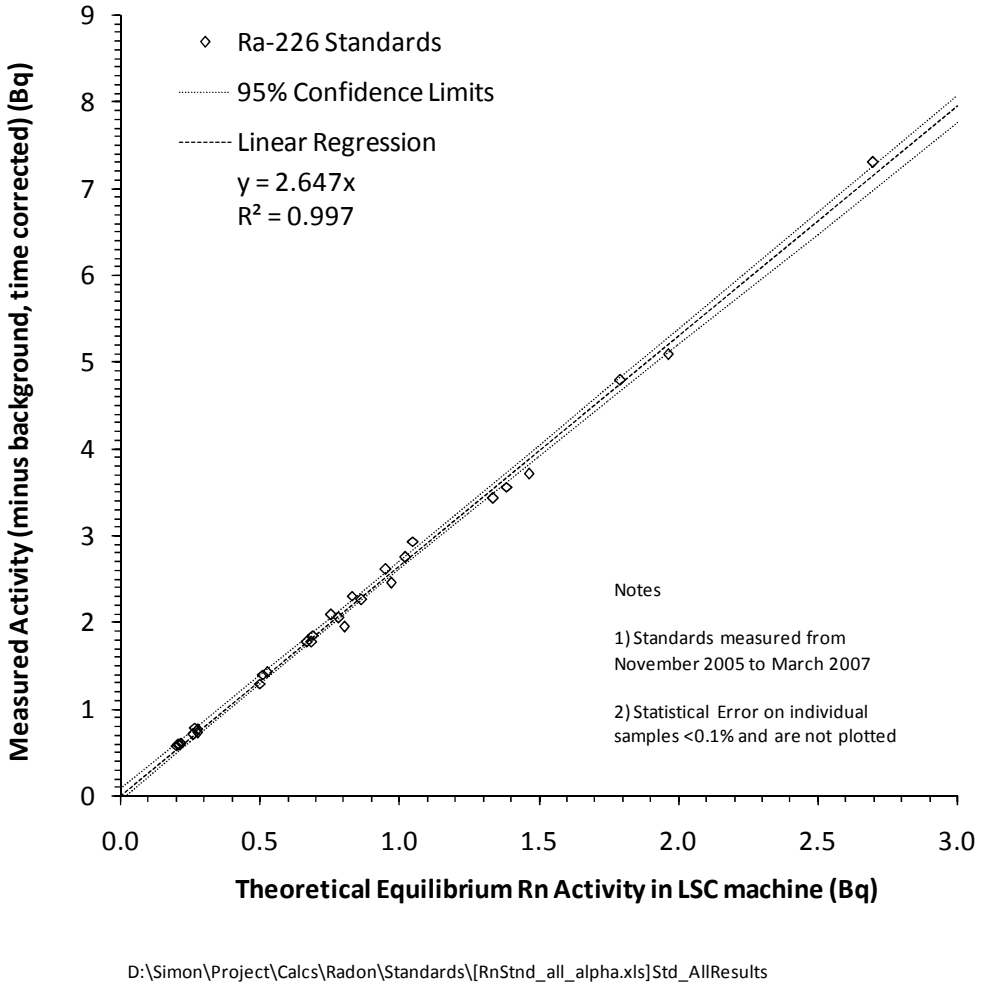

Figure 4—19 Calibration curve for Packard TriCarb 2900TR using radium-226 standard solutions.

4.2.4 Detection limits

A detection limit in its most general form can be described as the signal required above background which indicates the presence of the nuclide of interest. However, as noted by others, no universal method is employed for calculating such a value, due in part to the statistical nature of particle counting (e.g. Prichard et al., 1992).

Currie (1968) describes a method for calculating limits that are based on the probability of detection are particularly suitable to radiochemistry. Three distinct levels of detection are defined, each of which is based on hypothesis testing. They can be defined as follows:

i. a "decision" limit, L_C, at which level it is possible to conclude with a given probability that a signal has been "detected", (for Type I errors only – i.e. the probability of detecting the presence of a substance when it is in fact not present),

ii. a "detection limit, L_D, greater than L_C,, which also incorporates the effect of failing to detect the presence of a substance when it is in fact present (i.e. Type II errors), and,

iii. a "determination limit", L_Q, which is defined at the minimum signal above background that not only indicates detection but can also be reliably quantified, i.e. the standard deviation of the signal is a small fraction of the true signal value.

In the case of radioactivity counting, Currie assumes that the signal variation can be approximated to a Poisson distribution and provides a working example of the methodology applied where the risk of both making both Type I and II errors is set to 5% respectively. This methodology is applied to the case of counting on both the TriCarb 2260XL and 2900TR, and the results for each level are presented in Table 4—7.

Finally, the detection limit is expressed in terms of the actual physical quantity inferred from the net signal. This calculation is related therefore to the extraction efficiency during sample preparation, the counting efficiency of the machine, the count time, as well as the original volumes of sample collected in the field. In a manner similar to Pates and Mullinger (2007), the "minimum detectable activity" (MDA) is calculated for the radon extraction method, following calibration using known radium standards (Table 4—7).

The benefit of using α/β discrimination is now clear – the minimum detectable activity is less than half (0.025 Bq l^{-1}) of that determined previously using non discriminated counts (0.059 Bq l^{-1}). Refinement to the Pulse Decay Discriminator would be expected to lower this limit still further, given that most data available in the calculation was recorded using a value of 139 and not 165 (see above). However, the results are close to the detection limits quoted by others for similar sample preparation techniques (e.g. Hoehn and Von Gunten, 1989 [0.02 Bq/l, 1 litre samples]; Freyer et al., 1997 [0.05 Bq/l, 1 litre]; Pates and Mullinger, 2007 [0.02 Bq/l, 570ml]).

Table 4—7 Count Parameters and Calculation of Detection Limits based on Currie (1968)

	Tri Carb 2600XL *(low level count mode)*	*Tri Carb 2900TR* *(alpha channel only)*
Count Window (keV)	100 – 1000	250 - 800
Count Time (mins)	200	200
Background counts (long term average) B	2581.4[A]	444.0[B,C]
Equivalent Count Rate (CPM)	12.91 (± 0.06)[D]	2.22 (± 0.02)[D]
Critical level, L_C $2.33B^{½}$	*118* *(~0.6 CPM)*	*49* *(~0.25 CPM)*
Detection level, L_D $2.71 + 4.65B^{½}$	*239* *(~1.2 CPM)*	*101* *(~0.50 CPM)*
Determination Limit, L_Q $50\left\{1+\left[1+\frac{B}{12.5}\right]^{½}\right\}$	*818* *(~4.1 CPM)*	*352* *(~1.76 CPM)*
Minimum Detectable Activity (MDA)[F,G] $\frac{L_D}{tE_\alpha XV \cdot 60}$	*0.059 Bq.l*$^{-1}$	*0.025 Bq.l*$^{-1}$

[A]Based on 19 independent measurements totalling 3800 minutes count time. [B]Based on 21independent measurements totalling 7250 minutes count time. [C]Pulse Decay Discriminator set at 139. [D]Error calculated from long term count and associated standard deviation. [E]For a 200 minute count time. [F]Represents the smallest radon concentration that yields a net count above the background with a 95% probability (i.e. a true signal is reported 95% of the time) and no greater than a 5% probability of calling a blank a true signal (Prichard et al., 1992) [G] t = count time (200 mins), E_α *= counting efficiency for the a count window (264.7%), X = radon extraction efficiency for 10ml toluene removed from sample bottle (estimated from partition theory at 25.2%, i.e. 75.5%/3).*

4.2.5 Treatment of error in radioactive counting

As described in Section 2.1.1, radioactive decay is a purely spontaneous and random process. One consequence of this probabilistic behaviour is that, if the same long lived sample was measured many times, the total number of counts recorded by detection equipment, such as a liquid scintillation analyzer, would vary between analyses.

This process may be modelled mathematically by use of the binomial distribution, as each particle has two possible states (i.e. decayed or not decayed) with fixed probabilities. However it may be shown (e.g. Boas, 1983; Ivanovich and Harmon, 1992; Turner, 1995) that the distribution of the individual count rates may be approximated to a Poisson distribution if:

i. the number of atoms present is large;
ii. the number at atoms that decay in a given count time is small in relation to the total; and
iii. the probability of particle decay is very small.

If these conditions are met, and the Poisson distribution is assumed, it is then possible to estimate the standard deviation of the mean count rate simply from the square root of the total number of counts recorded – i.e.,

$$\sigma_{cps} = \frac{\sqrt{n}}{t} \qquad (4\text{-}10)$$

where σ_{cps} is the standard deviation of the count rate (in counts per second), n is the total number of counts and t is the count time (s)

Given this natural, unpreventable, signal variation it is necessary to state both the count rate and the count rate standard deviation when reporting count results – i.e.,

$$r = \frac{n}{t} \pm \frac{\sqrt{n}}{t} \qquad (4\text{-}11)$$

where r is the count rate.

The net count rate for a sample is defined as the gross count rate minus any background. As both of these quantities have their own associated error, so will the net result. The calculation of this quantity requires propagation of all individual errors, normally by assuming that they are uncorrelated (e.g. Faires and Boswell, 1981).

By definition,

$$r_{Net} = r_g - r_b = \frac{n_g}{t_g} - \frac{n_b}{t_b} \equiv \left(\frac{n_s}{t_g} + \frac{n_b}{t_g}\right) - \frac{n_b}{t_b} \qquad (4\text{-}12)$$

where r_x is the count rate, n_x is the number of counts, and t_x is the count time for the sample (s), gross (g) and background (b) components.

In radioactive counting, it is important to note the gross signal will also include a background count with its own associated error. By separating the gross count rate into its two components, and from the definition of standard deviation in Equation *(4-10)*, the standard deviation of the net count rate can be calculated:

$$\sigma_{Net} = \sqrt{(\sigma_s + \sigma_b) + \sigma_b} = \sqrt{\left(\frac{n_s}{{t_g}^2} + \frac{n_b}{{t_g}^2}\right) + \frac{n_b}{{t_b}^2}} \qquad (4\text{-}13)$$

In the specific case of the radon decay series, the total number of counts recorded within the alpha channel will also be a function of both the width of the count window. However, assuming that the count window is sufficiently wide to include all alpha counts produced from the radon decay chain there will be three alpha counts generated for each radon parent. Given their short half lives, it is clear that the ^{218}Po ($t_{½}$ = 3.05 min) and ^{214}Po ($t_{½}$ = 1.64×10^{-4} sec) decay events are entirely dependent on the presence of ^{222}Rn, any influence from co-extraction into toluene rendered insignificant within *c.*20 minutes after preparation of the vial (i.e. after *c.*7 ^{218}Po half-lives, when less than 0.8% of any unsupported daughter products would remain).

Therefore, it is not appropriate to calculate the standard deviation of the true sample by simply taking the square root of the total number of sample counts, as this assumes that each alpha count is an independent and random event. Rather, the value must be calculated from the number of inferred independent events for which the Poisson approximation is valid, i.e. $n_s/3$. (Inherent in this equation is the assumption that the detection efficiency of the machine does not vary for each of the three alpha particles emitted).

From this assumption it follows that,

$$n_s = 3n_{Rn}$$

$$\sigma_{Rn} = \sqrt{\frac{n_{Rn}}{{t_g}^2}} \qquad (4\text{-}14)$$

where n_{Rn} is the number alpha counts produced by the decay of ^{222}Rn alone, and σ_{Rn} is the standard deviation in the count rate.

By proportionality and then substitution,

$$\sigma_s = 3\sigma_{Rn} = 3\sqrt{\frac{n_{Rn}}{{t_g}^2}} \equiv 3\sqrt{\frac{n_s}{3{t_g}^2}} = \sqrt{\frac{3n_s}{{t_g}^2}} \qquad (4\text{-}15)$$

Hence, from Equation *(4-13)* a modified estimate of the net count rate error can be made for the specific case of radon decay series alpha counting:

$$\sigma_{Net} = \sqrt{\left(\frac{3n_s}{{t_g}^2} + \frac{n_b}{{t_g}^2}\right) + \frac{n_b}{{t_b}^2}} \qquad (4\text{-}16)$$

Finally, a further simplification can be made by setting the count times for the sample and the background vials to the same value, i.e. $t_g = t_b = T$

$$\sigma_{Net} = \frac{1}{T}\sqrt{3n_s + 2n_b} \qquad (4\text{-}17)$$

A worked example for the overall determination of sample activity and its associated error is provided in Table 4—8.

Note on the validity of the Poisson approximation to the background count

Implicit in the above working is that the background signal error can be estimated in a similar fashion to that of the true sample, i.e. that the standard deviation is equal to the square root of the total number of counts. Currie (1998) questioned this assumption when using low-level counting systems which include anti-coincidence circuitry to suppress background counts and argued that the use of such signal suppression may result in a deviation of the total background count from the Poisson distribution, due the background signal consisting of a range of sources, including "spurious, counter-generated events".

Table 4—8 Example of sample activity determination of a field sample

Quantity	*Value*	*Governing Equation*
Gross Signal Count Rate (CPM, 200 minute count time)	35.61[A]	-
Background Count Rate (CPM, 200 minute count time)	1.78 ± 0.07	*(4-11)*
Gross signal minus Background	33.83 ± 0.72	*(4-17)*
Representative time since field sampling (minutes)	1550	*(4-20)*
Time corrected Net count rate (CPM)	41.11 ± 0.87 (equivalent to 0.685 ± 0.015 Bq)	$A = A_0 e^{-\lambda t}$ *(2-3)*
Radon activity in vial (Bq)	0.259 ± 0.005	Calibration curve, Figure 4—19
Inferred radon activity of original sample (Bq.l^{-1})	2.00 ± 0.04	*(4-8)*

[A]Sample quoted is UCL070705-T29, Source d:\simon\project\calcs\radon\pumptests\monitoring\ [rnconc_5july07_alpha.xls]calcs_timecorrected

However, given the high signal to background ratio of the current method, as well as taking into account additional errors introduced though separate aspects of the sampling technique (see discussion in following section), the potential for this effect to produce erroneous error estimates in the final quoted sample activity is considered negligible.

Note on representative time since field sampling

The example presented above includes the calculation of the inferred radon activity of the original source, by correcting for the time that has elapsed since collection in the field. One important point to note is that as the normal count time for field samples (200 mins) is equivalent to *c.*0.036 ^{222}Rn half-lives. By use of the radioactive decay law (as developed previously in Section 2.1.1), the relative decrease in vial activity that would be expected to occur during this time is *c.*2.5% of the starting value. This effect necessitates the calculation of a "representative time since field sampling", to ensure that the count rate may be assigned to a time equivalent to that if it the sample activity was measured near instantaneously (i.e. without *in situ* decay). This correction is illustrated in Figure 4—20.

Using the decay law, the average count rate may be calculated by dividing the total number of counts by the count time. The activity of an equivalent representative time t_r can then be set equal to this value, i.e.,

$$\frac{1}{t_2 - t_1} A_0 \int_{t_1}^{t_2} e^{-\lambda t}\, dt = A_0 e^{-\lambda t_r} \qquad (4\text{-}18)$$

where A_0 is the intial sample activity, at time t_s

By integration, rearrangement, and taking logs,

$$t_r = -\frac{1}{\lambda} \ln \left[\frac{e^{-\lambda t_1} - e^{-\lambda t_2}}{(t_2 - t_1)\lambda} \right] \qquad (4\text{-}19)$$

By further substitution of $t_2 = t_1 + \Delta T$, Equation *(4-19)* may be simplified further and the value of $t_r - t_1$ (i.e. the time elapsed since counting began) may be shown to be simply a function of the decay constant λ, and the count time, ΔT,

$$t_r - t_1 = -\frac{1}{\lambda} \ln \left[\frac{1 - e^{-\lambda \Delta T}}{\Delta T \lambda} \right] \qquad (4\text{-}20)$$

In the specific case of counting ^{222}Rn decay for 200 mins (i.e. λ_{Rn}=2.079×10^{-6} s^{-1}, ΔT = 12000 s), the value of $t_r - t_1$ is equal to 99.79 min (5987s), or just less than the mid point of the total count time.

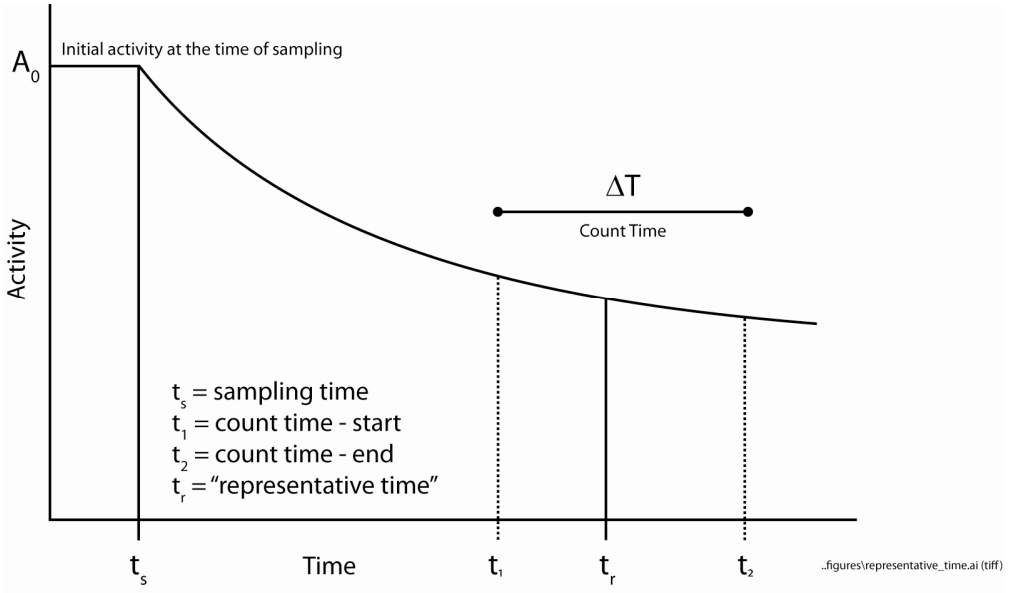

Figure 4—20 Schematic representation of the sample decay during analysis.

Comparison between individual and replicate errors

Following calibration of the machine, replicate samples were often measured in an attempt to assess the relative importance of the errors introduced through sampling, laboratory work and eventual vial counting. Representative examples are provided in Table 4—9 to highlight the degree of uncertainty from each stage. From counting errors alone, the standard deviation for a well known standard (that has a radon activity close to expected field values) are *c.*1.3% of the mean value. This value is calculated from combining the errors from the sample minus the background signal and, as explained previously, assumes Poisson statistics. Repeated measurements of this same standard over time permits some indication of the variation that may occur during radon partitioning, toluene extraction and vial preparation. As may be seen, inter-sample count variation may approach double that introduced by counting alone (*c.*2.6%).

Finally, variation in the activity of field sample duplicates can indicate the reliability of the sampling method. Waters collected by peristaltic pump and sub-surface tubing show significantly less variation (*c.*1.1%) than those taken by submersion of the sample bottle at the surface of the water feature (*c.*7.4%). This is to be expected, as less opportunity exists for radon to be lost to the atmosphere as the sample bottles are being filled.

Further comment on the standard deviation of individual and duplicate radon samples – field results.

To illustrate the effect of counting error values of sample standard deviation, it is considered useful at this stage to present results for all spring samples collected in this study (the full details of which are presented Chapter 6). These results are plotted in Figure 4—21 and highlight some particular characteristics of scintillation counting – namely that,

i. the relative standard deviation decreases with greater sample activity. Fitting a regression line to the data confirms that this relationship approximates to an inverse power law of order 2 (i.e. $\sigma \propto {}^{1}/_{\sqrt[2]{A}} \equiv A^{-0.5}$), as would be expected from Poisson statistics; and that

ii. the reduction in background count as a result of α/β separation reduces the sample error term, compared with samples of the same activity where discrimination has not taken place.

As an extension to this work, the standard deviation of duplicates could be calculated to estimate the error of each pair mean. However, this result would be of little statistical merit, given that the number of degrees of freedom is low (i.e. d.f. = 1).

Table 4—9 Comparison between individual and replicate errors.

Stage	*Mean and associated error*	*Error as percentage of mean*	*Notes*
Count error (TriCarb 2900TR)	13.36 ± 0.18 CPM	1.3%	Time corrected count error on a single measurement of standard #1A (1.563 $Bq.l^{-1}$). Value reported is the vial radon activity only (inferred from the calibration curve)[A]
Radon extraction into toluene	13.32 ± 0.35 (SD) CPM	2.6%	Evaluated from 5 repeat measurements of radon standard #1A (1.563 $Bq.l^{-1}$). Value reported is the **inter-sample** mean and standard deviation and does not take into account the counting error of each result.[A]
Field sample duplicates (sampled using peristaltic pump)	2.99 ± 0.03 (SD) $Bq.l^{-1}$ 2.99 ± 0.02 (SEM) $Bq.l^{-1}$	1.1% 0.8%	Based on 2 sample bottles from Kimber spring (Ref: UCL061012-T30,38). Value reported is the **inter-sample** mean, standard deviation and standard error and does not take into account the counting error of each result. [B]
Field sample duplicates (sampled using bottle submersion)	2.13 ± 0.16 (SD) $Bq.l^{-1}$ 2.13 ± 0.09 (SEM) $Bq.l^{-1}$	7.4% 4.3%	Evaluated from 3 sample bottles taken at the same time from Great Shefford Spring (Ref: UCL070705-T34,16,29)[B] Value reported is the **inter-sample** mean, standard deviation and standard error and does not take into account the counting error of each result. [B]

[A] *Source d:\simon\project\calcs\radon\standards\RnStnd_all_alpha.xlsm*

[B] *Source d:\simon\project\data\filedrecords_v2.xlsm*

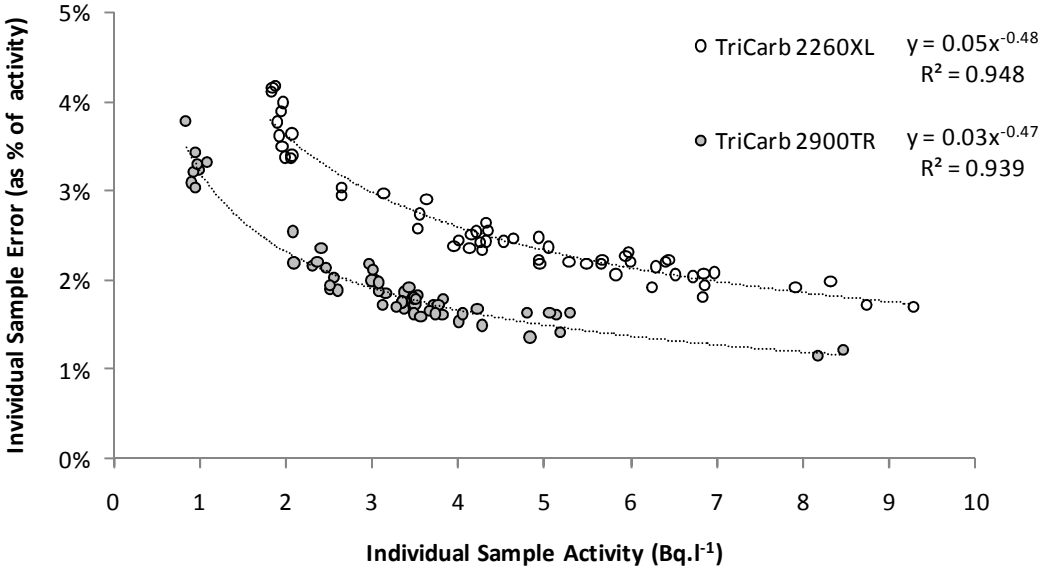

Figure 4—21 Standard deviation of individual field samples, expressed as a percentage of activity.

An alternative approach, suggested by Taylor (1987), is to calculate a global estimate of the standard deviation from many duplicates of a similar nature.

Making the assumption that the precision of the measurement process is the same for all the samples of similar activity (reasonable given the results presented in Figure 4—21), the standard deviation may be calculated by:

$$\sigma_d = \sqrt{\frac{\sum_{i=1}^{N} {d_i}^2}{2N}} \qquad (4\text{-}21)$$

where

d_i is the absolute difference between duplicate measurements

N is the number sets of duplicate samples (and also, by definition, the number of degrees of freedom)

The result of this calculation for all duplicate spring survey samples (grouped according to sample activity) is presented in Figure 4—22. The results demonstrate that, for samples analysed by the TriCarb 2900TR, the standard deviation tends to decrease with activity. This suggests that either –

i. the inter sample variability is due primarily to statistical counting error, or
ii. that there are other systematic errors present in the sampling and analysis procedures that do not depend of sample activity.

The former explanation is preferred, given the robust goodness of fit of the calibration curve presented in Section 4.2.3 which suggests that no significant systematic bias should be present during sample preparation.

Results from the TriCarb 2260XL (no discrimination) show no clear trend in the error term, although they are typically higher than that from the new machine, in line with the single sample error terms presented previously.

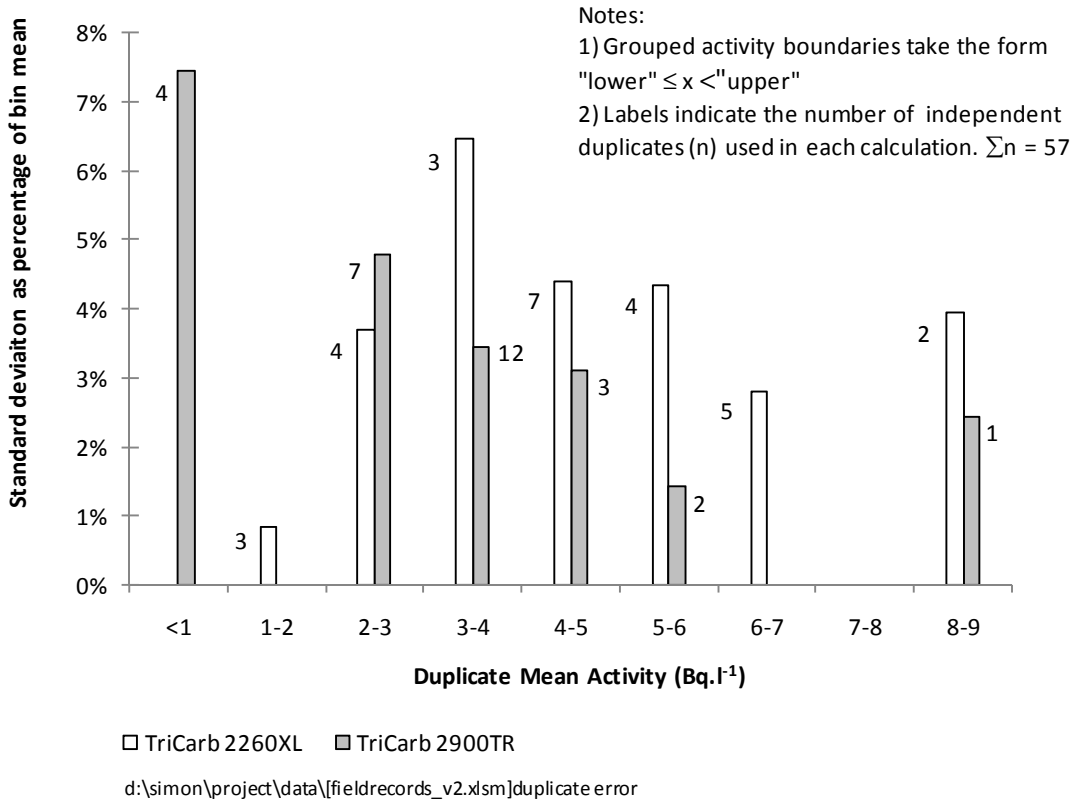

Figure 4—22 Standard deviation of field sample duplicates expressed as a percentage of mean activity.

4.3 Radium (^{226}Ra) activity in rock

4.3.1 Radium analysis by radon ingrowth.

Energy-discriminated liquid-scintillation (LSC) has been shown to be a simple and reliable method for the determination of ^{226}Ra by measurement of its ^{222}Rn decay product (Prichard and Gesell, 1977; Prichard et al., 1992). Hence, as a method for ^{222}Rn measurement by LSC has already been developed and validated in this thesis, the extension to permit radium assay in solid samples was evaluated. The method has been based on the preparation of a series of powdered and acid-dissolved chalk samples and by allowing secular equilibrium between ^{226}Ra and ^{222}Rn to be achieved. Although there are limitations to the method with regards to the necessity for a relatively large sample mass (*c.*3g) and the long run-in time required for analysis (samples must be stored for a month beforehand), dissolved Chalk samples may be analysed for ^{226}Ra without the need to resort to more expensive techniques such as γ-spectrometry (King et al., 1982; Wood et al., 2004)

4.3.2 Sampling

A sub-set of these samples prepared for uranium analysis were chosen in relation to the results of the uranium assay, but also on the proximity to those fractures likely to be the most transmissive – in total 20 samples throughout the 1 m sections and 10 samples from the detailed fracture bound block were prepared.

4.3.3 Sample Preparation

Samples were dissolved in a similar way to that for uranium analysis (as outlined in Section 4.1.2). However, the total mass used at the initial stage was increased to 3 g per sample (as opposed to 0.5 g) in light of preliminary calculations to assess the mass of radium required per sample to be detectable by liquid scintillation. Details of the actual detection limits inferred for the method are discussed in Section 4.3.5.

Small Winchester sample bottles (60 ml) were prepared by acid washing and rinsing in ultra pure deionized water. 20 ml of toluene were pipetted into the bottle, followed by the addition of the dissolved Chalk sample. The bottles were then filled to the brim by additional 2 % (w/w) HNO_3 and sealed by plastic cap. (Note that the partitioning of radon between water and toluene for a mix of 40ml water, and 20ml toluene results in a theoretical extraction efficiency of 96.4%, much higher than that used in the method for groundwater radon measurements – see Section 4.2.2 for the details of this calculation).

To ascertain if a proportion of total radium was present in the acid insoluble phase of the Chalk, a selection of samples separate bottles were prepared where the filter papers from the sample dissolution phase were added and made up with nitric acid as before.

The bottles were then stored in an inverted position for *c.*5 weeks, to allow for the ingrowth of radon due to radium decay.

4.3.4 Measurement

The same liquid scintillation equipment and cocktail were used for the analysis of radon ingrowth. However, changes to the pulse decay discriminator (PDD) were made in light of the work summarized in Figure 4—15. A PDD value of 165 was adopted, which provided a further reduction in the number of background counts within the alpha channel, without introducing significant alpha count misclassification. The benefits of this change are reflected in a lower limit of detection compared to the spring survey sample configuration, the details of which are provided in Table 4—10.

4.3.5 Calibration and uncertainty

The linearity of detection of the TriCarb 2900TR has been demonstrated previously (i.e. Figure 4—19, which was for a PDD setting of 135).

In the interests of the limited time that was available for radium analysis, an assumption is now made that the measurement of a repeated single standard for the new PDD setting of 165 may be used to determine an overall detection efficiency of the new settings (i.e. the both the extraction efficiency and the alpha count efficiency), without recourse to undertaking a new calibration curve. An inherent risk of this approach is that the initial extraction efficiency has been miscalculated. However, from the evidence of good repeatability of previous standards (with over 30 independent extractions resulting in a well constrained calibration curve), this risk was considered low.

Following an analysis of the background counts under the new discriminator settings, a re-evaluation of the theoretical detection limits, as defined by Currie (1968), has been made and is presented in Table 4—10. These limits have in turn been used to determine the lowest limit of radium activity that may be detected. This value (0.84 $Bq.l^{-1}$) is considered quite high, but is still below that expected from Chalk core (e.g. a ^{238}U concentration of 0.2 $mg.kg^{-1}$ would, from theory, result in a radium activity of 2.47 $Bg.kg^{-1}$, assuming secular equilibrium throughout the decay series had been achieved).

Table 4—10 Liquid Scintillation Count Parameters and Calculation of Detection Limits for radium by radon emanation, using Currie (1968)

	Tri Carb 2900TR (alpha channel only)
Pulse Decay Discriminator	165
Count Window (keV)	250 - 800
Count Time (mins)	200
Background counts (2 measurements) B	53.0[A]
Equivalent Count Rate (CPM)	0.27 (± 0.03)[D]
Critical level, L_C $2.33B^{½}$	*17* *(~0.08 CPM)*
Detection level, L_D $2.71 + 4.65B^{½}$	*37* *(~0.18 CPM)*
Determination Limit, L_Q $50\left\{1+\left[1+\frac{B}{12.5}\right]^{½}\right\}$	*165* *(~0.83 CPM)*
Minimum Detectable Activity (MDA)[F,G] $\frac{L_D}{tE_\alpha XV \cdot 60}$	*0.063 Bq.l^{-1}*
Minimum radium rock activity detectable for chosen configuration $\frac{MDA \times V\ (40\text{ml})}{sample\ mass\ (3\text{g})}$	*0.84 Bq.kg^{-1}*

[A]Based on 2 independent measurements totalling 400 minutes count time. [D]Error calculated from total count and associated standard deviation. [F]Represents the smallest radon concentration that yields a net count above the background with a 95% probability (i.e. a true signal is reported 95% of the time) and no greater than a 5% probability of calling a blank a true signal (Prichard et al., 1992) [G] t = count time (200 min), E_α = counting efficiency for the a count window (254.8%), X = radon extraction efficiency for 10ml toluene removed from sample bottle (originally containing 20ml toluene, c.40ml water) estimated from partition theory at 48.2% (i.e. 96.4%/2).

4.4 Radon (^{222}Rn) emanation from rock fractions

To measure radon emanation rates, powders of Chalk material were prepared for analysis by radon ingrowth (see Figure 4—23). Particles of varying size were prepared by gentle crushing of several Chalk blocks, sourced from different elevations from the core material of the Trumpletts Farm PL10A borehole. Disaggregation was achieved by use of an ultra-sonic bath followed by passing the sediment through a brass sieve. All powders were then placed into a sealed sample bottle filled with deionized water and radon ingrowth was permitted for *c.*5 weeks to allow for secular equilibrium to be achieved. Each sample bottle was shaken and rotated 2-3 times a week to ensure that the solutions did not compact and potentially impair radon release to the surrounding water.

In order to estimate an overall 'bulk' emanation rate, a small cube of competent solid block was cut from the main sample and placed in a similarly filled bottle. A fully dissolved sample was also prepared in order to estimate the maximum possible emanation from the same mass of Chalk, assumed to be indicative of the total source term concentration.

The dimensions and mass of each sample prepared is presented in Table 4—11. Radon assay was performed using liquid scintillation analysis, using the same approach adopted for radium analysis described above.

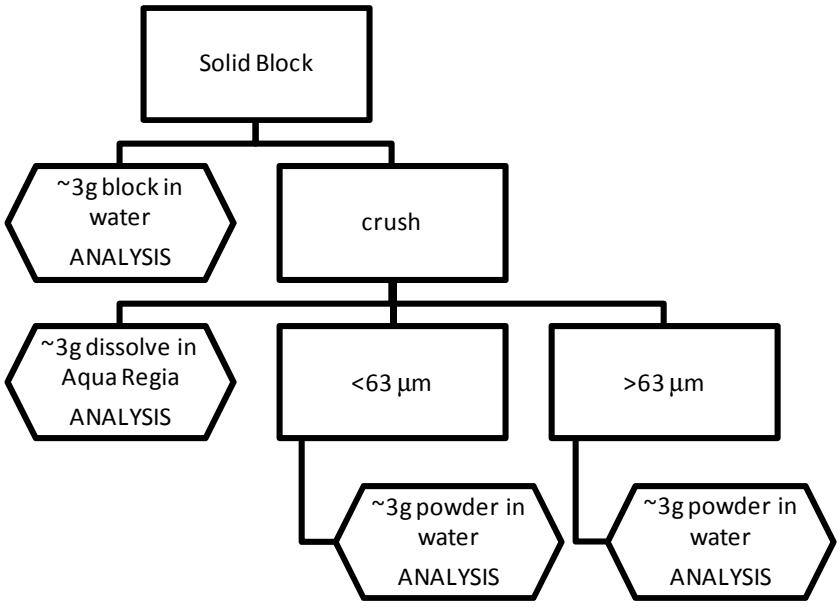

Figure 4—23 Preparation of samples for emanation analysis – process chart

Table 4—11 Samples prepared for emanation study

	Sample	TF81.3m) very well cemented block	TF86.3m light grey marly chalk, friable	TF23.0m white chalk, very easy to break apart
Solid Block	*Mass, g*	3.26	3.55	3.06
	Dimensions, cm	1.3 × 1.4 × 0.8	1.5 × 1.35 × 0.8	1.4 × 1.6 × 0.6
	Volume, cm^3	1.46	1.62	1.34
	Density g.cm^3	2.24	2.19	2.28
<63μm solid	*Mass, g*	3.00	2.99	3.00
>63μm solid	*Mass, g*	3.00	2.99	N/A
Dissolved Sample	*Mass, g*	2.99	3.00	3.02

4.5 Other Standard Methods Employed

4.5.1 IC for anions (Wolfson Geochemistry Laboratory)

Filtered, non-acidified, water samples were analysed for major anions using ion chromatography. Each sample was prepared for analysis by re-filtering using 0.2 μm filters. 100 μl of sample was added to a vial and mixed with to 900 μl ultrapure deionized H_2O to achieve a dilution factor of ten. Samples were assayed by a machine configuration consisting of a Dionex IC 2500 with ED50 conductivity detector, EG50 eluant generator (which generates high-purity carbonate-free eluent), an AS50 autosampler and a AS50 thermal compartment.

Ongoing calibration of the machine and formatting of the results was then undertaken by Wolfson Laboratory staff. The detection limits for major anions using the method configuration employed are presented in Table 4—12.

Table 4—12 Ion Chromatography Detection Limits (Dionex IC 2500)

Analyte	*Detection Limit[A] ($mg.l^{-1}$)*
F^-	0.009
Cl^-	0.014
NO_3^-	0.023
SO_4^{2-}	0.020
PO_4^{3-}	0.002

[A]Source: T Osborn, Chief Technician, Wolfson Geochemistry Laboratory, Department of Earth Sciences, UCL: (pers comm)

4.5.2 ICP-AES for cations (RHUL)

ICP-AES is a comparative technique that does not give the absolute value for the concentration of an element. Compositions are quantified by comparing the signal intensity measured for elements in the unknown sample, with the signal intensities for an external calibration solution containing a known amount of the elements of interest. Calibration standards are matrix matched for the samples, so that they behave the same way as the sample solutions during transport and in the plasma. A blank solution is also analysed so that the data are corrected for any background signal. The blank is subtracted from the signal for the calibration standards before calibration.

Drift correction

A drift monitor is analysed repeatedly during the course of an analytical run. This allowed all data to be corrected for instrumental drift during the course of an analytical run (e.g. due to fluctuations in nebulizer efficiency). Typical sample uncertainty is reported for each element of interest in Table 4—13 and is regarded as low, in relative terms, for most elements of interest in this study.

Table 4—13 ICP-AES Detection Limits for elements of interest in this study

Element	*Detection Limit*[A] *(mg.l^{-1})*	*[Stnd Dev]/[Mean]*[A,B] *(%) (repeat samples)*
Ca	0.10	0.4%
Na	0.10	0.6%
K	0.50	1.3%
Mg	0.01	0.5%
Fe	0.10	0.6%
Ba	0.01	not known
Mn	0.01	0.8%
Sr	0.01	0.7%

[A]*Data supplied by Dr Emma Tomlinson, former NERC ICP-AES facility, Royal Holloway University of London.*
[B]*Assessed by running an internal NERC laboratory standard multiple times (n=20).*

4.5.3 Field measurements

Dissolved Oxygen

Measurements of dissolved oxygen (DO) were made at all locations during water sampling. Initially two methods were tested to assess their robustness and accuracy under field conditions – a traditional membrane electrode method and a new luminescence probe (Camlab Ltd).

As described by Jackson (2004), membrane electrodes have a thin organic membrane covering a layer of electrolyte and two metallic electrodes. When placed in solution, oxygen diffuses through the membrane and is electrochemically reduced at the cathode. The rate of diffusion is observed to be proportional to the dissolved oxygen partial

pressure which is reflected in the induced current between the electrodes. Typically, such field equipment also includes a temperature sensor so that the signal may be corrected for variations in oxygen diffusion rate and solubility. However, a newly proposed alternative method is based on the observed quenching of a luminescent dyes by the presence of oxygen (proposed EPA Method 360.3). Oxygen is permitted to diffuse through a permeable polymer, which also contains such a luminophore. The polymer is excited repeatedly by a LED light source contained within the probe and the resulting emission signal is compared against an internal instrument calibration curve. The recorded emission signal is observed to be inversely proportional to the dissolved oxygen concentration.

Although both methods performed satisfactorily, the new luminescence method proved easier to calibrate under field conditions. It also had the additional benefits that there were no additional consumables required in the field, such as membranes or filling solutions and, unlike the former procedure, oxygen is not consumed at the sensor-water interface. However, it was also noted that the new method was susceptible to overestimating oxygen content (e.g. often reporting >100% saturation in stagnant surface waters) if water samples contained high levels of suspended organic material. The mechanism for this result was not clear, but may suggest that (luminescent) humic acids present in organic material may interfere with the signal recorded by the probe sensor.

Other

Standard approaches were adopted for the analysis of other field measurements. These included a three point, temperature corrected, pH meter (Sension 1 portable meter with gel filled electrode, HACH Inc), a titration approach for the determination of alkalinity (HACH Inc), and temperature compensated electrical conductivity using a graphite probe (DiST 5, Hanna Inc).

5 Uranium and Radium distribution within the Chalk matrix

This chapter describes the results of the uranium and radium analysis of Chalk core from the Trumpletts Farm research borehole, PL10A (as described in Chapter 3). Results are presented predominantly in graphical form to aid interpretation, although for reference all raw data are tabulated in Appendices A and B.

Firstly, the sampling undertaken of the Trumpletts Farm borehole core is described. Access to dried core material was provided by the British Geological Survey, and sub-samples (at *c.*1 m vertical intervals) were selected with reference to their proximity to structural features such as fractures and hardbands as well as visible variations in marl content. To enable a more detailed investigation of a small vertical section of core, a competent block of Chalk bounded by two fractures was also selected.

Secondly, results from the uranium assay are discussed. The assayed results are grouped further according to location of sample relative to fracture/matrix block boundary, as well as the extent of Fe/Mn staining on fracture walls to ascertain whether there is a correlation with uranium content as suggested by other authors. The preparation of each sample also provides an indication of the variation in acid insoluble phase and this is discussed with reference to the sample's uranium content and lithology.

Thirdly, the results of the radium assay are provided for a selected sub set of the same samples. The uranium and radium results are compared and an assessment is made of the extent and variation in isotopic disequilibrium of the Chalk matrix.

Finally, a summary is provided of previous data with which the new results may be compared. This work includes studies of the Cretaceous Chalk both in the UK and northern France, with an emphasis placed on where the analyses also considered other factors which may potentially influence U-series content - such as lithology, location within the stratigraphic sequence and position relative to other hydrogeological features such as the water table and its seasonal zone of fluctuation or observed groundwater flow horizons.

5.1 Preparation of Trumpletts Farm A core

All details of the samples collected from the dried core at Trumpletts Farm are presented in Appendix A, which lists both the description of the rock fragments made during sampling, a cross reference to the laboratory sample subsequently prepared and the assayed uranium content. The rock fragments have also been classified into four broad sub-classes ('block surface', 'solid block', 'marl' and 'Fe/Mn staining') used for subsequent comparative analysis (noting however that each sample may belong to more than one class). Photographs of the recovered core, labelled with each sampling point, are provided in Appendix F. In addition to the sampling a *c.*1 m intervals, a 20 cm solid block of Chalk, bounded by fractures at the top and bottom was removed for more detailed analysis. This block (TF23) was sampled from *c.*34.4 mbgl, within the Seaford Chalk Formation (as described in Section 3.5).

5.2 Presentation of results

All three of the main suites of results from the analysis of the borehole core samples at Trumpletts Farm (i.e. uranium concentration, radium activity and inferred isotopic activity ratios) are presented together in two integrated plots.

Figure 5—1 presents the results from those samples taken at approximately 1 m intervals throughout the 92 m preserved core material that was made from the BGS Core Store in Keyworth. For each sample, the three sets of results are plotted in relation to their estimated depth below borehole datum. Additional information about the borehole is provided for reference – i.e. a caliper log and natural gamma count undertaken by the BGS shortly after drilling, plus an indication of the inferred Chalk stratigraphy (as supplied by A Williams, BGS, *pers comm.*). The plot also indicates the elevation of the ambient water table as recorded on the 30 June 2006 (during the period of packer and open hole testing, the results of which are described in Chapter 6), as well as the elevation of known flowing horizons that have been observed during the pumping of the Bottom Barn abstraction well, located *c.*35 m away (Butler et al., 2009). Values of Chalk matrix porosity (sourced from the LOCAR data repository) and hydraulic conductivity derived from packer testing (as reported by Williams et al., 2006), are also plotted for comparative purposes. Figure 5—2 presents the same uranium series data determined for samples derived from the single 20 cm Chalk block. In all cases, an estimate of the statistical error (1σ) is included.

The following sections of this Chapter now consider each set of results individually, before discussing the results in combination with data obtained from previous studies.

5.3 Uranium Assay

In total, 111 crushed and sieved chalk samples (including duplicates) were analyzed from the Trumpletts Farm core, which represented 84 unique sampling points. These results are summarized in Table 5—1, grouped according to stratigraphic unit. Of note is the general lower concentration and proportionally smaller variation in uranium content sourced from the white Seaford Chalk (0.29 ± 0.09 $mg.kg^{-1}$, n=58 locations), compared to the white/grey Lewes Nodular Chalk (0.67 ± 0.70 $mg.kg^{-1}$, n=20). The increase in concentration within the Lewes Nodular Chalk is particularly noticeable close to the base of the formation, considered to be located within the Chalk Rock group. Few samples from the New Pit Chalk were analysed, but these tend to show concentrations that have an intermediate uranium content, albeit with large variation (0.42 ± 0.23 $mg.kg^{-1}$, n=6).

However, the results from the single block analysis (Figure 5—2) still indicate that even at low overall concentrations patterns of variation do exist within the Chalk matrix of the Seaford Chalk and that uranium does not appear to be randomly distributed[4] across the block. Rather, it is clear that two local minima exist within the block, at *c.*5 cm and *c.*11 cm from the upper fracture that bounded the original core material.

Table 5—1 Uranium content of Chalk samples from Trumpletts Farm Borehole A

Stratigraphic Unit	*Average ($mg.kg^{-1}$)*	*Standard Deviation*	*Min ($mg.kg^{-1}$)*	*Max ($mg.kg^{-1}$)*	*n (minus duplicates)*
Seaford Chalk	0.29	±0.09	0.15	0.53	58
Lewes Nodular Chalk	0.67	±0.70	0.21	3.00	20
New Pit Chalk	0.42	±0.23	0.23	0.76	6
All Samples	0.39	±0.38	0.15	3.00	84

[4] It should be noted that the analysis of these samples was not undertaken in stratigraphic order and hence it is considered unlikely that the pattern of uranium concentration results from either inconsistency in the preparation method or as by-product of systematic drift in machine calibration or in background signal.

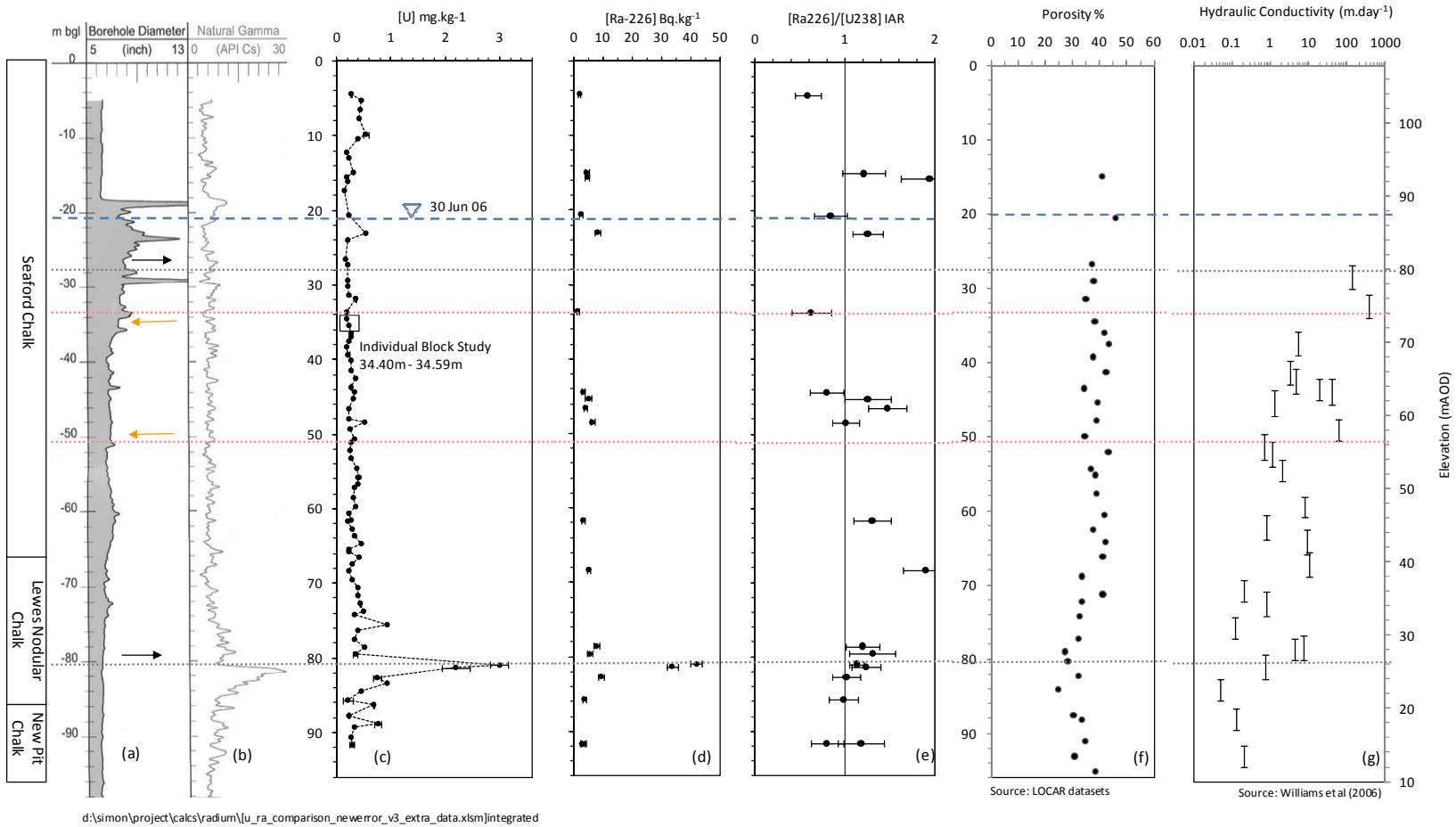

Trumplett's Farm integrated data plot

Figures (left to right)

a) borehole diameter (inch)
b) natural gamma log (API Cs)
c) total uranium concentration ($mg.kg^{-1}$)
d) radium-226 activity ($Bq.kg^{-1}$)
e) calculated $^{226}Ra/^{238}U$ isotope activity ratios
f) matrix porosity (%)
g) hydraulic conductivity from packer testing ($m.day^{-1}$)

Black horizontal lines – recorded in-flowing horizons

Red horizontal lines recorded out-flowing horizons

Dashed horizontal line – measured water table 30 Jun 2006 before packer testing

Figure 5—1 Trumpletts Farm integrated data plot (for 1 m samples)

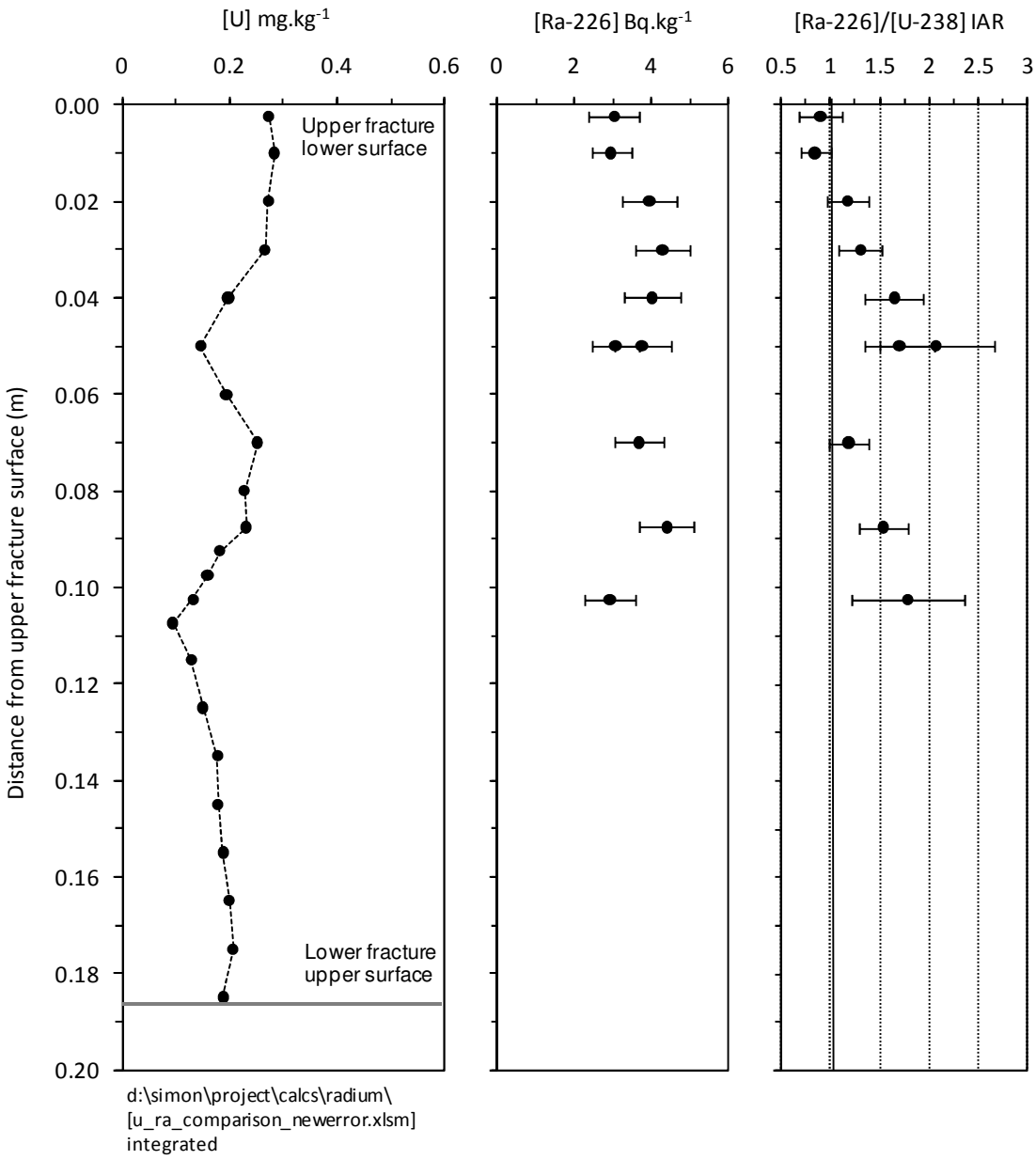

Figure 5—2 Uranium concentration, radium-226 activity and inferred isotope ratios in a competent Chalk block bounded on both sides by fractures

5.3.1 Acid insoluble content

The distribution of the acid-insoluble fraction from the core material (as presented in Figure 5—3) is considered to reflect the lithological variations within the borehole. Most samples from the Seaford Chalk Formation have a generally low insoluble content (averaging around *c.*2%). However, samples from the Lewes Nodular and in particular in the vicinity of the Chalk Rock show a greater degree of lithification and lower carbonate content and this is reflected in the greater resistate components within the samples.

A frequency distribution of the entire dataset (111 samples) is presented in Figure 5—4. The modal value of between 1-2% is consistent with other literature values of petrographic analyses of Upper Cretaceous white chalk facies, the higher values similar to those for hard-ground chalk facies (as reported in Hancock, 1975). The highest observed insoluble fraction was determined at 23.6% for sample TF80 (86.3 mbgl), noted to be a marl rich solid block. Its depth suggests that this sample is taken from a hardband located at the boundary between the Lewes Chalk and New Pit Chalk Formations (i.e. within the Chalk Rock group of mineralized hardgrounds).

Uranium content as a function of acid insoluble phase

Following Pacey's (1984) demonstration of the strong positive relationship between the non-carbonate fraction of Chalk material and the sample's natural background gamma activity (which was subsequently used as a proxy for uranium content), a similar plot considering uranium as a function of acid insoluble phase was prepared for the dissolved samples at Trumpletts Farm. However, this analysis demonstrates no clear relationship between insoluble fraction and uranium content of the dissolved sample (Figure 5—5), and indicates both that high values of uranium content are observed in very pure Chalk samples and that low to average uranium content (for the samples analyzed) may be found in chalk powders that have a high acid insoluble component.

However, it should be noted that the two methods of preparation differ significantly which makes a meaningful comparison rather limited. Pacey (1984) used a dilute acid to dissolve the carbonate fraction alone, whereas the method described in Chapter 4 employs reverse Aqua Regia. Although of limited value in comparison with these previous results, the new data do not contradict Pacey's (1984) hypothesis that the uranium bearing mineral phases in Chalk may be dominated by francolite, a pelletal apatite $Ca_5(PO_4)_3(OH,F,Cl)$, which although not readily dissolved by dilute acids, would be expected to be fully dissolved by stronger acid solutions (e.g. as demonstrated by Evans et al., 2005).

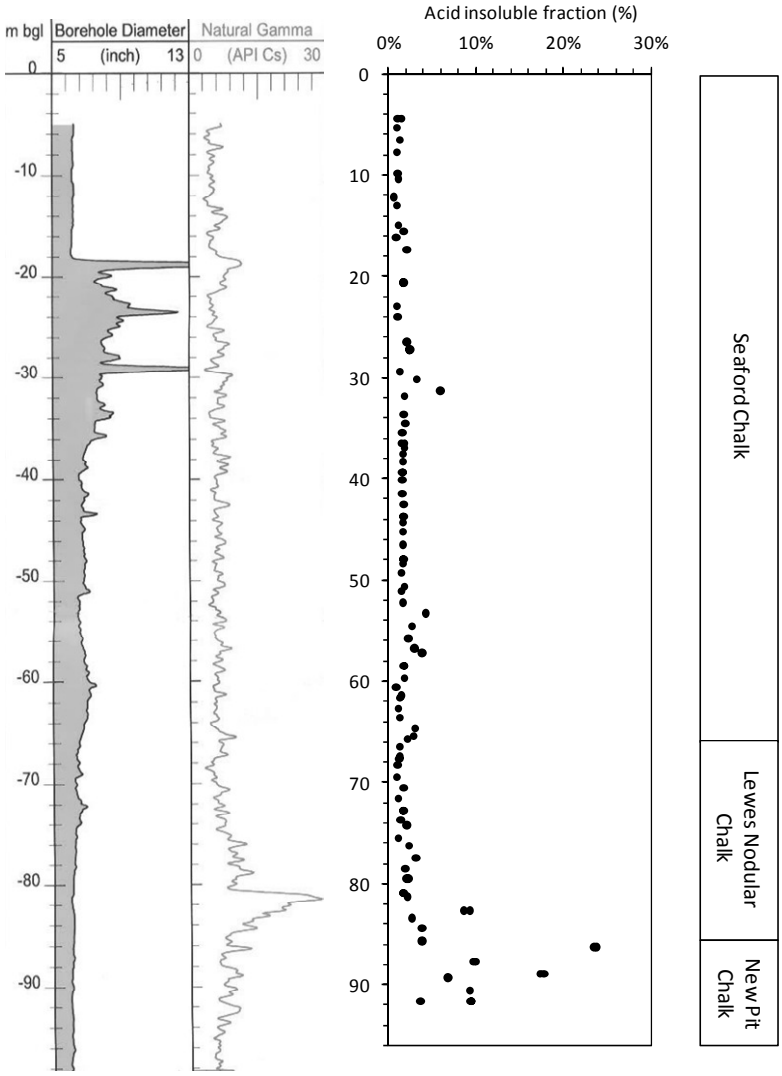

d:\simon\project\calcs\radium\[u_ra_comparison_newerror.xlsm]integrated_insoluble

Figure 5—3 Acid insoluble fraction of core samples in relation to their sampling location.

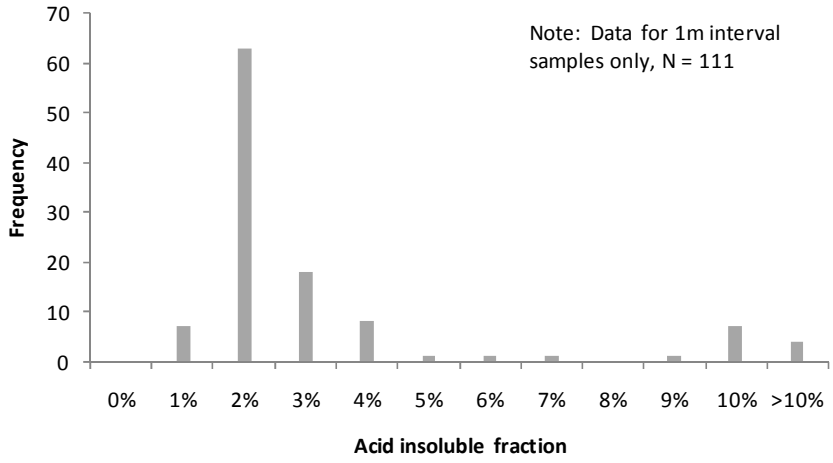

d:\simon\project\data\uranium\ls55\u_chalk\trumpfarma\[uchalkresults_trumpfarm_all_v2.xlsm]

Figure 5—4 Frequency distribution of acid insoluble fraction of core samples.

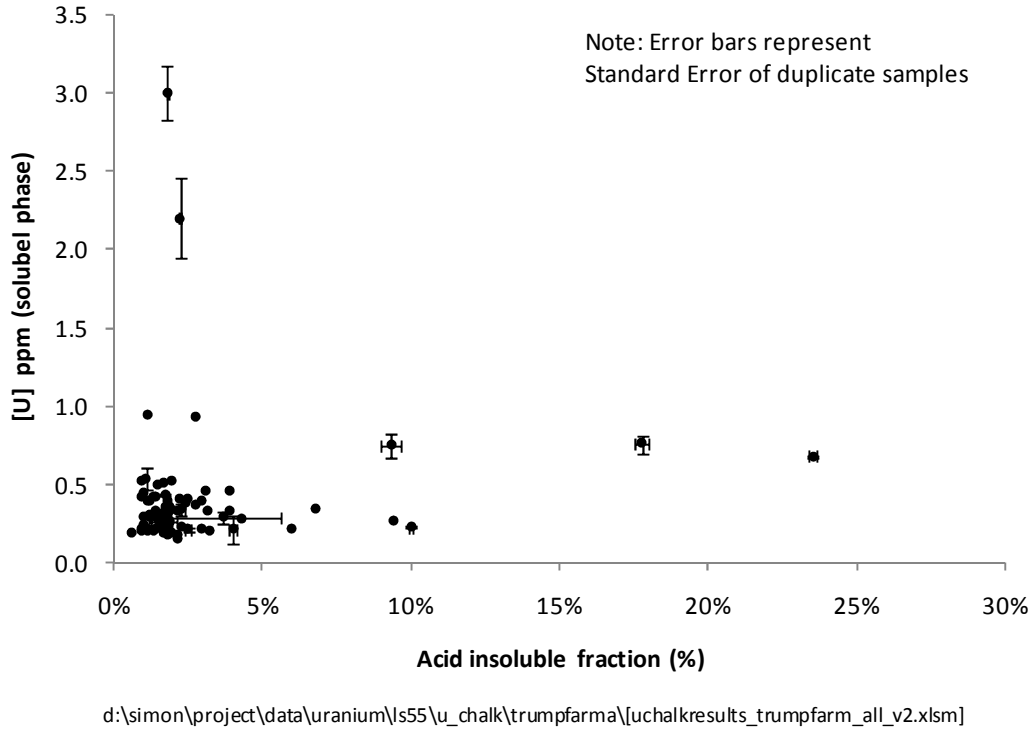

Figure 5—5 Uranium content of dissolved samples as a function of the percentage of acid insoluble phase.

Comparison with down borehole gamma signal (BGS)

Pacey (1984) also demonstrated by use of gamma ray spectrometric analysis that between 70-100% of the total background gamma activity in Chalk samples could be ascribed to the presence of uranium isotopes, in contrast to *c.*15% from isotopes of thorium and less than 5% from ^{40}K. In such a way, down hole logs of natural gamma intensity were considered useful indicators of the magnitude of uranium content through a series of alternative Chalk facies (white, gray and marl rich Chalks).

For this current study, a natural gamma log from Trumpletts Farm A, produced shortly after the time of drilling, was obtained from the BGS for the purposes of comparison with the new uranium data. The gamma plot, obtained in graphical form (i.e. as presented in Figure 5—1), was initially digitized and then smoothed using a interval size of 20cm with an averaging window of ±35 cm. This provided a interpreted data series where any artefacts from the digitization process were removed, but which was still considered to reflect the magnitude and variation of the original data set. For each Chalk sample, uranium content was then plotted against the closest gamma signal recorded (Figure 5—6).

Although this method of comparison is subject to error in both the uranium content and the representative gamma signal (e.g. the down-borehole gamma log signal is naturally depth integrated and not representative of a single point), the results indicate that there is a positive correlation between the two variables. Calculation of the 95% confidence belt for the results emphasizes, however, that there is a high degree of uncertainty in the linear regression at uranium concentrations greater than *c.*0.5ppm, as most samples cluster at values less than this amount.

The result suggests that use of gamma signal intensity as a proxy for uranium content may be justified in Chalk boreholes, although it would be desirable to obtain further data from regions of elevated uranium content to improve the confidence of the regression.

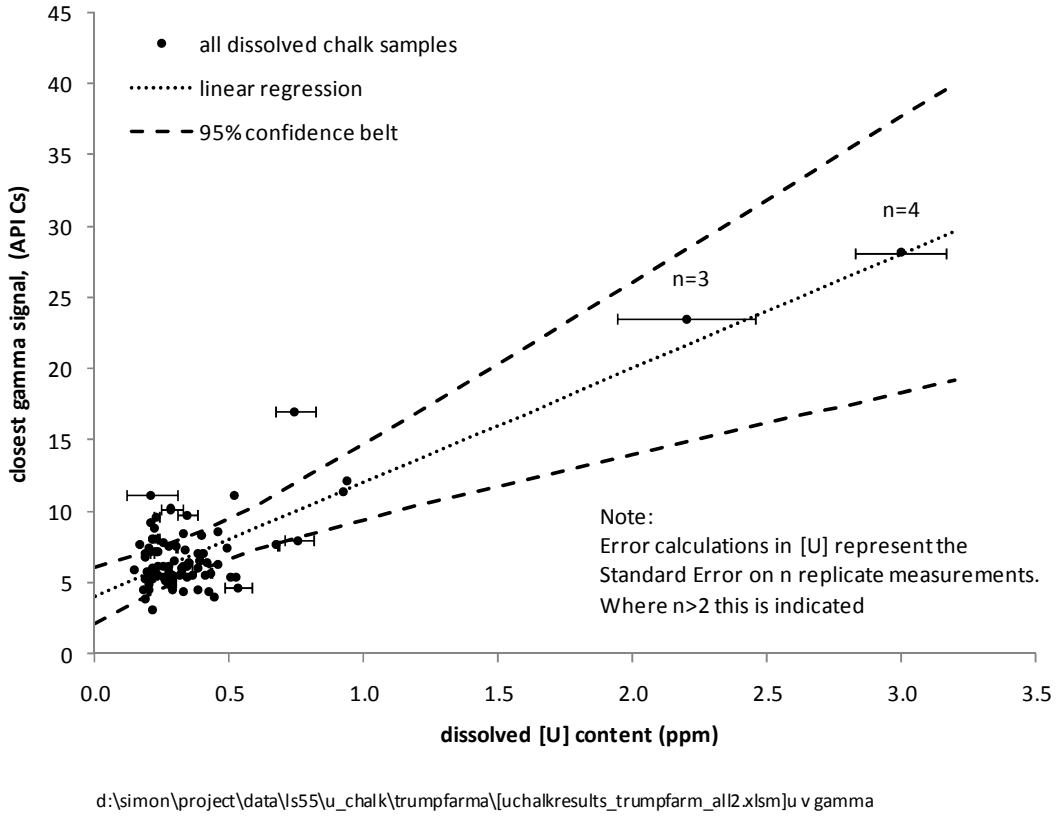

Figure 5—6 Comparison between dissolved uranium content and down borehole natural gamma signal.

Uranium content of sample sub sets

Several previous authors have observed variation in uranium content for particular sub-sets of Chalk samples. For example, in the analysis of a single sample from the 'Trunch' borehole in East Anglia, Low (1996b) demonstrated that uranium was preferentially concentrated in the non-carbonate fraction of the bulk matrix material. Ward (1989) reports analyses of Chalk samples taken from quarries (in East Anglia), that also demonstrated some differences in uranium concentrations within fracture linings when compared to the block material. For example, at South Pickenham (NGR TF 853 042), the uranium content of an iron rich fracture lining was calculated at *c.*0.63ppm compared with *c.*0.36ppm within the Chalk block. At Caistor St. Edmund (NGR TG 238 046), no statistically significant difference between the block material and iron rich linings was found, although higher uranium concentrations were observed in material sourced from solution-enhanced fracture walls (*c.*1.44 ppm U compared with *c.*1.07 ppm of the block material).

To investigate the potential for uranium variation according to provenance, each new uranium data sample was re-grouped according to four non-independent sub-classes, (namely 'block surface', 'solid block', 'marl' and 'Fe/Mn staining present'), based on their location with the core and proximity to fractures observed at the time of sampling (as defined in Appendix A and presented in photographs in Appendix F). For each sub-class, whisker plots of the uranium content were produced to help illustrate the variation and spread of each dataset. Figure 5—7 illustrates the difference for samples considered to be sourced from the block surface or from within the block material. Overall, the average and inter-quartile range of each dataset is similar, reflecting the global average value of uranium content of *c.*0.3 $mg.kg^{-1}$. Some high outliers do exist for the matrix material – e.g. at 2.99 $mg.kg^{-1}$ (sample TF74, a nodular Chalk taken from solid core with iron stained nodules) and 2.20 $mg.kg^{-1}$ (sample TF75, a very well cemented 2 cm section taken from solid block). Figure 5—8 compares the uranium content for Chalks samples that contain or lack the presence of visible marl content (typically classified according both to colour during the initial sampling as well as evidence of the 'wispy' nature of marl sedimentation observed in such samples). In general, the results suggest, based on such a qualitative classification, that there is very little difference in either the median of the uranium content or in the sub-sample variation according to the presence of marl banding. Figure 5—9 compares the uranium content for samples where there is the presence or absence of staining either on the fracture surface or within the chalk block, usually in the form of reddish-brown or black mottling. Once again, it is apparent that the median uranium

content of both sub-sets is similar, although those samples with staining do show greater overall variation. From this analysis, the sample with the highest recorded uranium content (TF74) can be summarised as a non marly solid chalk block with the presence of Fe/Mn staining.

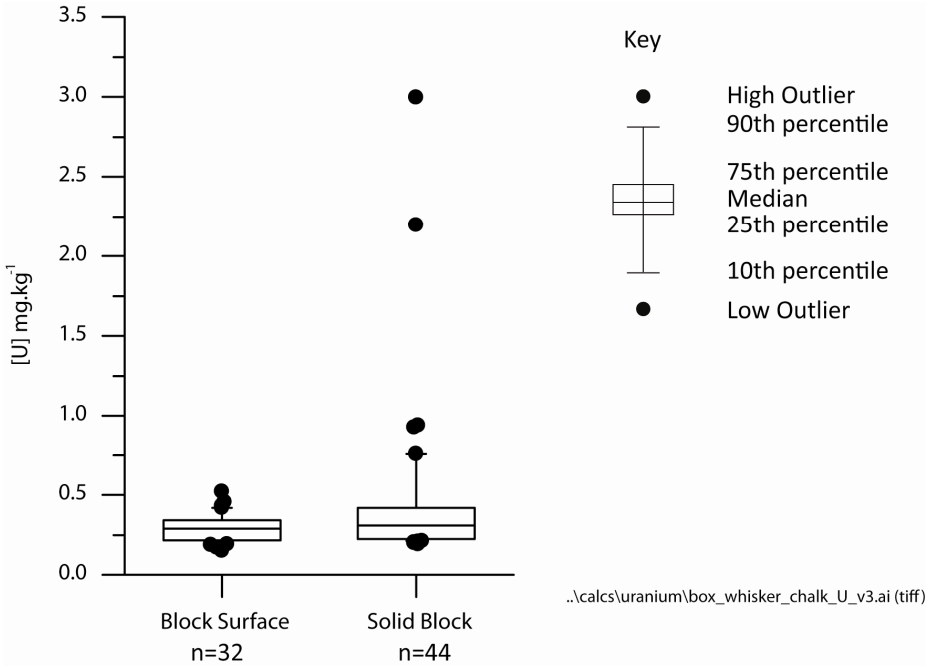

Figure 5—7 Box-whisker plots of uranium content for Chalk samples grouped according to location of sample relative to matrix blocks.

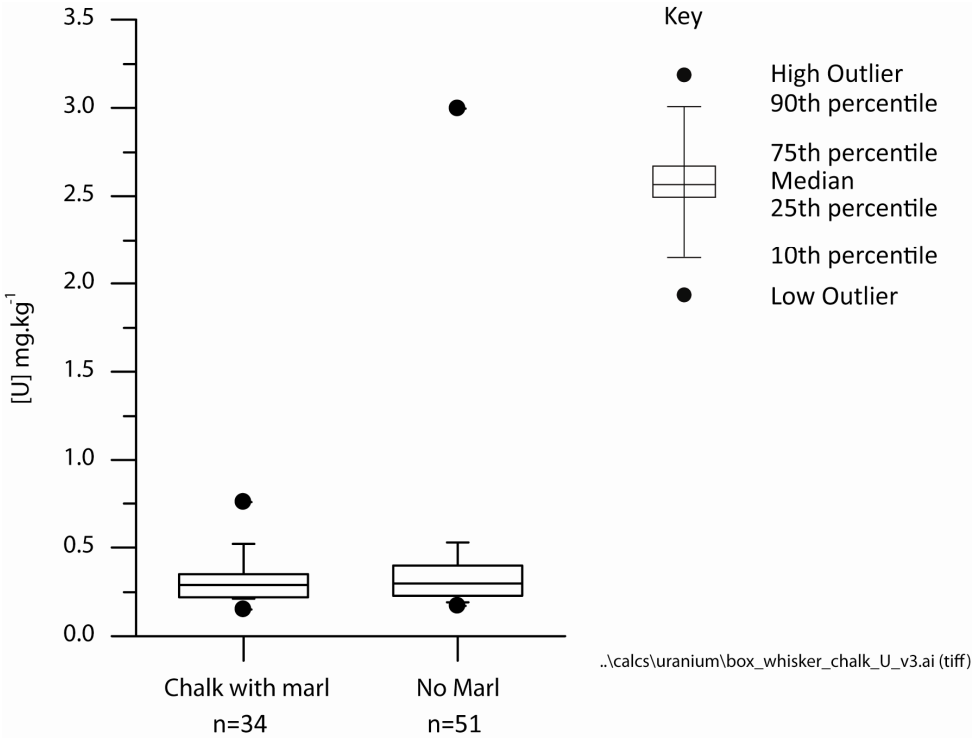

Figure 5—8 Box-whisker plots of uranium content for Chalk samples with the presence or absence of marl sequences

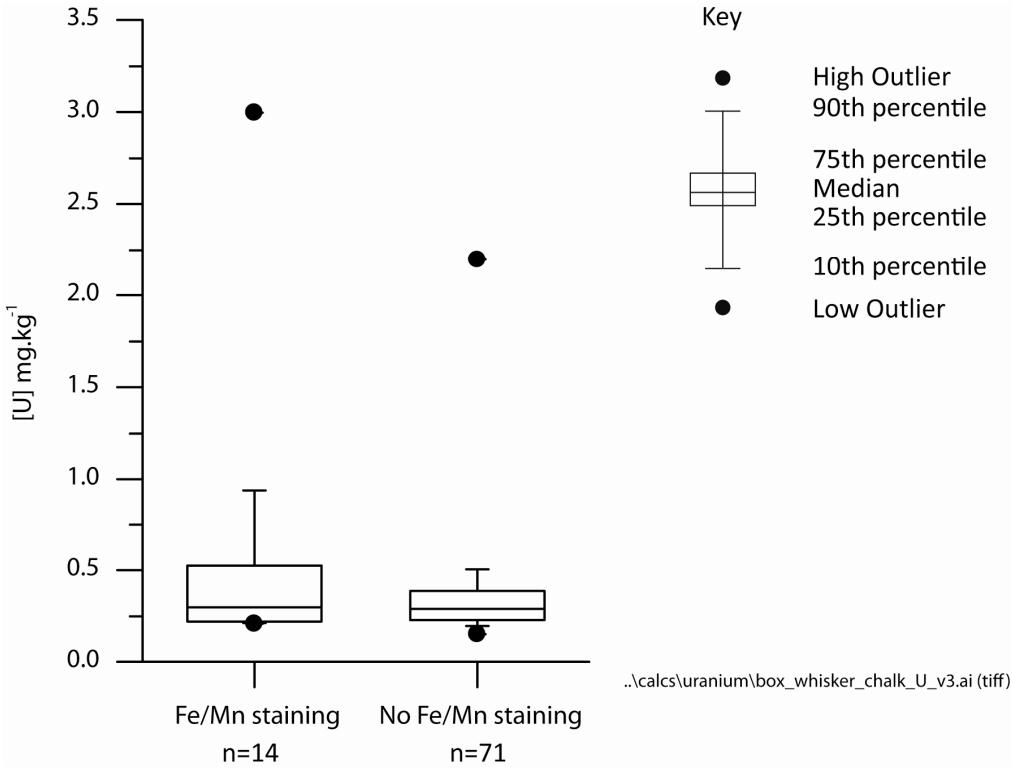

Figure 5—9 Box-whisker plots of uranium content for Chalk samples with the presence or absence of Fe/Mn staining.

Comment on sample error

An assessment of both individual sample and duplicate measurement error for a series of uranium standard solutions has been presented previously in Chapter 4. However, it is of interest to compare these results with the recorded error on actual samples. These results are presented in Figure 5—10 and demonstrate that inter-sample standard errors are in general much greater than the individual errors, produced by variation in signal intensity from the luminescence spectrometer. For individual samples, the percentages are generally lower for higher uranium content (*c.*2-3%), reflecting in part the increased signal-to-noise ratio as concentration increases.

However, it is noticeable that for all samples the fractional error is never less that *c.*1%, i.e. that that the absolute error is in part proportional to the uranium content. Such results suggest that some signal variation may also be a function of the analytical method employed, or may indicate the presence of an interfering (i.e. randomly quenching) species within the sample solution.

Replicate errors are generally an order of magnitude greater than individual samples (up to 20% of the averaged concentration). This variation is considered to reflect the natural range of uranium content within each sub-sample of crushed chalk powder, although may also indicate analyte loss during the dissolution and multiple refluxing procedure. In all

calculations, where possible, replicate error has been calculated and taken into consideration in the calculation of subsequent terms (such as activity and isotopic activity ratios).

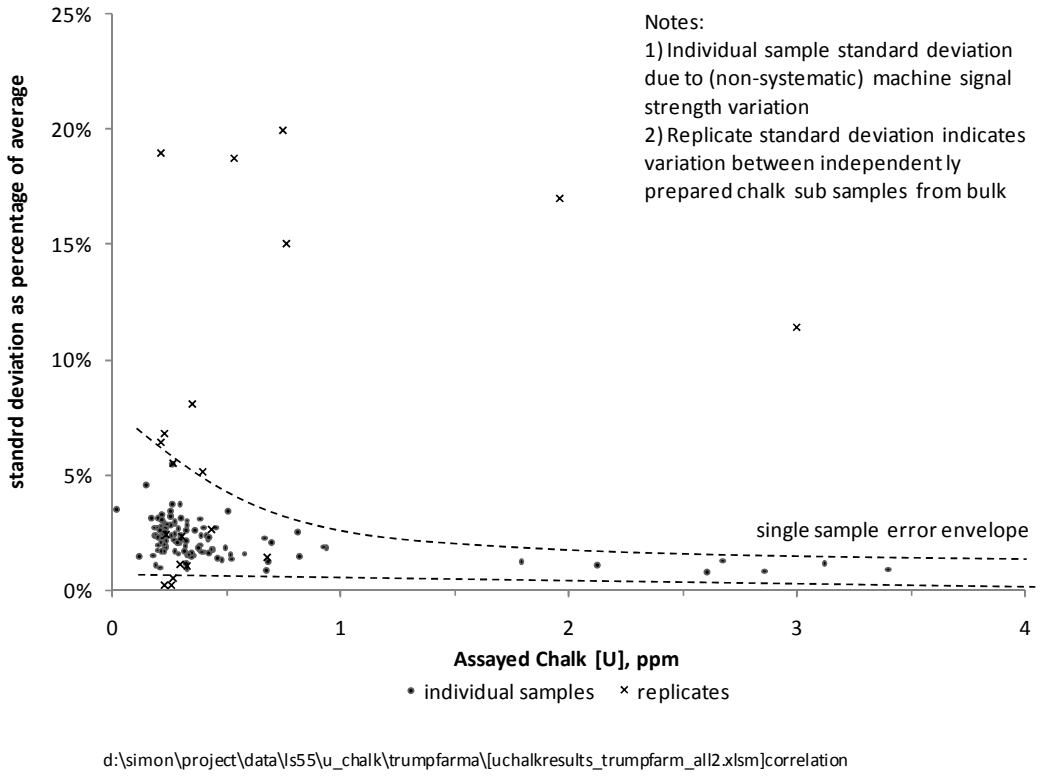

Figure 5—10 Standard deviation of chalk samples analyzed using the Perkin Elmer LS55 luminescence spectrometer.

5.4 Radium Assay

The radium activity of a sub-set of the same samples analyzed for uranium are presented in Figure 5—1 and Figure 5—2. A complete record of the results is also provided in Appendix B for reference.

For the 1 m samples, there is a wide range of relative activity (min 1.4 $Bq.kg^{-1}$, max 41.9 $Bq.kg^{-1}$) with an average of 7.9 $Bq.kg^{-1}$. However, in a similar way as for uranium, there are clear differences in content and variation between the three Chalk stratigraphic units represented within the borehole (see Table 5—2). Samples within the white Seaford Chalk have a generally low and tightly constrained activity (4.05 ± 1.98 $Bq.kg^{-1}$) throughout the sequence, compared to samples from the Lewes Nodular Chalk, where the average activity is four times greater, albeit with a large standard deviation (17.17 ± 16.20 $Bq.kg^{-1}$). Only three samples from the New Pit Chalk were analyzed, but all have activities similar to that observed in the Seaford Chalk.

The ten samples analysed from the single block of Seaford Chalk have a mean activity of 3.61 ± 0.57 $Bq.kg^{-1}$, reflecting a similar activity to other samples points in the same stratigraphic unit. Qualitatively, the results also suggest that there may be a systematic variation in activity throughout the block, initially increasing away from the block surface, but also more broadly correlated with uranium content (Figure 5—2). However, also of note is the large individual sample error, which is comparable in magnitude to the inter-sample standard variation. Such large relative errors make the direct comparison with other variables more uncertain and necessarily limit the strength of the conclusions that may be drawn.

Table 5—2 Radium activity of Chalk samples from Trumpletts Farm Borehole A

Stratigraphic Unit	*Average ($Bq.kg^{-1}$)*	*Standard Deviation*	*Min ($Bq.kg^{-1}$)*	*Max ($Bq.kg^{-1}$)*	*n*
Seaford Chalk	4.05	±1.98	1.39	8.14	11
Lewes Nodular Chalk	17.17	±16.20	5.06	41.88	6
New Pit Chalk	3.28	±0.39	2.92	3.69	3
All Samples	7.87	±10.50	1.39	41.88	20

Such results are similar to those recorded by Ward (1989) at South Pickenham, where radium activity ranged from 3.35 $Bg.kg^{-1}$ (for 'block material') to 6.67 $Bg.kg^{-1}$ (for an iron-rich lining of a fracture). This site was described as a quarry exposure of predominantly 'extremely weathered and highly fractured Chalk', but with very little clay material apparent on fracture surfaces. Results from Caistor St Edmund were greater, reflecting the higher uranium series content also recorded at this location (11.37 to 23.52 $Bg.kg^{-1}$). Ward's (1989) data suggested that the higher activity may have been related to the extensive iron staining and clay material observed on the fracture walls and linings at this site.

Cuttell *et al* (1989) determined radium activity for ten samples sourced from three sites in Lincolnshire, with an average of 1.44 ± 0.55 $Bq.kg^{-1}$ for nine white chalk samples, generally lower than that recorded at Trumpletts Farm. However, they also recorded a single value of 16.87 $Bq.kg^{-1}$ for a marl sample ('Goxhill 9 m'), which they hypothesized may have resulted from a combination of radium mobilization combined with preferential adsorption onto clay rich material.

5.5 U-Ra Isotope Activity Ratios

As outlined in Chapter 2, analysis of uranium series isotope activity ratios may be useful to aid understanding of the relative mobility of each daughter product, and in particular to ascertain whether radium may be concentrated in mineral linings of fractures (regarded as an important observation to make especially in terms of developing a realistic diffusion model). Such data are also important for testing the original assumption by Atkinson et al (2001) that the unconfined solid Chalk matrix may be regarded as effectively 'closed', i.e. that sufficient time has elapsed to permit secular equilibrium between ^{238}U and ^{226}Ra, enabling uranium concentration to be used as a suitable proxy for radium activity (and hence radon production) within the matrix. Although ^{238}U isotope activity was not measured directly in this study, an estimate may be made by using the total uranium concentration assayed previously (using the method described in Section 4.1.4). Comparisons may be made therefore between inferred ^{238}U activity and measured ^{226}Ra activity, but with care taken to ensure that all errors are combined to reflect the overall uncertainty of the calculation.

A plot of the uranium content and ^{226}Ra activity for those samples where both measurements were made is presented in Figure 5—11. Similar data from other Chalk studies (i.e. Cuttell et al., 1986; Ward, 1989) are re-plotted for comparative purposes. The figure also includes the calculated activity that would be present for a given uranium content, assuming that secular equilibrium had been achieved. From this comparison, it is apparent that the results from Trumpletts Farm are generally similar to other studies in terms of the degree of deviation from secular equilibrium over several orders of magnitude in uranium content. However, as is also apparent in Figure 5—1, from the calculated $[^{226}Ra]/[^{238}U]$ isotopic activity ratios, that the majority of the results indicate greater radium activity than would be expected at secular equilibrium. This effect is more evident particularly when uranium content is low – made clear from the further re-working of the data in the form of a plot of activity ratio with uranium content as presented in Figure 5—12.

Although there is significant sample variation, the average isotopic ratio for all 1 m section samples is calculated at 1.15. Such an overall isotopic ratio greater than 1 may be explained by either a) radium enrichment with respect to uranium or possibly b) that uranium is being preferentially leached from the samples, although it should be recognised that these mechanisms would be expected to operate on very different timescales.

Assuming pure radium enrichment would suggest that the current disequilibrium has occurred within the last few thousand years, given that the half life of ^{226}Ra is 1620yr – i.e. as unsupported radium (in excess of that produced by its immediate parent ^{230}Th) would have decayed to *c.*3% of its original activity with *c.*8000 years (5 half lives) and so would not be detected. However, if uranium is being leached from the samples then the timescale over which the mechanism has been operating could be much longer, given that the intervening isotope ^{230}Th has a half life of *c.*75,000 years, but with a much lower solubility than uranium. Hence, uranium leaching within the order of 10^5 years could result in an overall reduction in sample uranium isotopic activity whilst maintaining a radium activity that was close to the original activity achieved at secular equilibrium, given that it will be supported by the decay of ^{230}Th.

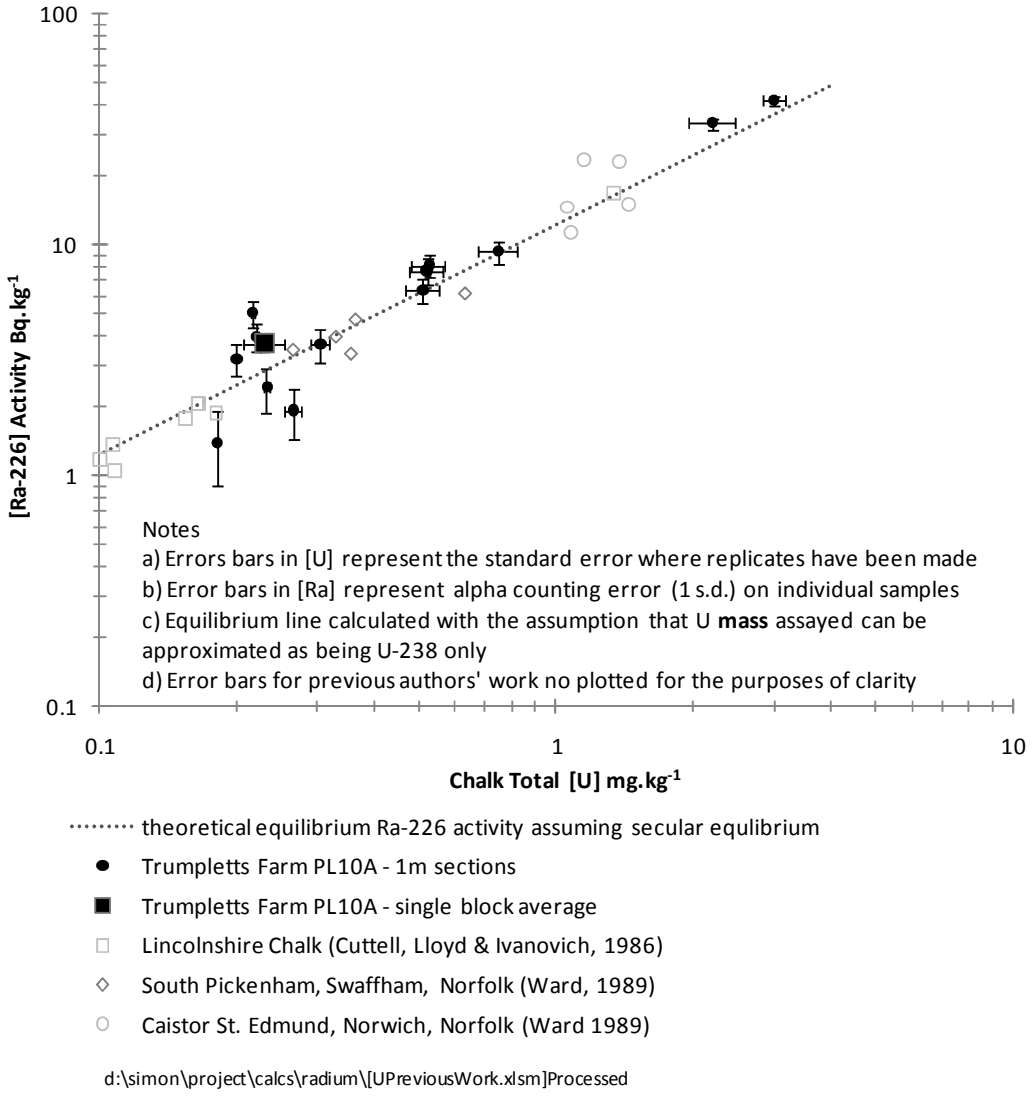

Figure 5—11 Radium activity versus total uranium content for all Trumpletts Farm Chalk core samples, including measurement error.

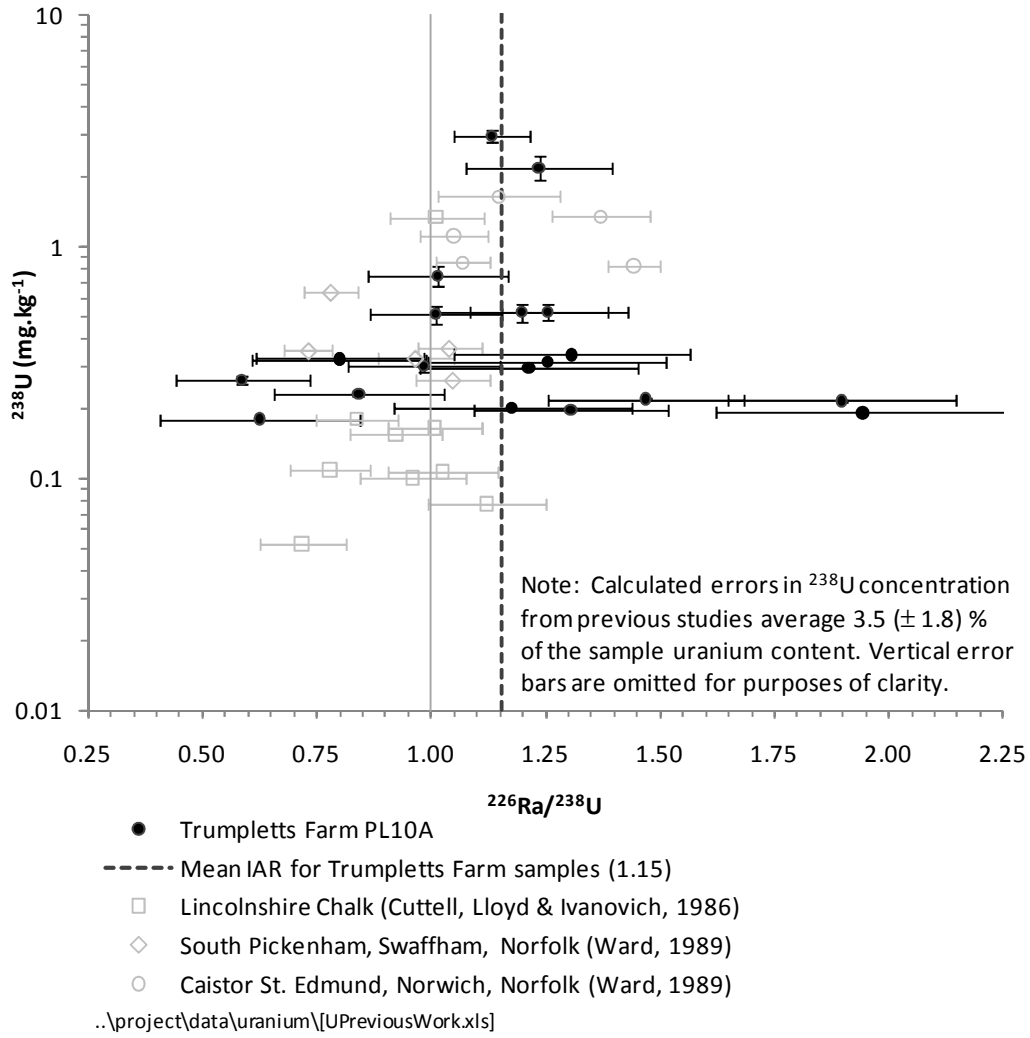

Figure 5—12 Comparison between ^{226}Ra/^{238}U and bulk uranium concentration for all Chalk samples.

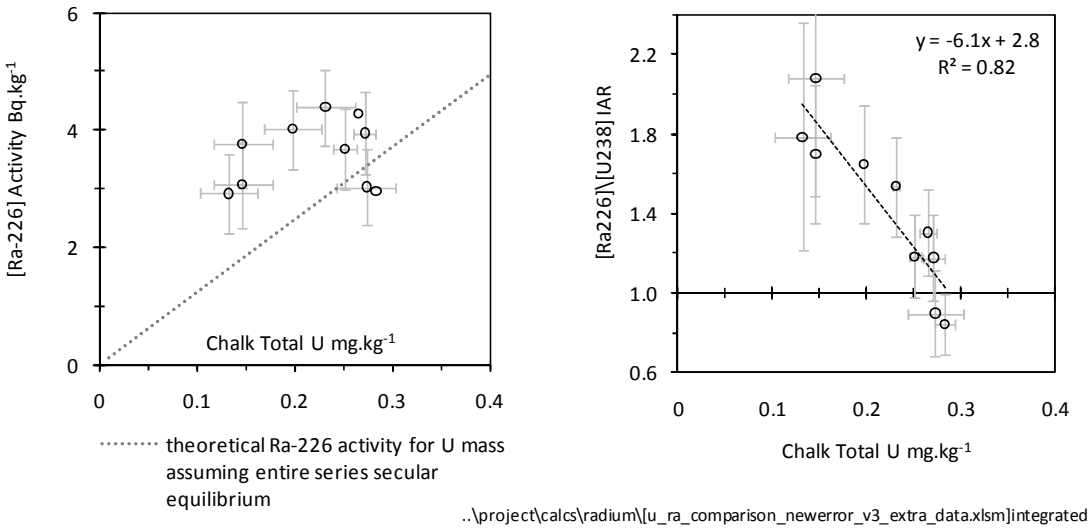

Figure 5—13 Comparison between ^{226}Ra/^{238}U and bulk uranium concentration for samples from an individual 20cm matrix block.

Figure 5—13 (right panel) compares [^{226}Ra]/[^{238}U] versus bulk uranium concentration for samples from the individual 20 cm matrix block and suggests that there is a strong negative correlation between the two results (R^2=0.82). This supports the hypothesis than uranium has been leached from most samples – i.e. the regression line placed through the data indicates that, if samples had their uranium content increased to 0.29 mg.kg^{-1} but that their radium content was maintained, then all would have a [^{226}Ra]/[^{238}U] isotopic activity ratio close to 1.

Naturally, the removal of uranium from the decay series would eventually result in a reduction in ^{230}Th activity as well, with near complete decay achieved within 0.38 Ma if left totally unsupported by the decay of its immediate parent ^{234}U. Therefore, some degree of correlation between ^{226}Ra activity and uranium concentration may also be expected over time – and this is evident from Figure 5—13 (left panel), where for those samples that deviate most from secular equilibrium there is a general positive correlation between the two results.

Combining these observations, and assuming uranium leaching is the dominant mechanism controlling disequilibrium, would suggest that up to 50% of the original uranium content has been leached from the 20 cm Chalk block.

Comparison

It is useful to compare these new data with the work of Hubert et al (2006), who measured U-series isotopic data from both solid Chalk samples and groundwaters form the Upper Cretaceous Chalk in the Paris Basin (France). In total, 16 water samples sourced from springs, rivers and boreholes were analysed for ^{238}U, ^{234}U, ^{230}Th and ^{232}Th activity using ICP-MS. A further 26 samples of solid Chalk samples obtained from 4 boreholes and surface outcrop were analysed by Thermal Ionization Mass Spectrometry (TIMS). Solid core samples were selected to ensure that a wide range of depths and varying proximity in relation the to the water table were represented.

In all but one sample analysed within the study area, the authors reported [^{234}U]/[^{238}U] activity ratios greater than 1.0 for all water types. They also demonstrated that [^{234}U]/[^{238}U] ratios in solid samples were predominantly less than unity, although there were exceptions from samples located within the zone of observed water table fluctuation The results supported their original hypothesis that ^{234}U was preferentially released from Chalk above the water table (potentially as a consequence of chemical weathering), but which may be re-deposited near the water table as a result of calcite precipitation.

In addition, for all solid samples, [^{230}Th]/[^{234}U] ratios were consistently greater than one, indicating that uranium was depleted relative to the more immobile thorium. Hence, these results suggest that the process of uranium leaching is apparent not only at the cm scale (as suggested by the results from the single block), but may also operate on a larger scale, e.g. comparable to the vertical dimensions to the Trumpletts borehole in this study.

However, given that some samples plotted in Figure 5—13 do exhibit [^{226}Ra]/[^{238}U] less than 1, uranium leaching cannot be the only mechanism present. Rather, some degree of depletion by radium migration must also operate. This is supported by Cuttell et al's (1986) isotopic data, who reported an average ^{226}Ra/^{238}U ratio of 0.91±0.13 for nine non-marl rich Chalk samples. Given the extremely low radium content reported for Chalk groundwaters (see Chapter 6), some form of radium re-deposition within aquifer material seems likely. Cuttell et al (1986) suggested that this could be explained in terms of the lack of affinity of radium to the apatite lattice structure, assuming that the Chalk uranium content was preferentially concentrated in the same crystal, i.e. as evidenced by Pacey (1983). Unfortunately, they did not cite further details of the location of the Chalk samples in relation to stratigraphy, so it is unclear whether there was variation between Chalk units, as suggested by the results from Trumpletts Farm. What is clear however, is that disequilibrium of this nature will only be observed if radium migration has occurred within the last few thousand years.

Remaining uncertainty

Implicit in the above discussion is that radium and uranium are both uniformly distributed within the sample analysed. If this was not the case and rather uranium was preferentially located within distinct grain coatings (say), then aggregated results may give the misleading impression of equilibrium, even where none exists. The solution to this uncertainty would lie in a much more detailed investigation of uranium and radium content for each component of Chalk matrix material, at a much finer resolution that undertaken in this study.

Finally, if the uranium mass has been under-reported this would also lead to the appearance of uranium depletion relative to radium. This result could occur if the majority of uranium content is located within the acid-insoluble fraction of the Chalk sample, which has not been considered. However, given that the samples were prepared using a combination of strong HNO_3/HCl, and that XRF data confirm that the resistate components of the dissolution process are predominantly quartz (Section 4.1.2), it is considered very likely that

all uranium originally present in Chalk sample has been dissolved and hence is reported in the analysis[5].

[5] *Note that this preparation method is in contrast to the work of Low (1996), who used 0.1M HNO_3 to prepare the initial soluble phase and then a combination of perchloric and hydrofluoric acids to dissolve the remaining insoluble fraction, and whose result for a single sample at the 'Trunch' borehole in East Anglia did indicate a large difference in uranium content between the two phases – i.e. 0.45 $\mu g.g^{-1}$ (acid soluble) cf 8.04 $\mu g.g^{-1}$ (acid insoluble).*

6 Radon in Chalk groundwaters

This chapter summarises and discusses the results from radon measurements made in the Pang and Lambourn catchments from a series of boreholes and springs sites in 2005 and 2006. Repeated measurements at each selected site were considered an important part of the characterisation of the radon signatures across the study area. In particular, given the initial work of Gresswell (2004) in the same catchment, it was apparent that significant differences in radon activity between sites have been observed, but that there was at the time no clear understanding of the underlying controlling factors. As such, it was felt that only through a much longer period of monitoring (in combination with the collection of other environmental data) could a better hypothesis be developed and subsequently tested.

Firstly, the spatial and temporal results from spring sites are presented which indicate that activities are similar to those reported from the Chalk aquifer by others, but that within this range there may exist significant variation. It is also apparent that the seasonal temporal patterns are very different to observations in the Carboniferous Limestone made by Andrews and Wood (1972) and Zereshki (1983). Results are also compared to other environmental variables, which some previous emanation and transport models have also considered as part of their formulation (e.g. rainfall sequences, river flows and groundwater levels).

Secondly, the results for four 'depth-integrated' sampling rounds of boreholes are presented, selected on the basis of additional flow characterisation data being available from previous single borehole dilution testing (Maurice, 2008). Longer open hole pump tests were also performed at Trumpletts Farm, two from the large augmentation scheme abstraction borehole at Bottom Barn and another from PL10A – the same borehole from which core material has been analyzed. Results from packer tests undertaken at the same location are also reported. These results are compared to similar work by Ward (1985) and the differences in observed responses to the abstraction rate are discussed.

Thirdly, a comparison is made between radon activity from both spring and boreholes with the major ion chemistry of samples collected at the same time – noting that some spring samples indicate that they are potentially a mix of water from different sources. Finally, measurements of radon emanation from Chalk material are presented, indicating levels similar to those observed by Zereshki (1983), but much lower than predicted by Andrew and Wood's (1972) model of radon release from solid carbonate grains.

6.1 Temporal spring and borehole surveys

In total, fifteen 4-6 weekly sampling rounds of spring locations and four borehole sampling rounds (described previously in Chapter 3) were completed between January 2005 and July 2007; and on each occasion both radon and major ion chemistry samples were collected and analyzed. The results from the temporal surveys are presented in Figure 6—1 and Figure 6—2, with data tabulated for reference in Appendix C. Where duplicate samples were taken (the majority of cases), the standard error is also plotted. The reader is referred to Figure 3—2 for a map of all sampling locations.

Several noticeable features that are common to all locations. Namely that,

i. the absolute activity of all spring sites is with the range of 1 to 10 $Bq.l^{-1}$, which is consistent with the results of others who have measured radon activity within similar unconfined Chalk aquifer systems (e.g. Zereshki (1981), Cuttell (1986), Ward (1989), Low (1996), Elliot at al (1999)),
ii. that during 2005 there was a general rising trend in spring radon activity throughout the first half of the year, with peak levels recorded at most locations during the autumn (September/October),
iii. that in most locations there was a rapid reduction in activity between October and December 2006, and that by the beginning of 2006 activities had generally decreased to levels similar to those of January 2005.
iv. that in 2006 there was much less variation in spring activity over time than in the previous year, with levels remaining at the lower limits of that recorded the previous year,
v. that although fewer data were collected, radon activities recorded from boreholes did not indicate as much variation as the spring sites during the monitoring period, and,
vi. that the sample error was low in comparison to the magnitude of the monthly variations and therefore, there is a high degree of confidence that the difference is not accounted for solely from individual sample counting error, or from errors incurred during taking of duplicate samples.

Only two of three main spring sites located near the River Lambourn were sampled over the duration of the study. Lynch Wood, and the associated ponds, located at the top of the catchment near the village of Lambourn were observed to dry completely during the summer of 2005 and no further sampling was possible after July 2005. The natural outflow

from this location, which fed the nominal source of the river Lambourn, was also recorded as dry, indicating ephemeral conditions typical of bourne features within unconfined Chalk catchments.

The boggy nature of Great Shefford spring was also subject to periods of drying, and during such times sampling was restricted to small ponds of water near the centre of the site. However, on no occasion did the spring site dry completely and outflow that fed the main river channel further downstream was observed during both summer periods. The pond at Weston spring remained full throughout the monitoring period and samples were taken away from the pond edge by use of a long length of tubing attached to the peristaltic pump.

Although classified as a spring, the samples from the Jannways estate were taken from the outfall of a shallow pumped borehole that fed a series of inter-connected ponds. However, evidence of natural issue of water directly into the pond was inferred from the presence of clear gravel patches on the pond bottom. Anecdotal evidence from local residents also suggested that upwelling of water from the base of the pond has regularly been observed. The pond location is close to the deeper penetrating and open hole observation borehole at Bagnor (which shows similar levels of radon activity). The Winterbourne observation borehole is located further up the catchment of Winterbourne stream, beyond its perennial head. This borehole has radon activities consistently higher than that observed at Bagnor.

Within the Pang catchment, the three spring locations close to the village of Stanford Dingley all show similar radon activities and variation. In particular, Ingle spring and Jewell's spring are closely matched in both magnitude and timing. However, although situated very close to each other (less than 500 m apart – see Figure 3—16) the nature of each site is quite different. Jewell's spring issues water to the surface from beneath a tree stump into the beginning of a short stream course, before joining the main river channel, whereas Ingle spring is a covered shallow well that penetrates the Chalk, and with no overlying bed material. Such similarity in results suggest that the water sample from Ingle spring is representative of shallow groundwater and that little opportunity for mixing or degassing on the surface is present.

Results from Kimber spring (part of the Blue Pool complex) are similar to the other spring issues, although the highest recorded radon activity was measured much earlier in the year (April), with a general reduction over the remainder of the 2005. In 2006, levels of radon activity remain generally constant for those months when samples were taken.

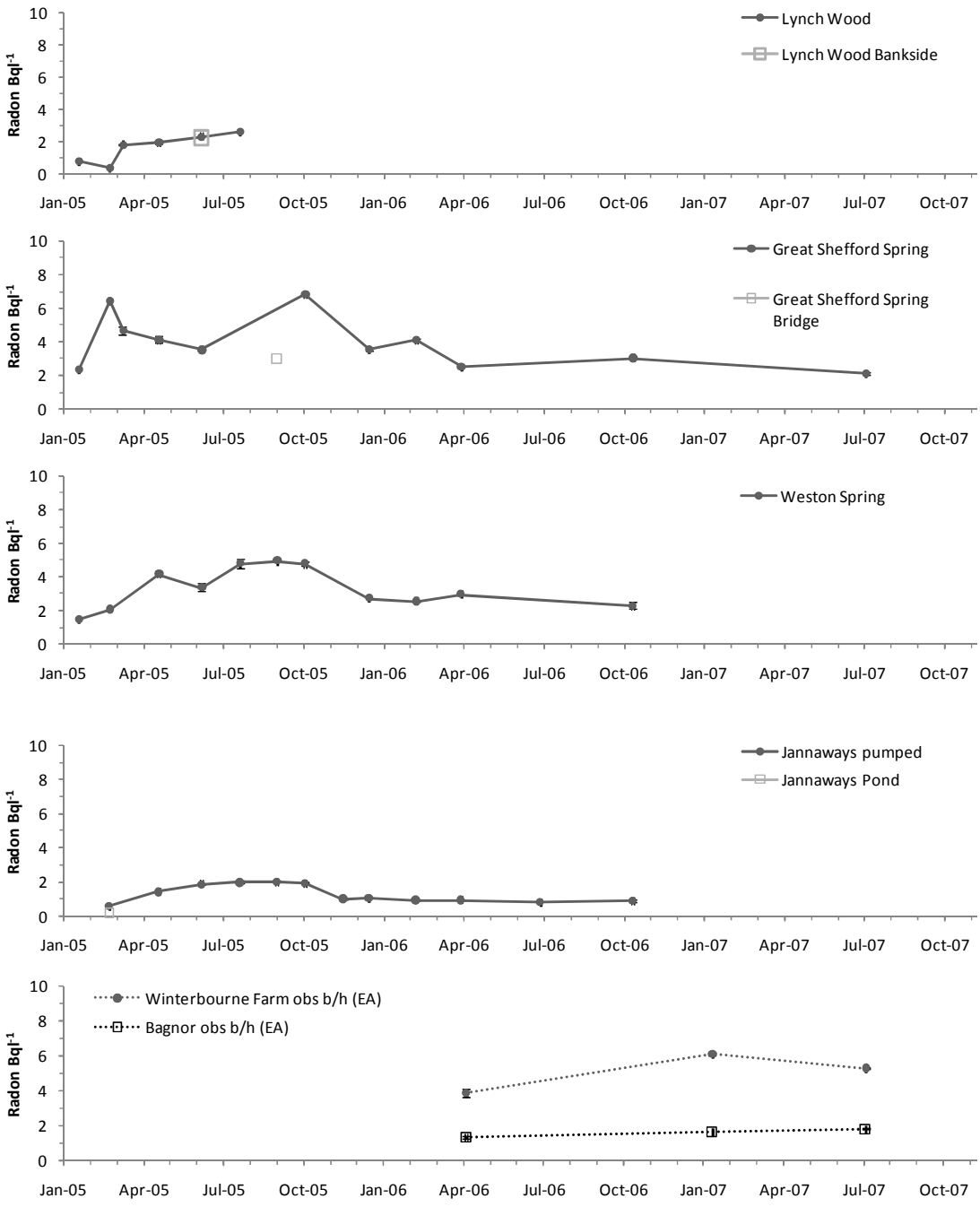

d:\simon\project\data\[fieldrecords_v2.xlsm]rnpivot_quinn

Note: Errors, where plotted, represent the **standard errror** calculated from multiple samples.

Figure 6—1 Temporal variation in radon activity from spring and borehole locations within the River Lambourn surface water catchment (including the Winterbourne Stream)

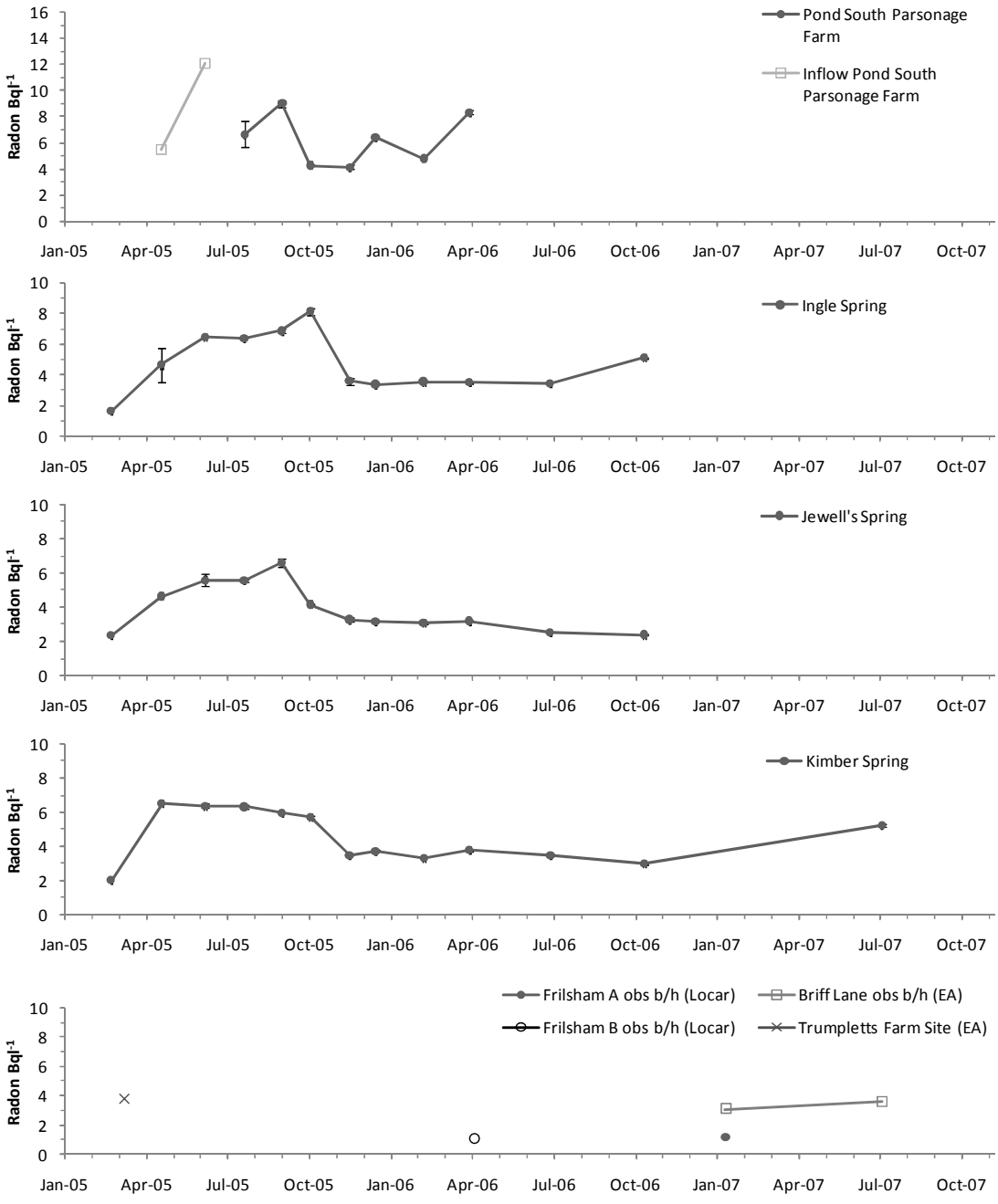

d:\simon\project\data\[fieldrecords_v2.xlsm]rnpivot_quinn

Note: Errors, where plotted, represent the **standard errror** calculated from multiple samples.

Figure 6—2 Temporal variation in radon activity from spring and borehole locations within the River Pang surface water catchment

The pond at Parsonage Farm proved difficult to sample due to the high sediment load of the water. During the early summer of 2005, the pond dried completely and the bottom surface was exposed, which consisted of thick sequences of soil and other rotting detritus that appear to have been deposited by a small inflowing field drainage stream. Even so, small patches of Chalk were also exposed at the centre of the pond which suggested that the pond was potentially a location of upwelling groundwater. From the temperature of the water (>10 deg C) it was apparent that the pond often acted as a surface store and that relatively little water flowed out to the main river channel. Hence, measurements made at this location are not considered directly comparable to the other spring sites, which were less subject to potential mixing and degassing possible in more stagnant surface ponds.

Although limited, the single pumped samples from the four boreholes within the catchment have radon activities between 1 and 4 $Bq.l^{-1}$, similar to those within the Lambourn. A more detailed sampling of the Trumpletts Farm boreholes is discussed in Section 6.2.

Discussion

Before considering the results in detail, it is useful to make reference to two related studies that have also been conducted in the same catchments. Gresswell (2004) undertook a series of borehole and spring measurements in both the catchments between December 2004 and February 2004. The samples were collected from three springs in the Lambourn (Great Shefford, Weston, and Winterbourne) and two springs in the Pang (Ingle and Jewell's), all identical in location to those locations sampled in this study with the same name. In addition, a stream survey of 10 samples was completed on the Lambourn from Maidencourt Farm to Boxford (see Figure 3—2 for a map of the study area where these additional locations are marked).

The results indicated low activities of radon in the stream water, with majority of samples exhibiting values below 1 $Bq.l^{-1}$ which contrasted with higher radon activities observed in the spring samples (see Table 6—1). Gresswell suggested that this difference was consistent with the idea that a greater proportion of radon is lost from the stream surface due to longer atmospheric exposure, coupled with radioactive decay of unsupported radon due to a negligible amount of radium in the surface water.

Groundwater samples were collected from piezometers installed within LOCAR borehole PL11e at Frilsham Meadow, close to the River Pang, with generally low activity (0.16 ± 0.04 $Bq.l^{-1}$, n=8)

Table 6—1 Radon activity of spring samples reported by Gresswell (2004)

Spring Name	*Average (Bq.l^{-1})*	*Standard Deviation*	*Min (Bq.l^{-1})*	*Max (Bq.l^{-1})*	*n*
Great Shefford (Lambourn)	3.19	± 0.02	3.17	3.21	3
Weston (Lambourn)	1.86	± 0.75	1.34	3.15	5
Jannways (Winterbourne Str)	0.97	± 0.04	0.95	1.00	2
Ingle Spring (Pang)	3.05	± 0.51	2.50	3.5	3
Jewells Spring (Pang)	3.24	± 0.98	2.59	4.36	3

Source: ..project\data\[fieldrecords_v2.xlsm]gresswell

In a further investigation of groundwater-surface water interaction, Mullinger et al (2007) undertook a series of radon surveys between May 2003 and February 2005 of both surface waters and of piezometers with a range of sampled depths below ground surface. Borehole samples indicated higher and more variable radon concentrations close to the ground surface (*c.*12 Bq.l^{-1}), with a general reduction (to *c.*1-3 Bq.l^{-1}) with increasing depth. The authors attributed this profile to changes in not only Chalk properties (i.e. the degree of weathering), but also the presence of overlying clay material considered to have higher radium content. Overall, samples taken from both catchments displayed similar vertical profiles, especially when the thickness of Chalk regarded as highly weathered was taken into account. For those samples taken below the zone of weathering, radon activities of the order of *c.*1 Bq.l^{-1} were generally observed.

By collecting quarterly stream samples down the length of both the Pang and Lambourn, Mullinger et al (2007) combined the results of radon activity and stream flow to assess the strength and variability of the groundwater radon source term. Although not all stream variation could be explained by the two mixing models investigated, the results did suggest that the calculated groundwater radon activity that fed the rivers correlated in part with the rate of flow accretion – i.e. in their example high rates of accretion were associated with periods that would also require high radon input from groundwater. The authors suggest that this may be expected given that at times of higher flow accretion "more inflow to the river travels through the near surface alluvial gravel deposits". The profiles of radon activity observed within the near river boreholes support this hypothesis, given that a potentially greater proportion of water may pass through overlying deposits that have potentially higher radium content.

To illustrate the overall average and variability for each of the major spring location samples, in the current study, the data have been presented as a box-whisker plot[6]. Activities are consistent with the winter observations made by Gresswell (2004).

In general, the results are more variable than observed other Chalk or limestone aquifer studies. For example, in the seasonal study of radon levels in East Anglian Chalk, Low (1996) found few spring sites with greater than 10% variation from the mean value, and these showed approximately equal numbers of summer and winter maxima. Andrews and Wood (1972) also recorded seasonal variations in radon activity (over the period September 1969 to August 1970) at two springs from the Carboniferous Limestone in north Somerset (Rickford and Holwell). In both cases, the highest activities were recorded during the winter period (with a maxima of 10 $Bq.l^{-1}$ and 19 $Bq.l^{-1}$ recorded at each site respectively in February), and with the lowest activity record in June. A qualitative correlation with rainfall totals for 30 days prior to the radon measurement was also noted. In an subsequent study, Zereshki (1983) noted that the radon activity of the Shipham borehole (located *c.* 6km to the west of Rickford spring) was generally 'uniform and invariable' with season, when the effects of intense rain events were ignored. However, given the influences of rainfall, a four-fold variation in activity between each monthly sample was observed, which suggested that the radon signature was controlled by a much more complex interaction between both 'slow percolation' (possibly through small fractures or void space) and 'fast conduit water' (suggestive of much larger aperture fissures).

Therefore, one hypothesis for the relatively small variation observed in the Chalk springs may be that the predominant source of the water to these springs may be delivered through narrow aperture fractures within the Chalk aquifer, as such a system would be expected to result in water with longer aquifer residence times, resulting in generally constant radon levels. Seasonal variation may also be expected, with a tendency towards maximum values in summer when drainage of the very smallest voids in the aquifer supports river baseflow. However, an apparent contradiction to this hypothesis is evident from the results of catchment scale tracer tests conducted in the lower Pang (Banks et al., 1995; Maurice et al., 2006), as described in Section 3.4.2, which indicate that the delivery of water may be very rapid to the Blue Pool (in the same vicinity as Kimber Spring), and suggests that

[6] In this figure the lower and upper boundaries of the box indicate the 25th/75th percentiles and the solid line within the box indicates the median. Error bars above and below the box indicate the 10th/90th percentiles, and individual outliers are plotted as points.

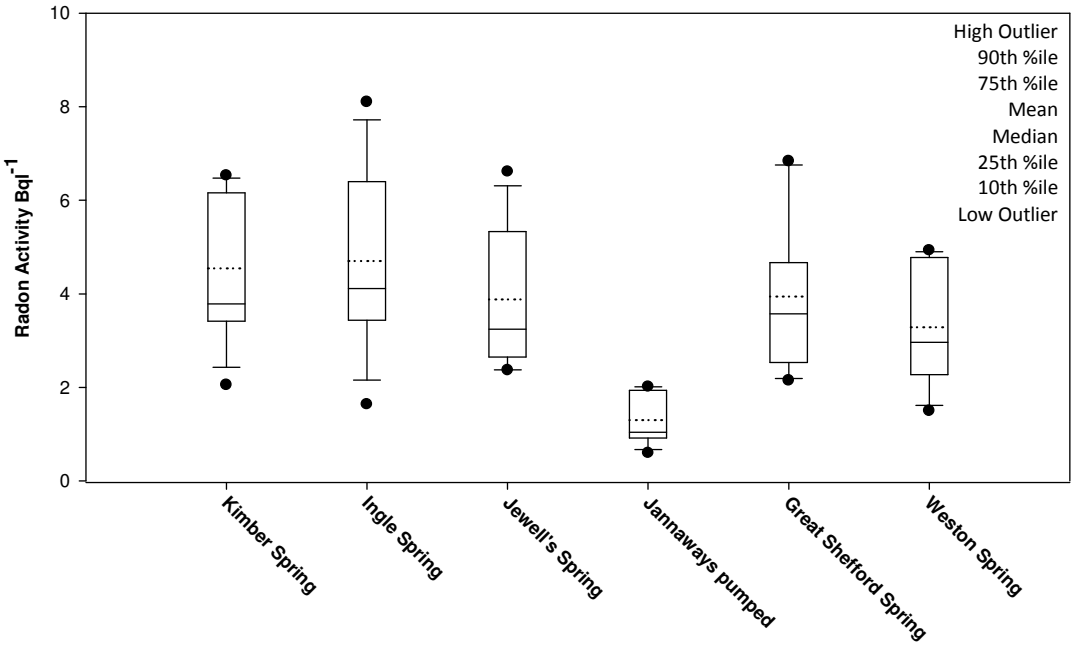

Figure 6—3 Radon activity from major springs sample in both the Pang and Lambourn catchments

fast flowing pathways must also contribute water to the same localities during periods of high rainfall. Hence, lower radon activities observed during winter periods may also indicate that the sample spring water includes a greater proportion of rapidly delivered water (possibly non-equilibrated in terms of radon activity), given the short residence times relative to that required to achieve secular equilibrium between ^{226}Ra and ^{222}Rn (*c.*25 days).

6.1.1 Radon activity at spring locations versus rainfall at MORECS weather stations.

Point to point tracer tests (Maurice, 2008) reveal that fast flowing pathways are likely to contribute at least some component of water to the Blue Pool complex. Hence, it may be hypothesised that radon activities will tend to be low during periods of high rainfall, as a consequence of the dilution of water from the Chalk pore space with low radon content water that has undergone rapid transport from the surface. To test this hypothesis, daily rainfall data were obtained from two MORECS weather stations located within the two catchments for the duration of the radon sampling period. As results from tracer testing previously described indicated travel times of between 60-70 hours from a catchment interfluve situated 5.75 km to the west, so it was considered that summing rainfall for the previous 10 days would provide sufficient time for any initial pulses of low radon content water from within the catchment to have reached the springs, accepting that other naturally occurring (and closer) sink-sources may provide water in less time. Due to the rapid equilibration of radon activity (which theoretically would be expected to be complete with

*c.*25 days), percolating water arriving at spring sources that was 'older' than 10 days was not considered.

Analysis was undertaken for the major spring sources, where the most complete datasets were available. The results, presented in Figure 6—4, demonstrate no clear correlation between preceding accumulated rainfall and radon activity and, as a consequence, no attempt at regression has been made. The lack of correlation is particularly obvious for the lower Pang springs (which includes Kimber Spring), where high radon content is observed during periods of both high and low rainfall. At no site does high rainfall result in a clear reduction in activity, as might be expected with the mixing hypothesis.

Similar uncorrelated radon variation is also reported for the Lower Pang by Mullinger et al (2007), who concluded that rainfall events did not appear to influence spring radon concentrations in a consistent manner, high and low radon corresponding with peak and base flow conditions. Such results suggest that, even though spring samples may consist of a mix of different groundwater ages from a range of sources, the radon activity of the major flow component is not dominated by rapidly percolated rainfall. In the case of Kimber Spring, although recorded increases in flow during periods of high rainfall have been noted (Maurice et al., 2006), it is still considered that this complex is likely to be fed predominantly by water sourced from a network of small fractures and fissures as a result of groundwater recession, rather than from fewer but larger 'karstic' conduits.

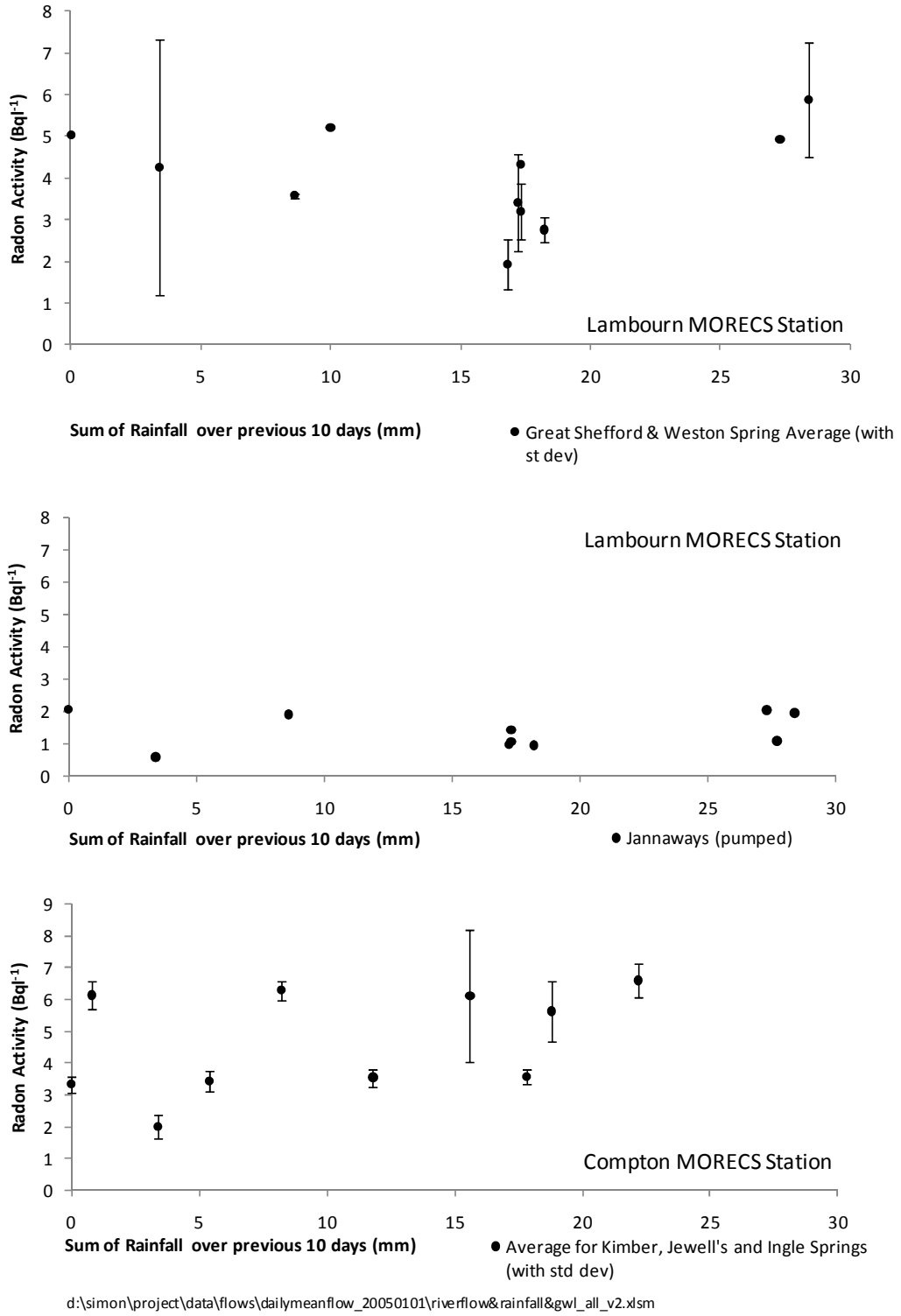

Figure 6—4 Radon activity from spring locations plotted against accumulated rainfall recorded at Lambourn and Compton MORECS weather stations.

6.1.2 Radon activity versus groundwater level changes

Through development of a five-component model of Chalk fissure-water, Low (1996b) suggested that radon activity at spring locations may be indirectly linked to groundwater level change. Namely that,

i. high radon activity matrix pore water may be released from storage (and supply the fracture network) during periods of groundwater level recession, as a consequence of elastic release and free drainage, but
ii. that high activities may also be expected during periods of recharge (and hence groundwater level rise), as a consequence of water being delivered to the fracture network via vertical piston flow within the matrix (estimated to contribute between 70% and 83% of the recharge delivered to the Chalk water table (Mathias et al., 2006b) and likely to have a residence time much greater than 25 days), but
iii. that, if present, rapid, direct recharge through a vertical fracture network (often referred to as 'bypass recharge') would be expected to reduce the overall activity of an integrated spring sample, given that insufficient time would have elapsed for radon equilibration to be achieved.

Low (1996b) presented plots of radon activity as a function of representative groundwater level for a series of spring samples in East Anglia, but concluded that it was not possible to identify a direct relationship between the two parameters. A further attempt to model a more detailed response at the Fleam Dyke research site permitted Low to suggest an advective flux of ^{222}Rn to the fissure space by drainage of matrix water from the unsaturated zone but that, in general, the results of the modelling exercise were considered poor.

For comparative purposes, this analysis was repeated for the major spring samples in this study, with the results presented in Figure 6—5 and Figure 6—6. In each case, all records were obtained for EA monitoring boreholes closest to the spring locations (see Figure 3—2). These data consisted typically of monthly dips, although some weekly data were available for the borehole at Bockhampton.

Figure 6—5 plots radon activity against the depth below groundwater level, and supports the conclusion by Low (1996a) that no simple relationship can be defined. However, the results do appear consistent with Low's (1996b) observations that the activity shows clear hysteresis, and that it is generally greater when groundwater levels fall compared to the onset of recharge and subsequent groundwater level rise. However, the data collected in

2006 are less supportive of this conclusion – and that, even though groundwater levels continue to change, radon activities remain similar throughout the year.

Given the proposed dependence of radon activity on the strength of the source term plus residence time, further work was undertaken to determine if spring activity was related to the rate of change of groundwater, as opposed to absolute level – based on an hypothesis that rapid changes in groundwater level will lead to an increase in the contribution of high radon content water from the matrix pore space to each spring.

Results from this analysis are presented in Figure 6—6, where the rate of change in groundwater level was calculated by considering the previous available dip measurement. For each result, the correlation coefficient was calculated, but linear regression analysis was not undertaken given the degree of scatter evident in the data. In each case, R values equal approximately -0.5, indicating a moderately strong correlation, but which is not considered strong enough to carry forward for predictive purposes. However, in qualitative terms the result do suggest that for each location the highest radon activities were observed during periods where rates of groundwater level recession were greatest.

Other authors have also considered groundwater rise as controlling factor on radon activity – for example in the Carboniferous Limestone, the storage aquifer for the thermal spring waters that issue at Bath (Andrews et al., 1982). Radon concentrations of water at the 'King's Spring' was observed to increase three-fold (from 38.1 to 98.1 $Bq.l^{-1}$) over the period 1977-79, and Andrews et al (1982) suggest that the increase may have been due to a 'delayed piezometric recovery following the drought conditions of 1976'.

Unfortunately, the authors do not explain explicitly the mechanism by which radon activity would be expected to increase. It is likely however, that the model envisaged is similar to a previously presented model (Andrews and Wood, 1972), where the radon source was thought not to be located primarily within the Carboniferous Limestone aquifer, but rather activity was elevated as a result of radium dissolution from deep percolation through Devonian Old Red Sandstone. However, such mechanisms are not considered relevant in this current study (there is assumed to be only one major aquifer system) and as a result no direct comparisons with this type of conceptual model is made.

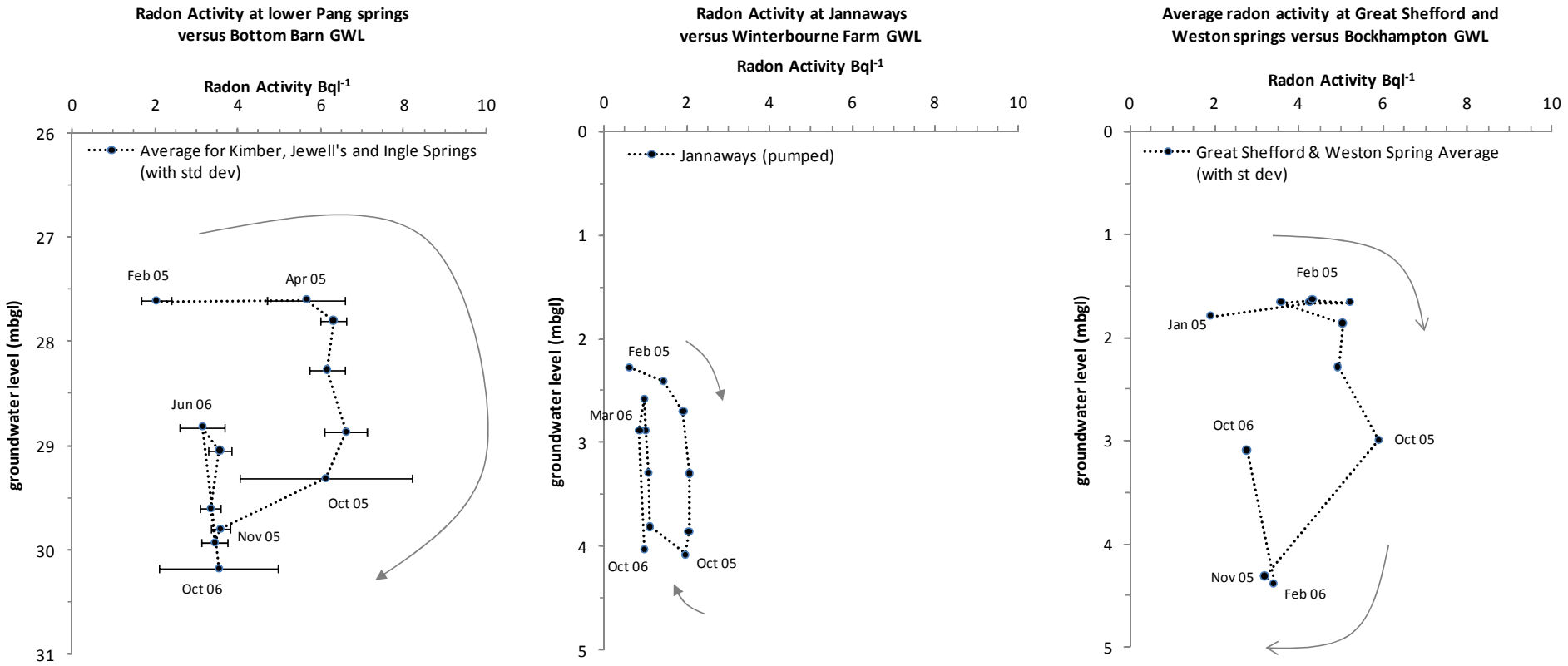

Figure 6—5 Radon activity from spring locations plotted against interpolated groundwater levels for selected boreholes (Jan 2005 to Oct 2006)

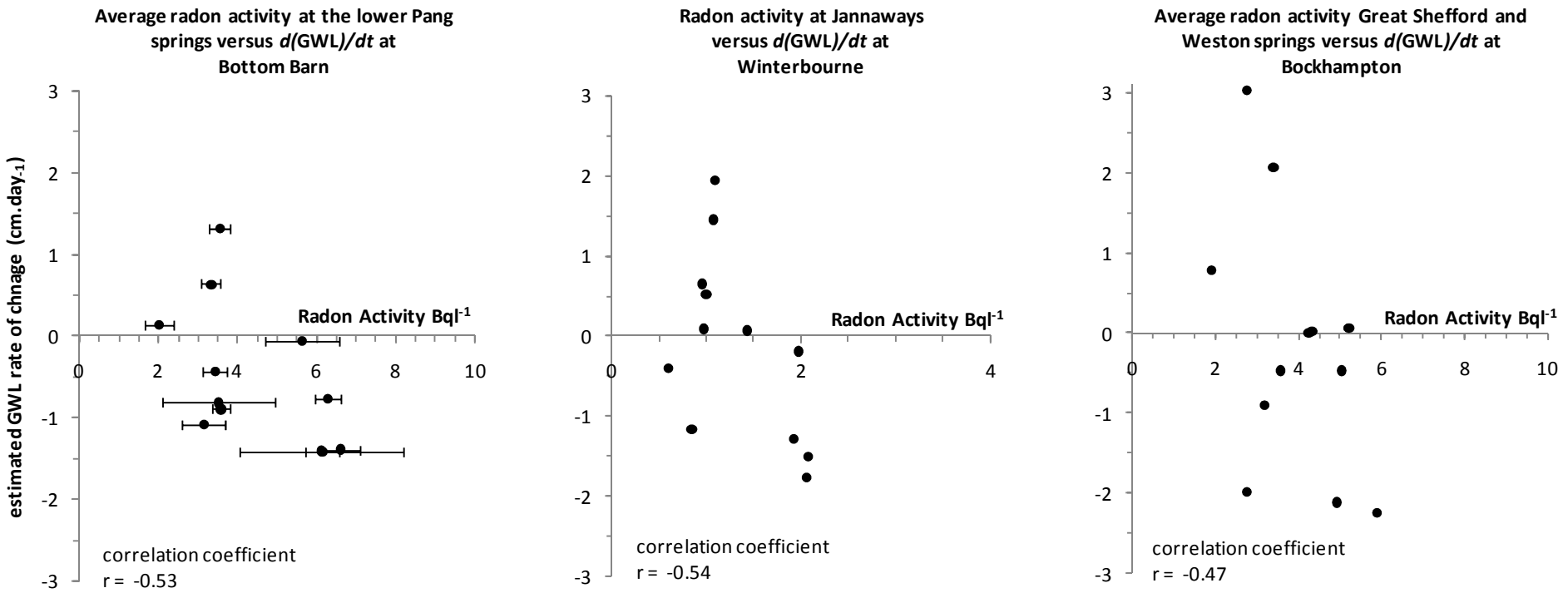

d:\...\flows\dailymeanflow_20050101\[riverflow&rainfall&gwl_all_v3.xlsm

Figure 6—6 Radon activity from spring locations plotted against estimated rate of change in groundwater levels (cm.day^{-1}) for selected boreholes (Jan 2005 to Oct 2006)

6.1.3 Spatial Distribution

Spatial plots of radon activity for all sites monitored are presented in Figure 6—7 (2004/2005), Figure 6—8 (2005/2006) and Figure 6—9 (2006/2007). All data collected have been classified in broad classes, representing two halves of the standard water year – 'winter', related to all data collected between October and March and 'summer', for data collected between April and September. Although there is no consistent spatial pattern to the activities recorded, several trends in activity may be noticed, namely,

i. the spring sources near the middle reaches of the southward flowing River Lambourn (i.e. Great Shefford, Weston) typically show the highest radon activity in this river system,
ii. Activities recorded at the Winterbourne OBH, at the top of Winterbourne Stream, are consistently greater than those at the spring site at Jannaways and Bagnor OBH, both located at the bottom of the same river valley,
iii. the springs that feed the Pang in its lower reaches have activities that are similar to borehole samples to the west (i.e. Briff Lane), but greater than borehole samples collected further upstream (i.e. Frilsham).

However, given the lack of spatial coverage, contouring was not considered appropriate at this stage. Both Zereshki (1981) and Low (1996) demonstrated that some trends in activity could be identified in sub-groups of their data – Zereshki identified a trend in borehole samples that related to the distance from extensive karst development, but observed no significant variation in the radon content of the spring water. Low (1996b) was able to delineate several regional zones of radon activity in Norfolk, with lower values recorded with increasing distance eastwards from the western edge of Chalk outcrop. This variation was attributed to the decreasing influence of high radon content groundwaters from the Lower Chalk units, which although exposed in the west increased in depth eastwards due to the regional dip. Several locally high activity anomalies in the east were thought to be due to samples that contained a mix of waters sourced from the Chalk and overlying glacial deposits, which were likely to have higher overall U-series content.

These data suggest that no clear pattern of variation in radon activity is evident across the catchments. In combination with the temporal results presented previously, it is now apparent that the integrated nature of spring samples (i.e. potentially a mixture of waters sourced from many different components of the regional groundwater flow system) does not provide a clear indication of either the strength or the location of the radon source term – but rather, must be interpreted on the basis of some form of mixing or dilution

model. However, the analysis undertaken has not demonstrated significant correlation with the catchment scale data sets, such as rainfall and changes in groundwater level, and suggests that better characterisation of individual sites is required.

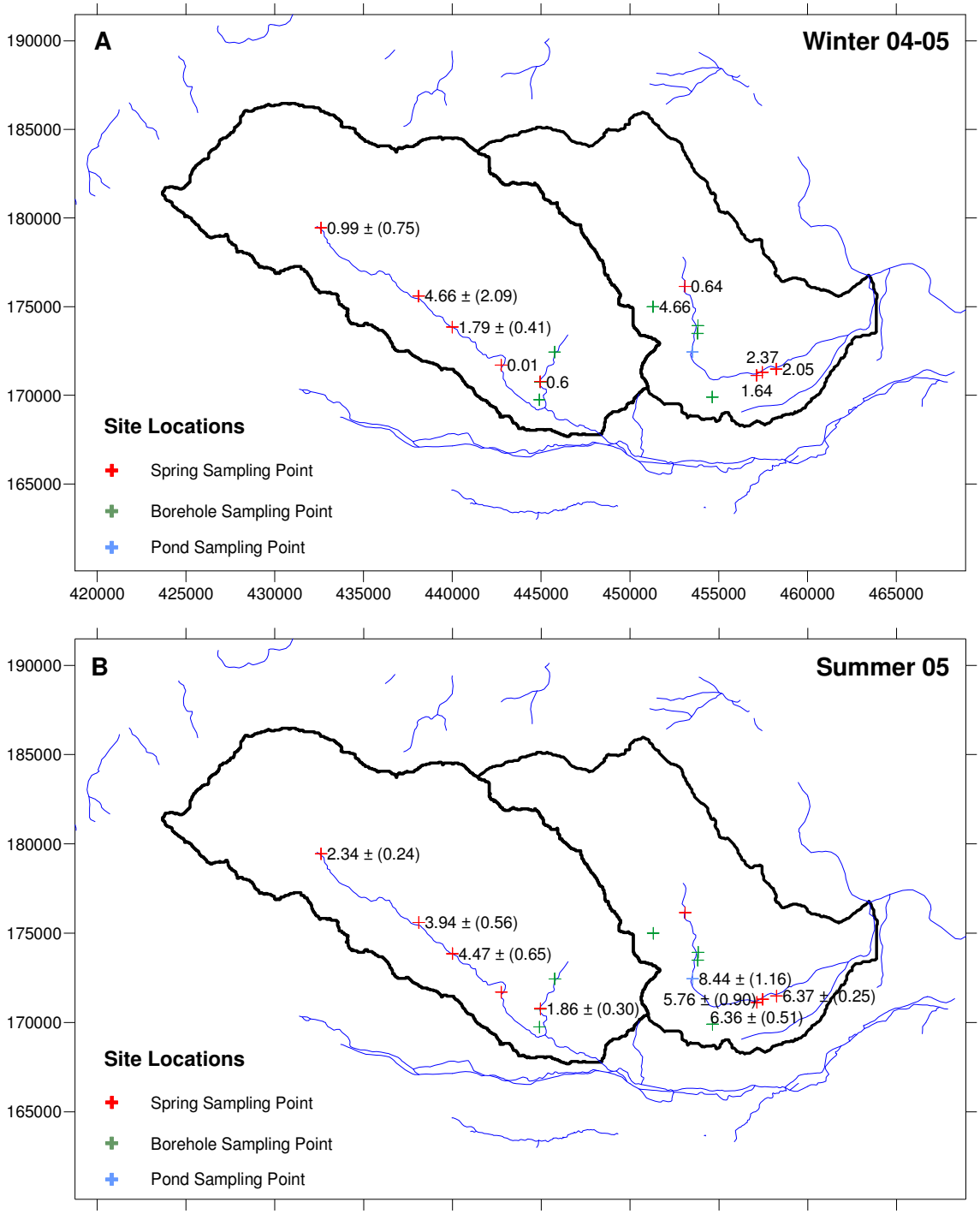

d:\simon\project\calcs\surfer\gwlcalcs\radon_temporal.srf

Figure 6—7 Radon activity (temporal plot), A) Winter 2004-05 and B) Summer 2005

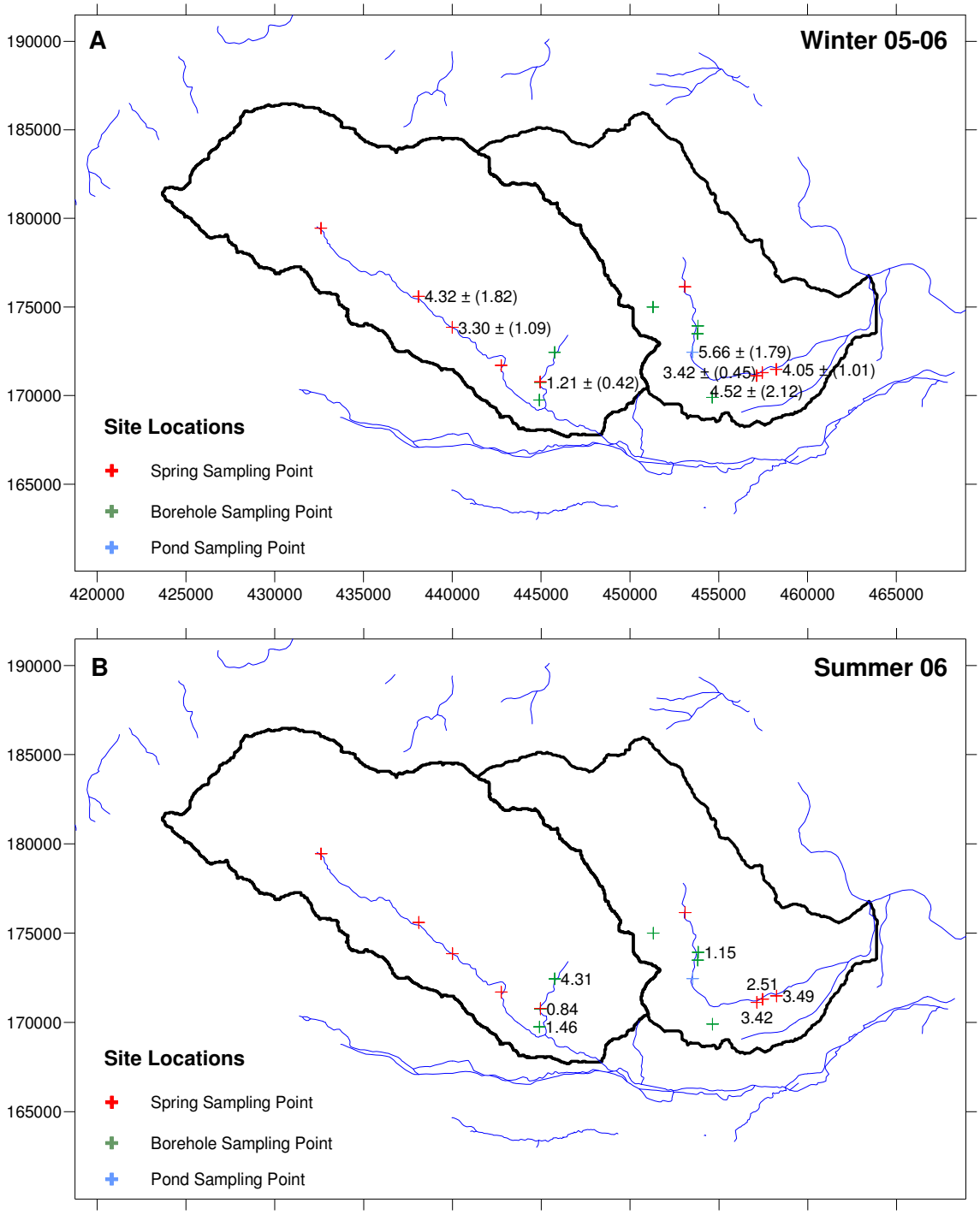

d:\simon\project\calcs\surfer\gwlcalcs\radon_temporal.srf

Figure 6—8 Radon activity (temporal plot), A) Winter 2005-06 and B) Summer 2006

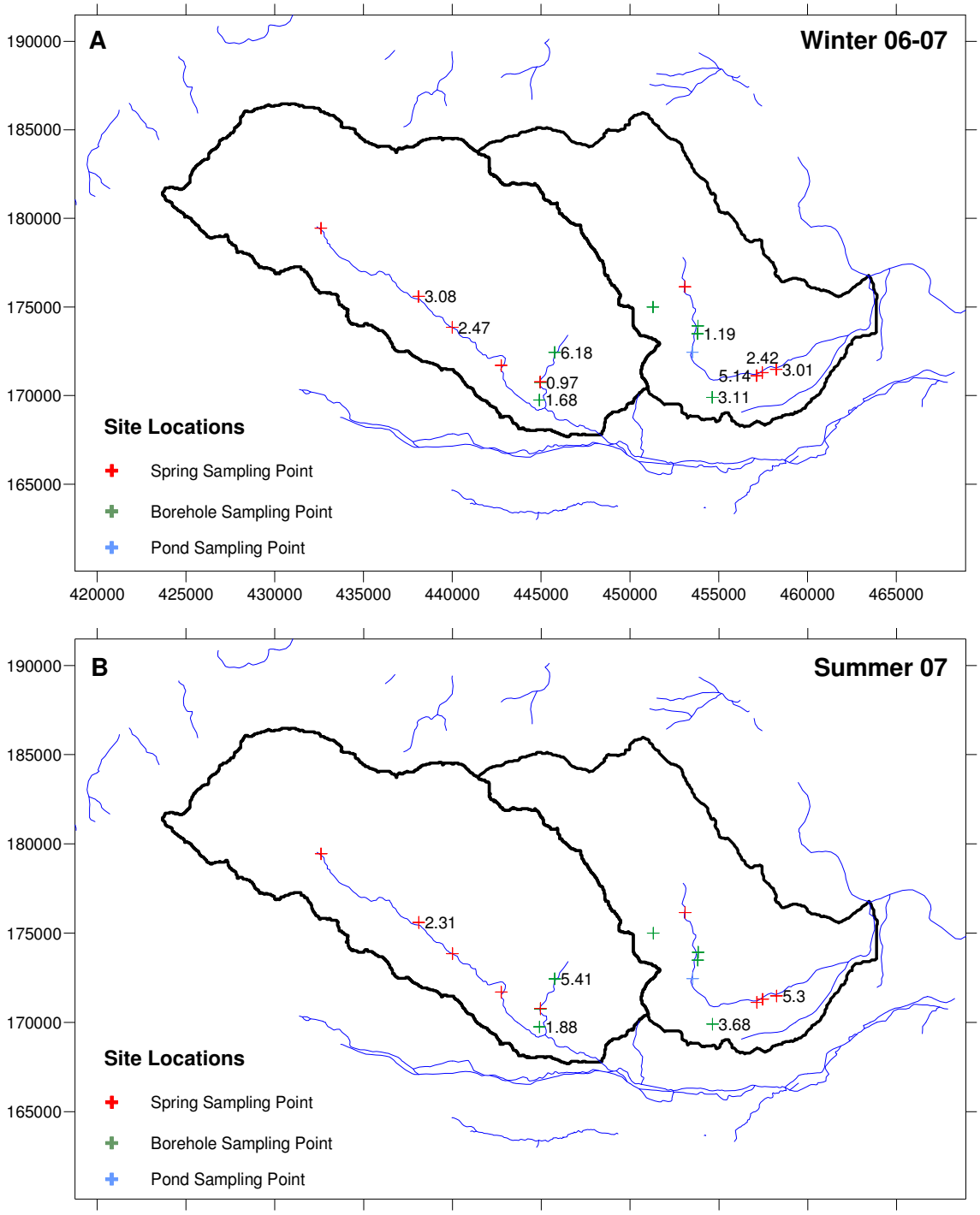

d:\simon\project\calcs\surfer\gwlcalcs\radon_temporal.srf

Figure 6—9 Radon activity (temporal plot), A) Winter 2006-07 and B) Summer 2007

6.2 Pumping Tests

6.2.1 Large scale pumping of Bottom Barn abstraction borehole.

Pumped groundwater was sampled for radon at two separate pump tests at the Environment Agency's augmentation abstraction borehole Bottom Barn, located in the vicinity of the Trumpletts Farm LOCAR site in summer 2005, as part of a tracer test conducted by Imperial College and BGS Wallingford (detailed by Butler et al., 2009).

The results are presented in Figure 6—10 and are compared with the work of Ward (1989), who undertook similar analysis of radon activity from Chalk boreholes in East Anglia. For comparative purposes, the results have been normalised for well volume to account for the larger diameter of the borehole at Bottom Barn. The details of each borehole and the pump test conditions are also provided for reference in Table 6—2.

(Note that the samples from the Trumpletts Farm tests were also analyzed for dissolved radium, although in each case no radium signature was recorded above the limit of detection of the LSC method (*c.*0.05 Bq.l^{-1}) and consequently, the results are not reported further).

Table 6—2 Comparison of pumping conditions between large scale Anglian and Berkshire Chalk pump tests that have measured radon activity.

	Anglian (Ward 1989)			*Berkshire (this study)*
	Well 3A	*Well 9A*	*Well 11A*	*Trumpletts Farm 9 & 27 Mar 05*
Depth (m)	85.34	84.43	115.82	86.90
Diameter (m)	0.457	0.457	0.457	0.800
Open Hole Length (m)	54.96	53.58	112.76	64.10
Pump rate (l.s^{-1}, Ml.day^{-1})	50.0 (4.3)	62.0 (5.4)	50.5 (4.4)	65.5 (5.7)
Well volumes per hour	20.0	25.4	9.8	8.1

Source: Anglian data abridged from Ward (1989), Trumpletts data d:\simon\project\calcs\radon \pumptests\[rnpumptests_all.xlsm]ward_compare

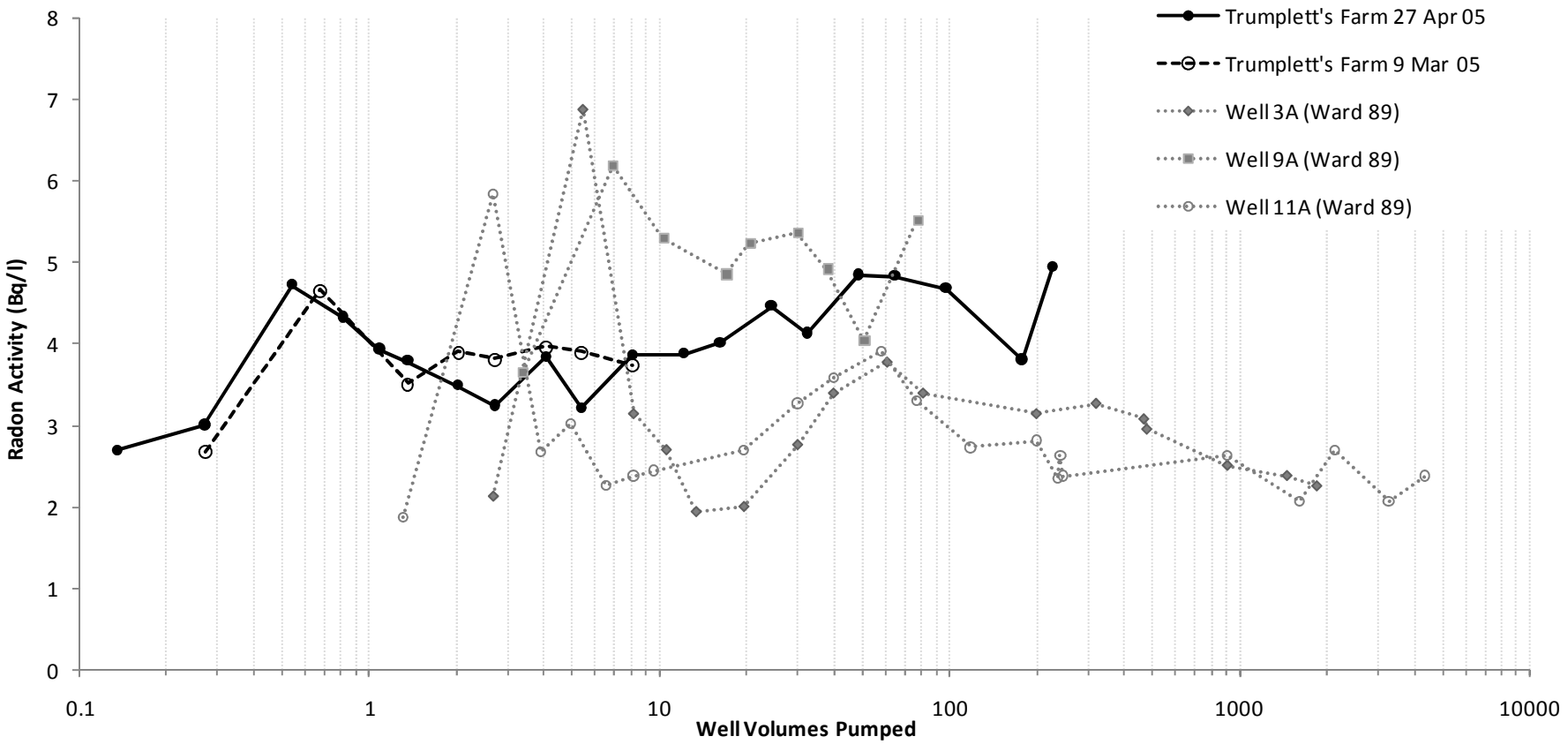

d:\simon\project\calcs\radon\pumptests\[rnpumptests_all.xlsm]ward_compare

Figure 6—10 Radon activity from two large scale pump tests of the EA groundwater abstraction borehole at Trumpletts Farm, compared with previous data from other Chalk boreholes collected by Ward (1989)

The two new tests show similar results to each other initially at the start of pumping, with radon activity rapidly rising from approximately 2.5 to 5 $Bq.l^{-1}$. Activity quickly reduces again, although not to the initial level. For the shorter test conducted on 9th March, there then follows a period of stabilisation where radon activity increases slightly from 3.3 to 3.8 $Bq.l^{-1}$ and remains fairly constant for the remainder of the pumping. However, results from the longer duration test illustrate that equilibrium is never achieved even after the equivalent of 200 well volumes have been abstracted, with activity gradually rising again from the first minimum and reaching levels similar to the first peak observed at the start of pumping.

Although there is clear difference in the timing of the peak levels, the results are quite similar in form to those reported by Ward (1989), in particular that an equilibrium radon activity is not quickly established – and that multiple peak and troughs may be observed. Such results have not been reported elsewhere in the literature and seem to be specific to the Chalk aquifer. For example, pumping from the Carboniferous Limestone (Zereshki, 1981) displayed a much simpler response consisting of a gradual rise in radon activity over time to reach a maximum after c1 hour (equivalent to 1.6 well volumes), and similar results are reported in fractured (but single porosity) meta-sedimentary aquifers (e.g. Cook et al., 1999). These data suggest that radon content of Chalk groundwater evolves in a much more complex fashion (that may be a function of both the duration and the rate of pumping), and that pumping does not necessarily provide samples that are representative of a specific radon source.

Ward (1989) suggested several distinct phases of radon evolution in a pumped Chalk borehole, which are now considered in relation to the new data. These phases may be summarised as follows – namely,

i. Water sampled at the immediate commencement of pumping will tend to have low radon activity, due to de-gassing and the decay of unsupported radon within the water column;
ii. That once stagnant water from the well has been removed, there will a rapid rise in radon activity as water close to the well is drawn into the borehole. The rapid rate of change in pumped water level and the elastic response of the aquifer would produce an influx of water from the smaller compressible voids, that form part of the surrounding rock matrix – i.e. that there will be rapid expansion of water close to the well, with an associated release from storage as the pressure is reduced;

iii. As the rate of change in water level reduces and a pressure equilibrium is gradually achieved between the porous matrix and larger fractures, there will be a reduction in the radon activity as water is drawn mainly from the fracture network, outside the initial 'elastic response' zone;

iv. That as the cone of depression spreads, there will be drainage of fissures (and larger matrix pores), and this water will now feed the fissure network to deliver water to the well. Characterized as form of 'delayed drainage' from the matrix pores, the radon activity would tend to rise again;

v. That as water is drawn from greater distances from the well, there would be a reduction in delayed drainage and eventually an equilibrium radon activity would be achieved, at a level that would be controlled through a combination of the (distant) source term and the ratio of the travel time to the well and the half life of radon.

It is suggested that at least the first four stages have been observed in the results from Bottom Barn. In both cases, radon activity started from a low level and rapidly rose to an initial peak, followed by a reduction and then gradual rise again as the test continued. However, the results seem to have much more temporal variation even after 100 well volumes have been pumped. This suggests that many different sources of water may continue to contribute to the sampled water, and that further characterization of the distribution of inflowing horizons, as well as the local piezometric response, may need to be considered.

6.2.2 Packer Testing

Results from the monthly spring sampling survey indicated that there was significant variation in radon activity over time from the same location, and it was considered that these samples were not representative of any one radon source but rather, were composed of a mix of waters reflecting the delivery of water many different delivery routes. Hence, to investigate further the relationship between radon production in the chalk matrix and radon activity in groundwater, it was considered necessary to take water samples from packered intervals for which uranium and radium assays of chalk material were also available (i.e. at Trumpletts Farm PL10-A). Such a configuration was thought to reduce the uncertainty in the source of water sampled, plus provide a direct indication of the potential strength of the radon source term.

Details of the packer system used at Trumpletts Farm have been described previously in Section 4.2.1. The elevations of each packered section are indicated by shaded regions in Figure 6—11. This figure also includes other related borehole data such as diameter, gamma signal, results from the uranium assay for bulk samples presented above, as well as values of hydraulic conductivity calculated by Williams et al (2006). The location of the pump intake used for a subsequent open hole test is also illustrated as a dashed shaded region (*c.*70 m bgl). Radon activities of pumped water sampled from the rising main are illustrated in Figure 6—12, with full details of the pump test (e.g. rate, water level, sampling times) provided in Appendix D. Given the volume of each test interval, calculated on the basis of caliper log data, the configuration ensured that at least 6 (and up to 14) interval volumes were pumped at each elevation.

The results demonstrate that groundwaters from packered sections all reached a steady radon activity more rapidly than from the larger scale open-hole pump tests conducted at Bottom Barn (where water was pumped at a rate 100 times greater than from the packered intervals). Samples from the top interval show a small rise in activity as soon at the pump is switched on, which is typical of pumping from initially undisturbed wells, and which indicates a degree of degassing and radon decay from the previously stagnant water column. A steady activity of 2.0 $Bq.l^{-1}$ is then rapidly achieved for the remainder of the test (30 mins). Similar results are observed from the lower sections, although all demonstrate an initial *decrease* in activity once the packers had been lowered and the pump restarted. Final radon activities from the lower packered intervals are lower than from the top section.

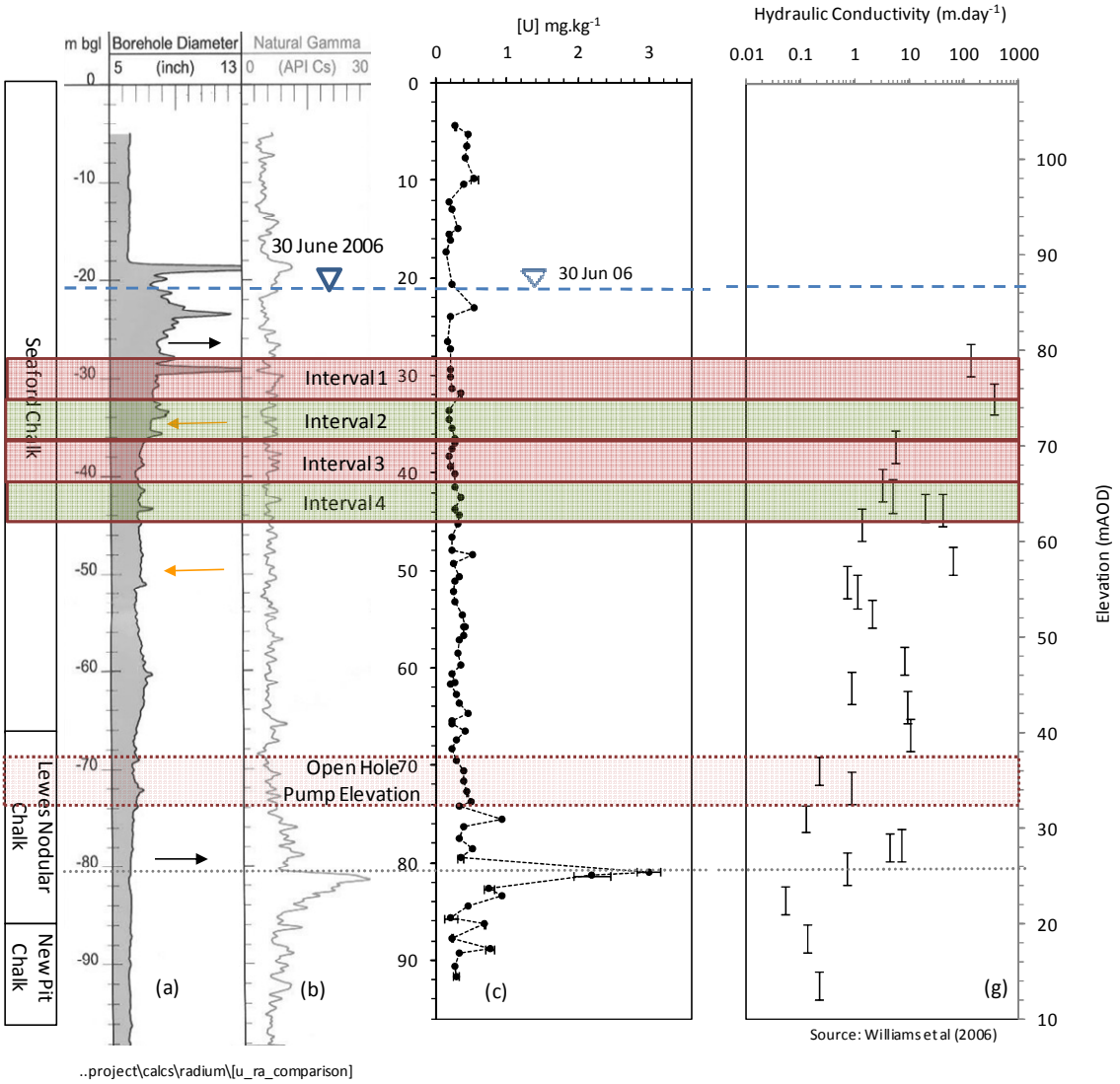

Trumplett's Farm integrated data plot

Figures (left to right) - borehole diameter (inch), natural gamma log (API Cs), hydraulic conductivity from previous packer testing ($m.day^{-1}$)

Horizontal arrows – recorded in-flowing horizons, Dashed horizontal line – measured water table 30 Jun 2006 before packer testing, coloured bars - packer test intervals

Figure 6—11 Packer Intervals pumped at Trumpletts Farm PL10A, July 2006.

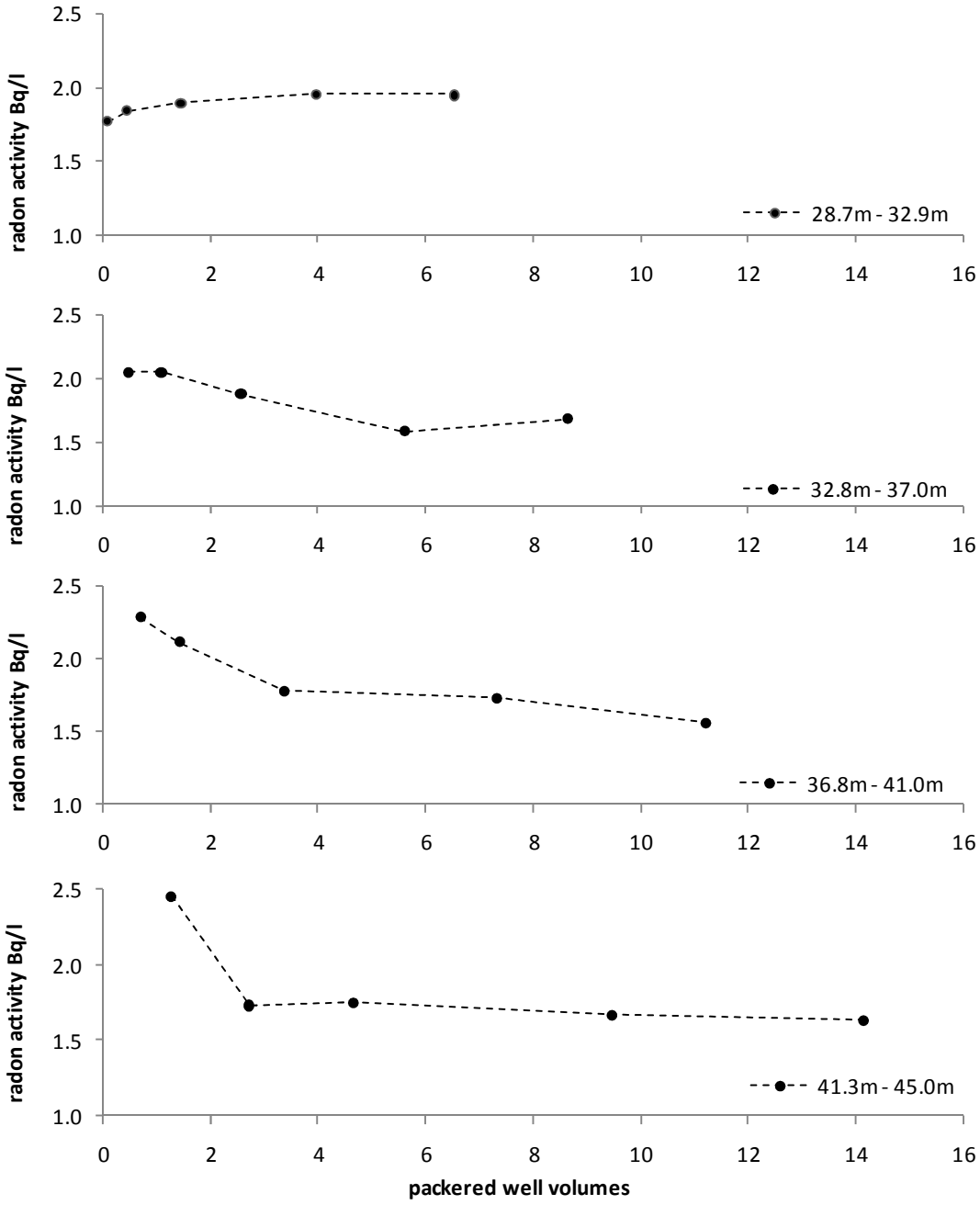

D:\Simon\Project\Calcs\Radon\PumpTests\[TrumpPacker_AllResults.xls]All packer results

Figure 6—12 Radon activity from packered sections of Trumpletts Farm PL10A, July 2006.

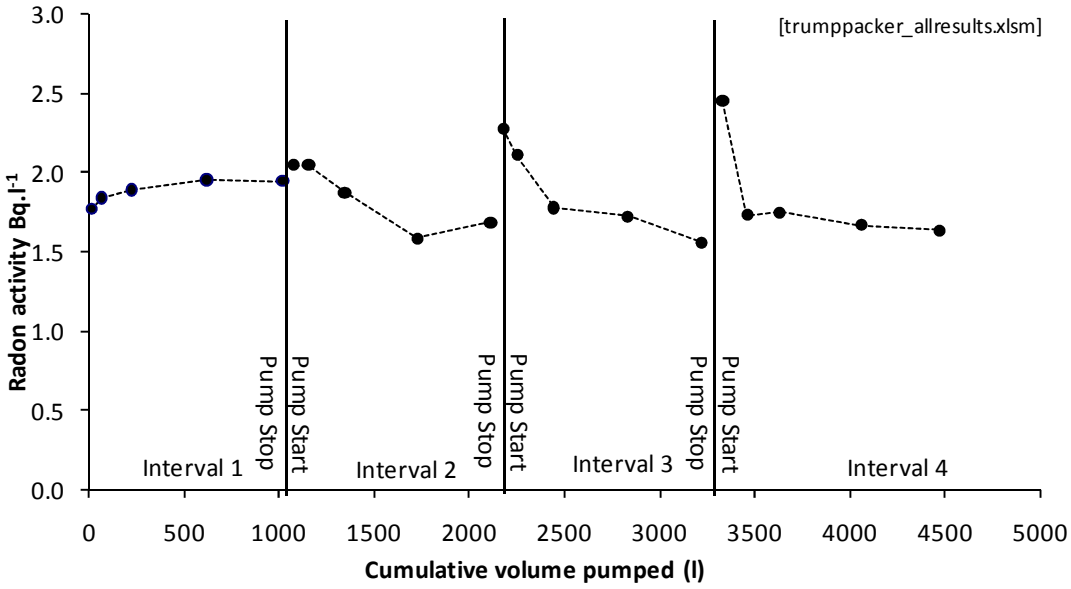

Figure 6—13 Radon activity Trumpletts Farm packer test as a function of cumulative volume pumped

Given the disturbed nature of the water column and surrounding fractures as a result of previous pumping, this initial decrease is difficult to interpret, but does not appear to reflect the activity of the water remaining in the rising main during the reconfiguration of the packer string. This difference is illustrated more clearly in Figure 6—13, where radon activity is plotted as a function of the cumulative pumped volume (noting that a period of several hours may exist between the cessation of pumping, reconfiguration of the packer string and the pump start). In each case, the initial radon activity from each section appears to increase as the string is lowered to the next packer interval, before a new equilibrium activity is achieved.

Considering the initial responses observed from the larger Bottom Barn abstraction and Ward's (1989) hypothesis, the results from the lower sections suggest that the initial higher radon activity may be controlled by release of water from smaller fractures and matrix pore space as the piezometric head drops within the packered interval. This response may therefore be analogous to the decrease from the first peak observed in the larger tests. However, given the much lower pump rates, it would not be expected that significant release from the surrounding matrix material would be apparent once a stable pressure head had been achieved. Rather, it is felt the steady radon activity achieved over 30 minutes is dominated by water sourced from the most transmissive fractures within the packered interval, and which are able to deliver water to the well without significant head gradients being induced through the bulk material.

6.2.3 Open hole pump test at PL10A

Following the cessation of the packer testing, the string was completely removed but the pump was lowered again to undertake a open hole test, with the intake point located at *c.*69 mbgl just above a restriction in the borehole. Water was pumped at an average rate of 1.8±0.1 l.s-1 for 7 hours, with radon samples taken at regularly intervals throughout the test. Results from the test are presented in Figure 6—14, with details collated in Table D5 of Appendix C.

The evolution of the radon signature is similar to that observed previously during the packer testing, with an equilibrium activity of *c.*2.3 Bq.l^{-1} being established after the equivalent of several well volumes had been pumped. A gradual rise in activity over time is then observed, but on much smaller magnitude of change when compared to the larger pump tests at Bottom Barn. (located 40 m to the east). The slightly higher radon activity from lower within the borehole suggests the pumped water may be derived from a fracture network that integrates a range of high and low activity waters. This hypothesis is supported by single borehole dilution testing (Williams et al., 2006), which identified a prominent inflow horizon associated with the Chalk Rock hardground (indicated on Figure 6—11), with upwards flow present in the borehole during ambient conditions. However, pumping from Bottom Barn was observed to flow horizons in additional horizons above this elevation, and which are likely to have contributed water to the pumped samples.

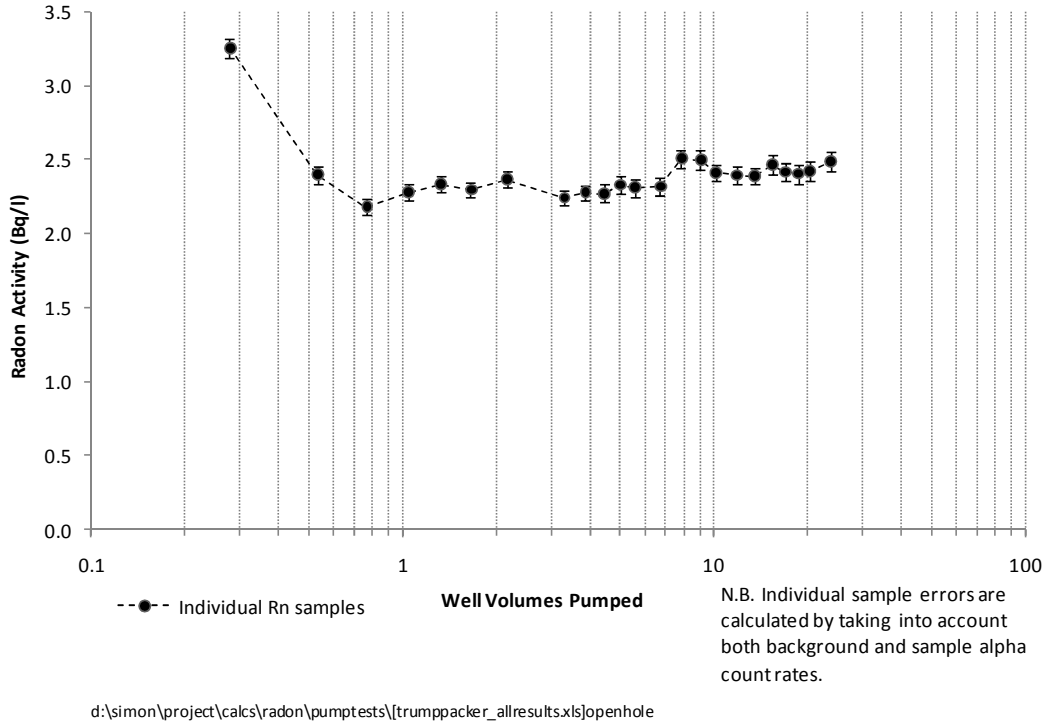

Figure 6—14 Radon activity from open hole pump test of Trumpletts Farm A, July 2006

6.3 Estimating fracture water radon activity

From the results of all the borehole samples undertaken, it is now clear that radon content is in part dependent on the rate at which water is pumped. For example, with lower pump rates radon activities are considered primarily representative of the surrounding fracture water, with little contribution from water drained from the matrix. The open hole discharge rate of 2 $l.s^{-1}$ indicated radon content settling in the range 1.7 to 2.5 $Bq.l^{-1}$, with plateau conditions achieved after *c.*4 well volumes had been pumped.

This is in contrast to the results from the large pump test at Bottom Barn and to some degree the packer testing of PL10A. The large scale tests illustrate the complexity of the evolution of the radon signatures from the Chalk and supports the previously discussed theory, developed by Ward (1989), that many different sources of water have been mixed together as the cone of depression develops and water is drawn from greater distances from the well. Of particular note is the large peak in radon activity observed soon after the start of pumping, which is thought to indicate the rapid release of water from the matrix pore space in the immediate vicinity of the well. Such water would be expected to have much higher radon activity that the fracture as suggested by Atkinson et al (2001). The fact that the sampled waters contained unsupported radon (i.e. the radium content of the water was negligible in comparison to that within the solid matrix) also supports the theory the water has been rapidly released from the matrix.

In contrast, low pumping rates would be expected to produce little or no drawdown, such storage effects are largely absent and radon activity is considered to reflect solely the ambient content in fractures. In the case of Trumpletts Farm, undisturbed fracture water is in the range 1.7 – 2.5 $Bq.l^{-1}$, although there is some variation between the fissures sampled in each packered section. The higher values obtained in the open-hole sampling (Figure 6-14) are thought to reflect the contribution from high U and high Ra Chalk in the lower part of the Lewes Nodular Formation, as evinced from the uranium assay work (i.e. as indicated Figure 6—11 and as previously presented in Figure 5—1).

In conclusion, it is considered that low pump rates provide the most appropriate indication of fracture water activity, as required by the model by Atkinson et al (2001), and which should now be carried forward for the calculation of transport parameters. In contrast, samples taken from boreholes with high pumping rates are unlikely to provide representative radon activities of ambient, undisturbed fracture water.

.

6.4 Groundwater geochemistry

The majority of waters sampled for radon were also assayed for major ion species as part of the sampling round, analysis being undertaken by ICP-MS and ion-chromatography (see Chapter 4). Other field measurements (pH, dissolved O_2, conductivity and temperature) were made on site, and alkalinity was determined by titration once the samples has been returned to the laboratory. All geochemical results are tabulated in Appendix E.

Major ion chemistry for all spring samples is presented in the form of a Piper diagram in Figure 6—15, each sample grouped according to the catchment from which it was obtained. The results indicate that the groundwaters are very similar in composition and that all may be classified as belonging to a calcium bicarbonate type hydro-chemical facies, similar to that described by Lloyd (in Downing et al., 1993, Ch 12) as 'modern' water (or 'Water Type Ia', with high concentrations of calcium and bicarbonate of between 80-150 mgl^{-1} and 250-350 mgl^{-1}, respectively). Total Fe concentrations are also confirmed as very low in such oxygenated waters (Appendix E).

Samples from Pang catchment (i.e. Jewell's, Ingle Spring and Kimber Spring) have slightly increased (Na+K)/Ca ratios which may suggest a degree of mixing from sources other than Chalk groundwaters. Previous work suggests that water sourced from overlying Palaeogene sediments may also feed the springs in the Lower Pang, as evinced from the spring water composition lying on the mixing line between the Chalk-Palaeogene spring sample end members (Wheater et al., 2007). Neal et al (2004) described the results from an extensive groundwater geochemistry sampling round from the same catchment and report similar findings. Their results also demonstrated that dissolved calcium, barium and strontium are derived predominantly from the weathering of the calcium carbonate matrix, with bicarbonate produced not only from the solubilisation of calcite, but possibly from near surface biogenic origin.

An alternative form of data presentation is the Schoeller diagram (Figure 6—16), where the ionic concentrations of the major ionic components are expressed as milli-equivalents per litre ($meq.l^{-1}$) and are plotted on a logarithmic vertical scale. Compared to a Piper diagram, the differences include a plotting of the absolute concentrations rather than relative percentages. The figure has been coloured according to the location of each spring (brown/orange - Lambourn, green – Winterbourne Stream, blue – Pang). Once again, the greater concentrations in Mg^{2+}, $Na^{+}+K^{+}$ and Cl^{-} are apparent in the Pang samples, which supports the hypothesis that these spring waters may consist of a mix of water facies.

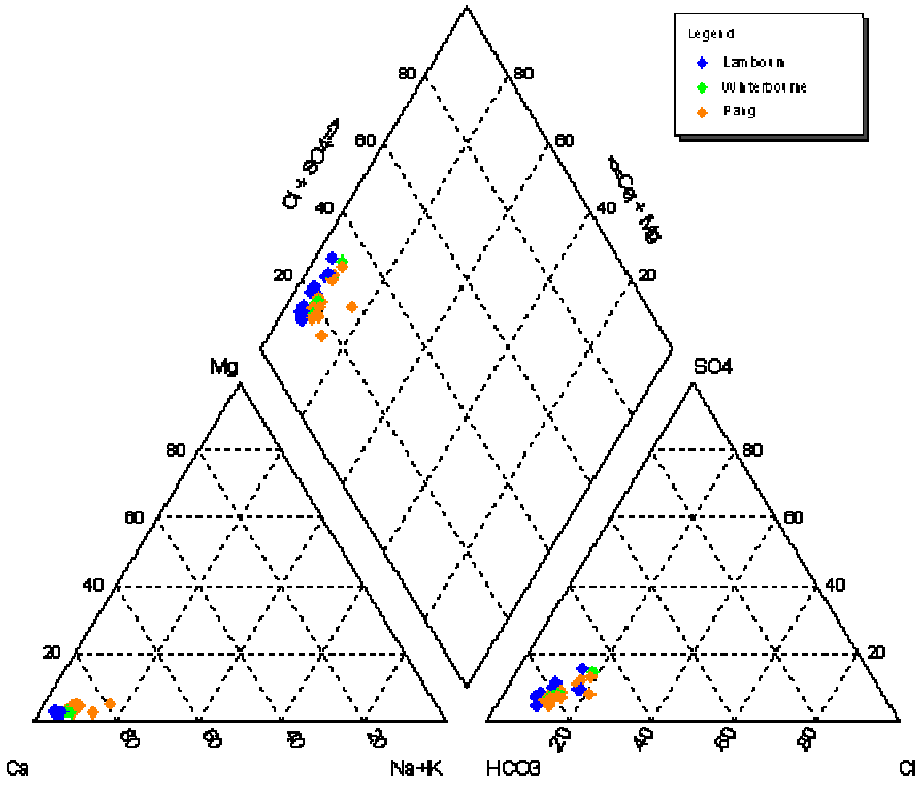

Figure 6—15 Piper Diagram for spring samples (Feb 2005- Oct 2006)

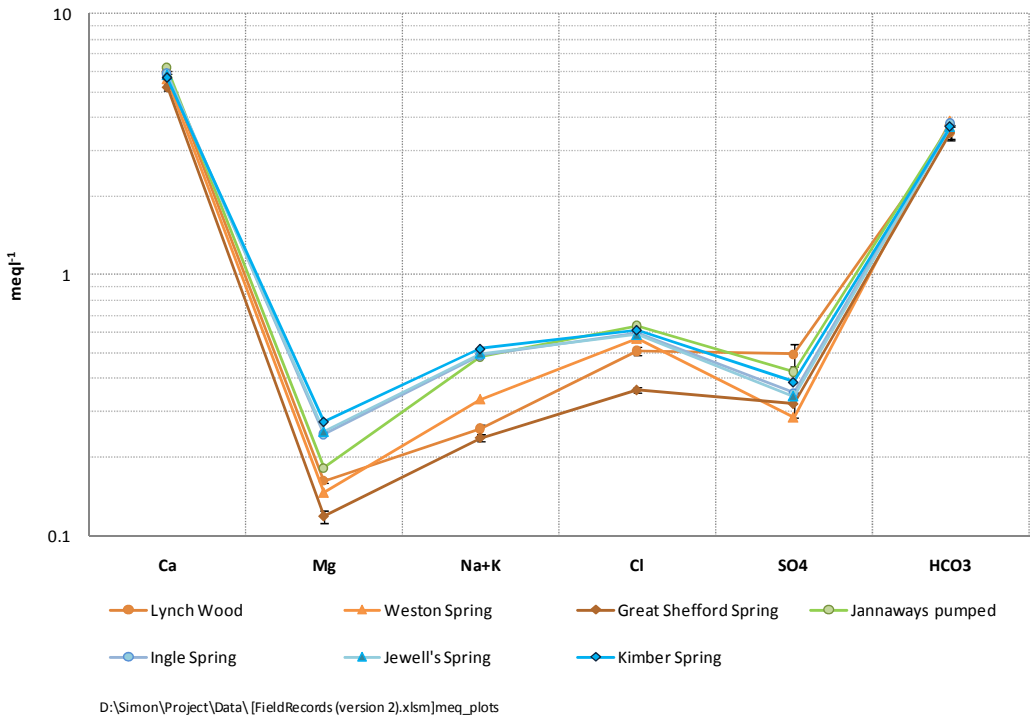

Figure 6—16 Schoeller diagram for major dissolved species at spring locations (mean results 2005-2006, average population size per site (n) = 5)

To test the hypothesis that Ca^{2+} enters solution via the dissolution of $CaCO_3$ by carbonic acid, a plot of the molar ratio of Ca^{2+} to HCO_3^- has been determined for those samples judged to have an acceptable ionic balance (i.e. where the ratio [anions-cations]/[anions+cations] was less than 0.05). The results are presented in Figure 6—17, which also includes the theoretical molar calcium concentration expected from carbonate stoichiometry. As all samples plotted lie above this line, the results suggest that other chemical processes contribute to the release of Ca^{2+} into solution – i.e. either (a) from another source (i.e. not supplied from the dissolution of carbonate), or (b) that a different acid is also involved in calcite dissolution.

In an investigation of Chalk groundwaters in Berkshire, Elliot et al (1999) considered the theoretical additional supply of Ca^{2+} from the concurrent dissolution of gypsum. Contribution from a solid solution impurity of $CaSO_4$ in calcite may also be possible, but is considered unlikely given the low concentration in the Chalk. Furthermore, as samples plotted were from taken from surface spring sources on agricultural land it could be hypothesised that some additional component of Ca^{2+} has also entered solution form the dissolution of nitrogenous fertilizer (or alternatively from the presence of nitric acid produced by the oxidation of organic matter). Ion exchange may also be a possible source of Ca^{2+} (with exchange of Na^+ from groundwater) - however there is no evidence to support this in the Ca^{2+}/Na^+ ratios obtained from the major samples (Table 6—3).

Considering these potential new sources and alternative acids, the Ca^{2+} data were adjusted by subtracting both the SO_4^{2-} and NO_3^- molar concentrations in the appropriate stoichiometric ratio for gypsum and fertilizer solution, and the plot redrawn (Figure 6—18).

For all samples it is clear that there is now more agreement with the calcium concentration expected from carbonate stoichiometry. This result supports the theory that, although calcite dissolution by carbonic acid is the predominant mechanism for the release of Ca^{2+} into solution, there is an observable and consistent contribution from other chemical processes. However, it is accepted that further more detailed analysis would be required to identify the exact source and/or acid(s) involved.

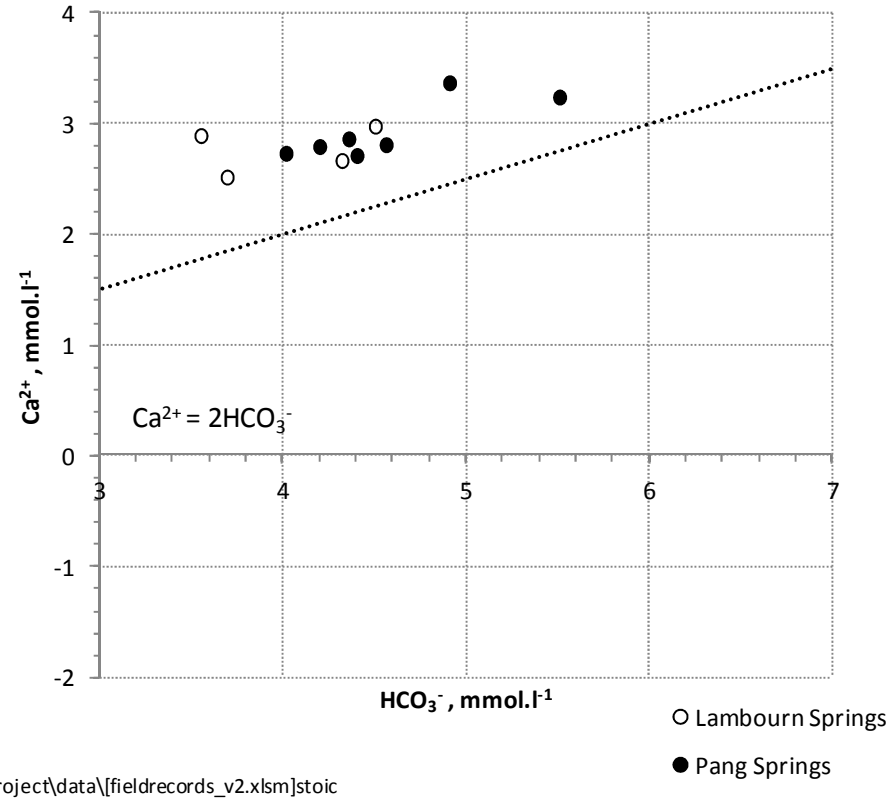

..project\data\[fieldrecords_v2.xlsm]stoic

Figure 6—17 Molar ratio of Ca^{2+} versus HCO_3^- for Chalk spring samples with ionic imbalances <5%.

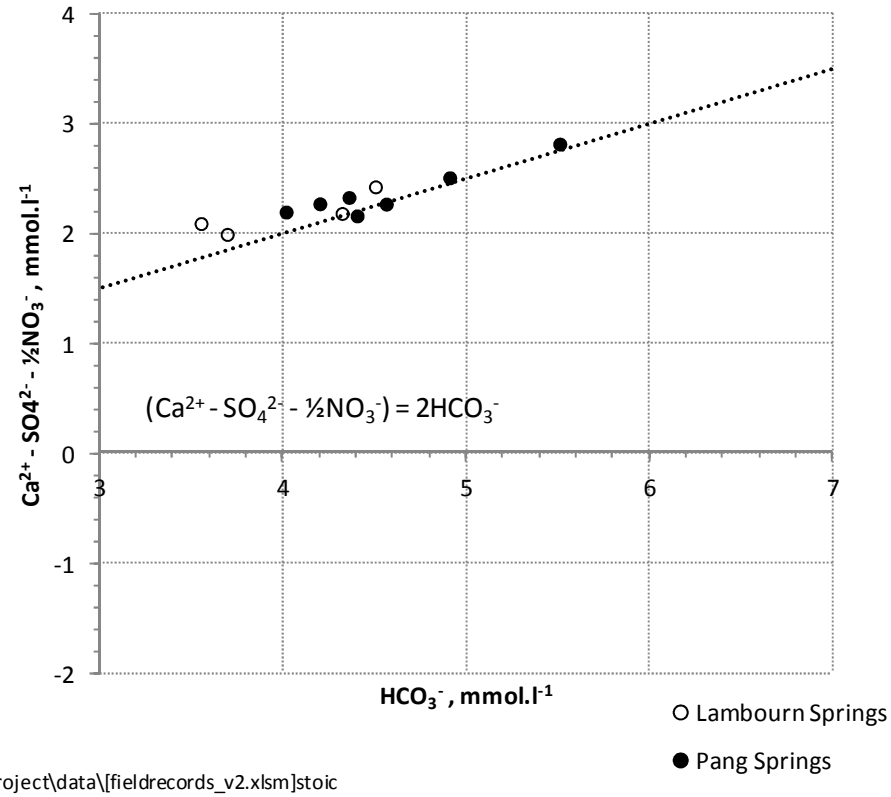

..project\data\[fieldrecords_v2.xlsm]stoic

Figure 6—18 Molar ratio of Ca^{2+}-SO_4^{2-}-$½NO_3^-$ versus HCO_3^- for Chalk spring samples with ionic imbalances <5%.

Table 6—3 Ca^2+/Na+ molar ratios for spring samples.

Spring Name	*Average (-)*	*St Dev (-)*	*Min (-)*	*Max (-)*	*n*
Lynch Wood	12.59	± 0.92	10.83	13.35	6
Great Shefford Spring	11.78	± 0.82	10.69	12.59	7
Weston Spring	8.81	± 1.03	6.55	9.89	10
Jannaways pumped	6.80	± 0.53	6.31	7.51	10
Ingle Spring	6.66	± 0.53	5.90	7.53	11
Jewell's Spring	6.68	± 0.47	6.22	7.54	11
Kimber Spring	6.10	± 0.54	5.23	7.06	11

Source: ..project\data\[fieldrecords_v2.xlsm]gresswell

Correlation of geochemistry with radon activity

The significance of the correlation between radon activity, major ion and other field chemistry results has been assessed using the "Student's" t test. This was initially applied to pooled results for the three major sampling locations in the Lower Pang (Kimber Spring, Ingle Spring and Jewell's Spring), for all dates where both radon and other chemical data were available. As illustrated previously, these three locations showed similar magnitude and temporal variability over the study period. They were also regarded as the most consistent and reliable locations from which groundwater samples were taken and provide the most reliable dataset for further statistical analysis.

From statistical theory, the distribution of a sample's correlation coefficient r_{XY} depends on the value of the population coefficient ρ_{XY}. When $\rho_{XY} = 0$, the sample variance of r_{XY} is equal to

$$S^2_{r_{XY}} = \frac{1 - r^2_{XY}}{n - 2} \qquad (6\text{-}1)$$

and the ratio

$$t = \frac{r_{XY} - 0}{S_{r_{XY}}} = \frac{r_{XY} - 0}{\sqrt{\frac{(1 - r^2_{XY})}{(n - 2)}}} \qquad (6\text{-}2)$$

will have the "Student's" t-distribution with (n-2) degrees of freedom (Chiang, 2003).

The t statistic has been used to test a null hypothesis that the underlying population sample correlation coefficient between the two variables is not significantly different from zero, i.e. $H_0: \rho_{XY} = 0$. The alternative hypothesis, H_1, is therefore that the sample coefficient is significantly different to zero, i.e. $H_0: \rho_{XY} \neq 0$. Hence, by this design, the test is 2-tailed.

A summary of the hypothesis testing is presented in Table 6—4. Two levels of significance (which determine the region of the t-statistic in which the null hypothesis will be rejected) have been examined, α=0.05 and α=0.10. In each case, the null hypothesis could not be rejected, as the magnitude of the t-statistic calculated was always less than the t value calculated for the level of significance at the given sample size.

The results show that there is no significant correlation between individual chemical variables and radon activity in groundwater, when a time series is taken at a group of sites with homogenous chemistry. Noticeably, this includes other Group 2 elements (Ba, Sr), which have a similar chemistry to radium and which may behave in an similar fashion to the radium, in terms of mobility of potential concentration on fracture walls (Baraniak et al., 1999; Hidaka et al., 2007).

Such a result suggests that radon may be controlled by different processes from solution chemistry. This is perhaps not surprising, as the radium content of groundwaters has been shown to not support radon activities. But rather, it is through the ejection of radon from the decay of radium located within the Chalk matrix or which has migrated and subsequently been absorbed to fracture walls, that is likely to control overall activity.

Table 6—4 Correlation Coefficient – Radon vs Water Chemistry (Lower Pang Springs)

Determinand	*Sample Correlation Coeff,* r_{XY} $\frac{\sum(X_i - \bar{X})(Y_i - \bar{Y})}{\sqrt{\sum(X_i - \bar{X})^2 \sum(Y_i - \bar{Y})^2}}$	*n*	*t-statistic* $\frac{r_{XY} - 0}{\sqrt{\frac{(1 - r_{XY}^2)}{(n-2)}}}$	*t-crit* (α=0.05) *2 tailed*	*t-crit* (α=0.10) *2 tailed*	*Null Hypothesis* $H_0: \rho_{XY} = 0$
pH	-0.18	34	-1.04	±2.04	±1.69	Not rejected at either level
DO (%)	-0.03	33	-0.17	±2.04	±1.70	Not rejected at either level
Conductivity	-0.06	30	-0.34	±2.05	±1.70	Not rejected at either level
Na^+	-0.17	33	-0.96	±2.04	±1.70	Not rejected at either level
K^+	-0.20	33	-1.15	±2.04	±1.70	Not rejected at either level
Mg^{2+}	0.11	33	0.61	±2.04	±1.70	Not rejected at either level
Ca^{2+}	0.27	33	1.55	±2.04	±1.70	Not rejected at either level
Sr^{2+}	-0.21	33	-1.20	±2.04	±1.70	Not rejected at either level
Ba^{2+}	0.18	33	1.00	±2.04	±1.70	Not rejected at either level
Alkalinity	0.38	18	1.64	±2.12	±1.75	Not rejected at either level
Cl^-	-0.07	31	-0.38	±2.05	±1.70	Not rejected at either level
SO_4^{2-}	0.01	31	0.03	±2.05	±1.70	Not rejected at either level

Source: ..\project\calcs\chemical\[plspring_chemplots2.xlsx]location_correl

6.5 Experiments on radon emanation from solid and disaggregated Chalk

As discussed in Section 1.4, an initial assumption of the radiochemical transport model of Atkinson et al (2001) relates to a fixed and known emanation rate of radon from the solid grains to the surrounding pore space. Based on the analysis of Andrews and Wood (1972), a working assumption of 100% emanation efficiency was adopted given the small particle size of the Chalk grains. Such high emanation rates were regarded as specific to the Chalk and would not generally be expected from other types of rock – for example, Rama and Moore (1984) determined the radon emanation rate from a selection of granites, monazite sands and zircons, and in all cases calculated values less than 3% for the smallest grain sizes (<73 μm). Zereshki (1981) calculated rates of ^{222}Rn emanation from samples of Keuper Marl and Tea Green Marl samples at 18% and 31% respectively (for particles with a diameter of 64μm, similar to the Chalk particles analyzed in this thesis).

Results from the radon emanation from three Chalk samples taken from the core of Trumpletts Farm PL10A (described previously in Section 4.4) are illustrated in Figure 6—19. In each case, emanation has been expressed relative to the results of a dissolved sample of the same material, and which is assumed to represent the theoretical maximum value possible. For the powdered samples, the emanation fraction is considered to represent the proportion of radon that is produced from within the solid material that has been ejected (or has diffused) into the surrounding pore space.

The results suggest that emanation is strongly controlled by particle size. A small solid block and larger particles of sample TF23.0m, both typical in terms of radium strength within the white Seaford Chalk, show very low rates of emanation compared to other samples (between 2.5-2.9%, albeit with large relative errors a result of the limits of liquid scintillation counting errors). A similar result is obtained for a sample with a radium content more representative of the Lewes Nodular Chalk (TF81.3m, which is sampled from a competent chalk block below a fracture, but with no staining). Consistently greater rates of emanation for all size fractions are observed for TF86.3m, which was sampled at and below a fractured marl band.

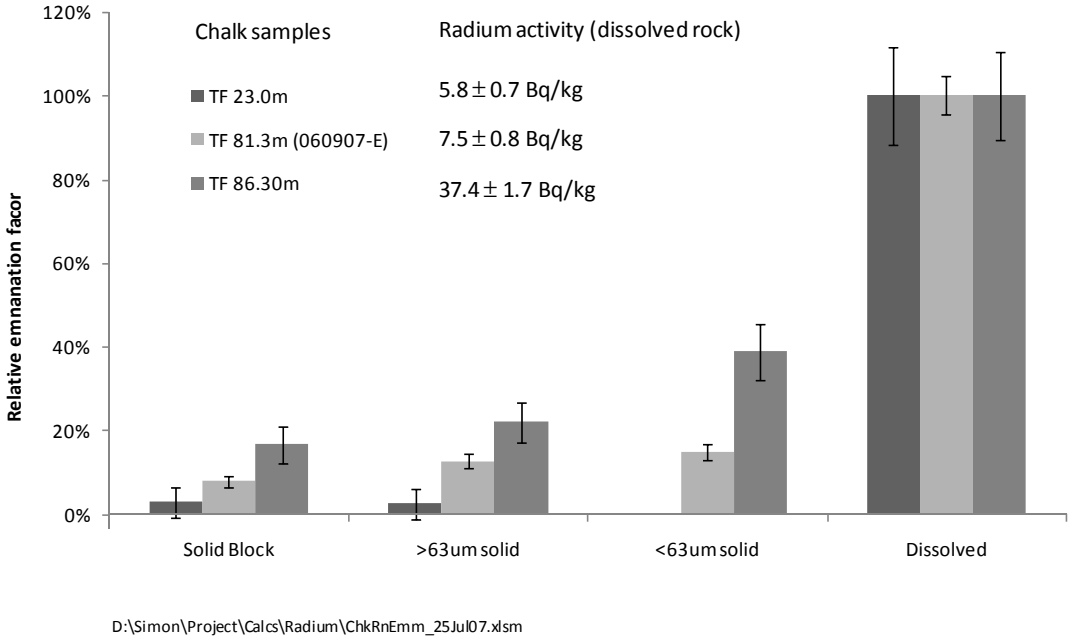

Figure 6—19 Radon emanation factors from selected Chalk samples from Trumpletts Farm A recovered core

All results are low in comparison to previous estimates of radon emanation in Lincolnshire Chalk samples (Cuttell et al., 1986), where emanation was estimated through the calculation of an in-situ "radon release factor", $\hat{}Rn$,

$$\hat{}Rn = \frac{\phi \cdot \left(\left[{}^{222}Rn \right]_s - \left[{}^{226}Ra \right]_s \right)}{(1-\phi) \cdot \left[{}^{226}Ra \right]_r} \qquad (6\text{-}3)$$

where ϕ is the matrix porosity, $\left[{}^{222}Rn \right]_s$ is the representative radon activity of groundwater and $\left[{}^{226}Ra \right]_s$ and $\left[{}^{226}Ra \right]_r$ are the radium activities of groundwaters and solid samples respectively.

Cuttell et al (1986) calculated a value of $\hat{}Rn$ of 62% from an analysis of the radium activity of 9 core samples (taken from 3 boreholes), in combination with the average radon content of groundwaters sourced from 11 boreholes. However, as the study did not measure the direct radon emanation from each rock fragment analysed for radium, a large degree of uncertainty exists in this result – especially as the radon content of groundwaters in the study area was observed to vary both temporally and seasonally.

An example of the range of possible emanation factors including the variation in radon activity in groundwater and radium activity observed by Cuttell et al (1986) is provided as

an example in Table 6—5. This indicates that, for the same site, the calculated radon release factor may vary from 18% to 93% depending on the input values selected. In addition, the approach adopted did not take into account the bulk density of the Chalk, which would be expected to affect the overall radium content of a Chalk block and which in combination with matrix porosity would control the radon content of pore waters.

Also, it has been assumed that radon activity of groundwater is representative of pore water activity and no account of fracture porosity has been taken into account. Table 6—6 illustrates the influence that fracture porosity could have on calculated emanation if a fracture porosity of 0.01 is used on the numerator of Equation 6-3 instead of matrix porosity. The average emanation rate is reduced from 27% to 0.9% as a result, a value which is closer in agreement with those determined for the solid block in this thesis.

Table 6—5 Example of variation in in-situ radon release factor for a single Chalk borehole using field data from Cuttell at al (1986)

"Sample 126"		Recorded groundwater radon activity measured between January 1982 and May 1982 (Bq.kg^{-1})		
Radium (rock) activity (Bq.kg^{-1}) measured at 3 boreholes (Goxhill, Barrow, Immingham)		Minimum	Average	Maximum
		0.86	0.92	1.01
Minimum	0.47	79%	84%	93%
Average	1.44	26%	27%	30%
Maximum	2.07	18%	19%	21%

Notes: Assumes that $[^{226}Ra]_s$ *is 0.003 Bq.kg^{-1} (i.e. negligible) and that Chalk porosity* ϕ *is 0.3, as assumed by Cuttell et al. Source: Project\Calcs\Radium\[ChkRnEmm_25Jul07.xlsm]Cutell*

Table 6—6 Variation in in-situ radon release factors calculated by Equation 6-3 but assuming Chalk fracture porosity is used on the numerator.

"Sample 126"		Recorded groundwater radon activity measured between January 1982 and May 1982 (Bq.kg^{-1})		
Radium (rock) activity (Bq.kg^{-1}) measured at 3 boreholes (Goxhill, Barrow, Immingham)		Minimum	Average	Maximum
		0.86	0.92	1.01
Minimum	0.47	2.6%	2.8%	3.1%
Average	1.44	0.9%	0.9%	1.0%
Maximum	2.07	0.6%	0.6%	0.7%

Notes: Assumes that $[^{226}Ra]_s$ *is 0.003 Bq.kg^{-1} (i.e. negligible) and that Chalk matrix porosity* ϕ *is 0.3,* ***but that Chalk fracture porosity is 0.01.*** *Source: Project\Calcs\Radium\[ChkRnEmm_25Jul07.xlsm]Cutell*

Overall, it is considered that, as pump tests in this current study have demonstrated that groundwaters sampled from boreholes are unlikely to give a realistic indication of pore water radon activity, it is difficult to make any direct comparison with the emanation results from the Trumpletts core.

6.5.1 Estimation of pore water radon activity

Given the potential variation in emanation rate, combined with new knowledge of the porosity and radium content of samples sources from the same core (Figure 5—1), it is possible to estimate the potential range in pore water concentration C_∞ that forms part of the radon transport model, described previously in Section 1.4, and which will be required in Chapter 7 in relation to the calculation of fracture diffusion time t_{cf}.

Results of this calculation are presented in Table 6—7 and Table 6—8 for two values of emanation (5% and 40%), which represent the range of values calculated above. Values of minimum, maximum and mean value of rock porosity and radium content have been used to calculate C_∞ for each emanation rate.

Of particular note is the wide range in pore water radon concentrations that are possible, as a result of the variation in emanation rate and radium content (i.e. between 0.49 $Bq.l^{-1}$ and 117.61 $Bq.l^{-1}$ depending on the values chosen). Such a result confirms the importance of accounting for the potential variability of each measurement when estimating the radon production rate from the solid matrix into the surrounding pore space.

Insufficient data and the large count errors make it difficult to draw firm conclusions about the control of emanation from these samples. However, qualitatively it may be stated that total radon emanation is likely to be controlled by both grain size and radium source strength. In addition, a sample with higher marl content has demonstrated greater emanation overall, which may suggest either 1) that radon is ejected from the decay of radium concentrated within clay material and which may diffuse more rapidly to the particle boundary or 2) that the radium source may be close to the particle surface.

The results also suggest that the assumption made by Atkinson et al (2001) based on extrapolation of the work of Andrews and Wood (1972), that 100% of radon emanated from Chalk grains is likely to rapidly diffuse to the Chalk matrix pore space, may be unrealistic.

Table 6—7 Estimates of pore water radon activity as a function of radium content and porosity assuming an emanation rate of 5%

Emanation Rate 5%		Porosity		
Radium content (Bq.kg^{-1}) of 1 m samples from Trumpletts Farm		0.25	0.35	0.45
Min	1.39	0.49 Bq.l^{-1}	0.35 Bq.l^{-1}	0.27 Bq.l^{-1}
Geometric Mean	5.77	2.03 Bq.l^{-1}	1.45 Bq.l^{-1}	1.13 Bq.l^{-1}
Arithmetic Mean	9.89	3.47 Bq.l^{-1}	2.48 Bq.l^{-1}	1.93 Bq.l^{-1}
Max	41.88	14.70 Bq.l^{-1}	10.50 Bq.l^{-1}	8.17 Bq.l^{-1}

Note: Assumes Bulk density of Chalk 1755 kg.m^{-3}

Table 6—8 Estimates of pore water radon activity as a function of radium content and porosity assuming an emanation rate of 40%

Emanation Rate 40%		Porosity		
Radium content (Bq.kg^{-1}) of 1 m samples from Trumpletts Farm		0.25	0.35	0.45
Minimum	1.39	3.91 Bq.l^{-1}	2.79 Bq.l^{-1}	2.17 Bq.l^{-1}
Geometric Mean	5.77	16.22 Bq.l^{-1}	11.58 Bq.l^{-1}	9.01 Bq.l^{-1}
Arithmetic Mean	9.89	27.77 Bq.l^{-1}	19.83 Bq.l^{-1}	15.43 Bq.l^{-1}
Maximum	41.88	117.61 Bq.l^{-1}	84.00 Bq.l^{-1}	65.34 Bq.l^{-1}

Note: Assumes Bulk density of Chalk 1755 kg.m^{-3}

7 Radon Model Comparison with Tracer Testing

This Chapter builds on the data collation and processing reported in Chapters 5 and 6, by assessing the applicability of the radon diffusion model described by Atkinson et al (2001) as a credible alternative to tracer testing in Chalk, where it is assumed that double-porosity diffusion is the dominant control on the migration of solutes.

Firstly, a brief review is given of previously published values of the characteristic diffusion time t_{cf} in Chalk, derived from the results of tracer tests. Emphasis is placed upon the work of Imperial College in particular (Mathias et al., 2006a; Mathias et al., 2007b; Mathias et al., 2009; Butler et al., 2009), whose work as part of the wider LOCAR programme has included testing at Trumpletts Farm, and hence which is most closely related to the new data presented in this thesis. However, other tracer tests are also included to provide some indication of the potential variability in transport properties in different Chalk aquifers.

Secondly, a summary is provided of the arguments required by the diffusion model, including a discussion of the possible range of each of the input datasets. By making use of a series of 'bootstrapped' mean values, a range of values of the diffusion time t_{cf} is calculated using a Monte Carlo sampling approach. A further exploration of the sensitivity of t_{cf} to input parameters is also undertaken, with conclusions drawn about the dominant controls on the model's performance.

Thirdly, a direct comparison is made between the results of the radon diffusion model and the values of t_{cf} derived from fitting tracer breakthrough curves to double porosity models. This work includes a more detailed summary of the convergent tracer testing undertaken at Trumpletts Farm, to demonstrate that a like for like comparison of t_{cf} is valid at this site. In particular, the applicability of applying a double porosity diffusion model to the results is discussed, and the potential uncertainty in the tracer derived t_{cf} is estimated.

Finally, any discrepancies between the modelling approaches are noted, with a discussion on the potential reasons why these may occur.

7.1 Tracer testing in double porosity media

7.1.1 Previous work

That matrix diffusion may play an important role in solute diffusion has been widely discussed in the literature. For example, Grisak and Pickens (1980) described the development of a model that has been used to predict solute transport by advection, hydrodynamic dispersion, plus diffusion between fracture and rock matrix. This model was used to interpret the results from a column study of a fractured clay-loam till, where variations in the form of breakthrough curve were explained in terms of either matrix diffusion alone, or enhanced matrix diffusion through the adsorption of some species to fracture walls. Grisak and Pickens (1981) subsequently presented an analytical solution to solute transport with matrix diffusion, assuming that the penetration depth of solute into the matrix was small in comparison to the fracture spacing. The model demonstrated that, for rocks with large matrix porosities (of the order of 0.3), solute transport could be dominated by retardation through matrix diffusion.

Maloszewski and Zuber (1985) extended the development of a solution to permit full penetration of the matrix and presented a series of theoretical breakthrough curves for the instantaneous injection of a tracer into a single fracture and multi fracture configuration. They demonstrated that for short duration tests (hours rather than days) tracer movement is not affected by fracture spacing and that results can be fitted assuming a single fracture model, with a resulting beneficial reduction in fitted parameters. This was also noted by Wright and Barker (2001), who concluded that short term tracer tests can give little information on the matrix properties of a double-porosity medium, whereas long term tests reflect total porosity and are dominated by matrix effects. Moench (1989, 1991) also provided solutions to advection-dispersion that later incorporated double porosity effects.

Brouyere et al (2000) reiterated that ignoring double porosity diffusion can lead to errors in the interpretation from tracer test breakthrough curves. This was illustrated by comparing theoretical breakthrough curves for a radially convergent flow tracer test for models that included or ignored double porosity. Brouyere (2002) explored breakthrough curve sensitivity to tracer injection, which can affect breakthrough interpretation and lead to errors in fitted parameters, but also in misleading identification of the active transport processes. For example, Brouyere (2002) demonstrated that theoretical breakthrough curves from advection-dispersion only models that had non-instantaneous injection could be fitted equally well to models which included the effects of double-porosity diffusion.

The importance of careful representation of the initial vertical tracer injection was demonstrated more recently by Mathias et al (2007b), who inferred the tracer concentration leaving the injection borehole by measuring temporal changes in conductivity.

7.1.2 Chalk Specific Tracer Tests

There are relatively few tracer studies in the Chalk aquifer whose breakthrough curves have been interpreted in terms of double porosity diffusion. However, Table 7—1 and Table 7—2 present those results from tracer tests in the UK Chalk where values have been reported, or where it has been possible to determine from the published breakthrough curves and subsequent analysis.

Of particular note, is that several authors have reinterpreted the tracer test at South Farm (Ward, 1989) and derived a range of travel and diffusion times dependent on the type of model selected and representation of the tracer injection. Atkinson et al (2001) fitted the breakthrough curve to three models – instantaneous tracer injection, exponential dilution of tracer and a formulation of Moench (1995) that included hydrodynamic dispersion. For each model, a value of t_{cf} was calculated which varied according to both the input term and whether hydrodynamic dispersion dominated.

Mathias et al (2009) fitted data from South Farm, as well as Horseheath in Cambridgeshire (Kachi, 1987), using a four parameter model that incorporated both radially convergent dispersion and Fickian diffusion. From the model results, Mathias et al (2009) stressed the importance of collecting early-time data (i.e. before the arrival of the tracer peak) when attempting to assess the importance of mechanical dispersion compared to the effects of double porosity diffusion. This uncertainly was subsequently addressed in the test at Trumpletts Farm, by continuous monitoring of tracer arrival by use of a flow-through fluorometer (Section 7.1.3).

Table 7—1 Tracer Tests in Chalk where double porosity effects have been modelled

Authors(s)	*Test Details*	*Model Details*	*Comments*	t_a *(mean transit time)*	t_{cf} *(fracture diffusion time)*
Maloszewski & Zuber (1985)	Radial Flow test in Dorset Chalk conducted by Ivanovitch & Smith (1978). Instantaneous injection of ^{82}Br, 8m separation	Fitted to a single fracture dispersion and piston flow model both that includes matrix diffusion	Short term tests can be fitted equally well to a single rather than a many fracture model (as tracer does not have time to penetrate matrix blocks)- enables the omission of one fitting parameter	90 min (with fracture dispersion) 75 min (without fracture dispersion)	Assuming same values calculated in paper i.e. $D_a = 10^{-10}$, a = 0.11 to 0.19 mm, n_e = 0.23 to 0.39 leads to t_{cf} between 9.5 to 9.8 mins
Atkinson at al (2001)	Radially convergent in Chalk at South Farm near Thetford (as described by Atkinson et al (2000). Tracer: Fluorescein	Fitted results to three models – a) instantaneous tracer injection, b) exponential dilution of tracer c) a formulation of Moench (1995) that includes hydrodynamic dispersion.	Models a) and b) give good fit to data but predict only 51-55% mass recovery. c) is formulated to maximise effects of hydrodynamic dispersion, and reduced significance of matrix diffusion.	a) 1195 mins b) 1195 mins b) 4997 mins	a) 230 mins (158 corrected for Rn) b) 83.5 (56) mins c) 13881 (9273) mins (considered an upper bound)
Mathias et al (2009)	Radially convergent test at South Farm (Norfolk) by Ward (1989), upper Chalk, pump rate 3.3 $Ml.d^{-1}$ separation 199 m. Tracer: Fluorescein	Data fitted to a single fracture dispersion mode, for multiple values of Peclet number to achieve a range of combinations of t_a, t_{cf} . Assumption of instantaneous injection	Noted that lack of early time data results in many parameter combinations that provide equally good fits. Also indentified well-bore mixing as a source of further uncertainty.	1317 – 5626 min depending on Peclet number	73.8 mins (single fracture model no dispersion)- 2178 mins (diffusion with increasing fracture dispersion)
Mathias et al (2009)	Radially convergent test at Horseheath (Cambridge) by Kachi (1987), Middle Chalk, pump rate 2.6 $Ml.d^{-1}$ separation 44 m. Tracer: Fluorescein	Data fitted to a single fracture dispersion mode, for multiple values of Peclet number to achieve a range of combinations of t_a, t_{cf} . Assumption of instantaneous injection	Noted that lack of early time data results in many parameter combinations that provide equally good fits.	125 – 473 min depending on Peclet number	8.4 mins (single fracture, no dispersion)– 171 min, (again depending on Peclet number)
Mathias et al (2007b)	Radially convergent test at Trumpletts Farm PL10B, Upper Chalk, pump rate 5.77 $Ml.d^{-1}$ separation 54 m, Amino-G	Data fitted to a single fracture model (no dispersion), taking into account the release of tracer from the source borehole.	Continuous monitoring of the breakthrough curve using in-line fluorometer, periodic monitoring of the input tracer concentration.	4.5 min	13.7 min

Table 7—2 Tracer Tests in Chalk where double porosity effects have been modelled (continued)

Authors(s)	*Test Details*	*Model Details*	*Comments*	t_a *(mean transit time)*	t_{cf} *(fracture diffusion time)*
Mathias et al (2007b)	Radially convergent test at Trumpletts Farm PL10A, Upper Chalk, pump rate 5.77 $Ml.d^{-1}$ separation 32 m. Tracer: Uranine (i.e. Fluorescein)	Data fitted to a single fracture model (no dispersion), taking into account the release of tracer from the source borehole.	Continuous monitoring of the breakthrough curve using in-line fluorometer, periodic monitoring of the input tracer concentration.	13.2 min	2.3 min

7.1.3 Trumpletts Farm tracer test

As part of the LOCAR research programme, an artificial tracer test was conducted by research staff at BGS and Imperial College at the Trumpletts Farm research site in the spring of 2005. Full details of the tracer test configuration and the results have been presented previously by Mathias et al (2007b), but they are restated here for purposes of clarity. It should also be noted that:

i. this is the same test during which the first suite of radon samples from the Bottom Barn abstraction borehole were obtained and which have been presented in Chapter 6 (i.e. as plotted in Figure 6—10 and discussed in Section 6.2.1); and,
ii. that the first tracer was released into PL10A, located *c.*32 m to the west of the abstraction borehole, and is the same borehole at which the packer and open hole pump test were undertaken (described in Sections 6.2.2 and 6.2.3 respectively), and from which core material was obtained for uranium and radium assay (Section 5.2).

The tracer test was a forced gradient radially convergent configuration, where the Bottom Barn abstraction borehole was pumped at a constant rate close to its normal operational limit (an average rate of 5.77 $Ml.d^{-1}$). Pumping ceased after 36 hours due to a technical fault. Forty minutes after the start of pumping, 10 g of uranine and 2 kg of NaCl (dissolved in 20 l of water) was slowly released into the water column of borehole PL10A by use of a plastic hose. The addition of NaCl to the tracer solution also permitted the dilution from within the injection borehole to be monitored at regular intervals through use of a conductivity probe. Geophysical logging and tracer measurements made at borehole PL10A during the pumping of Bottom Barn are presented in Figure 7—1. This figure also indicates the dominant inflow horizons, which were identified using the result of impeller and heat logs, in combination with conductivity measurements. In addition, inferred fracture flow rates were also estimated by fitting the down borehole tracer profiles to a simple mass balance model.

From the breakthrough curve, assuming a single fracture model gave t_a = 13.2 mins and t_{cf} = 2.3 mins assuming 100% mass recovery. However, it was noted that there was potential variation in the values of t_a and t_{cf} derived from the tracer test, if the effects of hydrodynamic dispersion were also included.

Finally, the authors noted that with such short tracer tests that it would not be expected to identify the characteristic matrix block diffusion time t_{cb} from the tail of the breakthrough

curve, given that in this test the solute was very unlikely to reach the centre of the blocks between fractures.

As an extension to the work previously published, the advection-diffusion model was re-run to investigate what difference there would be in the predicted breakthrough curve if hydrodynamic dispersion was permitted during the test at PL10A (S.A. Mathias, *pers comm*).

The variations in breakthrough curves from these new sets of model runs are presented graphically in Figure 7—2. This figure also includes the mean concentration of the tracer leaving the injection borehole over time, plus the breakthrough data as recorded by the fluorometer at the abstraction borehole.

A comparison of the goodness of fit of each new curve to the data is presented in Figure 7—3, with the numerical results listed in Table 7—3. The results indicate that, if hydrodynamic dispersion within the fracture network were permitted (as well as double porosity diffusion within the matrix), then the root mean square log error would be minimised if 100<P<150, where P is the Peclet number and equal to R/α_L (R being the distance between the pumping well and the injection well and α_L being dispersivity). For P = 100 this would yield a value of t_a = 18.1 mins and t_{cf} = 4.6 mins (or double that determined with no dispersion, P = ∞).

However, although introducing dispersion does improve fit slightly, the overall sensitivity is regarded as low (except when P is small). It should also be noted that the fit at the very start is best for P = ∞, (i.e. no dispersion) and that, regardless of the value of P, t_a is much less than the time of peak tracer concentration arrival. This result suggests that the shape of the breakthrough curve may in reality be dominated by the shape of the input function, which Mathias et al (2007b) acknowledge.

From the analysis of other Chalk tracer tests, Mathias et al (2009) have also demonstrated that a large set of P, t_a and t_{cf} values could lead to equally good model fits, especially when tracer breakthrough is not monitored continuously. They note that, without very early time data, it is generally impossible to conclude whether a single fracture model with matrix diffusion or a single fracture dispersion model is the most appropriate solution (given the many similar model fits possible as a result of parameter trade off).

Figure 7—1 Geophysical logging and tracer measurements made at borehole PL10A during the pumping of Bottom Barn ABH. (Data reproduced from Mathias et al ,2007 and Butler et al ,2009)

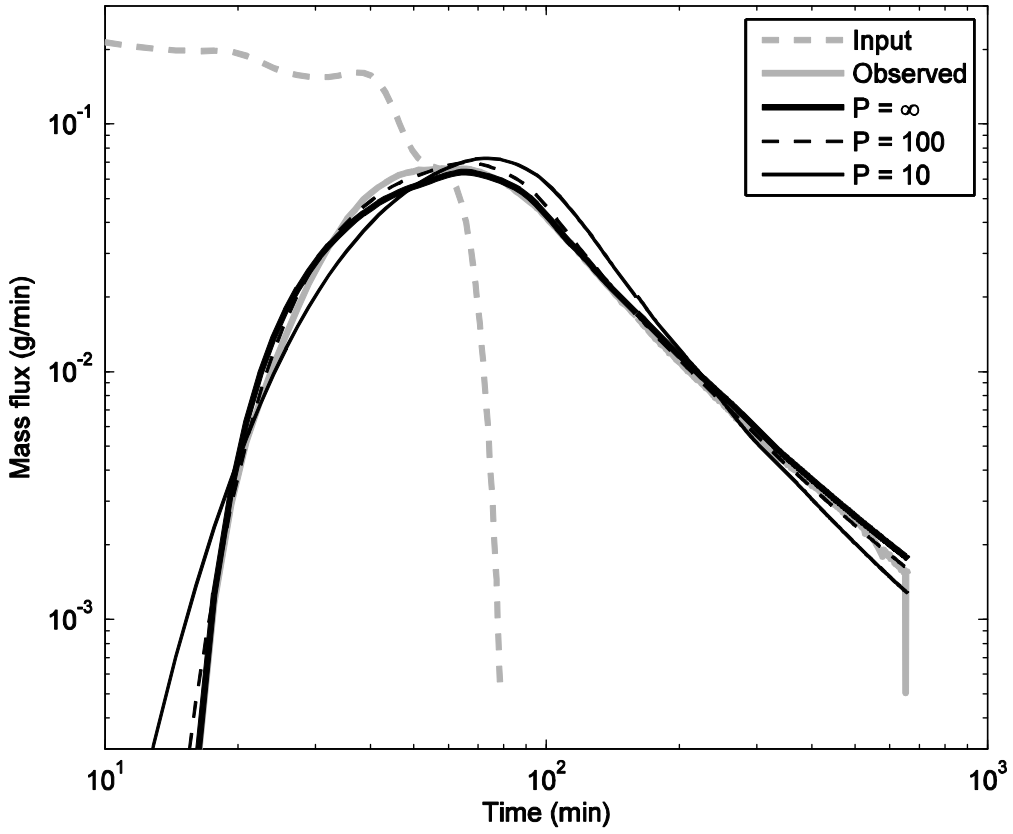

Figure 7—2 Variation in fit of Bottom Barn breakthrough curve as a function of Peclet number, P. (P=∞ equivalent to no hydrodynamic dispersion represented in model). Source: S.A. Mathias (pers comm)

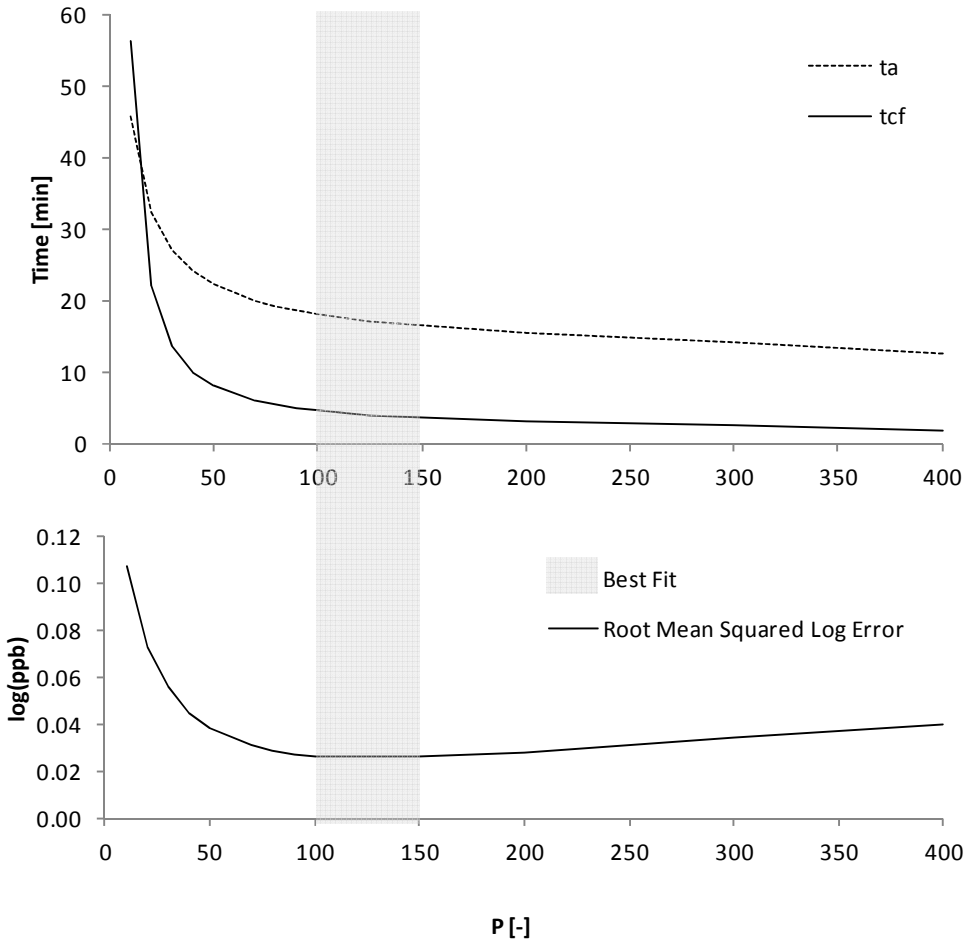

project\data\mathias\[tracer_fitting_peclet number.xlsx]rmsle

Figure 7—3 Variation in optimum t_a and t_{cf} as a function of Peclet number P for the Trumpletts Farm tracer test assuming using a "Single Fracture Dispersion Model" (SFDM). Source: S.A. Mathias

Table 7—3 Optimum "Single Fracture Dispersion Model" (SFDM) parameter sets for the Trumpletts Farm (Borehole A) tracer test assuming various values of Peclet number, P.

P *(-)*	t_a *(minutes)*	t_{cf} *(minutes)*	*RMSLE log(ppb)*
∞	**12.64**	**1.81**	**0.040**
400	12.64	1.81	0.040
300	14.26	2.52	0.034
200	15.59	3.15	0.028
150	16.46	3.63	0.026
125	17.12	4.02	0.026
100	**18.07**	**4.64**	**0.026**
90	18.58	4.99	0.027
80	19.20	5.44	0.029
70	19.98	6.05	0.031
50	22.31	8.10	0.038
40	24.21	10.05	0.045
30	27.14	13.62	0.056
20	32.43	21.92	0.073
10	**45.72**	**56.17**	**0.107**

Note: Bold figures indicate breakthrough curves plotted on Figure 7—2. Source: S.A. Mathias (pers comm)

7.2 Estimating t_{cf} using a radon diffusion model

The expected value for the characteristic diffusion time t_{cf} can be calculated on the basis of (ideally paired) measurements of radon and uranium content of groundwater and Chalk. Recalling the mathematical description of the radiochemical model described in Chapter 1, and rearranging, the value of t_{cf} may be estimated (assuming steady state conditions) by:

$$t_{cf} = \frac{1}{\lambda_{222}}\left(\frac{c_\infty}{c_f(\infty)} - 1\right)^2 \qquad (7\text{-}1)$$

where $c_f(\infty)$ is the steady state radon content of fracture water and $c_\infty = \frac{P_w}{\lambda_{222}}$ is the radon source concentration within the matrix where,

$$P_w = 2.53 \times 10^{24}\, E\, \frac{\rho_m}{\phi} \lambda_{238} U \left[\frac{^{226}Ra}{^{238}U}\right] \qquad (7\text{-}2)$$

and P_w = the production rate of radon per unit volume of pore water, as a result of emanation from within the matrix (atoms.m^{-3}.s^{-1}), $0 \leq E \leq 1$ = the efficiency of the emanation of radon from solid grains into the pores, ϕ = the matrix porosity, ρ_m = the bulk density of the rock (kg.m^{-3}), λ_{238} = the decay constant of the uranium isotope ^{238}U (seconds^{-1}), U = the uranium concentration of the solid matrix (kg.kg^{-1}), and $\left[^{226}Ra/^{238}U\right]$ is the isotope activity ratio between the two isotopes of radium and uranium.

7.2.1 Selection of input arguments

Before presenting values of t_{cf}, a summary of the available input data described in Chapters 5 and 6 is presented. The data have been divided in several sub categories, which reflect the main sources for the data collected. Namely,

i. uranium, radium and radon data collected from Trumpletts Farm only;
ii. other radon data from the wider spring and borehole study, and
iii. values of uranium and radon activity reported in the literature for UK Chalk.

Care has been taken in the case of radon measurements to distinguish values regarded as representing fracture waters from those altered by either high rates of pumping (producing mixing with pore waters and higher Rn values) or from spring waters (that may have spent

some time in transit towards the point of emergence and so have lower radon values than most fracture waters, because of decay while in transmissive fractures).

Note however, that is has been assumed that the inclusion of some results from spring waters is still appropriate, as they provide examples of fracture waters obtained close to springs. Uncertainly remains as to the validity of this assumption, given the likelihood that the radon signatures are potentially not representative of any one source but rather, are influenced by other controls such as recent mixing. However, it could be also argued that the highest spring values more closely represent bulk groundwater radon content, as these samples will have undergone least decay while in transit towards the spring sources in fractures with a spectrum of apertures.

As there are many more samples collected from spring sites overall (compared to borehole samples), the number of spring data points used in the subsequent calculation of t_{cf} has been limited further, by representing each spring by its highest, lowest and average values only, thus giving them effectively a similar weighting in terms of number of samples as the for borehole samples. All borehole samples have been included, with the exception of most obtained from the large pumping test at Bottom Barn, where the complex development of the radon signature over time suggests a high degree of mixing near the borehole.

A summary of the sources of input data used, and how they have been processed for each of the three classifications is provided in Table 7—4 and Table 7—5 The datasets derived in each case are presented graphically in Figure 7—4. These plots indicate both the overall spread of the data, and where most of the data cluster.

7.2.2 Propagating parameter variation and uncertainty

From the study of uranium and radium profiling of Chalk core presented in previous chapters, it is clear that both radionuclides are subject to litho-stratigraphic control and that both the concentration and isotope activity ratio are subject to significant variation. As illustrated in Figure 7—4, other physical properties such as porosity and bulk density may also vary significantly within the Upper Chalk sequence (e.g. matrix porosity ranges from 25% to 45% within the one core).

Therefore, before using such data in further calculations, it is useful to consider what range of values may be considered representative of each parameter and to what extent the natural variation observed should also be taken into account.

Table 7—4 Input data sets for radon diffusion model (Trumpletts Farm, plus Pang/Lambourn samples)

Grouping	*Input to radon diffusion model*	*Datasets used/ excluded*	*Data manipulation*	*n*
Trumpletts datasets	Uranium content of Chalk matrix	All data from 1 m sections and small block sample results	Only the average of any replicates included	105
	Ra226/U238 isotopic activity ratio	All data used from 1 m sections and small block results	No replicates, so all values used	31
	Radon activity of groundwater	Results from low rate pumping at site – e.g. packer test results (final activity only), open hole test (final activity only).	No replicates, so all values used	7
		Lowest values from larger pump test at Bottom Barn (adjacent to site), after the first radon peak (See Figure 6—10). Average of the large scale test not used (expected to be heavily influenced by pumping).		
	Chalk porosity	BGS reported values of porosity of borehole PL10A	None	38
	Chalk dry bulk density	BGS reported values of porosity of borehole PL10A	None	38
	Radon emanation factor	Solid block, <63µm and>63µm for 3 Chalk samples.	No replicates, so all values used.	8
		Total dissolved samples ignored		
Pang/Lambourn datasets	Uranium content of Chalk matrix	As for Trumpletts – no additional data known	As for Trumpletts	105
	Ra226/U238 isotopic activity ratio	As for Trumpletts – no additional data known	As for Trumpletts	31
	Radon activity of groundwater	Min, max and average for each routine spring location, all values for groundwater sampling, Trumpletts Farm packer test (end value), plus groundwater samples reported by Mullinger et al (2007)	Only using min, max, avg for springs (thereby reducing this dataset, to avoid dominating over smaller set of groundwater samples)	46
	Chalk porosity	As for Trumpletts – no additional data collected within catchment	None	38
	Chalk dry bulk density	As for Trumpletts – no additional data collected within catchment	None	38
	Radon emanation factor	Only data available is that for Trumpletts Farm	None	8

Table 7—5 Input data sets for radon diffusion model ('UK Chalk' dataset)

Grouping	*Input to radon diffusion model*	*Datasets used/excluded*	*Data manipulation*	*n*
'UK Chalk' datasets	Uranium content of Chalk matrix	Values from this study, plus all from Low (1996b), Ward (1989), Cuttell et al (1986) and Younger & Elliot (1995)	Value for Trumpletts averaged per Chalk unit (Table 5—1)	26
	Ra226/U238 isotopic activity ratio	Values from this study, plus all from Ward (1989) and Cuttell et al (1986).	All 1m sections from this study included. Detailed block results excluded.	40
	Radon activity of groundwater	Values from this study, plus all from Zereshki (1981), Ward (1989), Cuttell et al (1986), Low (1996b), Elliot et al (1999) (both confined and unconfined boreholes), plus Mullinger et al (2007)	Only spring and borehole sample averages from this study	110
	Chalk porosity	Trumpletts Farm data only	None	38
	Chalk dry bulk density	Trumpletts Farm data only	None	38
	Radon emanation factor	All values from this study, reworked value from Cuttell et al (1986), Zereshki's (1981) values for similarly sized particles from the Tea Green and Keuper Marls (29µm), plus Andrews et al (1979) values for Carboniferous Limestone	Cuttell et al's method was reworked (as summarised in Table 6—6).	

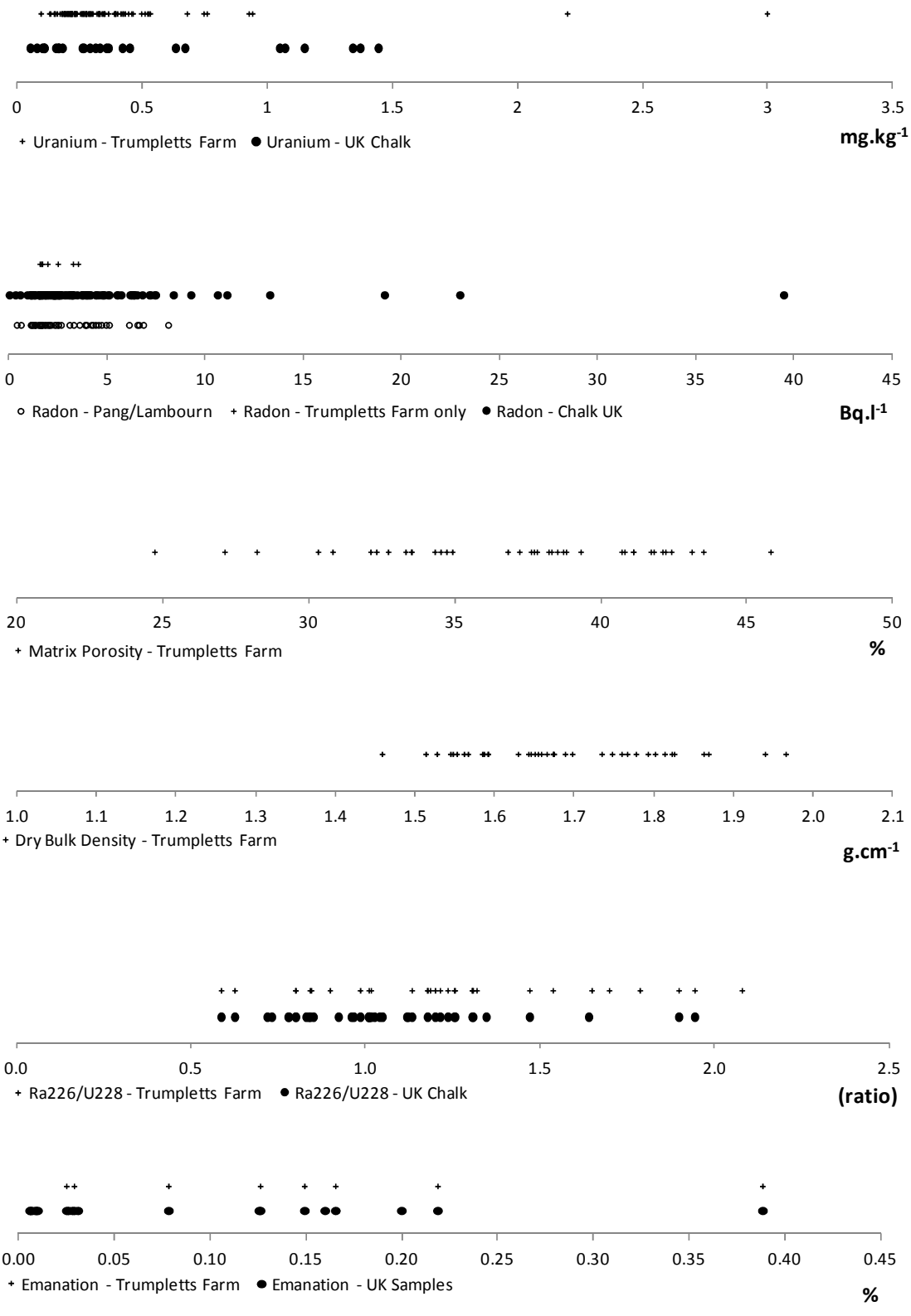

Figure 7—4 Variations in variables used in the calculation of transport parameter t_{cf} (grouped according to data sources)

One simple approach would be to take the arithmetic mean of each of the parameters and to calculate a value of t_{cf} directly. Other limiting values of each parameter could then be substituted, to provide an indication of the potential variation that might be expected, given the natural variation from the original dataset. However, such deterministic modelling using single-point estimates does not provide any indication of the likelihood of each result occurring and as such may provide an unrealistic range in the values of t_{cf}.

A more rigorous alternative approach is to assume that each of the datasets comprise of individual samples, selected from an underlying distribution of values. Values of t_{cf} could then be calculated by randomly sampling many times from these larger distributions (i.e. a Monte Carlo approach), with the results collated to provide an estimation both the mean and spread of the result.

However, it is clear from some of the data (e.g. uranium and radon concentrations), that the observed variation cannot be represented by a standard (normal) distribution. Therefore, before generating a set of input values to use in the radon diffusion model, the structure of the underlying dataset has been considered more carefully using the process of 'bootstrapping', as described by Efron and Tibsharini (1994).

Bootstrapping

Bootstrapping has been used in this thesis to gain a better feel for how the mean value of each of the input datasets may vary if a random selection of the existing data is made. This has been achieved as follows:

i. For each input variable (and for each sub-set, as outlined in Table 7—4 and Table 7—5) a selection of new values was generated by randomly sampling the dataset N times (where the total number of values was also N). This sampling was done *with replacement*, meaning that the same value could be selected more than once;
ii. The resulting bootstrap sample was then used to calculate a new mean value, which was stored. The random re-sampling process was then repeated 1,000 times.
iii. The large number of bootstrap replications were themselves then averaged to give a feel for the 'mean mean' value. As Efron and Tibsharini (1994) outlined, the standard deviation of the bootstrapped means tends towards the standard error of the mean value as the number of re-samples increases.

Using this process, a distribution was generated of the likely mean value of each variable, plus its likely variation, without the need to assume that the data conform to any form of parametric model. Another advantage to the approach is that the 1,000 mean values

generated (which in themselves reflect the variation) may also be sampled randomly, without the need to understand the underlying distribution.

The results of bootstrapping for each of the datasets are presented in Figure 7—5 to Figure 7—10. Interesting points to note include:

i. The mean value of uranium content in the UK Chalk is predominantly higher than that observed in the core analysed at Trumpletts Farm (which is well constrained between 0.2 – 0.4 $mg.kg^{-1}$). From the work of Ward (1989) and Low (1996), it is also clear that large variations may exist between samples taken from Chalk fracture walls (some of which may be iron stained) and the matrix;
ii. That UK radon values are generally higher than those recorded at either the Trumplett's Farm borehole or all the springs and boreholes within the Pang and Lambourn catchments. (e.g. the average value from all 17 spring and borehole sites monitored by Low (1996) was 5.6 ± 2.2 $Bq.l^{-1}$ compared to 3.1 ± 1.9 $Bq.l^{-1}$ within this current study);
iii. Variations in both porosity and dry bulk density are similar to that noted by Price (Price et al., 1982; Price et al., 1993);
iv. Although few data exist of $[^{226}Ra]/[^{238}U]$ isotopic activity ratios in UK Chalk, the spread of means obtained as part of this study is similar to that calculated when additional data from previously reported values are included.
v. Overall ratio values are generally greater than 1, indicating either radium enrichment or uranium depletion (assuming the systems had previously achieved isotopic equilibrium); and,
vi. That very few data exist on rates of radon emanation from Chalk, and that rates from other sediments with small particle sizes show a wide range in values.
vii. No data were reported for Chalk samples with emanation rates approaching 100%, which had been previously inferred by Atkinson et al (2001), based on previous theoretical calculations (Andrews and Lee, 1979).

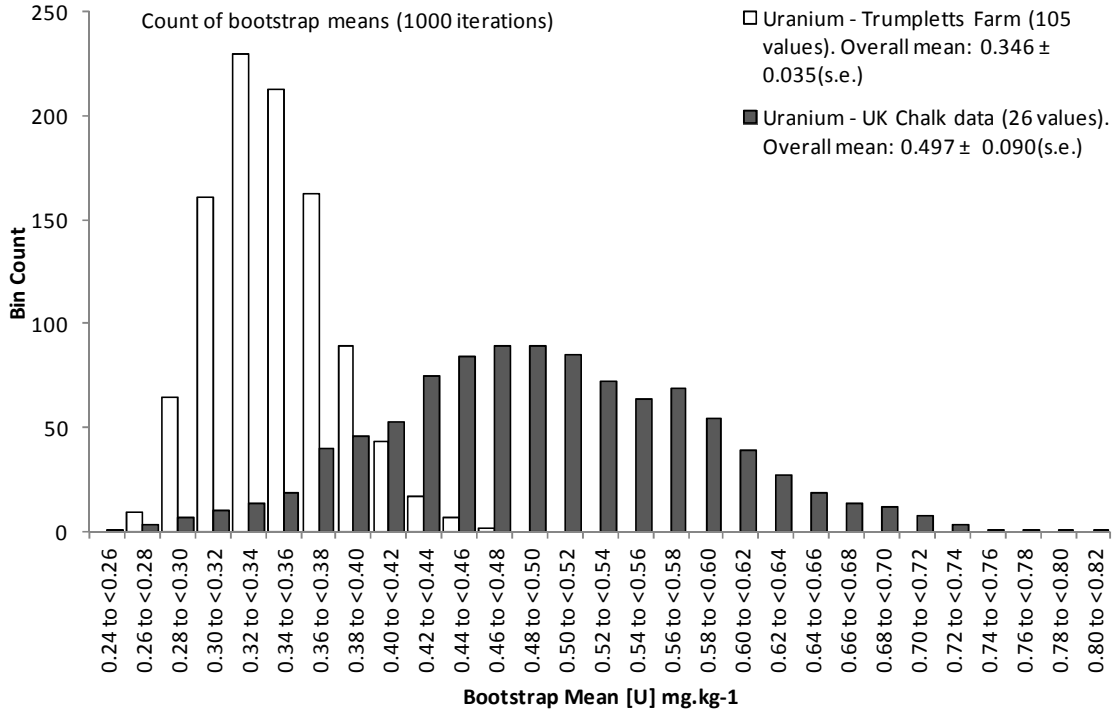

Figure 7—5 Bootstrap - Distribution of the means of 1000 random re-samples (with replacement) from the Chalk matrix uranium content dataset (for samples collected at Trumpletts Farm and other reported data)

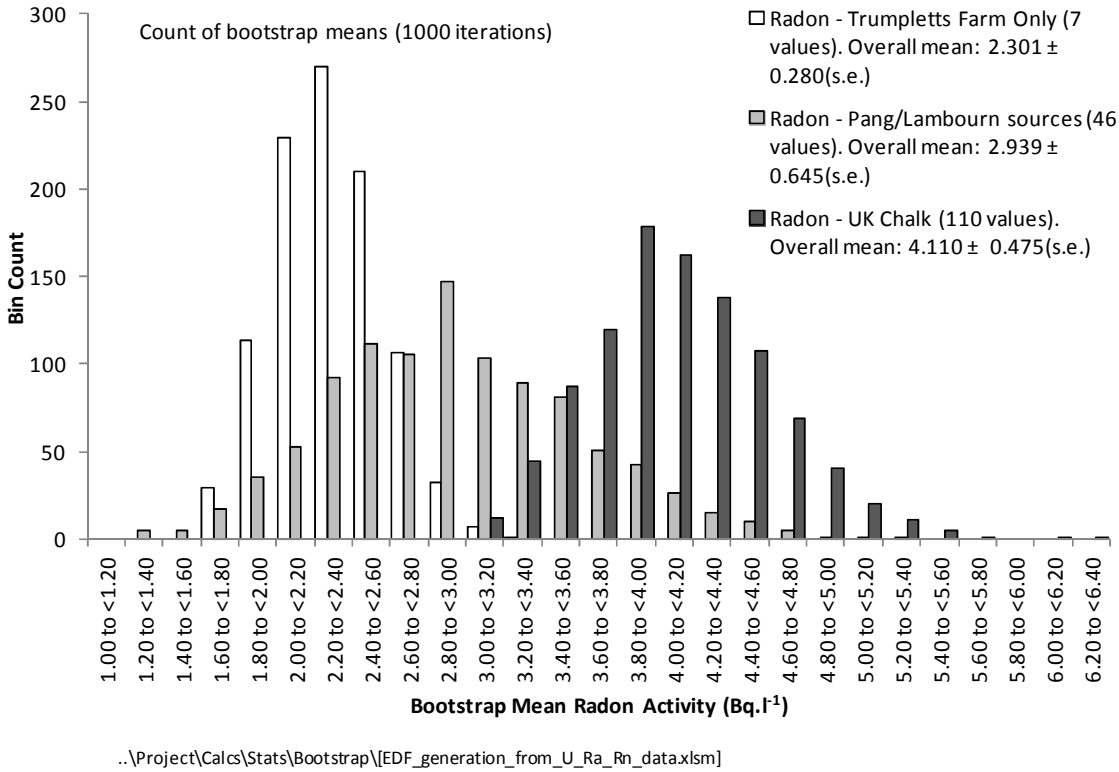

Figure 7—6 Bootstrap - Distribution of the means of 1000 random re-samples (with replacement) from the groundwater/spring radon content dataset (for samples collected at Trumpletts Farm and other reported data)

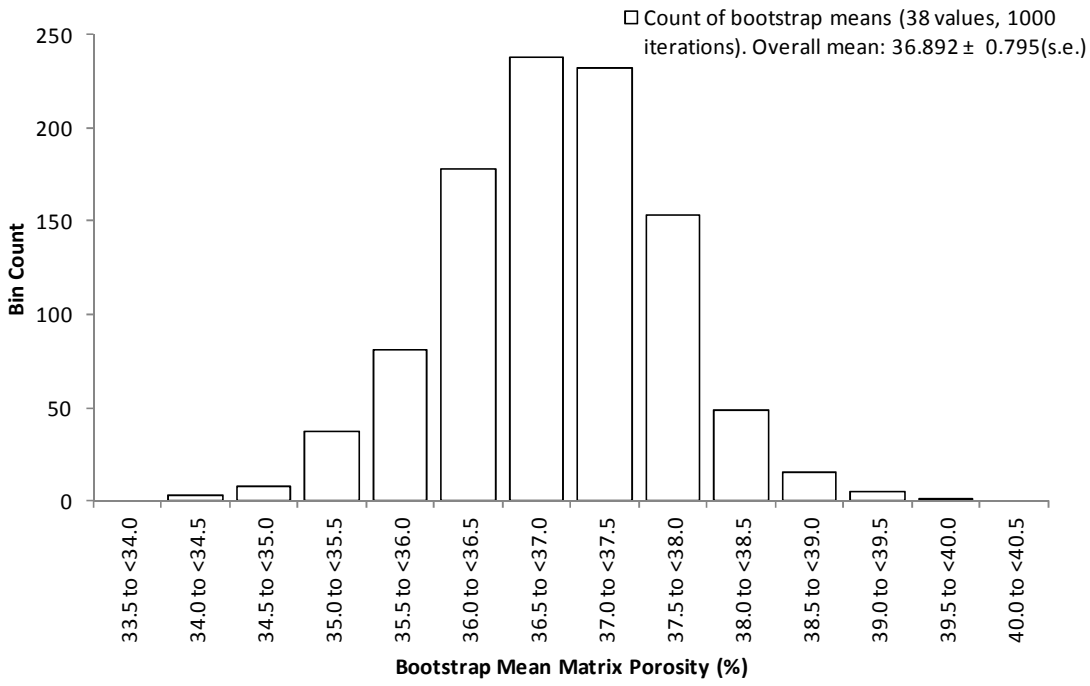

..\Project\Calcs\Stats\Bootstrap\[EDF_generation_from_U_Ra_Rn_data.xlsm]

Figure 7—7 Bootstrap - Distribution of the means of 1000 random re-samples (with replacement) from the matrix porosity dataset (for samples collected at Trumpletts Farm Borehole A)

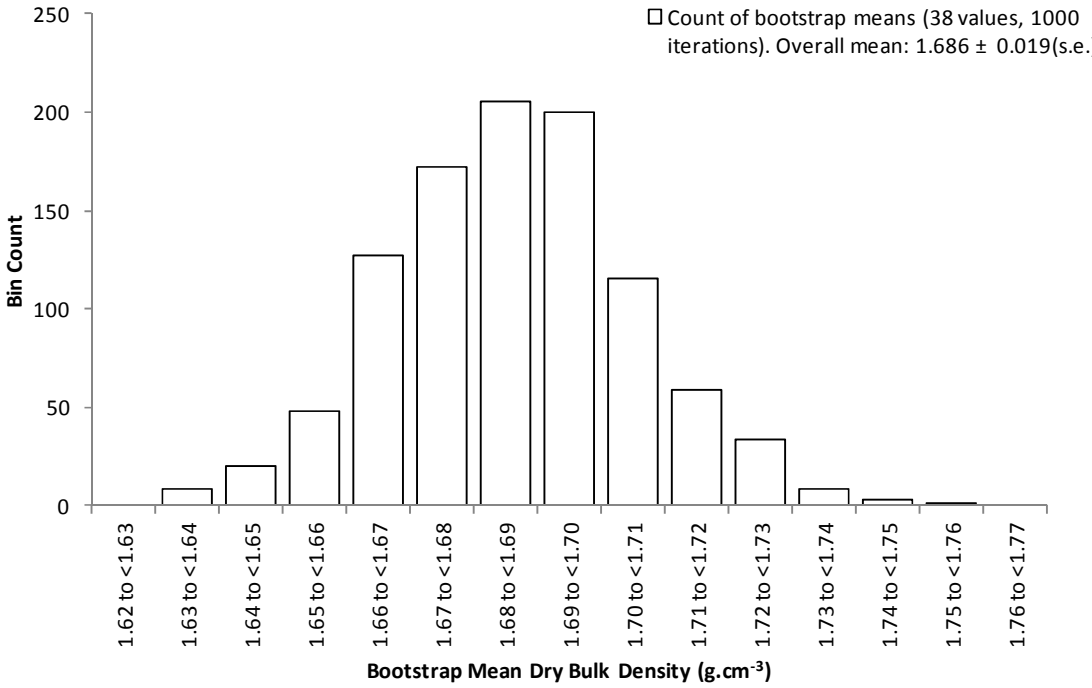

..\Project\Calcs\Stats\Bootstrap\[EDF_generation_from_U_Ra_Rn_data.xlsm]

Figure 7—8 Bootstrap - Distribution of the means of 1000 random re-samples (with replacement) from the dry bulk density dataset (for samples collected at Trumpletts Farm Borehole A)

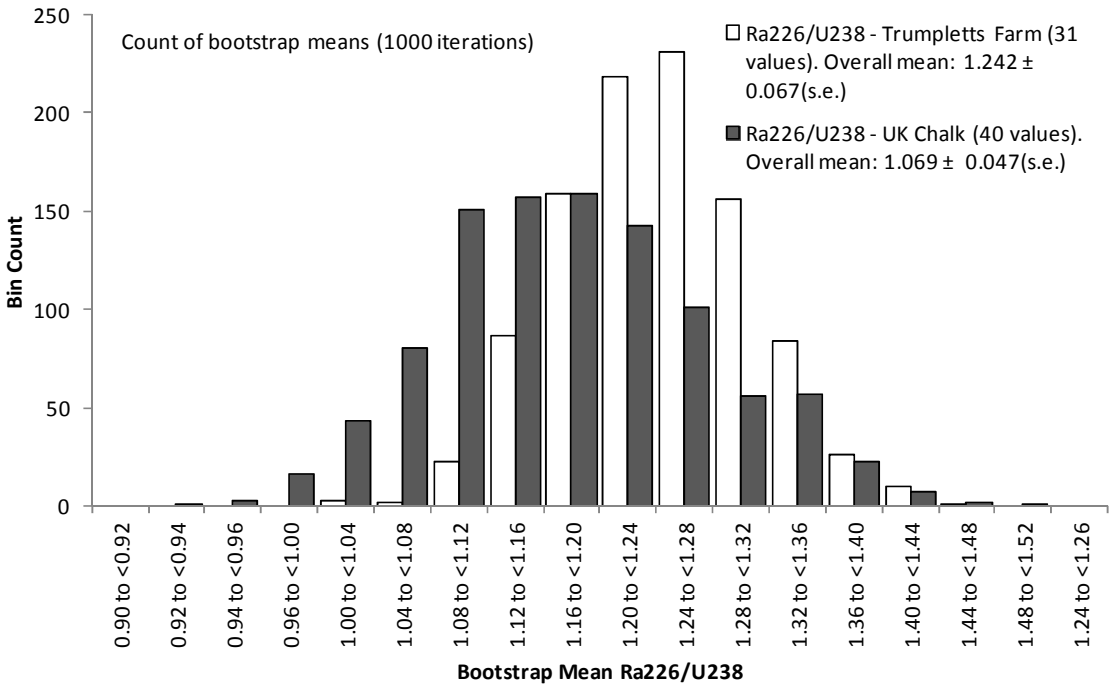

..\Project\Calcs\Stats\Bootstrap\[EDF_generation_from_U_Ra_Rn_data.xlsm]

Figure 7—9 Bootstrap - Distribution of the means of 1000 random re-samples (with replacement) from the Ra226/U228 activity ratio (for samples collected at Trumpletts Farm and other reported data)

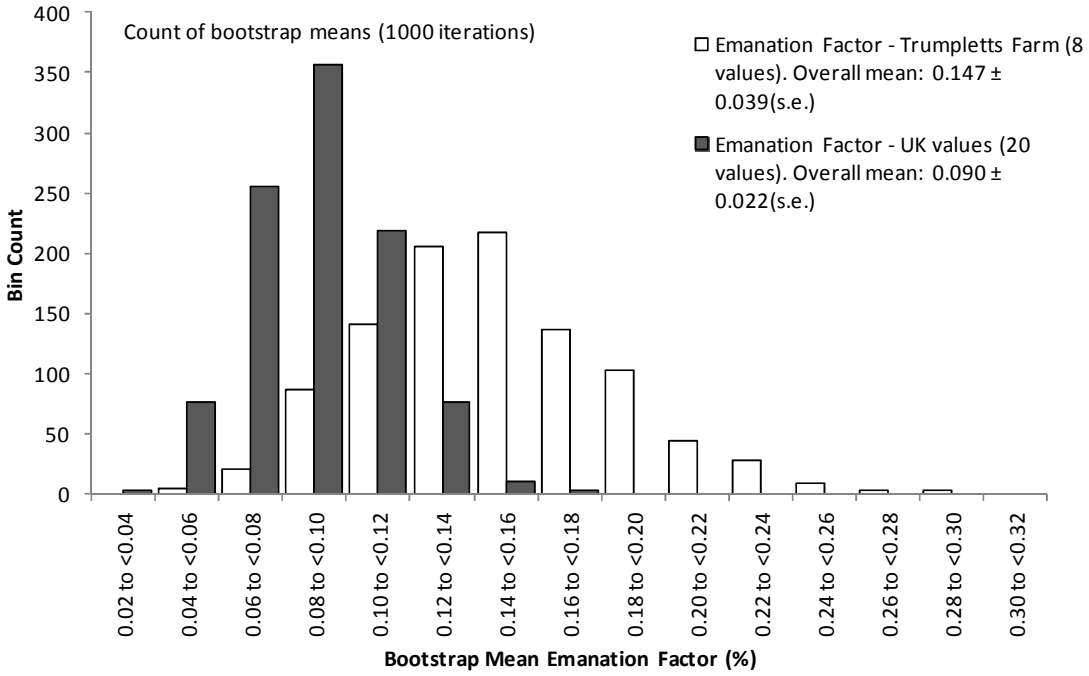

..\Project\Calcs\Stats\Bootstrap\[EDF_generation_from_U_Ra_Rn_data.xlsm]

Figure 7—10 Bootstrap - Distribution of the means of 1000 random re-samples (with replacement) from the calculated radon emanation factor (for samples collected at Trumpletts Farm and other reported data)

Calculation of t_{cf}. using Monte Carlo simulation

As described by Equations 7-1 and 7-2, the calculation of the characteristic diffusion time t_{cf} requires 5 independent arguments, for which probability distributions of mean values have been determined. A Monte Carlo simulation was designed to determine t_{cf}, which consisted of independent random sampling of each of the input variable distributions many times and generating new histograms of the resulting variation (and hence a likely probability distribution) in the derived diffusion time.

To achieve this, a computer code was written to record the result of 10,000 re-samples of the 1,000 mean values calculated for each of the 5 arguments. Given that the frequency of values within each of the sets already reflect the underlying probability distribution, a simple selection approach was adopted where values between 1 and 1000 were randomly generated and the value according to this position within the dataset was returned. Once a new set of 5 arguments had been returned, the value of t_{cf} was then calculated. Finally, the overall process was undertaken 3 times – once for each of the data classifications discussed in Section 7.2.1.

The resulting histograms for each simulation are presented in Figure 7—11. Each plot has been calculated by defining a series of 'bins' into which the 10,000 values of t_{cf} have been assigned. For the purposes of clarity, the frequency bins have been defined on a log scale, given the wide variation in results. The data have also been converted into a likelihood of occurrence by calculation of cumulative probability curves (as presented in Figure 7—12) This figure also includes a 50% probability line superimposed for reference.

Of particular note is

i. The difference in distribution between Trumpletts Farm site specific data and the inclusion of the mean radon values from within the Pang and Lambourn catchment, where higher values of radon activity reduce the value of t_{cf} by approximately an order of magnitude – with the value of t_{cf} with the highest probability decreasing from *c.*4 days to *c.*0.8 days. From this result, it may also be inferred that that groundwater radon activity should ideally be monitored at the same location from where Chalk uranium content has been assayed, to reduce the potential of such variation.
ii. The similarity in peak probability between the Pang/Lambourn and UK Chalk datasets (around the order of 1 day), but the distinct change in degree of negative skew, plus a lower limit on the highest values if t_{cf}, when mean values for all Chalk

samples are considered. Such a change is considered to be a combined impact of generally lower [^{226}Ra]/[^{238}U] isotopic activity ratios (which would decrease t_{cf}), combined with a lower and much narrower range in emanation rate (which again would produce lower values of t_{cf}).

iii. That, although the variation in t_{cf} in each scenario can cover over 6 orders of magnitude, the 50% probability values (i.e. where half the values of t_{cf} are greater and half are less in each distribution) are approximately of the same order (510, 1019 and 2034 mins respectively).

Sensitivity Analysis of individual parameters

The results from the Monte Carlo analysis naturally combine the impact of variation in each of the arguments used to calculate t_{cf}. However, it is also useful to consider the sensitivity of some of the most uncertain variables on the final value. Figure 7—13 illustrates the impact of the potential variation in [^{226}Ra]/[^{238}U] disequilibrium observed from previous studies and of emanation factor on the estimates of t_{cf}. The results demonstrate a 3-fold range from the extremes of disequilibrium in UK rock matrix data. In a similar style, Figure 7—14 reworks the model results to illustrate the potential variation on t_{cf} given a fixed emanation rate (100%), but allowing the uranium content within the matrix material to vary. The figures confirm that, although sensitive to uranium content, the value of t_{cf} is, in general, more sensitive to emanation rate overall.

In addition, the impact of assuming fixed values of parameters within the radon diffusion model, rather than permitting each argument to vary, is explored in Figure 7—15. In this example, the values assumed for each parameter in the original work by Atkinson et al (2001) are gradually imposed upon the mean bootstrap replicate distributions derived in Section 7.2.2. In this figure, the original distribution of t_{cf} calculated for Trumpletts Farm data is repeated, but new distributions are superimposed, having been calculated after single point estimates have been gradually introduced. Of particular note again is the influence of emanation rate on the distribution of predicted diffusion times, as well as the influence of assuming a fixed uranium concentration of the Chalk block that is lower than the mean data would suggest overall, but which is more representative of the white Chalk matrix.

Such results will be will discussed further in the following sections, where a comparison between the radon diffusion model and results from other tracer tests is made.

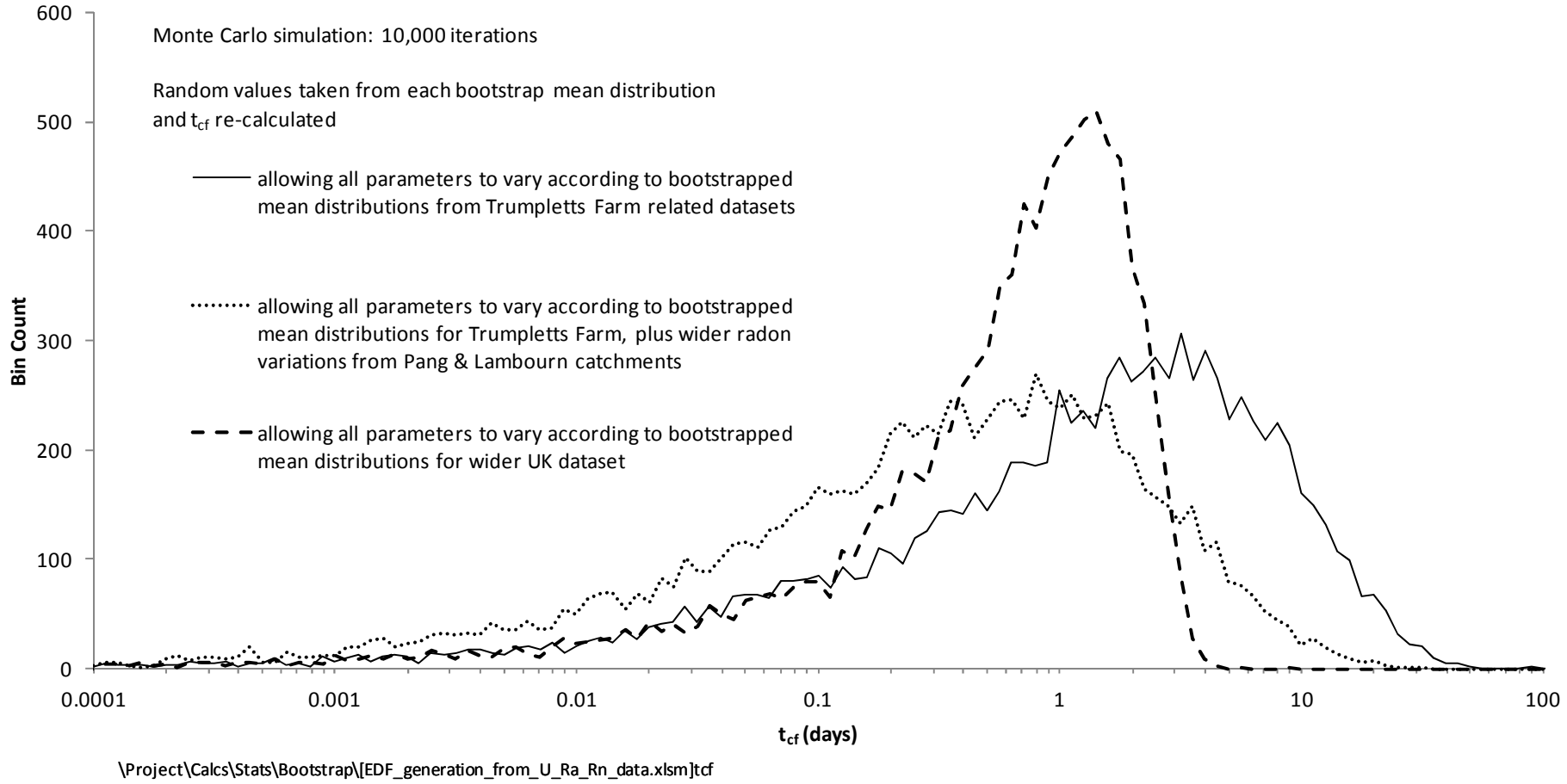

Figure 7—11 Variation in t_{cf} calculated using a Monte Carlo approach to the selection from bootstrap mean distributions of input values

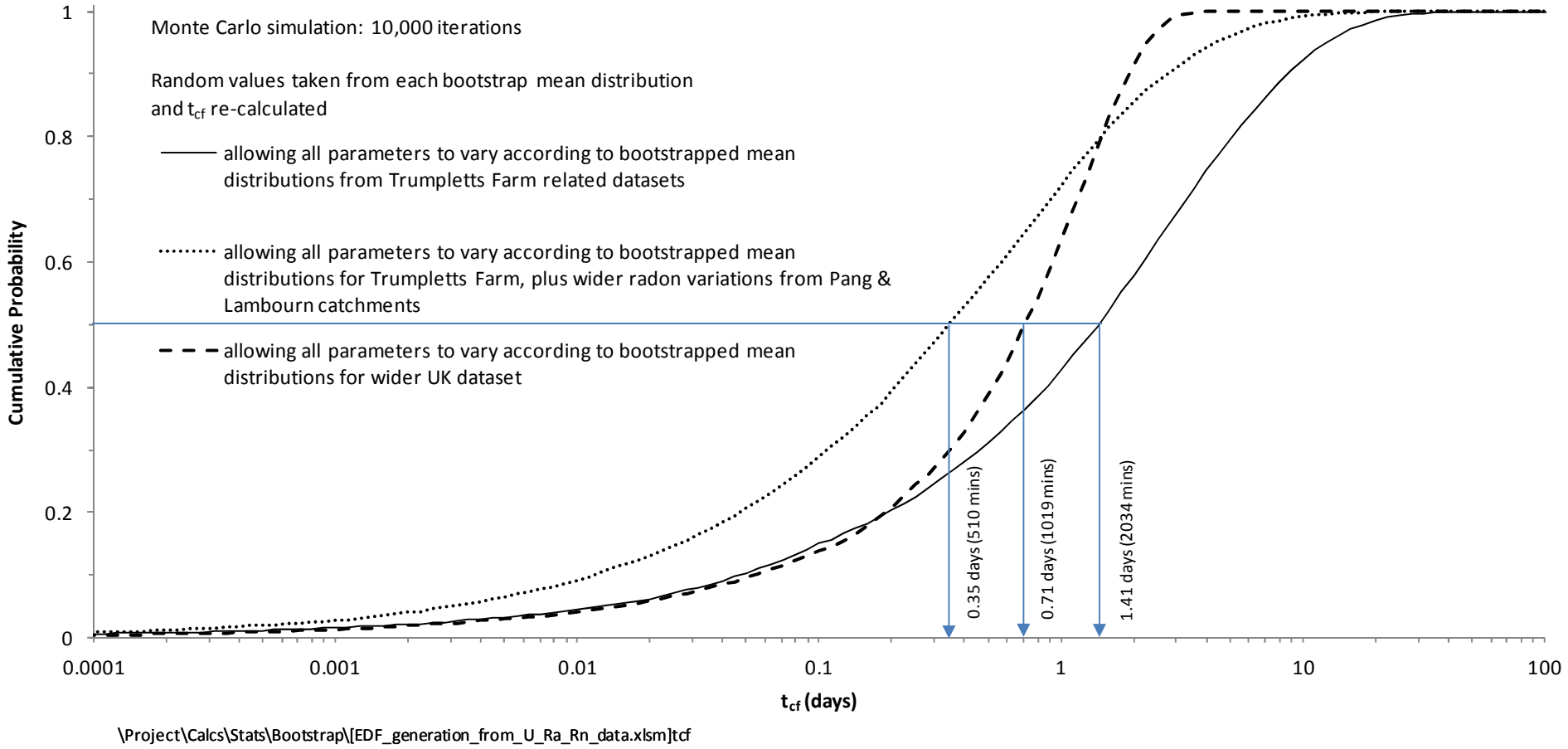

Figure 7—12 Cumulative probability distribution for values of t_{cf} calculated using a Monte Carlo approach for three datasets

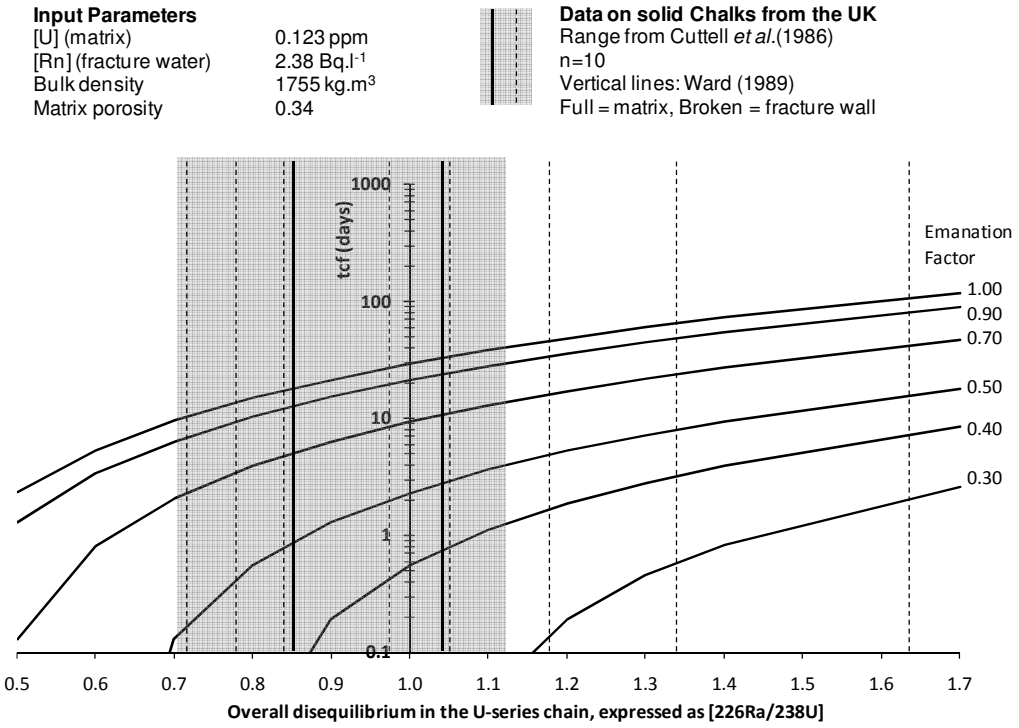

d:\simon\project\calcs\models\[uchalkresults_trumpfarm_modelcalcs_v3.xlsm]modelcalcs1

Figure 7—13 Theoretical values of t_{cf} as a function of [^{226}Ra]/[^{238}U] ratio and radon emanation factor, for a fixed matrix uranium and groundwater radon concentrations.

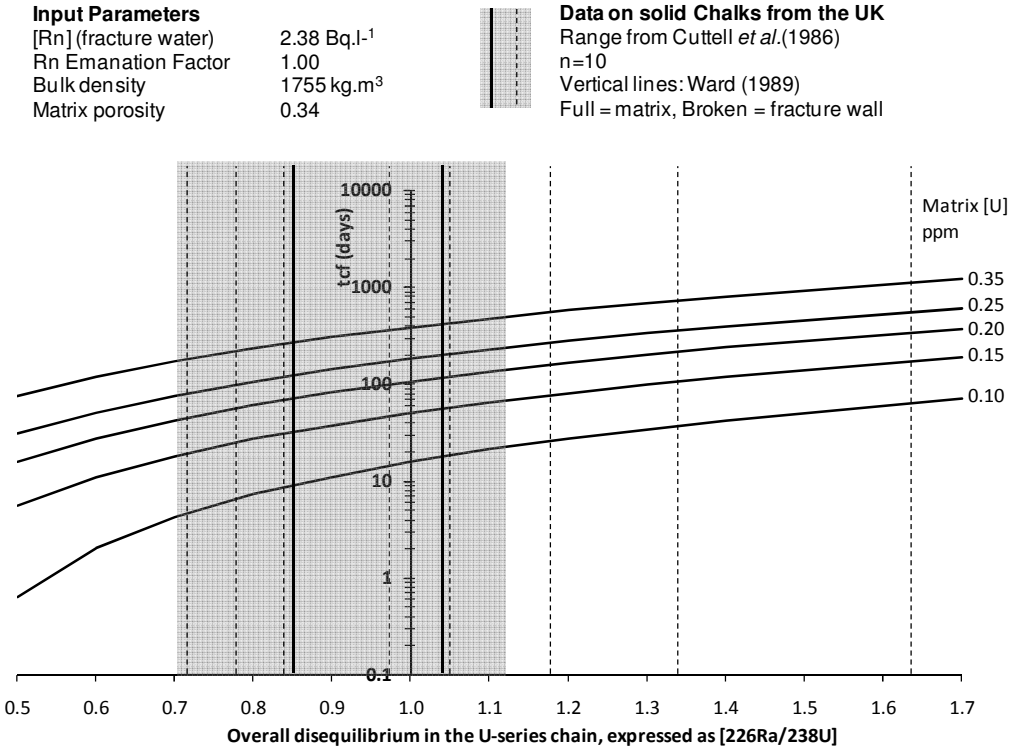

d:\simon\project\calcs\models\[uchalkresults_trumpfarm_modelcalcs_v3.xlsm]modelcalcs1

Figure 7—14 Theoretical values of t_{cf} as a function of [^{226}Ra]/[^{238}U] ratio and matrix [U] for a fixed radon emanation factor (E=1) and groundwater radon concentration

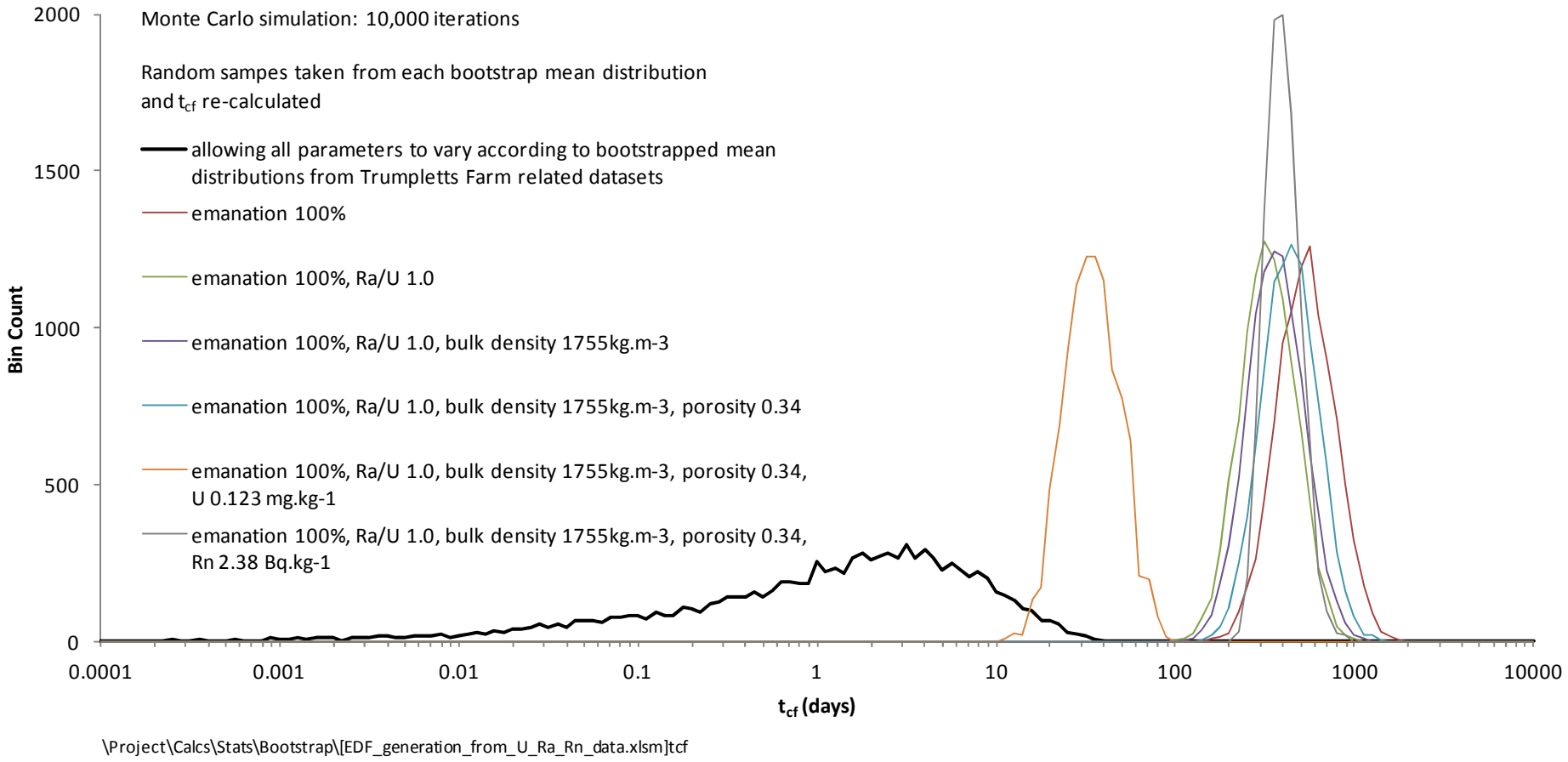

Figure 7—15 Sensitivity Analysis - Variation in t_{cf} using Trumpletts Farm datasets, holding combinations of parameters constant

7.3 Comparison between Tracer Test and Radon Model value of t_{cf}

In a similar way to that undertaken for the radon diffusion model, values of t_{cf} calculated from tracer testing in the Chalk have been processed further to obtain two sets of empirical distribution functions (EDF), that may be compared with those calculated for the radon diffusion model:

i. A 'pseudo' cumulative probability distribution for the results of the tracer test injected at PL10A and abstracted from the Bottom Barn borehole has been calculated by using the values of t_{cf} from P = 10 to P = ∞ presented in Table 7—3 and weighting them according to the reciprocal of the measure of goodness of fit 'RMSLE' (Root Mean Square Log Error). The relative contributions of each value of t_{cf} over the range of values have then been accumulated. As such, this method provides an approximate cumulative probability of occurrence which allows for variation in the extent of hydrodynamic dispersion, but reduces the contributions of values of t_{cf} derived for values of P that produce a poorer degree of fit to the observed breakthrough curve.

ii. An EDF of the mean value of t_{cf} has been calculated, using values calculated from other UK Chalk tracer tests, as presented in Table 7—1. To ensure a valid comparison with the radon diffusion model, only those values of t_{cf} derived assuming double-porosity diffusion *without* hydrodynamic dispersion have been included. (This criteria has limited the selection to 8 values.) An estimate of the potential distribution of the mean of these data was then calculated using the bootstrap method, similar to that described in Section 7.2.2.

The 'bootstrap' EDF of t_{cf} for UK Chalk values is compared with the previously presented results of t_{cf} derived from the radon diffusion model in Figure 7—16. The results have also been converted to a cumulative probability distribution and are presented alongside the pseudo EDF for Trumpletts Farm, plus the radon diffusion model results in Figure 7—17.

UK Chalk Data Comparison

As presented in Figure 7—16, it is evident that even with substantial variation from the results from the radon diffusion model, tracer tests generate representative fracture diffusion times that are substantially shorter overall; values differing by *c.*2 orders of

magnitude, i.e. in the order of days for the radon diffusion model, compared to 0.025 days derived for tracer tests. (Note that the results are plotted using a semi-log scale.)

However, it is also apparent that a degree of overlap exists between the two resulting EDFs. Explicitly that,

i. 100% of the t_{cf} mean distribution derived from tracer tests is contained with lowest 12% of values derived from the radon diffusion model (using UK Chalk data).
ii. Expressed alternatively, there is an 88% probability that values of t_{cf} calculated using the radon diffusion model will be greater than the maximum mean value calculated using standard tracer testing (where a double porosity diffusion model has been used which assumes that hydrodynamic dispersion may be ignored).
iii. This probability rises to 93% when compared to the median value of tracer test derived t_{cf}.

Trumpletts Farm Data Comparison

Figure 7—16 also indicates that there is a large discrepancy between the diffusion time estimated by the (well constrained) tracer test at Trumpletts and the predictions made by the radon diffusion model, where input data has been limited to that obtained from the same location. Note however:

i. That the pseudo cumulative distribution for t_{cf} assumes that hydrodynamic dispersion may be present and so a direct comparison with the results of the radon model values is not strictly valid;
ii. A value of t_{cf} of 2.3 mins (0.0016 days) obtained from tracer testing, where dispersion was ignored (i.e P=∞), is close to the smallest diffusion times predicted.

7.4 Comment on the discrepancy of results

By presenting the results from both types of model as empirical functions, the distribution in t_{cf}, as a consequence of the variability in the underlying datasets or models, has been explicitly taken into account during the comparison of results.

However, it is still apparent that there is a large discrepancy between the two types of approach and that, overall, there is a low probability that the radon diffusion model will provide values of t_{cf} that match those derived from tracer testing.

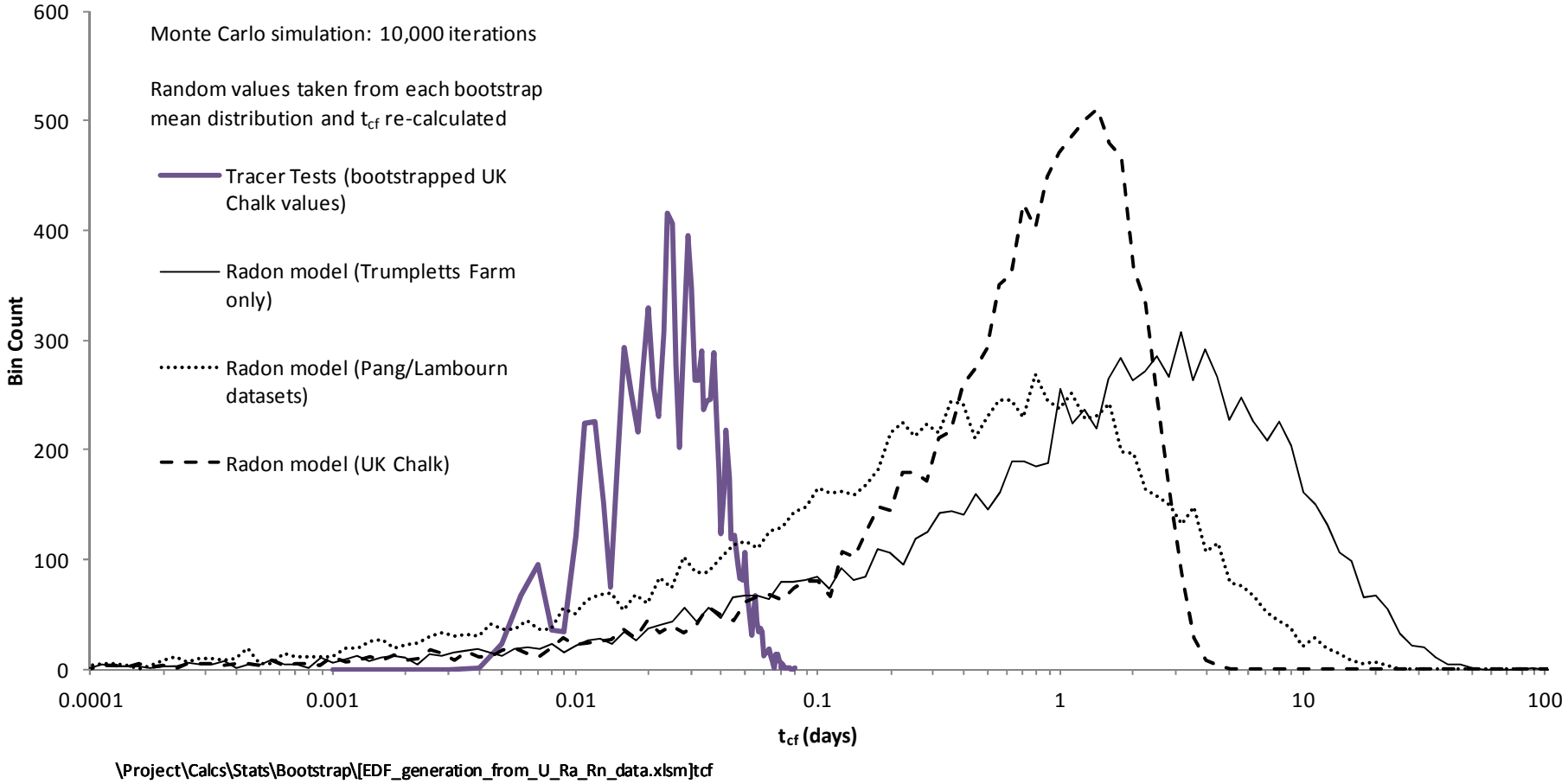

Figure 7—16 Comparison of t_{cf} from radon diffusion model and tracer tests in UK Chalk

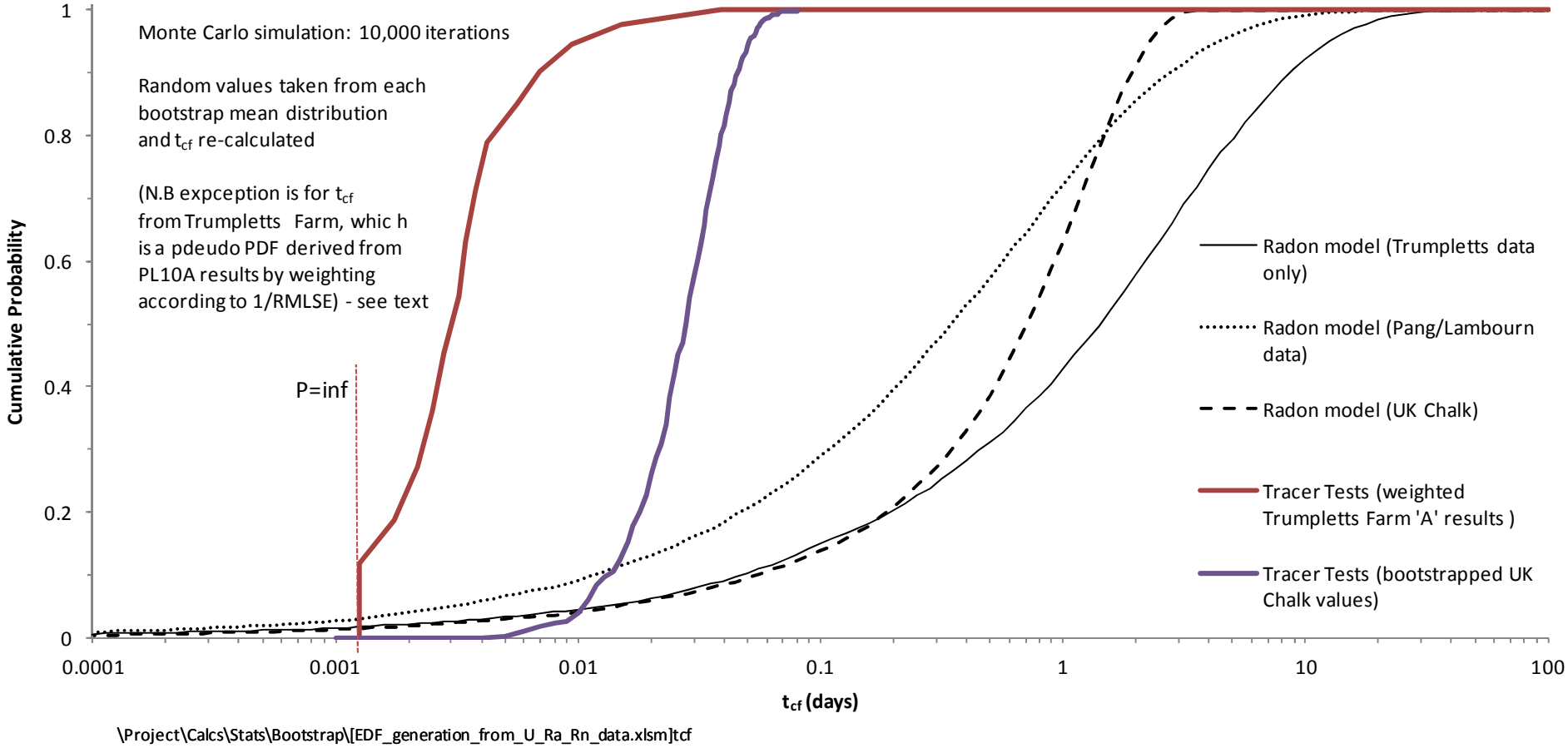

Figure 7—17 Cumulative probability distribution for values of t_{cf} for both radon diffusion model and Chalk tracer tests

The results suggest therefore that other factors, not considered as part of this current study, may require further exploration.

Poor understanding of the fracture system control on radon concentrations

It could be envisaged that the two types of test results may be dominated by different aspects of the same aquifer system. Given the short duration of the tracer tests, they can only ever be expected to reveal information localised around specific flowing horizons with the aquifer system. However, it may be possible that overall radon activity may reflect data about the entire Chalk fracture system, albeit potentially weighted by the contribution of each fracture's effective transmissivity.

Whereas tracer tests reflect only the properties of the largest two flowing fractures (in the case of pumping PL10A) and the surrounding matrix, radon activity measured at the site may reflect the wider distribution of fracture sizes that may contribute higher radon concentrations to pumped water. However, as represented in the radon diffusion model, assuming lower radon activity (which would be expected to occur in larger isolated fractures) would result in *higher* values of t_{cf}, increasing yet further the difference between model results.

Radon Sorption

The potential sorption of either uranine tracer to Chalk matrix or of radon to clay material (as discussed previously in Section 2.2.1) may affect the values of t_{cf} calculated by both type of model. In particular:

i. If in reality uranine sorption is occurring to fracture walls, but is not explicitly represented in the advection diffusion model used to fit to a tracer breakthrough curve, calculated values of t_{cf} will be too low. This will be as a consequence of the effect being interpreted in terms of a rapid loss of tracer to the aquifer matrix, i.e. that solute diffusion into the matrix block appears to be more rapid than is actually occurring. However, counter to this argument is evidence from Bottrell et al (2010), who demonstrated that sorption of Sodium Fluorescein on Chalk was very slight;
ii. Although inert, the sorption of radon onto clay sediments has been observed by Wong et al (1992). It could be envisaged that this phenomenon may be possible where clay material is present on fracture surfaces. In such a case, the retardation of dissolved radon within the fracture space would be expected to lead to higher values of t_{cf}.

To take the effects of radon sorption into account would require the incorporation of a additional retardation coefficient into the radon diffusion model, not investigated as part of this thesis. In addition, no known data exists for radon sorption within Chalk matrix.

Location of radon source

As formulated, the radon diffusion model currently assumes that the radium source term is uniformly distributed throughout the surrounding Chalk matrix. However, it could be envisaged, given radium's affinity to adsorption to clay, that long term migration from the original uranium parent location to fracture walls may have occurred over time. Wood et al (2004) used a diffusion/ion exchange model to explain how radium becomes concentrated on the fracture surfaces of metamorphic rocks, through diffusion through the matrix and sorption to weathered material on the fracture surfaces.

As source strength has been calculated using *bulk* uranium concentrations plus an assumption of a fixed *bulk* Ra226/U238 activity ratio, a miscalculation is this term could be possible, if in reality radium is preferentially located in fracture skins. Using bulk Chalk values may therefore not be sufficiently robust, and may lead to an underestimate of the potential for radon to diffuse much more rapidly from the fracture wall.

However, increasing the effective strength of the source term would again tend to *increase* values of t_{cf} for any given fracture water radon activity, and so this hypothesis is not supported from the results of tracer testing.

Scale Dependent Matrix Diffusion

With the advection-diffusion model, there is a general assumption that that the 'apparent' diffusion coefficient D_A (defined as the 'effective' diffusion coefficient divided by the matrix porosity i.e. D_E/ϕ_e) has a fixed value. However, recent reviews of tracer test results over varying distances suggest that effective matrix diffusion coefficients in fracture rocks may in fact be statistically scale-dependent (Liu et al., 2004; Zhang et al., 2006; Liu et al., 2007; Zhou et al., 2007). The enhancement of effective matrix diffusion with increased distance is considered possible, where other mass-transfer processes may begin to dominate. Examples include (Zhou, 2007):

i. where there is variability in the properties of fracture fill material;
ii. variability in fracture aperture within single fractures;
iii. the coexistence of fractures over a wide range of scales; or,
iv. where there is 'multi-rate' diffusion processes, caused by heterogeneity in matrix porosity.

Currently, it is unclear as to the impact that variable diffusion properties may have when comparing the two type of model investigated in this thesis and further analysis of the other Chalk tracer tests may be required to assess its significance. However, although scale-dependent porosity (due to the potential impact of sedimentary cycles within the Chalk), may be expected given its depositional environment, it is considered unlikely that the Trumpletts Farm tracer test was undertaken over sufficient distance or time for any of the effects described to dominate the form of the observed breakthrough curve.

8 Conclusions

This Chapter summarises the results achieved from the different strands of this study, and draws conclusions regarding the applicability and practicality of employing a radon diffusion model for the purposes of determining characteristic double-porosity diffusion times in the Chalk.

Each of the original study objectives are restated and comment is provided on the new information which has been gained, with an assessment on how successfully the objective has been met. Where uncertainties remain, these are discussed in relation to why they exist and, where possible, suggestions are made on how they may be reduced.

Finally, an assessment is made of the practicality of using uranium-series measurements to map spatially values of the fracture-matrix diffusion times t_{cf}, which has practical relevance when attempting to predict the capability of the Chalk aquifer as a whole to attenuate soluble contaminants.

8.1 Assessment against Study Objectives

Summary

The study's aims and objectives were formulated in detail in Chapter 1, after discussion of previous work which has demonstrated that,

a. double-porosity diffusion within the Chalk aquifer has been observed and quantified both in the field and in laboratory experiments;
b. that it may be used to explain the observed rapid attenuation of contaminants (such as nitrate, bromide and chloride),
c. as well as the long residence times of the same contaminants within the Chalk matrix.

The derivation of a radon diffusion model has been based on these observations, but incorporates values of *in situ* measurements of naturally occurring radionuclides, to derive information regarding the extent to which Chalk matrix can absorb and release non-sorbing solutes.

8.1.1 Comment on original assumptions of the radon diffusion model

In light of the new data gathered, the original assumptions of the radon-diffusion model as developed by Atkinson et al (2001) are now revisited.

- *That the Chalk aquifer system is at equilibrium with regards to the balance between radon diffusion from the matrix and the decay within the fractures.*
- *That sample points are far enough from any boundaries (e.g. low or high inputs) for the radon content of fissure water to be determined entirely by emanation of Rn from the matrix.*

(Note: Given that the half life of Rn atoms is 3.82 days, a state of equilibrium between production, diffusion and decay will occur if groundwater residence times are greater than about *c.*25 days.)

Seasonal variations in radon activity have been observed (Chapter 6), but it remains unclear as to the dominant factors that control the magnitude of change. Data collected during 2005 initially supported the hypothesis that radon activity from the chalk springs and groundwaters would tend to rise in summer, as a greater proportion of water is provided from the Chalk matrix as groundwater levels recede and water with high radon content is drained from the matrix to supply water to the fracture network. Winter springs flows (in particular at Blue Pool) may be expected to contain a greater proportion of water with short residence times delivered to the spring through the semi-karstic fracture network that has been suggested by the tracer tests result by Maurice (2008). Such water would not remain with the flow system for sufficient time to allow the radon activity to reach secular equilibrium and as a result would tend to dilute the overall activity of the water at the spring (given that precipitation has negligible radon content).

However, the results from 2006 did not fit this model as radon activities remained low throughout the year, even though groundwater levels continued to vary.

The period of monitoring did coincide with periods of low recharge compared to the long term average and, although there was still groundwater level fluctuation, radon activity remained low. Hence, it would have also been beneficial to make measurements during periods of average or high recharge.

The small number of measurements from boreholes did appear less variable than springs. With low pump rates (compared to that used during the large scale pump tests at Bottom Barn), radon activities were considered representative of the surrounding fracture water, with little contribution from water drained from the matrix.

Given this wide temporal variability of radon recorded at spring locations, the observations suggest that water sampled at these locations may not in fact be in steady state with the surrounding rock source, and may indicate either low groundwater residence times in the shallow aquifer system or a mixing between several sources.

This suggests that the fracture flow paths are either:

a. not sufficiently long to allow equilibrium to be achieved, or
b. that spring sources are in reality a complicated mix of equilibrated water (from the regional groundwater system) and shorter residence time Chalk waters delivered to the spring, either through the well characterised karstic flow system (e.g. Maurice, 2009) or, in the case of the Lower Pang springs, influenced by water derived from the overlying Palaeogene sediments.

Variations between spring sites also suggest that, either 1) the source term strength or 2) the radon diffusion coefficient for Chalk, may vary between sites. A greater density of monitoring would have been required to draw more robust conclusion regarding any potential seasonality of activity (as noted for example by Andrews and Wood, 1972).

Note that the above results are in distinct contrast to the results from the large pump test at Bottom Barn and to some degree the packer testing of PL10A, both at Trumpletts Farm. The large scale test illustrated the complexity of the evolution of the radon signatures from the Chalk and supported the theory developed by Ward (1989), that many different sources of water were mixed together as the cone of depression developed and the water was drawn from greater distances from the well. Of note was the large peak in radon activity observed soon after the commencement of pumping, which was considered to indicate the rapid release of water from the matrix pore space in the immediate vicinity of the well. Such water would be expected to have much higher radon activity than the fracture as predicted by Atkinson et al (2001) and others.

Finally, it should be noted that, if equilibrium has not been achieved, it is clear from Equation *(1-18)* (Chapter 1) that values of t_{cf} would be overestimated, and as a consequence would lead to an overestimate of effective aperture size.

- *That the radon that is measured in fracture waters is supported by transfer from the matrix alone and that this process can be represented by an effective (Fickian) diffusion coefficient.*

Radon has been measured in both groundwaters and springs using liquid scintillation analysis. Re-analysis of radon activity within the same samples after several months storage

has demonstrated that the radium content of Chalk groundwater is generally below the detection threshold. It is therefore highly likely that groundwater radon is unsupported from radium in the fracture water but rather, is derived from direct ejection or diffusion from the surrounding matrix. Andrews and Wood (1972) demonstrated that the contribution from direct alpha recoil is unlikely to contribute significantly to fracture water activity and rather that diffusion along grain boundaries is likely to dominate in such systems. However, note that no explicit controlled test to confirm that Fickian radon diffusion is occurring has been undertaken as part of this study. This may be a useful extension to this work.

- *That the distribution of uranium and radium, the immediate parent of radon, can be assumed to be uniform throughout the matrix.*

Chapter 5 demonstrated that variation in both uranium and radium is evident from within the core at Trumpletts Farm, and that these may be expected to vary at a range of scales. Greater levels of uranium were determined within the Lewes Nodular Chalk (compared to the Seaford Chalk), which may be associated with a greater reworking of uranium bearing sediments during the formation of hardgrounds.

Ward (1989) also reported variations in uranium content along fracture wall compared to the bulk matrix. Clearly, if radium is concentrated within the fracture walls, either by sorption or by the process of isotopic fractionation (discussed in Chapter 2), then the boundary conditions of the diffusion model will change substantially and bulk determinations of radium will tend to lead to an underestimate of the actual radon mass transfer rate from matrix to fractures.

Pacey (1984b; 1985) also suggested that the non-carbonate fraction of the Chalk may be the primary source of uranium series isotopes. Such a result has implications for the radon-emanation rate assumed in the double-porosity model. For example, if the radon source term were located in the non-carbonate fraction it may be envisaged that emanation and diffusion to surrounding fractures may be enhanced, given potentially shorter diffusion pathways.

Assay of radium from bulk samples does not provide any information in relation to the extent to which radium is located close to grain surfaces and within other secondary cementing material, (which Andrews and Wood (1972) suggested would lead to much more rapid rates of diffusion than from a single phase). Hence, assuming a lower source term strength than may be present, but associating it with observed fracture water radon activity,

would result in calculated rates of diffusion that were greater than in reality – i.e. the current model would tend to underestimate the value of t_{cf}.

- *The isotopic ratio between uranium-238 and radium-226 is known and does not vary, and hence allows uranium to act as a proxy for the source term.*

This assumption is beneficial in terms of laboratory analysis (Chapter 4), but as is clear, from the combination of Equations *(1-11)*, *(1-12)* and *(1-18)*, that uncertainty in this term will lead to a strong (second order) effect on estimates of t_{cf}. Atkinson et al (2001) cited data from studies on Chalk samples from Lincolnshire (Cuttell et al., 1986) to justify this assumption, but it was accepted that the data were few in number.

Isotopic Activity Ratios (IAR) derived from this study (Chapter 5), in combination with the bootstrapping techniques (Chapter 7), have demonstrated there is potentially a wide variation in isotopic disequilibrium within Chalk sediments Hence, it is not correct to assume that isotopic equilibrium has been achieved. Indeed most Chalk samples analyzed have shown 226Ra enrichment with respect to 238U.

This observation is particularly relevant for the measurements at the centimetre scale (Figure 5-2). Averages over the entire length of the core at Trumpletts Farm suggest a mean 226Ra/238U ratio of *c.*1.15. Combined with an average uranium content for the entire borehole (of *c.*20 samples for example), would produce an estimate of *c.*90% of the actual 226Ra source activity, if an IAR if 1 was assumed.

This suggests that it may not be practicable to use a single value of uranium concentration as a proxy for radium (i.e. the immediate parent of radon), and that additional knowledge of the uranium series disequilibrium would be required to constrain the radon-diffusion model. Given these results, the assumption of isotopic equilibrium could lead to a significant underestimation of source strength.

- *That 100% of radon produced within solid Chalk is ejected into the surrounding pore space and is able to diffuse towards larger fractures.*

From the analysis of solid and disaggregated core material, it has been demonstrated that the radon emanation rate from chalk particles to the matrix pores cannot be assumed to be 100%. In fact, for silt particles (*c.*63 μm), average rates of *c.*20% are more common. This is in line with values determined by Cuttell (1986) in the Lincolnshire Chalk. This apparent emanation may be enhanced if a large amount of rapid diffusion occurs along grain boundaries, as suggested by Andrews and Wood (1971), or if radium is concentrated on the

surface of grains and not uniformly distributed through the material. Andrews and Wood (1971) did not perform radon release experiments of Chalk material, but they did consider a range of particle size fractions for a crushed and sieved sample of Carboniferous Limestone. Calculated emanation rates were *c.*13% for particles less than 149 μm in diameter, decreasing rapidly with an increase in particle diameter. They also suggested that, as particle sizes decrease, the emanation may be controlled by the diameter of particles of any cementing phase and suggest that radon release and diffusion within such phases are very easy processes. Hence, given the small diameter of individual Chalk laths (a few microns), 100% radon emanation would be anticipated. However, the results from the emanation study do not support this hypothesis.

8.1.2 Comment on analytical method for uranium assay

The laboratory method used to assay for uranium with dissolved Chalk samples utilised the natural phosphorescence of the $[UO_2]^{2+}$ species. Potential quenching effects of other dissolved species was minimised though the preferential extraction from solution using tri-butyl-phosphate, combined with signal enhancement through complexing with EDTA (Chapter 4).

After significant development to improve the measurement repeatability, the method was considered to be a relatively simple yet sensitive approach to uranium assay. However, several limitations of the method became clear, namely,

i. that the sample dissolution technique used reverse Aqua Regia, which was assumed to be able to dissolve all constituents of the samples with the exception of silicate material (as confirmed using XRF analysis), and that all uranium would enter solution. However, this assumption was not tested by performing complete dissolution through the use of stronger acid techniques (e.g. making use of HF) and it may be possible that the uranium content was underestimated;
ii. that it may have been useful to differentiate between carbonate and non-carbonate fractions as well as the total sample – as per the small number of samples analyzed by Low (1996b) seemed to suggest that uranium was concentrated in non carbonate fractions. Pacey (1984b) also suggests this conclusion, in a study employing energy discriminated gamma spectrometry;
iii. that assay is necessarily for total uranium mass and that it does not differentiate between uranium isotopes. Hence, it was necessary to assume that the measurements reflected effectively 238U content and that the relative contribution of 234U at equilibrium would be negligible.

iv. It was not possible to determine potential 238U/234U disequilibrium within the scope of this thesis.

8.1.3 Comparison with independent tracer test data

Results from a series of tracer test undertaken at a research site with the Pang catchment, were reported by Mathias et al (2007b), and studies on borehole geophysics and groundwater flow heterogeneity at the same site reported by Williams et al (2006). A comparison of the values of t_{cf} (Chapter 7) has demonstrated that radon derived values are much higher than those from tracer tests, even after the potential variations and uncertainties in measured parameters have been taken into account.

Of the potential reasons why values may be so different that were explored in this thesis, it is considered that there are three leading factors which may have potentially a large control on the calculated value of t_{cf}, namely

a. uncertainly in the location of the radium source in relation to the fractures,
b. uncertainly in the effective radon emanation rate from carbonate grains (or other secondary material within the matrix), and,
c. that other factors dominate, not currently included in the formulation of the radon diffusion model, e.g. the sorption of radon onto complex substrates, such as amorphous phosphates, oxides or organic matter.

Of these options, least is known about the degree to which radon sorbs to other material. If in reality sorption dominates within the fracture system, then rates of diffusion would be reduced and the current model would overestimate the value of t_{cf}. This would be in agreement with the current disparity between results.

8.2 Overall Conclusion

These conclusions and subsequent discussion suggest that it may be difficult to deduce reliable transport parameters by routine application of the radon model described, as it is likely that each site would require detailed characterisation. It is also considered that results obtained are not currently sufficient to establish the applicability of the proposed method and that large uncertainties still remain surrounding the controls of radon diffusion from the Chalk matrix to the fracture system.

There are two mechanisms in particular which this work suggests may benefit from further study – the physical nature of radon diffusion from within the Chalk matrix (into both the

surrounding pore space and then the transmissive fracture network), plus the role of clays in the potential sorption of radon once ejected into the pore space.

A more rigorous examination of overall radon emanation could be achieved through the design of a new experiment, where water surrounding saturated Chalk blocks sealed within an airtight vessel could be regularly sampled over time to observed the evolution of radon activity. More detailed analyses of disaggregated Chalk samples may also help to identify the exact location of the radium source term.

The role of radon sorption has been assumed to be negligible within the Chalk's carbonate matrix, but no explicit studies are known. However, as discussed, previous work has identified that radon may sorb to clay material within soils. Hence, it is conceivable that significant sorption may also exist within clay lined fractures. If observed through experimentation, explicit radon retardation may therefore need to be included in the radon diffusion model presented by Atkinson et al (2001).

References

Adams, B., D. Peach and J. Bloomfield, The LOCAR Hydrogeological Infrastructure for the Pang/Lambourn Catchment, British Geological Survey, 2004.

Alibrahim, M. and H. Shlewit, Solvent extraction of uranium (VI) by tributyl phosphate/dodecane from nitric acid medium, *Periodica Polytechnica Chemical Engineering, 51*(2), 57-60, 2007.

Andrews, J. N., W. G. Burgess, W. M. Edmunds, R. L. F. Kay and D. J. Lee, The thermal springs of Bath, *Nature, 298*(5872), 339-343, 1982.

Andrews, J. N. and D. J. Lee, Inert gases in groundwater from the Bunter sandstone of England as indicatoirs of age and palaeoclimatic trends, *Journal of Hydrology, 41*, 233-252, 1979.

Andrews, J. N. and D. F. Wood, Mechanism of radon release in rock matrices and entry into groundwaters, *Transactions of the Institution of Mining and Metallurgy, B81*, 198-209, 1972.

Asikainen, M., State of Disequilibrium Between U-238, U-234, Ra-226 and Rn-222 in Groundwater from Bedrock, *Geochimica et Cosmochimica Acta, 45*(2), 201-206, 1981.

Atkinson, T. C., J. A. Barker, R. S. Ward and R. Low, Radon: An indicator of solute transport in double-porosity aquifers, paper presented at Proceedings - International Association of Hydrogeologists Congress, Netherlands, 2001.

Atkinson, T. C. and D. I. Smith, Rapid groundwater flow in fissures in the chalk: an example from south Hampshire, *Quarterly Journal of Engineering Geology and Hydrogeology, 7*(2), 197-205, 1974.

Atkinson, T. C., R. S. Ward and E. O'Hannelly, A radial-flow tracer test in Chalk; comparison of models and fitted parameters, Tracers and modelling in hydrogeology (ed A. Dassargues); TraM'2000, IAHS-AISH Publication 262, 2000.

Balogh, Z., S. L. S. Stipp, K. Bechgaard and E. Johnson, Reactive nanoparticles in chalk: implications for sequestration of metals from groundwater, *Mineralogical Magazine, 72*, 373-376, 2008.

Banks, D., C. Davies and W. Davies, The Chalk As A Karstic Aquifer - Evidence from A Tracer Test at Stanford-Dingley, Berkshire, Uk, *Quarterly Journal of Engineering Geology, 28*, S31-S38, 1995.

Baraniak, L., M. Thieme, G. Bernhard and H. Nitsche, Sorption behavior of radium on sandy and clayey sediments of the upper Saxon Elbe river valley, *Journal of Radioanalytical and Nuclear Chemistry, 241*(3), 511-517, 1999.

Barker, J. A., Transport in fractured rock, in Applied groundwater hydrology: a British perspective, edited by R. A. Downing and W. B. Wilkinson, pp. 199-216, Clarendon Press, Oxford, 1991.

Barker, J. A. and S. S. D. Foster, A Diffusion Exchange Model for Solute Movement in Fissured Porous Rock, *Quarterly Journal of Engineering Geology, 14*(1), 17-24, 1981.

Barker, J. A., T. E. J. Wright and B. A. Fretwell, A pulsed-velocity method of double-porosity solute transport modelling, Tracers and modelling in hydrogeology (ed A. Dassargues); TraM'2000, IAHS-AISH Publication 262, 2000.

Bateman, H., Solution of a system of differential equations occuring in the the theory of radioactive transformations, *Proceedings of the Cambridge Philosophical Society, 15*, 423-427, 1910.

Becquerel, E., La lumière, ses causes et ses effets, l'Academie des Sciences de L l'Institut de France, Paris, 1867.

Bem, H., Y. Y. Y. Bakir and P. Bourabee, An Improved Method for Low-Level Rn-222 Determination in Environmental Waters by Liquid Scintillation-Counting with Pulse-Shape Analysis, *Journal of Radioanalytical and Nuclear Chemistry-Letters, 186*(2), 119-127, 1994.

Benson, P., A. Cox, T. J. Kemp and Q. Sultana, Concentration and temperature quenching of the excited state of the uranyl ion in aqueous solution by laser flash photolysis, *Chemical Physics Letters, 35*(2), 195-197, 1975.

Betson, M., J. Barker, P. Barnes, T. Atkinson and A. Jupe, Porosity Imaging in Porous Media Using Synchrotron Tomographic Techniques, *Transport in Porous Media, 57*(2), 203-214, 2004.

Bevan, T. G. and P. L. Hancock, A late Cenozoic regional mesofracture system in southern England and northern France, *Journal of the Geological Society, 143*(2), 355-362, 1986.

Bibby, R., Mass-Transport of Solutes in Dual-Porosity Media, *Water Resources Research, 17*(4), 1075-1081, 1981.

Bloomfield, J., Characterisation of hydrogeologically significant fracture distributions in the Chalk: An example from the Upper Chalk of southern England, *Journal of Hydrology, 184*(3-4), 355-379, 1996.

Bloomfield, J., L. J. Brewerton and D. J. Allen, Regional trends in matrix porosity and dry density of the Chalk of England, *Quarterly Journal of Engineering Geology, 28*, S131-S142, 1995.

Boas, M. L., Mathematical methods in the physical sciences, J. Wiley & Sons, New York ; Chichester, 1983.

Bonotto, D. M., J. N. Andrews and D. P. F. Darbyshire, A laboratory study of the transfer of U-234 and U-238 during water-rock interactions in the Carnmenellis granite (Cornwall, England) and implications for the interpretation of field data, *Applied Radiation and Isotopes, 54*(6), 977-994, 2001.

Bottrell, S., S. Thornton, M. Spence, S. Allshorn and K. Spence, Assessment of the use of fluorescent tracers in a contaminated Chalk aquifer, *Quarterly Journal of Engineering Geology and Hydrogeology, 43*(2), 195-206, 2010.

Boulton, G. S., Quaternary, in Geology of England and Wales, edited by P. M. D. Duff and A. J. Smith, pp. 413-444, The Geological Society, London, 1992.

Bradford, R. B., Controls on the discharge of Chalk streams of the Berkshire Downs, UK, *The Science of The Total Environment, 282-283*, 65-80, 2002.

Bristow, C. R., R. N. Mortimore and C. J. Wood, Lithostratigraphy for mapping the Chalk of Southern England, *Proceedings of the Geologist's Association, 109*, 293-315, 1997.

Brooks, F. D., Development of organic scintillators, *Nuclear Instruments and Methods, 162*(1-3), 477-505, 1979.

Brouyere, S. and A. Dassargues, Reliability of transport models calibrated on field tracer experiments: Breakthrough curve sensitivity to tracer injection conditions, *Acta Universitatis Carolinae Geologica, 46*(2-3), 331-334, 2002.

Brouyere, S., A. Dassargues, R. Therrien and E. A. Sudicky, Modelling of dual porosity media: comparison of different techniques and evaluation of the impact on plume transport simulations, *Calibration and Reliability in Groundwater Modelling: Coping with Uncertainty,*(265), 22-27, 2000.

Burgess, W. G., J. A. Barker, S. J. Watson and B. A. Fretwell, Contaminant retardation by double-porosity diffusive exchange in the Chalk: implications for monitoring, *Bringing Groundwater Quality Research to the Watershed Scale (Proceedings of GQ2004), IAHS Publ. 297*, 191-196, 2005.

Burki, P. M., L. S. Dent Glasser and D. N. Smith, Surface coatings on ancient coccoliths, *Nature, 297*(5862), 145-147, 1982.

Butler, A. P., S. A. Mathias, A. J. Gallagher, D. W. Peach and A. T. Williams, Analysis of flow processes in fractured chalk under pumped and ambient conditions (UK), *Hydrogeology Journal, 17*(8), 1849-1858, 2009.

Carneiro, J., The evolution of the Tilmanstone contaminant plume., MSc thesis University College London, UK, 1996.

Catt, J. A. and J. M. Hodgson, Soils and geomorphology of the Chalk in south-east England, *Earth surface processes, 1*, 181-193, 1976.

CEH, The 2004-06 Drought (on line), *http://www. nwl. ac. uk/ih/nrfa/water_watch/dr2004_06/index. html,* 2008.

Chiang, C. L., Statistical methods of analysis, World Scientific, River Edge, N.J., 2003.

Clever, H. L., Krypton, Xenon, and Radon: Gas Solubilities. IUPAC solubility data series; vol 2., Pergamon, 1979.

Cook, P. G., A. J. Love and J. C. Dighton, Inferring ground water flow in fractured rock from dissolved radon, *Ground Water, 37*(4), 606-610, 1999.

Cothern, R. C., Properties (of radon), in Environmental Radon, vol. 25, edited by R. C. Cothern and E. S. Smith, pp. 1-27, Plenum Press, New York, 1987.

Coy, V., A study of matrix block geometry with respect to dual-porosity models and tracer test analysis, M.Sc. Thesis, University College London, 2001.

Currie, L. A., Limits for Qualitative Detection and Quantitative Determination - Application to Radiochemistry, *Analytical Chemistry, 40*(3), 586-&, 1968.

Currie, L. A., E. M. Eijgenhuijsen and G. A. Klouda, On the validity of the Poisson hypothesis for low-level counting: Investigation of the distributional characteristics of background radiation with the NIST individual pulse counting system, *Radiocarbon, 40*(1), 113-127, 1998.

Curry, D., Tertiary, in Geology of England and Wales, edited by P. M. D. Duff and A. J. Smith, pp. 389-411, The Geological Society, London, 1992.

Cuttell, J. C., J. W. Lloyd and M. Ivanovich, A Study of Uranium and Thorium Series Isotopes in Chalk Groundwaters of Lincolnshire Uk, *Journal of Hydrology, 86*(3-4), 343-365, 1986.

Demidova, M. G. and A. I. Saprykin, Determination of uranium and thorium isotope ratios by inductively coupled plasma mass spectrometry, *Journal of Analytical Chemistry, 59*(1), 45-49, 2004.

Downing, R. A., F. J. Pearson and D. B. Smith, The flow mechanism in the Chalk based on radio-isotope analyses of groundwater in the London Basin, *Journal of Hydrology, 40*(1-2), 67-83, 1979.

Downing, R. A., M. Price and G. P. Jones, The hydrogeology of the chalk of north-west Europe, Clarendon Press, Oxford, 1993.

Edmonds, C., Improved groundwater vulnerability mapping for the karstic chalk aquifer of south east England, *Engineering Geology, 99*(3-4), 95-108, 2008.

Edmunds, W. M., P. Doherty, K. J. Griffiths and P. Shand, Baseline Report Series - 4: The Chalk of Dorset, BGS Report CR/02/268N, 2002.

Efron, B. and R. J. Tibshiranu, An introduction to the bootstrap, Chapman & Hall/CRC, London, 1994.

Elliot, T., J. N. Andrews and W. M. Edmunds, Hydrochemical trends, palaeorecharge and groundwater ages in the fissured Chalk aquifer of the London and Berkshire Basins, UK, *Applied Geochemistry, 14*(3), 333-363, 1999.

EPA, Microwave assisted acid digestion of sediments, sludges and oils (on line), *http://www. epa. gov/osw/hazard/testmethods/sw846/pdfs/3051a. pdf,* 2007.

EPA, Microwave assisted acid digestion of sediments, sludges and oils (on line), *http://www. epa. gov/osw/hazard/testmethods/sw846/pdfs/3051a. pdf,* 2009.

Escobar, V. G., F. V. Tome, J. C. Lozano and A. M. Sanchez, Determination of Rn-222 and Ra-226 in aqueous samples using a low-level liquid scintillation counter, *Applied Radiation and Isotopes, 47*(9-10), 861-867, 1996.

Evans, N. J., J. P. Byrne, J. T. Keegan and L. E. Dotter, Determination of uranium and thorium in zircon, apatite, and fluorite: Application to laser (U-Th)/He thermochronology, *Journal of Analytical Chemistry, 60*(12), 1159-1165, 2005.

Faires, R. A. and G. G. J. Boswell, Radioisotope laboratory techniques, Butterworths, London, 1981.

Faure, G., Principles of isotope geology, Wiley, Ney York, 1986.

Fetter, C. W., Contaminant hydrogeology, Prentice Hall, Upper Saddle River, N.J., 1999.

Foster, S. S. D., The Chalk groundwater tritium anomaly -- A possible explanation, *Journal of Hydrology, 25*(1-2), 159-165, 1975.

Francois, C. A., Rapid Spectrophotometric Determination of Submilligram Quantities of Uranium, *Analytical Chemistry, 30*(1), 50-54, 1958.

Fretwell, B. A., W. G. Burgess, J. A. Barker and N. L. Jefferies, Redistribution of contaminants by a fluctuating water table in a micro-porous, double-porosity aquifer: Field observations and model simulations, *Journal of Contaminant Hydrology, 78*(1-2), 27-52, 2005.

Freyer, K., H. C. Treutler, J. Dehnert and W. Nestler, Sampling and measurement of radon-222 in water, *Journal of Environmental Radioactivity, 37*(3), 327-337, 1997.

Gaus, I., P. Shand, I. N. Gale, A. T. Williams and J. C. Eastwood, Geochemical modelling of fluoride concentration changes during Aquifer Storage and Recovery (ASR) in the Chalk aquifer in Wessex, England, *Quarterly Journal of Engineering Geology and Hydrogeology, 35*(2), 203-208, 2002.

Giridhar, P., K. A. Venkatesan, T. G. Srinivasan and P. R. Vasudeva Rao, Extraction of uranium(VI) from nitric acid medium by 1.1M tri-n-butylphosphate in ionic liquid diluent, *Journal of Radioanalytical and Nuclear Chemistry, 265*(1), 31-38, 2005.

Goh, T. B., D. W. Oscarson and M. Cheslock, Effect of Sorption Barriers on the Radon Fluence Rate from Soil, *Health Physics, 63*(2), 213-214, 1992.

Grapes, T. R., C. Bradley and G. E. Petts, Dynamics of river-aquifer interactions along a chalk stream: the River Lambourn, UK, *Hydrological Processes, 19*(10), 2035-2053, 2005.

Grapes, T. R., C. Bradley and G. E. Petts, Hydrodynamics of floodplain wetlands in a chalk catchment: The River Lambourn, UK, *Journal of Hydrology, 320*(3-4), 324-341, 2006.

Gresswell, R., Radon in Chalk groundwater: Development of a new methodology for determining low-level radon in water by Liquid Scintillation Counting, University College London (Unpublished MSci Thesis), 2004.

Griffiths, J., A. Binley, N. Crook, J. Nutter, A. Young and S. Fletcher, Streamflow generation in the Pang and Lambourn catchments, Berkshire, UK, *Journal of Hydrology, 330*(1-2), 71-83, 2006.

Grisak, G. E. and J. F. Pickens, Solute Transport Through Fractured Media .1. the Effect of Matrix Diffusion, *Water Resources Research, 16*(4), 719-730, 1980.

Grisak, G. E. and J. F. Pickens, An Analytical Solution for Solute Transport Through Fractured Media with Matrix Diffusion, *Journal of Hydrology, 52*(1-2), 47-57, 1981.

Gustard, A., A. Bullock and J. M. Dixon, Low flow estimation in the United Kingdom, Institute of Hydrology, 1992.

Hancock, J. M., The formation and diagenesis of chalk, in The hydrogeology of the chalk of north-west Europe, edited by R. A. Downing, M. Price and G. P. Jones, pp. 14-34, Clarendon Press, Oxford, 1993.

Hancock, J. M., The petrology of the Chalk, *Proceedings of the Geologists' Association, 86*(4), 499-535, 1975.

Headworth, H. G., S. Puri and B. H. Rampling, Contamination of a Chalk aquifer by mine drainage at Tilmanstone, East Kent, U.K, *Quarterly Journal of Engineering Geology and Hydrogeology, 13*(2), 105-117, 1980.

Henry, R., D. Koller, M. Liezers, O. T. Farmer, C. Barinaga, D. W. Koppenaal and J. Wacker, New advances in inductively coupled plasma - mass spectrometry (ICP-MS) for routine measurements in the nuclear industry, *Journal of Radioanalytical and Nuclear Chemistry, 249*(1), 103-108, 2001.

Hidaka, H., K. Horie and F. Gauthier-Lafaye, Transport and selective uptake of radium into natural clay minerals, *Earth and Planetary Science Letters, 264*(1-2), 167-176, 2007.

Hoehn, E. and H. R. Von Gunten, Radon in Groundwater: A Tool to Assess Infiltration From Surface Waters to Aquifers, *Water Resour. Res., 25*, 1989.

Hough, M. N. and R. J. A. Jones, The United Kingdom Meteorological Office rainfall and evaporation calculation system: MORECS version 2.0-an overview, *Hydrol. Earth Syst. Sci., 1*(2), 227-239, 1999.

Hubert, A., B. Bourdon, E. Pili and L. Meynadier, Transport of radionuclides in an unconfined chalk aquifer inferred from U-series disequilibria, *Geochimica et Cosmochimica Acta, 70*(22), 5437-5454, 2006.

Ivanovich, M. and R. S. Harmon, Uranium-series disequilibrium applications to earth, marine, and environmental sciences, Clarendon Press ; Oxford University Press, Oxford, 1992.

Ivanovich, M. and D. B. Smith, Determination of aquifer parameters by a two-well pulsed method using radioactive tracers, *Journal of Hydrology, 36*(1-2), 35-45, 1978.

Jackson, C. B., Report on the Validation of Proposed EPA Method 360.3 (Luminescence) for the Measurement of Dissolved Oxygen in Water and Wastewater, Hach Company, Laboratory Sciences Business Unit, 2004.

Jarvis, I., Geochemistry of Phosphatic Chalks and Hardgrounds from the Santonian to Early Campanian (Cretaceous) of Northern France, *Journal of the Geological Society, 137*(NOV), 705-721, 1980.

Jarvis, I., Sedimentology, Geochemistry and Origin of Phosphatic Chalks - the Upper Cretaceous Deposits of Nw Europe, *Sedimentology, 39*(1), 55-97, 1992.

Kachi, S., Tracer studies in the Chalk aquifer near Cambridge, MPhil Thesis, University of East Anglia, 1987.

Kaminski, R., F. J. Purcell and E. Russavage, Uranyl Phosphorescence at the Parts-Per-Trillion Level, *Analytical Chemistry, 53*(7), 1093-1096, 1981.

Khan, M. H., A. Ali and N. N. Khan, Spectrophotometric determination of thorium with disodium salt of Arsenazo-III in perchloric acid, *Journal of Radioanalytical and Nuclear Chemistry, 250*(2), 353-357, 2001.

Khorfan, S., Y. Koudsi and W. Rafool, The influence of cations in phosphoric acid on the extraction of uranium, *Journal of Radioanalytical and Nuclear Chemistry, 250*(1), 147-152, 2001.

Kigoshi, K., Alpha-Recoil Thorium-234: Dissolution into Water and the Uranium-234/Uranium-238 Disequilibrium in Nature, *Science, 173*(3991), 47-48, 1971.

King, P. T., J. Michel and W. S. Moore, Groundwater Geochemistry of Ra-228, Ra-226 and Rn-222, *Geochimica et Cosmochimica Acta, 46*(7), 1173-1182, 1982.

Komarneni, S., N. Kozai and W. J. Paulus, Environment: Superselective clay for radium uptake, *Nature, 410*(6830), 771, 2001.

Krishnaswami, S., W. C. Graustein, K. K. Turekian and J. F. Dowd, Radium, Thorium and Radioactive Lead Isotopes in Groundwaters - Application to the Insitu Determination of Adsorption- Desorption Rate Constants and Retardation Factors, *Water Resources Research, 18*(6), 1663-1675, 1982.

Krishnaswami, S. and D. E. Seidemann, Comparative-Study of Rn-222, Ar-40, Ar-39 and Ar-37 Leakage from Rocks and Minerals - Implications for the Role of Nanopores in Gas-Transport Through Natural Silicates, *Geochimica et Cosmochimica Acta, 52*(3), 655-658, 1988.

L'Annunziata, M. F. and M. J. Kessler, Liquid Scintillation Analysis: Principles and Practice, in Handbook of Radioactivity Analysis: Second Edition, edited by M. F. L'Annunziata, M. M. El Baradei and W. Burkart, pp. 347-537, Academic Press, 2003.

Lakowicz, J. R., Principles of fluorescence spectroscopy, Kluwer Academic/Plenum, New York, 1999.

Liu, H. H., G. S. Bodvarsson and G. Zhang, Scale Dependency of the Effective Matrix Diffusion Coefficient, *Vadose Zone J, 3*(1), 312-315, 2004.

Liu, H. H., Y. Q. Zhang, Q. Zhou and F. J. Molz, An interpretation of potential scale dependence of the effective matrix diffusion coefficient, *Journal of Contaminant Hydrology, 90*(1-2), 41-57, 2007.

Low, R., Radon as a natural groundwater tracer in the chalk aquifer, UK, *Environment International, 22*, S333-S338, 1996a.

Low, R., Radon in the groundwater in the Chalk of East Anglia, Ph.D. Thesis, University of East Anglia, 1996b.

MacDonald, A. M. and D. J. Allen, Aquifer properties of the Chalk of England, *Quarterly Journal of Engineering Geology and Hydrogeology, 34*, 371-384, 2001.

Maloszewski, P. and A. Zuber, On the Theory of Tracer Experiments in Fissured Rocks with A Porous Matrix, *Journal of Hydrology, 79*(3-4), 333-358, 1985.

Maloszewski, P. and A. Zuber, Tracer Experiments in Fractured Rocks - Matrix Diffusion and the Validity of Models, *Water Resources Research, 29*(8), 2723-2735, 1993.

Marcos, N., J. Suksi, H. Ervanne and K. Rasilainen, Fracture smectite as a long-term sink for natural radionuclides - indications from unusual U-series disequilibria, *Radiochimica Acta, 88*(9-11), 763-766, 2000.

Mathias, S. A., A. P. Butler, T. C. Atkinson, S. Kachi and R. S. Ward, A parameter identifiability study of two chalk tracer tests, *Hydrol. Earth Syst. Sci. Discuss., 3*(4), 2437-2471, 2006a.

Mathias, S. A., A. P. Butler, T. C. Atkinson, S. Kachi and R. S. Ward, A parameter sensitivity analysis of two Chalk tracer tests, *Quarterly Journal of Engineering Geology and Hydrogeology, 42*, 237-244, 2009.

Mathias, S. A., A. P. Butler, A. M. Ireson, B. M. Jackson, N. McIntyre and H. S. Wheater, Recent advances in modelling nitrate transport in the Chalk unsaturated zone, *Quarterly Journal of Engineering Geology and Hydrogeology, 40*(4), 353-359, 2007a.

Mathias, S. A., A. P. Butler, B. M. Jackson and H. S. Wheater, Transient simulations of flow and transport in the Chalk unsaturated zone, *Journal of Hydrology, 330*(1-2), 10-28, 2006b.

Mathias, S. A., A. P. Butler, D. W. Peach and A. T. Williams, Recovering tracer test input functions from fluid electrical conductivity logging in fractured porous rocks, *Water Resources Research, 43*(7), 2007b.

Maurice, L. D., Investigations of rapid groundwater flow and karst in the Chalk, Unpublished PhD Thesis, PhD University College London, London, 2008.

Maurice, L. D., T. C. Atkinson, J. A. Barker, J. P. Bloomfield, A. R. Farrant and A. T. Williams, Karstic behaviour of groundwater in the English Chalk, *Journal of Hydrology, 330*(1-2), 63-70, 2006.

McDowell, P. W., J. Coulton, C. N. Edmonds and A. J. Poulsom, The nature, formation and engineering significance of sinkholes related to dissolution of chalk in SE Hampshire, England, *Quarterly Journal of Engineering Geology and Hydrogeology, 41*(3), 279-290, 2008.

Meinrath, G., Uranium(VI) speciation by spectroscopy, *Journal of Radioanalytical and Nuclear Chemistry, 224*(1-2), 119-126, 1997.

Meinrath, G., P. Volke, C. Helling, E. G. Dudel and B. J. Merkel, Determination and interpretation of environmental water samples contaminated by uranium mining activities, *Fresenius Journal of Analytical Chemistry, 364*(3), 191-202, 1999.

Moench, A. F., Convergent Radial Dispersion in A Double-Porosity Aquifer with Fracture Skin - Analytical Solution and Application to A Field Experiment in Fractured Chalk, *Water Resources Research, 31*(8), 1823-1835, 1995.

Morgan Jones, M., Mineralogy of the non-carbonate material from the Chalk of Berkshire and Oxfordshire, England, *Clay Minerals, 12*(4), 331-344, 1977.

Mortimore, R. N., Chalk: A stratigraphy for all seasons (annual conference of the Ussher Society), Proceedings of Geoscience in south-west England, 2001.

Mortimore, R. N., C. J. Wood and R. W. Gallois, Transitional Province, England, in British Upper Cretaceous Stratigraphy, edited by R. N. Mortimore, C. J. Wood and R. W. Gallois, Joint Nature Conservation Committee, Peterborough, 2001.

Mullinger, N. J., A. M. Binley, J. M. Pates and N. P. Crook, Radon in Chalk streams: Spatial and temporal variation of groundwater sources in the Pang and Lambourn catchments, UK, *Journal of Hydrology, 339*(3-4), 172-182, 2007.

Murphy, A. M., Sediment and groundwater geochemistry of the Chalk in southern England, Ph.D. Thesis, University of London, 1998.

Neal, C., H. P. Jarvie, A. J. Wade, M. Neal, R. Wyatt, H. Wickham, L. Hill and N. Hewitt, The water quality of the LOCAR Pang and Lambourn catchments, *Hydrology and Earth System Sciences, 8*(4), 614-635, 2004.

Nichols, E. L. and H. L. Howes, On the phosphorescence of the uranyl salts, *Phys. Rev., 9*(4), 292-304, 1917.

Owen, M., Thames groundwater scheme, in Case-studies in groundwater resources evaluation, edited by J. W. Lloyd, pp. 186-202, Clarendon Press, Oxford, 1981.

Pacey, N. R., Bentonites in the Chalk of central eastern England and their relation to the opening of the Northeast Atlantic, *Earth and Planetary Science Letters, 67*(1), 48-60, 1984a.

Pacey, N. R., Some aspects of the natural radioactivity of the English Chalk, *Modern Geology, 8*, 199-206, 1984b.

Pacey, N. R., The Mineralogy, Geochemistry and Origin of Pelletal Phosphates in the English Chalk, *Chemical Geology, 48*(1-4), 243-256, 1985.

Panczer, G., M. Gaft, R. Reisfeld, S. Shoval, G. Boulon and B. Champagnon, Luminescence of uranium in natural apatites, *Journal of Alloys and Compounds, 277*, 269-272, 1998.

Passo, C. J. and G. T. Cook, Handbook of Environmental Liquid Scintillation Spectrometry - A Compilation of Theory and Methods, Packard Instrument Company, Meriden, CT, USA, 1994.

Pates, J., G. Cook, A. Mackenzie and J. Thomson, The development of an alpha/beta separation liquid scintillation cocktail for aqueous samples, *Journal of Radioanalytical and Nuclear Chemistry, 172*(2), 341-348, 1993.

Pates, J. M. and N. J. Mullinger, Determination of 222Rn in fresh water: Development of a robust method of analysis by [alpha]/[beta] separation liquid scintillation spectrometry, *Applied Radiation and Isotopes, 65*(1), 92-103, 2007.

Peedell, S., Investigation of the mine water pollution plume at Tilmanstone, East Kent., MSc thesis, University College London, UK, 1994.

Peters, E. and H. A. J. van Lanen, Separation of base flow from streamflow using groundwater levels - illustrated for the Pang catchment (UK), *Hydrological Processes, 19*(4), 921-936, 2005.

Price, M. and D. Banks, The Chalk as a karstic aquifer: Evidence from a tracer test at Stanford Dingley - Discussion, *Quarterly Journal of Engineering Geology, 29*, 257-258, 1996.

Price, M., R. A. Downing and W. M. Edmunds, The Chalk as an aquifer, in The hydrogeology of the chalk of north-west Europe, edited by R. A. Downing, M. Price and G. P. Jones, pp. 35-58, Clarendon Press, Oxford, 1993.

Price, M., R. G. Low and C. McCann, Mechanisms of water storage and flow in the unsaturated zone of the Chalk aquifer, *Journal of Hydrology, 233*(1-4), 54-71, 2000.

Price, M., B. Morris and A. Robertson, A study of intergranular and fissure permeability in Chalk and Permian aquifers, using double-packer injection testing, *Journal of Hydrology, 54*(4), 401-423, 1982.

Price, M., Fluid flow in the Chalk of England, *Geological Society, London, Special Publications, 34*(1), 141-156, 1987.

Prichard, H. M. and T. F. Gesell, Rapid Measurements of Rn-222 Concentrations in Water with A Commercial Liquid Scintillation-Counter, *Health Physics, 33*(6), 577-581, 1977.

Prichard, H. M., E. A. Venso and C. L. Dodson, Liquid-Scintillation Analysis of Rn-222 in Water by Alpha-Beta Discrimination, *Radioactivity & Radiochemistry, 3*(1), 28-36, 1992.

Rama and W. S. Moore, Mechanism of transport of U-Th series radioisotopes from solids into ground water, *Geochimica et Cosmochimica Acta, 48*(2), 395-399, 1984.

Rasmussen, N. C., Nuclear Wastes: Technologies for Separations and Transmutations., National Academy Press, 1996.

Rawson, P. F., The Cretaceous, in Geology of England and Wales, edited by P. M. D. Duff and A. J. Smith, pp. 355-388, The Geological Society, London, 1992.

Rawson, P. F., D. J. Allen and A. S. Gale, The Chalk Group - a revised lithostratigraphy, *Geoscientist,*(11), 21, 2001.

Reynolds, G. T., F. B. Harrison and G. Salvini, Liquid Scintillation Counters, *Phys. Rev., 78*(4), 488, 1950.

Rivett, M. O., J. W. N. Smith, S. R. Buss and P. Morgan, Nitrate occurrence and attenuation in the major aquifers of England and Wales, *Quarterly Journal of Engineering Geology and Hydrogeology, 40*(4), 335-352, 2007.

Rushton, K. R., B. J. Connorton and L. M. Tomlinson, Estimation of the groundwater resources of the Berkshire Downs supoported by mathematical modelling, *Quarterly Journal of Engineering Geology and Hydrogeology, 22*, 329-341, 1989.

Sasaki, T., Y. Gunji and T. Okuda, Radon emanation dependence on grain configuration, *Journal of Nuclear Science and Technology, 41*(10), 993-1002, 2004.

Sasaki, T., Y. Gunji and T. Okuda, Theoretical study of high radon emanation, *Journal of Nuclear Science and Technology, 42*(2), 242-249, 2005.

Schubert, M., K. Lehmann and A. Paschke, Determination of radon partition coefficients between water and organic liquids and their utilization for the assessment of subsurface NAPL contamination, *Science of The Total Environment, 376*(1-3), 306-316, 2007.

Semkow, T. M., Recoil-Emanation Theory Applied to Radon Release from Mineral Grains, *Geochimica et Cosmochimica Acta, 54*(2), 425-440, 1990.

Sill, C. W. and H. E. Peterson, Fluorescence Test for Uranium in Aqueous Solution, *Analytical Chemistry, 19*(9), 646-651, 1947.

Skoog, D. A., D. M. West and F. J. Holler, Analytical Chemistry, Saunders College Publishing, 1994.

Skoog, D. A., Fundamentals of analytical chemistry, Brooks/Cole, Pacific Grove, Calif., 2004.

Spink, T. W., The CIRIA Chalk description and classification scheme, *Quarterly Journal of Engineering Geology and Hydrogeology, 35*(4), 363-369, 2002.

Stein, L., The Chemistry of Radon, *Radiochimica Acta, 32*(1-3), 163-171, 1983.

Stein, L., New Evidence That Radon Is A Metalloid Element - Ion-Exchange Reactions of Cationic Radon, *Journal of the Chemical Society-Chemical Communications,*(22), 1631-1632, 1985.

Stuart, M. E., P. J. Chilton, D. G. Kinniburgh and D. M. Cooper, Screening for long-term trends in groundwater nitrate monitoring data, *Quarterly Journal of Engineering Geology and Hydrogeology, 40*(4), 361-376, 2007.

Suksi, J., K. Rasilainen and P. Pitkanen, Variations in 234U/238U activity ratios in groundwater--A key to flow system characterisation?, *Physics and Chemistry of the Earth, Parts A/B/C, 31*(10-14), 556-571, 2006.

Taylor, J. K., Quality assurance of chemical measurements, Lewis Publishers (Chelsea, Mich.), 1987.

Tessier, A., P. G. C. Campbell and M. Bisson, Sequential Extraction Procedure for the Speciaiton of Particulate Trace Metals, *Analytical Chemistry, 51*(7), 844-851, 1979.

Theodorsson, P., A new method for automatic measurement of low-level radon in water, *Applied Radiation and Isotopes, 47*(9-10), 855-859, 1996.

Thomson, J., Di-isopropylnaphthalene - a new solvent for liquid scintillation counting, in Liquid Scintillation Counting and Organic Scintillators, edited by H. Ross, J. E. Noakes and J. D. Spaulding, pp. 19-34, CRC Press, Oak Ridge National Laboratory, University of Georgia, 1991.

Trenn, T. J., The self-splitting atom the history of the Rutherford-Soddy collaboration, Taylor and Francis, London, 1977.

Turner, J. E., Statistics, in Atoms, Radiation and Radiation Protection, pp. 289-347, J Wiley & Sons, Inc, New York ; Chichester, 1995.

Veselsky, J. C., B. Kwiecinska, E. Wehrstein and O. Suschny, Determination of Uranium in Minerals by Laser Fluorimetry, *Analyst, 113*(3), 451-455, 1988.

Wanty, R., E. P. Lawrence and L. C. S. Gundersen, A theorertical model for the flux of radon from rock to groundwater, in Geologic controls on radon, edited by A. E. Gates and L. C. S. Gundersen, pp. 73-78, The Geological Society of America, Colorado, 1992.

Ward, R. S., Artificial tracer and natural ^{222}Rn studies of the East Anglian Chalk aquifer., Ph.D. Thesis, University of East Anglia, 1989.

Watson, S., W. Burgess, J. Barker, J. Carneiro and S. Hazell, Measurements and models of solute behaviour in the dual-porosity Chalk aquifer of the UK: the applicability of tracer tests, *Tracers and Modelling in Hydrogeology,*(262), 347-352, 2000.

Wheater, H. S., C. Neal and D. Peach, Hydro-ecological functioning of the Pang and Lambourn catchments, UK: An introduction to the special issue, *Journal of Hydrology, 330*(1-2), 1-9, 2006.

Wheater, H. S., D. Peach and A. Binley, Characterising groundwater-dominated lowland catchments: the UK Lowland Catchment Research Programme (LOCAR), *Hydrology and Earth System Sciences, 11*(1), 108-124, 2007.

Williams, A., J. Bloomfield, K. Griffiths and A. Butler, Characterising the vertical variations in hydraulic conductivity within the Chalk aquifer, *Journal of Hydrology, 330*(1-2), 53-62, 2006.

Williams, A. and M. Price, Using a double-packer system to determine hydraulic conductivity and water quality in the alluvium of the Indus Valley, Pakistan, British Geological Survey, 1988.

Williams, A. T. R. and J. N. Miller, The Determination of Uranium in Aqueous Samples by Means of A Pulsed-Source Fluorescence Spectrometer, *Analytica Chimica Acta, 154*(NOV), 341-345, 1983.

Wong, C. S., Y. P. Chin and P. M. Gschwend, Sorption of Rn-222 to Natural Sediments, *Geochimica et Cosmochimica Acta, 56*(11), 3923-3932, 1992.

Wood, W. K., T. F. Kraemer and A. Shapiro, Radon (Rn-222) in ground water of fractured rocks: A diffusion/ion exchange model, *Ground Water, 42*(4), 552-567, 2004.

Woods, M. A., UK Chalk Group stratigraphy (Cenomanian-Santonian) determined from borehole geophysical logs, *Quarterly Journal of Engineering Geology and Hydrogeology, 39*, 83-96, 2006.

Woods, M. A. and D. T. Aldiss, The stratigraphy of the Chalk Group of the Berkshire Downs, *Proceedings of the Geologists Association, 115*, 249-265, 2004.

Wright, T. E. J. and J. A. Barker, Calibration of a doub;e-porosity solute transport model using short and long term tracer tests, in New Approaches Characterizing Groundwater Flow, vol. 1 and 2, edited by K. P. Seiler and S. Wohnlich, pp. 683-688, 2001.

Younger, P. L., Devensian periglacial influences on the development of spatially variable permeability in the Chalk of southeast England, *Quarterly Journal of Engineering Geology and Hydrogeology, 22*(4), 343-354, 1989.

Younger, P. L. and T. Elliot, Chalk fracture system characteristics: implications for flow and solute transport, *Quarterly Journal of Engineering Geology and Hydrogeology, 28*, S39-S50, 1995.

Younger, P. L. and T. Elliot, Chalk fracture system characteristics: Implications for flow and solute transport - Reply, *Quarterly Journal of Engineering Geology, 29*, 94-96, 1996.

Zereshki, A., The solution of 222-Rn by groundwaters, Ph.D. Thesis, University of Bath, 1981.

Zhang, Y. Q., H. H. Liu, Q. L. Zhou and S. Finsterle, Effects of diffusive property heterogeneity on effective matrix diffusion coefficient for fractured rock, *Water Resources Research, 42*(4), 2006.

Zhou, Q. L., H. H. Liu, F. J. Molz, Y. Q. Zhang and G. S. Bodvarsson, Field-scale effective matrix diffusion coefficient for fractured rock: Results from literature survey, *Journal of Contaminant Hydrology, 93*(1-4), 161-187, 2007.

Zimmerman, R. W., D. W. Chen and N. G. W. Cook, The effect of contact area on the permeability of fractures, *Journal of Hydrology, 139*(1-4), 79-96, 1992.

Appendix A | Uranium Assay Results

Table A1 – Trumpletts Farm U assay (1m core samples)

							Sub Classification			
Sample Ref	**Depth (mbgl)**	**Result (mg.kg^{-1})**	**Error (+/-)**	**Notebook comments (at time of sampling)**	**Lab Ref (Analysis)**	**Lab comments (during prep)**	**Insoluble Fraction**	**Block Surface**	**Solid Block**	**Marl**	**Staining**
TF1	4.40	0.264 0.265	0.014 0.010	disturbed block from top barrel(?)	TF060321-A TF060321-A2	single lump	1.1% 1.6%				
TF2	5.30	0.444	0.008	block in broken chalk	TF060321-B	single lump	1.0%		✓		
TF3	6.50	0.423	0.007	block in broken chalk	TF060321-C	lump split into two	1.3%		✓		
TF4	7.75	0.413	0.010	block from within densely fractured run, below flint	TF060321-D	cut section	0.9%		✓		
TF5	9.88	0.480 0.580	0.006 0.009	block from within densely fractured run, below flinty zone	TF060321-E TF060321-E2	includes iron nodule/staining	1.1% 1.1%		✓		✓
TF6	10.36	0.387	0.012	block from within densely fractured run	TF060321-F	from centre of block, surface scraped	1.1%		✓		
TF7	12.20	0.189	0.04	block from within densely fractured run	TF060321-G	surface scraped	0.6%		✓		
TF8	13.00	0.234	0.006	block at top of densely fractured zone	TF060321-H	surface scraped	1.0%		✓		
TF9	14.93	0.298	0.007	from Fe stained inclined fracture	TF060321-I2	two blocks	1.2%	✓			✓
TF10	15.60	0.192	0.005	block from blocky fractured chalk, representative of block	TF060321-J	surface scraped	1.7%	✓			
TF11	16.20	0.206	0.005	block from blocky fractured chalk, below flints, with brown surface coatings	TF060321-K	from centre of block, orientation unknown	0.9%		✓		✓

Table A1 – Trumpletts Farm U assay (1m core samples)

								Sub Classification		
Sample Ref	**Depth (mbgl)**	**Result (mg.kg^{-1})**	**Error (+/-)**	**Notebook comments (at time of sampling)**	**Lab Ref (Analysis)**	**Lab comments (during prep)**	**Insoluble Fraction**	**Block Surface**	**Solid Block**	**Marl**	**Staining**
TF12	17.36	0.149	0.007	adj. brown clayey (?phosphatic) lens in lightly fractured blocky Chalk	TF060321-L	block - surface scraped	2.1%	✓		✓	
TF13	20.60	0.229 0.234	0.007 0.004	block from blocky & fractured zone with brown surface coating & brown clay (?phosphatic) spalls(?)	TF060321-M TF060321-M2	no comment	1.7% 1.8%			✓	✓
TF14	23.00	0.525	0.007	block from Fe-stained surfaces from fractured blocky zone & flints	TF060321-N	from centre of block	1.0%		✓		✓
TF15	24.05	0.203	0.004	block from within fractured/blocky chalk at 0.10m flint zone	TF060321-O	surface scraped	1.1%	✓			
TF16	26.48	0.170	0.005	from within fractured/flinty zone	TF060321-P	cut from end of block, surface scraped	2.1%	✓			
TF17	27.24	0.205 0.218	0.005 0.004	block with marly fracture at & Fe nodule within	TF060321-Q TF060321-Q2	from centre of block	2.4% 2.5%		✓	✓	✓
TF18	29.43	0.213	0.002	at base of competent blocky ending in fracture	TF060321-R	including marly bands	1.4%	✓		✓	
TF19	30.15	0.203	0.006	block from fractured block zone	TF060321-S	from block	3.2%		✓		
TF20	31.30	0.217	0.007	adj. fractured marly chalk	TF060321-T	including marly bands	6.0%	✓		✓	

Table A1 – Trumpletts Farm U assay (1m core samples)

								Sub Classification		
Sample Ref	**Depth (mbgl)**	**Result (mg.kg^{-1})**	**Error (+/-)**	**Notebook comments (at time of sampling)**	**Lab Ref (Analysis)**	**Lab comments (during prep)**	**Insoluble Fraction**	**Block Surface**	**Solid Block**	**Marl**	**Staining**
TF21	31.87	0.360 0.332	0.005 0.005	marly chalk	TF060619-A TF060619-A2	fresh surface marly band	1.8% 1.9%	✓		✓	
TF22	33.60	0.180	0.003	piece from fractured blocky chalk	TF060619-B	fresh surface	1.8%				
TF23	*34.40*	*See Table A2*	*See Table A2*	*from marl-lined fracture at top to top surface of fracture ~= water loss zone through competent chalk*	*Additional detailed analysis of this section*	*no comment at this stage – See Table A2*	-	✓		✓	
TF24	34.53	0.189	0.005	below(?) water loss horizon of IC (incompetent chalk?)	TF060619-C	from fracture surface (0.5 cm thickness)	1.9%	✓			
TF25	35.48	0.219	0.007	marly block & Fe staining	TF060619-D	no comment	1.6%			✓	✓
TF26	36.50	0.257 0.257	0.007 0.008	below break (in competent chalk)	TF060619-E TF060619-E2	from fracture surface	1.5% 1.9%	✓			
TF27	37.00	0.259	0.006	clean milky white competent chalk	TF060619-F	solid matrix core	1.9%		✓		
TF28	37.58	0.226	0.005	from fracture through marl(?) above & into competent chalk	TF060619-G	from marl section	1.7%		✓	✓	
TF29	38.34	0.187	0.005	above blocky fractured zone	TF060619-H	from fracture surface	1.7%	✓			
TF30	39.33	0.192 0.232	0.002 0.004	block bordered by fractures above and marl lined fracture below	TF060619-I TF060619-I2	marly section	1.6% 1.7%		✓	✓	

Table A1 – Trumpletts Farm U assay (1m core samples)

								Sub Classification		
Sample Ref	**Depth (mbgl)**	**Result (mg.kg^{-1})**	**Error (+/-)**	**Notebook comments (at time of sampling)**	**Lab Ref (Analysis)**	**Lab comments (during prep)**	**Insoluble Fraction**	**Block Surface**	**Solid Block**	**Marl**	**Staining**
TF31	40.15	0.274	0.006	competent chalk below flint break and above blocky zone	TF060619-J	no comment	1.6%		✓		
TF32	41.43	0.275	0.005	competent chalk below broken & flints horizon (0.20m)	TF060619-K	matrix - not fracture	1.6%		✓		
TF33	42.50	0.347	0.005	competent chalk to broken flint horizon below (0.08m)	TF060619-L	matrix - not fracture	1.7%		✓		
TF34	43.70	0.257 0.272	0.009 0.006	competent chalk to ?(clean) break at top	TF060619-M TF060619-M2	matrix - not fracture	1.8% 1.7%		✓		
TF35	44.35	0.323	0.006	competent chalk with ? marl-lined fracture at base	TF060619-N	matrix with marl bands	1.7%		✓	✓	
TF36	45.26	0.317	0.005	competent chalk to shelly face on fracture surface at base	TF060619-O	fracture surface	1.7%	✓			
TF37	46.53	0.220	0.006	wispy marl in competent chalk	TF060619-P	marl bands with iron nodule	1.7%		✓	✓	✓
TF38	47.96	0.229 0.229	0.004 0.005	competent block above broken zone	TF060619-Q TF060619-Q2	matrix next to fracture fresh surface	1.7% 1.7%	✓			
TF39	48.45	0.509	0.017	fractured marl into competent chalk below	TF060619-R	dark marl layer	1.7%		✓	✓	
TF40	49.35	0.236	0.005	competent chalk adjacent flint	TF060619-S	chalk matrix no fracture	1.5%		✓		

Table A1 – Trumpletts Farm U assay (1m core samples)

								Sub Classification		
Sample Ref	**Depth (mbgl)**	**Result (mg.kg^{-1})**	**Error (+/-)**	**Notebook comments (at time of sampling)**	**Lab Ref (Analysis)**	**Lab comments (during prep)**	**Insoluble Fraction**	**Block Surface**	**Solid Block**	**Marl**	**Staining**
TF41	50.70	0.329	0.003	from fracture at brecciated zone up into competent chalk	TF060619-T	chalk matrix	1.9%		✓		
TF42	51.15	0.275	0.007	fracture surface below broken & flint zone into competent chalk	TF060619-U	chalk with iron staining	1.5%	✓			✓
TF43	52.24	0.237	0.005	fracture up into competent chalk	TF060619-V	fracture surface	1.7%	✓			
TF44	53.28	0.276	0.008	marl & fracture up into competent chalk	TF060619-W	marl bands	4.3%	✓		✓	
TF45	54.60	0.364	0.009	block between fracture surfaces	TF060619-X	chalk matrix	2.7%		✓		
TF46	55.75	0.403 0.383	0.006 0.007	brecciated piece adj. sub vertical fracture & flint zone	TF060619-Y TF060619-Y2	crushed chalk matrix flint	2.2% 2.4%		✓		
TF47	56.75	0.392	0.006	block with marl bands between fracture surfaces	TF060619-Z	marl bands	3.0%		✓	✓	
TF48	57.22	0.325	0.008	fracture surface to competent chalk	TF060619-AA	marl bands	3.9%	✓		✓	
TF49	58.50	0.298 0.305	0.011 0.007	fracture below flint zone down into competent chalk	TF060619-AB TF060619-AB2	fracture side	1.8% 1.8%	✓			
TF50	59.72	0.349	0.005	marl bands up into fracture	TF060814-A	fracture surface and internal marl bands	1.8%	✓		✓	
TF51	60.56	0.218	0.005	from fracture up into competent chalk	TF060814-B	solid core	0.9%		✓		
TF52	61.45	0.276	0.008	pure milky white competent chalk	TF060814-C	solid core	1.5%		✓		

Table A1 – Trumpletts Farm U assay (1m core samples)

								Sub Classification		
Sample Ref	**Depth (mbgl)**	**Result (mg.kg^{-1})**	**Error (+/-)**	**Notebook comments (at time of sampling)**	**Lab Ref (Analysis)**	**Lab comments (during prep)**	**Insoluble Fraction**	**Block Surface**	**Solid Block**	**Marl**	**Staining**
TF53	61.65	0.198	0.005	horizontal fracture & clay	TF060814-D	solid core	1.3%		✓	✓	
TF54	62.70	0.294	0.006	orange staining	TF060814-E	solid core	1.2%		✓		✓
		0.291	0.008		TF060814-E2		1.2%				
TF55	63.60	0.328	0.009	from flint band surface upwards into competent chalk	TF060814-F	solid core	1.4%		✓		
TF56	64.65	0.457	0.012	through fracture (?intersect) ?Mn staining	TF060814-G	heavily stained fracture	3.1%	✓			✓
TF57	65.40	0.216	0.006	dark marl bands	TF060814-H	solid core	2.9%		✓	✓	
TF58	65.68	0.231	0.004	sub-v fracture with mineralization and clays	TF060814-I	broken up pieces of chalk	2.2%	✓		✓	
TF59	66.48	0.420	0.009	marl bands & fracture surface	TF060814-J	solid core	1.4%	✓		✓	
TF60	67.43	0.292	0.005	fracture surface up into marl bands	TF060814-K	chalk lump	1.4%	✓		✓	
TF61	67.70	0.019	0.001	brecciated pieces & flint fragments	TF060814-L	chalk lump	1.3%				
TF62	68.33	0.216	0.004	from fracture (?Mn mineralization) upwards into competent chalk	TF060814-M	solid core	1.1%		✓		
TF63	69.53	0.288	0.006	from fracture upwards through marls	TF060814-N	marly fracture with shells	1.0%	✓		✓	
TF64	70.56	0.391	0.009	from fracture upwards	TF060814-O	solid core	1.8%	✓			
TF65	71.60	0.388	0.007	below (different) brecciated section	TF060814-P	solid core	1.2%		✓		

Table A1 – Trumpletts Farm U assay (1m core samples)

								Sub Classification		
Sample Ref	**Depth (mbgl)**	**Result (mg.kg^{-1})**	**Error (+/-)**	**Notebook comments (at time of sampling)**	**Lab Ref (Analysis)**	**Lab comments (during prep)**	**Insoluble Fraction**	**Block Surface**	**Solid Block**	**Marl**	**Staining**
TF66	72.75	0.425 0.436	0.010 0.008	above brecciated section	TF060814-Q TF060814-Q2	solid core fracture surface	1.8% 1.7%	✓			
TF67	73.68	0.496	0.009	small block within clays & flint nodules	TF060814-R	fragments	1.4%			✓	
TF68	74.25	0.324	0.004	horizontal fracture	TF060814-S	solid core and fracture	2.1%				
TF69	75.52	0.939	0.017	block with Fe staining	TF060814-T	brown staining flaky chalk	1.1%		✓		✓
TF70	76.24	0.400	0.011	sub-vertical fracture	TF060814-U	solid core & fracture surface	2.4%				
TF71	77.48	0.329	0.005	horizontal fracture with marl bands	TF060907-A	solid core marly bands	3.2%	✓		✓	
TF72	78.55	0.520	0.008	top of block to include marl band	TF060907-B	solid core marly bands	2.0%	✓		✓	
TF73	79.50	0.303 0.380	0.007 0.007	block above flowing horizon	TF060907-C TF060907-C2	solid core marly bands	2.1% 2.3%	✓		✓	
TF74	80.96	2.859 3.120 3.399 2.605	0.022 0.035 0.029 0.019	nodular chalk & glauconite	TF060907-D TF060907-D_rpt TF060907-D1 TF060907-D2	solid core with iron staining nodules	1.7% 1.7% 1.8% 1.8%		✓		✓

Table A1 – Trumpletts Farm U assay (1m core samples)

								Sub Classification		
Sample Ref	**Depth (mbgl)**	**Result (mg.kg^{-1})**	**Error (+/-)**	**Notebook comments (at time of sampling)**	**Lab Ref (Analysis)**	**Lab comments (during prep)**	**Insoluble Fraction**	**Block Surface**	**Solid Block**	**Marl**	**Staining**
TF75	81.30	2.125	0.022	whole block (81.30-81.40)	TF060907-E	very well cemented	2.3%		✓		
		1.792	0.021		TF060907-E2	top 2cm	2.2%				
		2.674	0.033		TF060907-E_rpt		2.2%				
TF76	82.67	0.670	0.015	marl/chalk sequence next to	TF060907-F	solid block but v	8.7%			✓	
		0.819	0.012	fracture	TF060907-F-rpt	marly easy to cut	9.3%				
TF77	83.40	0.926	0.017	top of block, orange staining with mineralization	TF060907-G	solid block	2.8%		✓		
TF78	84.40	0.461	0.006	bottom of section, Fe staining	TF060907-H	iron staining	3.9%				✓
TF79	85.70	0.304	0.009	competent chalk with wispy marls	TF060907-I	solid block	3.8%		✓	✓	
		0.118	0.002	(bioturbated?)	TF060907-I2		4.0%				
TF80	86.30	0.683	0.008	in bioturbated marly chalk zone	TF060907-J1	solid block very	23.8%		✓	✓	
		0.674	0.006		TF060907-J2	marly	23.5%				
TF81	87.75	0.242	0.007	in competent chalk run below	TF060907-K	solid chalk	9.7%		✓		
		0.232	0.006	fracture (no staining)	TF060907-K1		9.9%				
		0.212	0.005		TF060907-K2		10.0%				
TF82	88.88	0.701	0.014	marl above fracture in bioturbated	TF060907-L	solid chalk with marl	17.3%		✓	✓	
		0.815	0.020	run	TF060907-L_rpt	easily fractured surface	17.8%				
TF83	89.28	0.338	0.005	around inclined fracture in marly chalk	TF060907-M1	solid chalk	6.8%		✓	✓	
TF84	90.62	0.258	0.008	at and below fractured marl band	TF060907-N	solid chalk	9.4%		✓	✓	

Table A1 – Trumpletts Farm U assay (1m core samples)

								Sub Classification		
Sample Ref	**Depth (mbgl)**	**Result ($mg.kg^{-1}$)**	**Error (+/-)**	**Notebook comments (at time of sampling)**	**Lab Ref (Analysis)**	**Lab comments (during prep)**	**Insoluble Fraction**	**Block Surface**	**Solid Block**	**Marl**	**Staining**
TF85	91.67	0.326	0.007	at and below fractured marl band	TF060907-O1	fracture	9.5%	✓		✓	
		0.329	0.010		TF060907-O2		9.4%				
TF86	91.67	0.201	0.003	at and below fractured marl band	TF060907-P	inner surface	3.7%	✓		✓	

Source: d:\simon\project\data\uranium\ls55\u_chalk\trumpfarma\[uchalkresults_trumpfarm_all_v2.xlsm]1m_interval_summary

Table A2 – Trumpletts Farm U assay (Detailed core sections)

Sample Ref	Sampling depth from top fracture (cm)	Chalk conc. ($mg.kg^{-1}$)	Error (+/-)	Insoluble fraction
TF060302-1 A1	18.50	0.210	0.008	1.1%
TF060302-1 A2	18.50	0.167	0.007	1.6%
TF060302-1 B1	17.50	0.217	0.004	1.0%
TF060302-1 B2	17.50	0.195	0.007	-
TF060302-1 C1	16.50	0.205	0.006	1.3%
TF060302-1 C2	16.50	0.050	0.006	-
TF060302-1 D1	15.50	0.187	0.006	0.9%
TF060302-1 D2	15.50	0.189	0.005	-
TF060302-1 E1	14.50	0.182	0.006	1.1%
TF060302-1 E2	14.50	0.174	0.003	1.1%
TF060302-1 F1	13.50	0.187	0.011	1.1%
TF060302-1 F2	13.50	0.168	0.006	-
TF060302-1 G1	12.50	0.148	0.004	0.6%
TF060302-1 G2	12.50	0.154	0.008	-
TF060302-1 H1	11.50	0.113	0.008	1.0%
TF060302-1 H2	11.50	0.144	0.008	-
TF060302-1 I1	10.75	0.094	0.009	-
TF060302-1 I2	10.75	compromised	-	1.2%
TF060302-1 J1	10.25	0.112	0.005	1.7%
TF060302-1 J2	10.25	0.153	0.006	-
TF060302-1 K1	9.75	0.160	0.004	0.9%
TF060302-1 KRpt	9.75	0.157	0.006	-
TF060302-1 L1	9.25	0.182	0.003	2.1%
TF060302-1 M1	8.75	0.232	0.006	1.7%
TF060302-1 N1	8.00	0.228	0.006	1.0%
TF060302-1 O1	7.00	0.252	0.009	1.1%
TF060302-1 P1	6.00	0.175	0.003	2.1%
TF060302-1 P22	6.00	0.213	0.008	-
TF060302-1 Q1	5.00	0.146	0.004	2.4%
TF060302-1 R1	4.00	0.198	0.006	1.4%
TF060302-1 S1	3.00	0.266	0.007	3.2%
TF060302-1 T1	2.00	0.263	0.003	6.0%
TF060302-2 T2	2.00	0.280	0.008	-
TF060302-1 U1	1.00	0.283	0.007	-
TF060302-1 V1	0.25	0.252	0.008	-

Table A2 – Trumpletts Farm U assay (Detailed core sections)

Sample Ref	Sampling depth from top fracture (cm)	Chalk conc. ($mg.kg^{-1}$)	Error (+/-)	Insoluble fraction
TF060302-1 V22	0.25	0.295	0.007	-

Source: d:\simon\project\data\uranium\ls55\u_chalk\trumpfarma\[uchalkresults_trumpfarm_all_v2.xlsm]

Appendix B | Radium Survey Results

Table B1 - 1m Core Samples

Table B2 - Detailed Core Samples

Table B1 – Trumpletts Farm Ra Assay (1m core samples)

Ref	Mass (g)	Comments	Sub-class	Depth (mbOD)	Activity[1] Bq.kg^{-1}	Uncertainty[1] Bq.kg^{-1}
Batch 1						
TF060321-I	3.0020	-	-	14.93	4.46	0.86
TF060321-J	3.0000	-	-	15.60	4.60	0.76
TF060620-N	3.0000	-	-	44.35	3.18	0.74
TF060620-O	2.0010	-	-	45.26	4.91	0.99
TF060907-C	3.0030	-	-	79.56	5.51	0.90
TF060907-O	3.0010	-	fracture	91.67	3.24	0.74
TF060907-P	3.0010	-	inner surface	91.67	2.92	0.65
Batch 2						
TF060907-L	3.0025	Not used - compromised	-	88.88	-	-
TF060907-I	2.9999	wispy marls	core	85.70	3.69	0.60
TF060907-F	3.0017	marl/chalk sequence to fracture	core	82.70	9.34	1.05
TF060907-E	3.0052	whole block	nodules	81.30	33.52	1.88
TF060907-D	3.0013	nodular chalk and glauconite	nodules	80.96	41.88	1.89
TF060907-B	3.0016	top of block to include marl band	core	78.55	7.69	1.00
TF060814-M	3.0030	from fracture upwards into competent chalk	core	68.33	5.06	0.66
TF060814-D	2.9996	horizontal fracture and clay	core	61.65	3.20	0.52
TF060620-R	3.0005	fractured marl into competent chalk below	core	48.45	6.35	0.75
TF060620-P	3.0015	wispy marl in competent chalk	core	46.53	3.99	0.58
TF060619-B	2.9996	fractured blocky chalk	surface	33.60	1.39	0.49
TF060321-N	3.0009	fractured zone, brown coating	core	23.00	8.14	0.88
TF060321-M	2.9994	fractured zone, brown coating	core	20.60	2.41	0.53
TF060321-A	3.0030	disturbed block	-	4.40	1.91	0.47

Notes [1]Activity for all rock sample, assuming no radium in un-dissolved fraction

Table B2 – Trumpletts Farm Ra Assay (Detailed core samples)

Ref	Mass (g)	Comments	Sub-class	Distance from top fracture (cm)	Activity[1] Bq.kg^{-1}	Uncertainty[1] Bq.kg^{-1}
Batch 1						
060302-1 'V'	3.0000	-	block	0.0025	3.03	0.65
060302-1 'T'	3.0020	-	block	0.0200	3.95	0.70
060302-1 'Q'	3.0050	-	block	0.0500	3.76	0.73
060302-1 'J'	3.0030	-	block	0.1025	2.92	0.67
Batch 2						
TF060302-1 'M'	3.0039	-	block	0.0875	4.39	0.71
TF060302-1 'O'	3.0043	-	block	0.0700	3.68	0.64
TF060302-1 'Q'	2.9990	-	block	0.0500	3.07	0.63
TF060321-1 'R'	3.0031	-	block	0.0400	4.02	0.73
TF060321-1 'S'	3.0010	-	block	0.0300	4.28	0.69
TF060321-1 'U'	3.0020	-	block	0.0100	2.96	0.52

Notes 1Activity for all rock sample, assuming no radium in un-dissolved fraction

Appendix C | Spring & Borehole Radon Results

Table C1 - River Lambourn catchment - Springs

		Radon Activity (Bql^{-1})			
Site Name	**Date**	**Bottle 1**	**Bottle 2**	***Average***	***± 1σ***
Boxford Spring	22-Feb-05	0.01		*0.01*	-
				-	-
Gt Shefford Spring	18-Jan-05	2.36		*2.36*	-
	22-Feb-05	6.43		*6.43*	-
	09-Mar-05	4.12	4.27	*4.19*	*0.11*
	19-Apr-05	4.33	3.94	*4.14*	*0.28*
	07-Jun-05	3.54	3.52	*3.53*	*0.01*
	03-Oct-05	6.83	6.84	*6.84*	*0.01*
	15-Dec-05	3.49	3.66	*3.58*	*0.12*
	07-Feb-06	4.22	4.04	*4.13*	*0.13*
	30-Mar-06	2.56	2.51	*2.53*	*0.03*
	12-Oct-06	3.00	3.08	*3.04*	*0.06*
	05-Jul-07	2.31	2.09	*2.20*	*0.15*
Gt Sheffford (Bridge)	01-Sep-05	2.99		*2.99*	-
Jannaways (pumped)	22-Feb-05	0.60		0.60	-
	19-Apr-05	1.43		1.43	-
	07-Jun-05	1.91	1.87	1.89	0.03
	21-Jul-05	2.06	1.93	2.00	0.09
	01-Sep-05	2.05	1.98	2.02	0.05
	03-Oct-05	1.96	1.95	1.95	0.01
	16-Nov-05	0.96	1.08	1.02	0.09
	15-Dec-05	1.06		1.06	-
	07-Feb-06	0.99	0.90	0.95	0.06
	30-Mar-06	0.93	0.95	0.94	0.01
	29-Jun-06	0.84		0.84	#DIV/0!
	12-Oct-06	0.85	0.97	0.91	0.09
Lynch Wood	18-Jan-05	0.76		*0.76*	-
	22-Feb-05	0.38		*0.38*	-
	09-Mar-05	1.82	1.83	*1.83*	*0.00*
	19-Apr-05	2.06	1.88	*1.97*	*0.12*
	07-Jun-05	2.33		*2.33*	-
	21-Jul-05	2.64	2.64	*2.64*	*0.00*
				-	-
Lynch Wood (Bank)	07-Jun-05	2.26		*2.26*	-

		Radon Activity (Bql^{-1})			
Site Name	**Date**	**Bottle 1**	**Bottle 2**	***Average***	***± 1σ***
Weston Spring	18-Jan-05	1.50		*1.50*	-
	22-Feb-05	2.09		*2.09*	-
	19-Apr-05	4.00	4.32	*4.16*	*0.22*
	07-Jun-05	3.62	3.12	*3.37*	*0.35*
	21-Jul-05	4.52	5.03	*4.78*	*0.36*
	01-Sep-05	4.93	4.93	*4.93*	*0.00*
	03-Oct-05	4.63	4.92	*4.78*	*0.20*
	15-Dec-05		2.73	*2.73*	-
	07-Feb-06	2.52	2.59	*2.56*	*0.05*
	30-Mar-06		2.96	*2.96*	-
	12-Oct-06	2.47	2.08	*2.27*	*0.27*

Source: d:\simon\project\data\[fieldrecords_v2.xlsm]radon_pivot_all

Table C2 - River Lambourn catchment – Pond & Stream Samples

Site Name	**Date**	**Bottle 1**	**Bottle 2**	***Average***	***± 1σ***
Jannaways (Pond)	22-Feb-05	0.18	-	0.18	-
Brockhampton	18-Jan-05	0.76	-	0.76	-
East Garston Bridge	18-Jan-05	0.71	-	0.71	-
Eastbury Bridge	18-Jan-05	0.38	-	0.38	-
Maidencourt Farm	18-Jan-05	1.35	-	1.35	-

Source: d:\simon\project\data\[fieldrecords_v2.xlsm]radon_pivot_all

Table C3 - River Pang catchment - Springs

		Radon Activity (Bql^{-1})			
Site Name	**Date**	**Bottle 1**	**Bottle 2**	***Average***	***± 1σ***
Ingle Spring	22-Feb-05	1.64		1.64	-
	19-Apr-05	5.72	3.54	4.63	1.54
	07-Jun-05	6.42		6.42	-
	21-Jul-05	6.35		6.35	-
	01-Sep-05	6.95	6.71	6.83	0.17
	03-Oct-05	8.30	7.90	8.10	0.28
	16-Nov-05	3.82	3.37	3.59	0.32
	15-Dec-05	3.37	3.35	3.36	0.01
	07-Feb-06	3.56	3.50	3.53	0.05
	30-Mar-06	3.53	3.43	3.48	0.07
	29-Jun-06	3.42		3.42	-
	12-Oct-06	5.14	5.05	5.10	0.06
Jewell's Spring	22-Feb-05	2.37		2.37	-
	19-Apr-05		4.65	4.65	-
	07-Jun-05	5.28	5.93	5.61	0.46
	21-Jul-05	5.48	5.64	5.56	0.11
	01-Sep-05	6.83	6.39	6.61	0.31
	03-Oct-05	4.14	4.20	4.17	0.04
	16-Nov-05	3.16	3.40	3.28	0.17
	15-Dec-05	3.16		3.16	-
	07-Feb-06	3.04	3.08	3.06	0.03
	30-Mar-06	3.13	3.28	3.20	0.11
	29-Jun-06	2.51		2.51	-
	12-Oct-06	2.42	2.36	2.39	0.04
Kimber Spring	22-Feb-05	2.05		2.05	-
	19-Apr-05	6.53		6.53	-
	07-Jun-05	6.28	6.51	6.40	0.16
	21-Jul-05	6.24	6.43	6.34	0.13
	01-Sep-05	5.96	5.99	5.98	0.02
	03-Oct-05	5.82	5.66	5.74	0.11
	16-Nov-05	3.50	3.49	3.50	0.01
	15-Dec-05	3.71	3.77	3.74	0.04
	07-Feb-06	3.34	3.34	3.34	0.00
	30-Mar-06	3.83	3.74	3.78	0.07
	29-Jun-06	3.49		3.49	-

		Radon Activity (Bql^{-1})			
Site Name	**Date**	**Bottle 1**	**Bottle 2**	***Average***	***± 1σ***
	12-Oct-06	2.96	3.01	2.99	0.03
	05-Jul-07	5.30	5.18	5.24	0.08

Source: d:\simon\project\data\[fieldrecords_v2.xlsm]radon_pivot_all

Table C4 - River Pang catchment – Pond & Stream Samples

		Radon Activity (Bql^{-1})			
Site Name	**Date**	**Bottle 1**	**Bottle 2**	***Average***	***± 1σ***
Pond south of Parsonage Farm	21-Jul-05	5.62	7.62	6.62	1.41
	01-Sep-05	8.73	9.27	9.00	0.38
	03-Oct-05	4.24	4.32	4.28	0.06
	16-Nov-05	4.01	4.28	4.14	0.19
	15-Dec-05	6.43		6.43	-
	07-Feb-06	4.79	4.83	4.81	0.02
	30-Mar-06	8.45	8.16	8.31	0.21
				-	-
Ditch south of Parsonage Farm	19-Apr-05	5.46		5.46	-
	07-Jun-05	12.03		12.03	-
				-	-
Bucklebury Bridge	19-Apr-05	0.15		0.15	-
				-	-
Downstream of Hampstead Norreys STW	19-Apr-05	4.26		4.26	-
	07-Jun-05	4.18		4.18	-
				-	-
Manor Farm	22-Feb-05	0.64		0.64	-

Source: d:\simon\project\data\[fieldrecords_v2.xlsm]radon_pivot_all

Table C5(A) - River Lambourn catchment – Boreholes

Winterbourne Farm (EA obs)

Pump Test at Winterbourne Farm - Results			
Date of Test	**05-Apr-06**		
Sample Depth	12.80	m below datum	
Water level (start)	2.52	m below datum	
Water level (end)	2.52	m below datum	
Pump rate	0.044	litres/sec	(measured by bucket method)

Output Files used: D:\Simon\Project\Calcs\Radon\
RnConc_5apr06_alpha.xls

				Winterbourne Farm 12.8m
Time	Elasped Time (hours)	**Volume Pumped (L)**	Sample Bottle	Radon Activity Bql-1
14:11	0	**0.0**	-	-
14:18	0.117	**18.5**	Q11	4.023
14:26	0.250	**39.6**	Q17	3.168
14:38	0.450	**71.4**	W19	4.004
14:50	0.650	**103.1**	W34	4.310

Table C5(B) - River Lambourn catchment – Boreholes

Winterbourne Farm (EA obs)

Pump Test at Winterbourne Farm - Results

Date of Test	**11-Jan-07**		
Sample Depth	15.60	m below datum	
Water level (start)	1.67	m below datum	
Water level (end)	1.67	m below datum	
Pump rate	0.471	litres/sec	(measured by bucket method)

Output Files used: D:\Simon\Project\Calcs\Radon\PumpTests

RnConc_11jan07_alpha.xls

				Winterbourne Farm 15.6m						
Time	Elasped Time (mins)	**Volume Pumped (L)**	Sample Bottle	Radon Activity Bql-1	Error	pH	Cond (uS/cm)	DO%	DO mg/l	Temp deg C
16:10	0	**0.0**	-	-	-	-	-	-	-	-
16:20	10.0	**282.6**	-	-	-	6.62	617	93.5	10.5	10.9
16:40	30.0	**847.9**	T6 Wint 1640	6.038	0.045	-	-	-	-	-
16:42	32.0	**904.4**	T20 Wint 1640(2)	6.176	0.046	-	-	-	-	-

Table C5(C) - River Lambourn catchment – Boreholes

Winterbourne Farm (EA obs)

Pump Test at Winterbourne Farm - Results

Date of Test	**05-Jul-07**	
Sample Depth	15.60	m below datum
Water level (start)	1.22	m below datum
Water level (end)	1.22	m below datum
Pump rate	0.555	litres/sec (measured by bucket method)

Output Files used: D:\Simon\Project\Calcs\Radon\PumpTests

RnConc_5july07.xls

Winterbourne Farm 15.6m

Time	Elasped Time (mins)	**Volume Pumped (L)**	Sample Bottle	Radon Activity Bql-1	Error	pH	Cond (uS/cm)	DO%	DO mg/l	Temp deg C
16:46	0	**0.0**	-	-	-	-	-	-	-	-
17:00	14.0	**466.6**	Q17	**5.19**	**0.08**	-	-	-	-	-
17:06	20.0	**666.5**	T6	**5.41**	**0.08**	-	-	42.50%	-	-
17:14	28.0	**933.2**	-	-	-	-	650	-	-	11.0
17:16	30.0	**999.8**	T27	**5.19**	**0.08**	-	-	-	-	-
17:26	40.0	**1333.1**	T15	**5.37**	**0.08**	-	-	-	-	-

Table C5(D) - River Lambourn catchment – Boreholes

Bagnor (EA obs)

Pump Test at Bagnor Manor - Results			
Date of Test	**05-Apr-06**		
Sample Depth	**16.50**	m below datum	
Water level (start)	2.33	m below datum	
Water level (end)	2.33	m below datum	
Pump rate	0.106	litres/sec	(measured by bucket method)

Output Files used: D:\Simon\Project\Calcs\Radon\
RnConc_5apr06_alpha.xls

Bagnor Manor 16.5m

Time	Elasped Time (hours)	**Volume Pumped (L)**	Sample Bottle	Radon Activity Bql-1
12:46	0	**0.0**	-	-
12:51	0.083	**31.9**	W20	1.228
13:01	0.250	**95.7**	Q3	1.464
13:10	0.400	**153.2**	W32	1.381
13:21	0.583	**223.4**	W31	1.310

Table C5(E) - River Lambourn catchment – Boreholes

Bagnor (EA obs)

Pump Test at Bagnor Manor - Results

Date of Test	**11-Jan-07**					
Sample Depth	**26.60**	m below datum	(assumes 0.6m from top of casing to board)	Datum	Board within housing	
Water level (start)	1.96	m below datum		Datum	86.02	mAOD
Water level (end)	2.03	m below datum		Depth Well	33.33	mbd
Pump rate	0.451	litres/sec	(measured by bucket method)	Volume	0.983	m2
				Assumes diameter of 200mm		

Output Files used: D:\Simon\Project\Calcs\Radon\PumpTests

RnConc_11jan07_alpha.xls

Time	Elasped Time (hours)	**Volume Pumped (L)**	**Well Volumes**	Sample Bottle	Radon Activity Bql-1	Error Bql-1	pH	Cond (uS/cm)	DO%	Temp deg C
14:42	0	**0.0**	**0.0**	-	-	-	-	-	-	-
15:12	0.500	**812.3**	**0.8**	QX	**1.68**	**0.02**	-	-	-	-
15:14	0.533	**866.4**	**0.9**	T25	**1.65**	**0.02**	-	-	-	-

Table C5(F) - River Lambourn catchment – Boreholes

Bagnor (EA obs)

Pump Test at Bagnor Manor - Results

Date of Test	**05-Jul-07**					
Sample Depth	**26.60**	m below datum	(assumes 0.6m from top of casing to board)	Datum	Board within housing	
Water level (start)	2.13	m below datum		Datum	86.02	mAOD
Water level (end)	2.14	m below datum		Well Depth	33.33	mbd
				Well		
Pump rate	0.556	litres/sec	(measured by bucket method)	Volume	0.980	m2
				Assumes diameter of 200mm		

Output Files used: D:\Simon\Project\Calcs\Radon\PumpTests
RnConc_5july07.xls

Time	Elasped Time (mins)	**Volume Pumped (L)**	**Well Volumes**	Sample Bottle	Radon Activity Bql-1	Error Bql-1	pH	Cond (uS/cm)	DO%	Temp deg C
15:05	0	**0.0**	**0.0**	-	-	-	-	-	-	-
15:09	4	**133.5**	**0.1**	-	-	-	7.29	-	-	10.9
15:10	5	**166.9**	**0.2**	-	-	-	-	-	85.50%	11
15:13	8	**267.0**	**0.3**	-	-	-	7.33	-	85.60%	-
15:15	10	**333.7**	**0.3**	T11	**1.85**	**0.05**	-	-	-	-
15:16	11	**367.1**	**0.4**	-	-	-	-	570	-	-
15:20	15	**500.6**	**0.5**	-	-	-	7.37	-	-	-
15:21	16	**533.9**	**0.5**	-	-	-	-	-	82.90%	-
15:24	19	**634.0**	**0.6**	-	-	-	7.36	-	84.70%	-
15:25	20	**667.4**	**0.7**	T7	**1.82**	**0.05**	-	-	83.40%	-
15:35	30	**1001.1**	**1.0**	QX	**1.88**	**0.04**	-	-	-	-
15:45	40	**1334.8**	**1.4**	T28	**1.81**	**0.05**	-	-	-	-

Table C5(G) - River Lambourn catchment – Boreholes

Briff Lane (EA obs)

Pump Test at Briff Lane - Results

Date of Test	**11-Jan-07**				
Sample Depth	**40.00**	m below datum		Datum	Board within housing
Water level (start)	33.90	m below datum		Datum	96.4 mAOD
Water level (end)	34.05	m below datum		Depth	56.94 mbd
Pump rate	0.407	litres/sec	(measured by bucket method)	Well Volume	0.719 m2
				Assumes diameter of 200mm	

Output Files used: D:\Simon\Project\Calcs\Radon\PumpTests
RnConc_11jan07_alpha.xls

Time	Elasped Time (hours)	**Volume Pumped (L)**	**Well Volumes**	Sample Bottle	Radon Activity Bql-1	Error Bql-1	pH	Cond (uS/cm)	DO%	Temp deg C
13:04	0	**0.0**	**0.0**	-	-	-	-	-	28.6%	11.3
13:07	0.050	**73.2**	**0.1**	-	-	-	6.12	584	12.4%	11.3
13:10	0.100	**146.3**	**0.2**	-	-	-	6.54	-	9.4%	11.4
13:15	0.183	**268.3**	**0.4**	-	-	-	7.04	-	9.5%	11.4
13:19	0.250	**365.9**	**0.5**	T11	**0.59**	**0.01**	-	-	-	-
13:20	0.267	**390.2**	**0.5**	Q9	**0.62**	**0.01**	-	-	-	-
13:25	0.350	**512.2**	**0.7**	-	-	-	6.96	606	9.6%	11.5
13:30	0.433	**634.1**	**0.9**	-	-	-	7.01	607	10.8%	11.6
13:34	0.500	**731.7**	**1.0**	T4	**3.11**	**0.03**	-	-	-	-
13:36	0.533	**780.5**	**1.1**	T28	**3.03**	**0.03**	-	-	-	-

Table C5(H) - River Lambourn catchment – Boreholes

Briff Lane (EA obs)

Pump Test at Briff Lane - Results

Date of Test	**05-Jul-07**		
Sample Depth	**46.00**	m below datum	
Water level (start)	33.55	m below datum	
Water level (end)	33.57	m below datum	
Pump rate	0.403	litres/sec	(measured by bucket method)

Datum	Board within housing	
Datum	96.4	mAOD
Depth	56.94	mbd
Well Volume	0.734	m2
Assumes diameter of 200mm		

Output Files used: D:\Simon\Project\Calcs\Radon\PumpTests
RnConc_5july07.xls

Time	Elasped Time (mins)	**Volume Pumped (L)**	**Well Volumes**	Sample Bottle	Radon Activity Bql-1	Error Bql-1	pH	Cond (uS/cm)	DO%	Temp deg C
12:47	0	**0.0**	**0.0**	-	-	-	-	-	10.10%	12
12:49	2.000	**48.3**	**0.1**	-	-	-	7.26	-	-	-
12:51	4.000	**96.6**	**0.1**	-	-	-	-	-	3.00%	-
12:54	7.000	**169.1**	**0.2**	-	-	-	7.3	-	2.60%	11.8
13:00	13.000	**314.1**	**0.4**	T38	**2.81**	**0.06**	-	-	-	-
13:01	14.000	**338.3**	**0.5**	-	-	-	7.32	-	4.20%	-
13:06	19.000	**459.1**	**0.6**	-	-	-	-	-	3.60%	-
13:07	20.000	**483.2**	**0.7**	T4	**3.53**	**0.06**	-	556	3.50%	-
13:17	30.000	**724.8**	**1.0**	T14	**3.69**	**0.07**	-	539	7.60%	12
13:27	40.000	**966.4**	**1.3**	T25	**3.47**	**0.06**	-	-	-	-

Table C6 (A) - River Pang catchment – Boreholes

Frilsham A (LOCAR obs)

Pump Test at Frilsham A - Results

Date of Test	**11-Jan-07**					
Sample Depth	27.70	m below datum		Datum	Top of outer casing	
Water level (start)	1.16	m below datum		Datum	77.52	mAOD
Water level (end)	1.21	m below datum		Depth	43.00	mbd
Pump rate	0.525	litres/sec	(bucket method)	Minimum Well Volume	1.334	m2
				Assumes diameter of 200mm		

Output Files used:
D:\Simon\Project\Calcs\Radon\PumpTests

RnConc_11jan07_alpha.xls

Frilsham A 27.7m

Time	Elasped Time (hours)	Volume Pumped (L)	Well Volumes	Sample Bottle	Radon Activity Bq.l^{-1}	Error Bql^{-1}	pH	Cond (uS/cm)	DO%	Temp deg C
11:12	0	**0.0**	**0.0**	-	-	-	-	-	-	-
11:39	0.450	**851.1**	**0.6**	Q10	**1.19**	**0.02**	-	-	-	-
11:40	0.467	**882.6**	**0.7**	Q17	**1.18**	**0.02**	-	-	-	-
11:52	0.667	**1260.8**	**0.9**	T18	**1.17**	**0.02**	-	-	-	-
11:58	0.767	**1450.0**	**1.1**	T7	**1.16**	**0.02**	-	-	-	-

Table C6 (B) - River Pang catchment – Boreholes

Frilsham B obs b/h (LOCAR obs

Pump Test at Frilsham B - Results

Date of Test	05/04/2006		
Sample Depth	21.00	m below datum	
Water level (start)	1.39	m below datum	
Water level (end)	1.40	m below datum	
Pump rate	0.132	litres/sec	(measured by bucket method)

Output Files used: D:\Simon\Project\Calcs\Radon\
RnConc_5apr06_alpha.xls

Frilsham B 21m

Time	Elasped Time (hours)	**Volume Pumped (L)**	Sample Bottle	Radon Activity Bql^{-1}
05/04/2006 10:39	0	**0.0**	-	-
05/04/2006 10:42	0.050	**23.7**	Q2	0.581
05/04/2006 10:49	0.167	**78.9**	Q6	1.142
05/04/2006 10:53	0.233	**110.5**	Q14	1.150
05/04/2006 10:59	0.333	**157.9**	Q16	1.095
05/04/2006 11:14	0.583	**276.3**	QX	1.078

Table C6 (C) - River Pang catchment – Boreholes

Trumplett's Farm (EA obs)

Pump Test at Trumpletts Farm - Results

Date of Test 09-Mar-05

Pump rate 5.66 Ml/day
(measured after 26 mins of pumping)

Output Files used: D:\Simon\Project\Calcs\Radon\
RnConc_10MR05.xls
RnConc_10MR05_2.xls

Time	Elasped Time (hours)	**Well Volumes Pumped**	Sample Bottle	Radon Activity Bql-1
9/05/05 10:11	0	**-**	-	-
9/05/05 10:13	0.033	**0.27**	Q8	2.67
9/05/05 10:16	0.083	**0.67**	Q9	4.66
9/05/05 10:21	0.167	**1.34**	Q10	3.51
9/05/05 10:26	0.250	**2.02**	Q11	3.89
9/05/05 10:31	0.333	**2.69**	Q12	3.81
9/05/05 10:41	0.500	**4.03**	Q13	3.96
9/05/05 10:51	0.667	**5.38**	Q14	3.90
9/05/05 11:11	1.000	**8.07**	Q15	3.74

Table C6 (D) - River Pang catchment – Boreholes

Trumplett's Farm (EA obs)

Date of Test 27-Apr-05 Pump rate 5.66 Ml/day

Output Files used: D:\Simon\Project\Calcs\Radon\
RnConc_29APR05 (&_2).xl s

Time	Elasped Time (hours)	**Well Volumes Pumped**	Sample Bottle	Radon Activity Bql-1
27/04/2005 10:19	0.000	**-**	-	-
27/04/2005 10:20	0.017	**0.13**	Q4	2.70
27/04/2005 10:21	0.033	**0.27**	Q6	3.01
27/04/2005 10:23	0.067	**0.54**	Q8	4.73
27/04/2005 10:25	0.100	**0.81**	Q10	4.33
27/04/2005 10:27	0.133	**1.08**	Q13	3.94
27/04/2005 10:29	0.167	**1.34**	Q15	3.80
27/04/2005 10:34	0.250	**2.02**	Q3	3.49
27/04/2005 10:39	0.333	**2.69**	Q17	3.25
27/04/2005 10:49	0.500	**4.03**	W36	3.85
27/04/2005 10:59	0.667	**5.38**	W20	3.22
27/04/2005 11:19	1.000	**8.07**	Q1	3.87
27/04/2005 11:49	1.500	**12.10**	W27	3.89
27/04/2005 12:19	2.000	**16.14**	W18	4.02
27/04/2005 13:19	3.000	**24.20**	W21	4.47
27/04/2005 14:19	4.000	**32.27**	W19	4.13
27/04/2005 16:19	6.000	**48.41**	Q2	4.85
27/04/2005 18:19	8.000	**64.54**	W33	4.84
27/04/2005 22:19	12.000	**96.81**	W34	4.68
28/04/2005 08:19	22.000	**177.49**	W28	3.81
28/04/2005 14:19	28.000	**225.89**	Q5	4.94

Appendix D | Packer Tests (Trumpletts Farm)

Table D1 – Packer Test Record Sheet (Interval 1)

Packer Testing Record Sheet

Hydrogeology Research Group - Department of Earth Sciences
UCL (University College London) - Gower Street - London - WC1E 6BT
Tel: +44 (0)20 7679 2364 Fax: +44 (0)20 7679 2433
Contact: Simon Quinn
Email: s.quinn@ucl.ac.uk Mobile +44 (0)7974 660003

Record Sheet completed by: SAQ/WGB/SC/ CF

Pumping Test at:	Trumplett's Farm	
NGR:	SU513750	
Details of packered section:	**28.7m - 32.9m**	**28.69m - 32.89m (below new datum) Interval 1**
	LARGE packer system	

Description of datum point:
Top of metal annulus (top section not removed)

SWL Annulus = 22.28mbd after inflation
Rising Main 22.28mbd after inflation
Height above ground level (meters): **0.48m (i.e. not 0.28m as previously used by BGS)**

Date	Time	Elapsed Time		Depth of water in annulus below datum (meters)	Drawdown (meters)	Transmitter reading mA	Flow Meter Reading m3	Radon Sample	Other Samples	Comments	Volume Pumped litres	Flow rate l/min	Radon Activity Bq/l
		Minutes	Hours										28.7m - 32.9m
27-Jun-06	13:28:00	0		22.23	0	4.7802	162.181			13:26 (SJC watch)	0	0	#N/A
		1		22.26	0.03		162.181				0	0	#N/A
		2		22.26	0.03	4.7745	162.190				9	9	#N/A
	13:31	3		22.26	0.03	4.7740	162.195	W20			14	5	1.770913136
		4		22.26	0.03	4.7738	162.198				17	3	#N/A
	13:34	5		22.26	0.03	4.7736	162.215				34	17	#N/A
		6		22.26	0.03	4.7735	162.252	W28			71	37	1.842022924
		7		22.26	0.03	4.7735	162.292				111	40	#N/A
		8		22.26	0.03	4.7734	162.322				141	30	#N/A
		9		22.26	0.03	4.7732	162.371				190	49	#N/A
	13:39	10		22.26	0.03	4.7733	162.408	Q3			227	37	1.892183917
		15		22.27	0.04	4.7730	162.606				425	39.6	#N/A
	13:49	20		22.27	0.04	4.7728	162.801	W32	CHEM		620	39	1.952544429
		25		22.27	0.04	4.7728	163.001				820	40	#N/A
	14:01	30		22.27	0.04	4.7727	163.201	Q11			1020	40	1.947231544
		40								14:00 (SJC watch)			

Recommended Radon Sampling Times

CHEM

Time of Sampling	13:48
Minutes of Pumping	20
Temp degC	11.6
DO (mg/l)	9.9
DO (%)	94%
pH	6.89
Cond (uS/cm)	536
Inorganic Ref (non acid)	UCL060627-1 F/UA
Inorganic Ref (acidified)	UCL060627-1 F/A

Table D2 – Packer Test Record Sheet (Interval 2)

Packer Testing Record Sheet

Hydrogeology Research Group - Department of Earth Sciences
UCL (University College London) - Gower Street - London - WC1E 6BT
Tel: +44 (0)20 7679 2364 Fax: +44 (0)20 7679 2433
Contact: Simon Quinn
Email: s.quinn@ucl.ac.uk Mobile +44 (0)7974 660003

Record Sheet completed by: SAQ/WGB/SJC/CMF

Pumping Test at:	Trumplett's Farm	
NGR:	SU513750	
Details of packered section:	**32.8m - 37.0m**	**32.8m - 37.0m (below new datum) Interval 2**
	LARGE packer system	

Description of datum point:

Top of metal annulus (top section not removed)

SWL Annulus = 22.23mbd at start

Height above ground level (meters): **0.48m (i.e. not 0.28m as previously used by BGS)**

Date	Time	Elapsed Time		Depth of water in annulus below datum (meters)	Drawdown (meters)	Transmitter reading mA	Flow Meter Reading m3	Radon Sample	Other Samples	Comments	Volume Pumped litres	Flow rate l/min	Radon Activity Bq/l
		Minutes	Hours										32.8m - 37.0m
27-Jun-06	15:23:00	0		22.23	0	5.4096	163.320			inflation at 14:50	0	0	#N/A
		1		22.27	0.04	4.7640	163.320			pump start at 15:23	0	0	#N/A
		2		22.27	0.04	4.6165	163.351			pump off after 33mins	31	31	#N/A
	15:26	3		22.27	0.04	4.5783	163.380	W19		pump off at 15:54	60	29	2.046271395
		4		22.27	0.04	4.5665	163.422				102	42	#N/A
	15:28	5		22.27	0.04	4.5594	163.456	Q9			136	34	2.045563444
		6		22.28	0.05	4.5613	163.494				174	38	#N/A
		7		22.28	0.05	4.5586	163.533				213	39	#N/A
		8		dipper stuck	#N/A	4.5555	163.572				252	39	#N/A
		9		dipper stuck	#N/A	4.5518	163.609				289	37	#N/A
	15:33	10		dipper stuck	#N/A	4.5483	163.644	W27			324	35	1.875401826
		15		dipper stuck	#N/A	4.5423	163.839				519	39	#N/A
	15:44	20		dipper stuck	#N/A	4.5395	164.028	Q16	CHEM		708	37.8	1.585616649
		25		22.28	0.05	5.5279	164.218				898	38	#N/A
	15:55	30		22.28	0.05	4.5244	164.411	W31			1091	38.6	1.683973759

Recommended Radon Sampling Times

CHEM

Time of Sampling	15:45
Minutes of Pumping	20
Temp degC	11.7
DO (mg/l)	9.9
DO (%)	93%
pH	7.16
Cond (uS/cm)	545
Inorganic Ref (non acid)	UCL060627-2 F/UA
Inorganic Ref (acidified)	UCL060627-2 F/A

Table D3 – Packer Test Record Sheet (Interval 3)

Packer Testing Record Sheet

Hydrogeology Research Group - Department of Earth Sciences
UCL (University College London) - Gower Street - London - WC1E 6BT
Tel: +44 (0)20 7679 2364 Fax: +44 (0)20 7679 2433
Contact: Simon Quinn
Email: s.quinn@ucl.ac.uk Mobile +44 (0)7974 660003

Record Sheet completed by: SAQ/WGB/ SC/CF

Pumping Test at:	Trumplett's Farm	
NGR:	SU513750	
Details of packered section:	**36.8m - 41.0m**	**36.8m - 41.0m (below new datum) Interval 3**
	LARGE packer system	

Description of datum point:

Top of metal annulus (top section not removed)

SWL Annulus = 22.22mbd at start Rising Main 22.27mbd at start

Height above ground level (meters): **0.48m (i.e. not 0.28m as previously used by BGS)**

Date	Time	Elapsed Time Minutes	Elapsed Time Hours	Depth of water in annulus below datum (meters)	Drawdown (meters)	Transmitter reading mA	Flow Meter Reading m3	Radon Sample	Other Samples	Comments	Volume Pumped litres	Flow rate 1/min	Radon Activity Bq/l 36.8m - 41.0m
27-Jun-06	17:32:00	0		22.22	0	6.0364	164.519				0	0	#N/A
		1		22.26	0.04	5.3900	164.519				0	0	#N/A
		2		22.26	0.04	5.2235	164.550				31	31	#N/A
	17:35	3		22.26	0.04	5.1830	164.587	Q10			68	37	2.277716087
		4		22.26	0.04	5.1779	164.623				104	36	#N/A
	17:37	5		#N/A	#N/A	5.1752	164.659	QX		affected by leak on rising main -	140	36	2.109695569
		6		#N/A	#N/A	5.1735	164.699				180	40	#N/A
		7		#N/A	#N/A	5.1692	164.738				219	39	#N/A
		8		#N/A	#N/A	5.1657	164.776				257	38	#N/A
		9		#N/A	#N/A	5.1654	164.815				296	39	#N/A
	17:43	10		#N/A	#N/A	5.1639	164.851	W34			332	36	1.776127833
		15		#N/A	#N/A	5.1617	165.046				527	39	#N/A
	17:52	20		#N/A	#N/A	5.1572	165.241	Q13	CHEM		722	39	1.72390672
		25		#N/A	#N/A	5.1563	165.435				916	38.8	#N/A
	18:03	30		22.27	0.05	5.1495	165.626	Q14			1107	38.2	1.556887875
		40											
		45											
		50											
		55											
		60	1										
		70											
		80											
		90											
		100											
		120	2										

Recommended Radon Sampling Times

CHEM

Time of Sampling	17:42
Minutes of Pumping	20
Temp degC	11.6
DO (mg/l)	9.7
DO (%)	93%
pH	7.17
Cond (uS/cm)	543
Inorganic Ref (non acid)	UCL060627-3 F/UA
Inorganic Ref (acidified)	UCL060627-3 F/A

Table D4 – Packer Test Record Sheet (Interval 4)

Packer Testing Record Sheet

Hydrogeology Research Group - Department of Earth Sciences
UCL (University College London) - Gower Street - London - WC1E 6BT
Tel: +44 (0)20 7679 2364 Fax: +44 (0)20 7679 2433
Contact: Simon Quinn
Email: s.quinn@ucl.ac.uk Mobile +44 (0)7974 660003

Record Sheet completed by: SAQ/WGB/SJC/CMF

Pumping Test at:	Trumplett's Farm A	
NGR:	SU513750	
Details of packered section:	**41.3m - 45.0m**	**41.25m - 45.00m (below new datum) Interval 4**
	SMALL packer system	

Description of datum point:

Top of metal annulus (top section not removed)

SWL Annulus = 22.26mbd at start, 22.27 after inflation
Rising Main 22.26mbd at start, 22.28 after inflation

Height above ground level (meters): **0.48m (i.e. not 0.28m as previously used by BGS)**

Date	Time	Elapsed Time Minutes	Elapsed Time Hours	Depth of water in annulus below datum (meters)	Drawdown (meters)	Transmitter reading mA	Flow Meter Reading m3	Radon Sample	Other Samples	Comments	Volume Pumped litres	Flow rate l/min	Radon Activity Bq/l 41.3m - 45.0m
28-Jun-06	19:31:00	0		22.26	0	#N/A	165.725				0	0	#N/A
		1		22.31	0.05	#N/A	165.751				26	26	#N/A
		2		#N/A	#N/A	#N/A	165.795				70	44	#N/A
	19:34	3		22.31	0.05	#N/A	165.837	T30			112	42	2.450323545
		4		22.31	0.05	#N/A	165.878				153	41	#N/A
		5		#N/A	#N/A	#N/A	165.923				198	45	#N/A
	19:37	6		#N/A	#N/A	#N/A	165.965	T29			240	42	1.733058941
		7		22.31	0.05	#N/A	166.007				282	42	#N/A
		8		22.31	0.05	#N/A	166.051				326	44	#N/A
		9		22.31	0.05	#N/A	166.098				373	47	#N/A
	19:42	10		22.31	0.05	#N/A	166.138	T25			413	40	1.749035651
		15		22.32	0.06	#N/A	166.356				631	43.6	#N/A
	19:51	20		22.31	0.05	#N/A	166.564	T24	CHEM		839	41.6	1.666145875
		25		22.32	0.06	#N/A	166.767				1042	40.6	#N/A
	20:03	30		22.32	0.06	#N/A	166.977	T28			1252	42	1.635087386

Recommended Radon Sampling Times

CHEM

Time of Sampling	19:51
Minutes of Pumping	20
Temp degC	11.4
DO (mg/l)	6.2
DO (%)	57%
pH	6.8
Cond (uS/cm)	555
Inorganic Ref (non acid)	UCL060628-1 F/UA
Inorganic Ref (acidified)	UCL060628-1 F/A

Table D5 – Open Hole Record Sheet

Hydrogeology Research Group - Department of Earth Sciences UCL (University College London) - Gower Street - London - WC1E 6BT Tel: +44 (0)20 7679 2364 Fax: +44 (0)20 7679 2433	**Record Sheet completed by: SAQ/WGB/CMF**

Pumping Test at:	Trumplett's Farm A	**Description of datum point:**
NGR:	SU513750	**Top of metal annulus (top section not removed)**
Details of packered section:	**Open Hole** / **Base of pump at 69.32m below datum**	Height above ground level (meters): **0.48m (i.e. not 0.28m as previously used by BGS)**
	Packers NOT INFLATED	Well Volume 1887.9 litres

Date	Time	Elapsed Time Mins	Elapsed Time Hours	Depth of water in annulus below datum (meters)	Drawdown (meters)	Flow Meter Reading m3	Radon Sample	Cond uS/cm	pH	DO%	Temp degC	Comments	Volume Pumped litres	Flow rate l/min	Well Volumes Pumped	Radon Activity Bq/l	Individual Sample Error
30-Jun-06	09:17:00	0		22.295	0	168.055							0	0.00	0.00	#N/A	#N/A
		5		22.400	0.105	168.580	T6						525	105.00	0.28	3.25	0.07
		10		22.405	0.110	169.060	T1	547					1005	96.00	0.53	2.40	0.06
		15		22.405	0.110	169.500	T4						1445	88.00	0.77	2.18	0.05
		20		22.410	0.115	170.025	T5			92.3%			1970	105.00	1.04	2.28	0.05
		25		22.410	0.115	170.550	T9	530					2495	105.00	1.32	2.33	0.06
		30		22.410	0.115	171.180	T8			93.2%			3125	126.00	1.66	2.30	0.05
		40		22.410	0.115	172.145	T2						4090	96.50	2.17	2.37	0.05
		50		22.415	0.120	173.215	T3	546			13.3		5160	107.00	2.73	#N/A	#N/A
		60	1	22.410	0.115	174.280	T7						6225	106.50	3.30	2.24	0.05
		70		22.415	0.120	175.340	T10			94.3%	12.2		7285	106.00	3.86	2.28	0.05
		80		22.420	0.125	176.405	T26						8350	106.50	4.42	2.27	0.06
		90		22.420	0.125	177.485	T23			94.3%	11.1		9430	108.00	5.00	2.33	0.06
		100		22.420	0.125	178.550	T21	548					10495	106.50	5.56	2.31	0.06
		120	2	22.420	0.125	180.720	T27	545		93.9%	11.2	Lancs Univ (NM/JP) take multiple samples	12665	108.50	6.71	2.32	0.06
		140		22.420	0.125	182.866	T37			93.1%	12.2		14811	107.30	7.85	2.51	0.06
		160		22.420	0.125	185.151	T39	556		92.8%	12.9		17096	114.25	9.06	2.50	0.06
		180	3	22.425	0.130	187.105	T33	540		93.3%	11.5		19050	97.70	10.09	2.41	0.06
		210		22.425	0.130	190.350	T36			96.0%			22295	108.17	11.81	2.40	0.06
		240	4	22.425	0.130	193.570	T34						25515	107.33	13.52	2.39	0.06
		270		22.425	0.130	197.110	T32	547	7.16	94.1%	11.0		29055	118.00	15.39	2.47	0.07
		300	5	22.425	0.130	200.015	T35	552	6.73	92.4%	11.1		31960	96.83	16.93	2.42	0.06
		330		22.430	0.135	203.200	T40	546	7.12	97.4%	11.7		35145	106.17	18.62	2.41	0.07
		360	6	22.430	0.135	206.385	T38	550	7.08	91.6%	11.0		38330	106.17	20.30	2.42	0.06
		420	7	22.430	0.135	212.825	T31	526	7.04	93.3%	11.6	Chemistry Samples	44770	107.33	23.71	2.48	0.07

Appendix E | Chemical Analyses

Table E1 – Chemical Analyses – Lambourn Catchment

Table E2 – Chemical Analyses – Pang Catchment

Table E1 – Chemical Analyses – Lambourn Catchment

			%	mg/l $HCO3^-$	$mS.cm^{-1}$	mg/l	mg/l	mg/l	mg/l	mg/l	mg/l	mg/l	mg/l	mg/l	mg/l	mg/l	meq/l	meq/l	meq/l
Site Name	**Date**	**pH**	**DO**	**Alk**	**Cond**	**SO_4^{2-}**	**NO_3^-**	**Cl^-**	**F^-**	**Ca**	**Na**	**Mg**	**K**	**Fe**	**Ba**	**Sr**	**Anions (ex alk)**	**HCO_3^-**	**Cations**
Boxford Spring	22/02/2005	7.9	78.1	167.1	625.0	15.1	21.5	15.7	0.2	132.3	8.4	2.1	1.1	0.0	0.0	0.3	1.1	2.7	7.2
Brockhampton	18/01/2005	-	-	-	273.0	-	-	-	-	-	-	-	-	-	-	-	-	-	-
Eastbury Bridge	18/01/2005	-	-	-	278.0	-	-	-	-	-	-	-	-	-	-	-	-	-	-
Great Shefford Spring	18/01/2005	7.2	88.4	-	526.0	17.8	51.5	13.8	0.2	113.9	5.3	1.6	0.7	0.0	0.0	-	1.6	-	-
	22/02/2005	7.9	81.6	100.9	525.0	17.5	50.3	13.1	0.1	108.5	5.1	1.5	0.8	0.0	0.0	0.2	1.6	1.7	5.8
	09/03/2005	-	-	-	-	-	-	-	-	-	-	-	-	-	-	-	-	-	-
	19/04/2005	7.2	0.0	203.1	512.0	15.6	45.6	13.0	0.0	106.3	4.9	1.5	0.8	0.0	0.0	0.2	1.4	3.3	5.7
	07/06/2005	7.2	93.2	215.0	567.0	13.4	39.7	12.4	0.7	105.1	4.8	1.5	0.8	0.0	0.0	0.2	1.3	3.5	5.6
	03/10/2005	7.0	87.8	-	502.0	-	-	-	-	-	-	-	-	-	-	-	-	-	-
	15/12/2005	-	-	-	-	15.4	45.3	13.0	0.6	103.4	5.4	1.4	0.8	0.1	0.0	0.2	1.4	-	5.5
	07/02/2006	6.7	91.6	-	530.0	14.7	41.3	12.3	0.5	99.3	5.3	1.3	0.8	0.1	0.0	0.2	1.3	-	5.3
	30/03/2006	6.8	101.2	225.3	510.0	14.8	44.5	12.7	0.6	100.7	5.2	1.3	0.8	0.1	0.0	0.2	1.4	3.7	5.4
Jannaways	22/02/2005	7.8	99.2	153.0	633.0	18.2	46.5	20.6	0.3	126.2	9.8	2.3	2.1	0.0	0.0	0.3	1.7	2.5	7.0
Jannaways pumped	22/02/2005	7.6	-	138.3	634.0	22.7	51.1	22.6	0.1	124.8	9.8	2.2	1.9	0.0	0.0	0.3	1.9	2.3	6.9
	19/04/2005	7.1	87.8	250.9	618.0	21.7	49.6	22.4	0.2	124.9	9.9	2.3	2.1	0.0	0.0	0.3	1.9	4.1	6.9
	07/06/2005	7.2	96.5	253.3	718.0	19.3	42.4	22.9	0.8	126.9	9.7	2.2	2.0	0.0	0.0	0.3	1.8	4.2	7.0
	21/07/2005	6.9	94.4	233.8	573.0	19.8	44.7	22.3	0.6	126.3	9.7	2.3	2.1	0.0	0.0	0.3	1.8	3.8	7.0
	01/09/2005	6.7	89.0	-	624.0	19.1	43.0	22.1	0.5	120.1	10.7	2.1	2.1	0.0	0.0	0.3	1.7	-	6.7

Table E1 – Chemical Analyses – Lambourn Catchment

			%	mg/l $HCO3^-$	$mS.cm^{-1}$	mg/l	mg/l	mg/l	mg/l	mg/l	mg/l	mg/l	mg/l	mg/l	mg/l	mg/l	meq/l	meq/l	meq/l
Site Name	**Date**	**pH**	**DO**	**Alk**	**Cond**	**SO_4^{2-}**	**NO_3^-**	**Cl^-**	**F^-**	**Ca**	**Na**	**Mg**	**K**	**Fe**	**Ba**	**Sr**	**Anions (ex alk)**	**HCO_3^-**	**Cations**
Jannaways	03/10/2005	6.9	84.6	224.1	624.0	-	-	-	-	-	-	-	-	-	-	-	-	3.7	-
Pumped	15/12/2005	-	-	-	-	18.9	45.3	23.5	0.6	118.7	10.6	2.0	2.1	0.1	0.0	0.3	1.8	-	6.6
	07/02/2006	6.8	89.1	-	653.0	18.7	44.3	21.8	0.4	118.6	10.7	2.1	2.1	0.0	0.0	0.3	1.7	-	6.6
	30/03/2006	7.0	93.6	274.6	627.0	18.3	43.4	22.4	0.7	119.0	10.8	2.0	2.1	0.1	0.0	0.3	1.7	4.5	6.7
	29/06/2006	7.1	89.8	-	599.0	18.5	44.2	22.4	0.6	117.9	10.7	2.0	2.0	0.1	0.0	0.3	1.8	-	6.6
	12/10/2006	6.5	83.6	277.0	613.0	-	-	-	-	118.2	10.6	2.0	2.1	0.1	0.0	0.3	-	4.5	6.6
Lynch Wood	18/01/2005	7.0	76.4	-	630.0	26.5	60.4	19.4	0.0	130.5	5.8	2.1	0.9	0.0	0.0	-	2.1	-	-
	22/02/2005	7.1	81.3	-	615.0	24.1	52.8	19.0	0.1	118.9	6.3	2.0	1.2	0.0	0.0	0.2	1.9	-	6.4
	19/04/2005	7.1	-	223.9	577.0	25.4	55.2	18.5	0.1	118.2	5.5	2.0	1.0	0.0	0.0	0.2	1.9	3.7	6.3
	07/06/2005	7.1	80.3	-	660.0	22.7	47.4	17.6	0.5	118.3	5.2	1.9	0.9	0.0	0.0	0.2	1.8	-	6.3
	21/07/2005	6.9	63.4	204.2	567.0	22.2	48.5	17.6	0.4	120.7	5.2	2.0	0.9	0.0	0.0	0.2	1.8	3.3	6.4
Maidencourt Farm	18/01/2005	7.1	96.8	-	581.0	21.6	44.6	27.1	2.8	114.6	12.5	2.2	2.7	0.0	0.0	-	2.1	-	-
Weston Spring	18/01/2005	7.1	84.5	-	580.0	14.2	50.7	18.7	0.1	126.4	7.9	2.0	1.3	0.0	0.0	-	1.6	-	-
	22/02/2005	7.7	81.9	125.0	570.0	12.6	49.1	17.1	0.1	114.6	6.8	1.8	1.2	0.0	0.0	0.3	1.5	2.0	6.2
	19/04/2005	7.2	-	228.8	555.0	13.3	49.8	17.7	0.1	113.8	6.9	1.8	1.1	0.0	0.0	0.2	1.6	3.8	6.2
	07/06/2005	7.2	83.4	239.8	652.0	9.8	930.6	16.5	0.0	113.2	6.8	1.8	1.2	0.0	0.0	0.2	15.7	3.9	6.1
	21/07/2005	7.1	53.7	216.6	547.0	21.7	69.8	32.1	0.7	115.6	6.7	1.9	1.7	0.0	0.0	0.2	2.5	3.6	6.3
	01/09/2005	7.1	79.0	-	561.0	12.0	44.9	18.0	0.6	109.9	7.9	1.7	1.3	0.0	0.0	0.3	1.5	-	6.0
	03/10/2005	6.6	72.4	215.5	568.0	-	-	-	-	-	-	-	-	-	-	-	-	3.5	-
	15/12/2005	-	-	-	-	10.5	1029.8	16.7	0.0	83.7	7.3	1.7	1.1	0.0	0.0	0.3	17.3	-	4.7

Table E1 – Chemical Analyses – Lambourn Catchment

			%	mg/l $HCO3^-$	$mS.cm^{-1}$	mg/l	mg/l	mg/l	mg/l	mg/l	mg/l	mg/l	mg/l	mg/l	mg/l	mg/l	meq/l	meq/l	meq/l
Site Name	**Date**	**pH**	**DO**	**Alk**	**Cond**	**SO_4^{2-}**	**NO_3^-**	**Cl^-**	**F^-**	**Ca**	**Na**	**Mg**	**K**	**Fe**	**Ba**	**Sr**	**Anions (ex alk)**	**HCO_3^-**	**Cations**
Weston Spr	07/02/2006	6.7	84.7	-	575.0	10.3	44.8	16.0	0.4	109.2	7.1	1.6	1.1	0.0	0.0	0.3	1.4	-	5.9
	30/03/2006	6.6	89.7	263.5	546.0	10.6	44.9	17.4	0.7	106.6	7.4	1.6	1.0	0.0	0.0	0.3	1.5	4.3	5.8
	12/10/2006	6.6	72.5	248.4	553.0	-	-	-	-	106.9	7.3	1.6	1.0	0.1	0.0	0.3	-	4.1	5.8

Table E2 – Chemical Analyses – Pang Catchment

		-	%	mg/l $HCO3^-$	$mS.cm^{-1}$	mg/l	mg/l	mg/l	mg/l	mg/l	mg/l	mg/l	mg/l	mg/l	mg/l	mg/l	meq/l	meq/l	meq/l
Name	**Date**	**pH**	**DO**	**Alk**	**Cond**	**SO_4^{2-}**	**NO_3^-**	**Cl^-**	**F^-**	**Ca**	**Na**	**Mg**	**K**	**Fe**	**Ba**	**Sr**	**Anions (excl HCO3)**	**HCO_3^-**	**Cations**
Bucklebury Bridge	19/04/2005	8.5	100.0	213.5	579.0	18.5	33.0	36.4	0.1	102.3	22.7	3.6	2.5	0.0	0.0	0.3	1.9	3.5	6.5
D/S Hampstead Norreys STW	19/04/2005	-	-	215.7	510.0	13.6	27.3	19.4	0.1	98.9	10.3	1.8	1.7	0.0	0.0	0.2	1.3	3.5	5.6
	07/06/2005	-	-	335.9	-	13.1	34.5	30.3	0.7	129.6	21.1	2.2	3.5	0.0	0.0	0.3	1.7	5.5	7.7
Ingle Spring	22/02/2005	7.6	65.5	154.6	628.0	17.9	48.6	20.6	0.1	120.0	9.7	3.0	2.3	0.0	0.0	0.3	1.7	2.5	6.7
	19/04/2005	7.2	66.6	238.7	603.0	18.3	48.3	20.9	0.0	120.8	10.1	3.2	2.4	0.0	0.0	0.3	1.8	3.9	6.8
	07/06/2005	7.1	74.2	252.0	686.0	15.3	43.5	21.9	0.9	117.4	9.0	3.0	2.2	0.0	0.0	0.3	1.7	4.1	6.6
	21/07/2005	6.9	64.6	-	598.0	14.6	43.1	19.5	0.5	119.9	9.2	2.9	2.3	0.0	0.0	0.3	1.6	-	6.7
	01/09/2005	7.1	65.4	-	594.0	0.0	0.0	0.0	0.5	113.1	10.3	2.6	2.2	0.1	0.0	0.3	0.0	-	6.4
	03/10/2005	7.0	65.5	229.1	603.0	-	-	-	-	-	-	-	-	-	-	-	-	3.8	-
	16/11/2005	7.0	66.8	-	615.0	14.7	44.2	19.6	0.3	113.1	10.1	2.7	2.2	0.0	0.0	0.3	1.6	-	6.4
	15/12/2005	-	-	-	-	15.5	43.7	19.5	0.4	114.1	10.5	2.8	2.3	0.0	0.0	0.3	1.6	-	6.5
	07/02/2006	6.7	66.5	-	613.0	14.7	44.1	19.5	0.6	114.7	10.4	2.7	2.2	0.0	0.0	0.3	1.6	-	6.5
	30/03/2006	6.8	69.5	278.2	605.0	15.9	45.2	21.4	0.7	112.4	10.9	2.7	2.3	0.1	0.0	0.3	1.7	4.6	6.4
	29/06/2006	7.0	67.1	-	600.0	14.6	44.1	21.7	1.2	113.9	10.1	2.7	2.2	0.1	0.0	0.3	1.7	-	6.4
	12/10/2006	6.5	65.2	261.0	594.0	-	-	-	-	112.0	9.8	2.6	2.1	0.1	0.0	0.3	-	4.3	6.3

Table E2 – Chemical Analyses – Pang Catchment

		-	%	mg/l $HCO3^-$	$mS.cm^{-1}$	mg/l	mg/l	mg/l	mg/l	mg/l	mg/l	mg/l	mg/l	mg/l	mg/l	mg/l	meq/l	meq/l	meq/l
Name	**Date**	**pH**	**DO**	**Alk**	**Cond**	**SO_4^{2-}**	**NO_3^-**	**Cl^-**	**F^-**	**Ca**	**Na**	**Mg**	**K**	**Fe**	**Ba**	**Sr**	**Anions (excl HCO3)**	**HCO_3^-**	**Cations**
Jewell's Spring	22/02/2005	7.6	66.0	145.7	608.0	18.7	50.2	20.5	0.1	120.0	9.7	3.1	2.3	0.0	0.0	0.3	1.8	2.4	6.7
	19/04/2005	7.2	66.1	236.0	602.0	18.1	47.7	20.7	0.1	120.3	10.2	3.2	2.5	0.0	0.0	0.3	1.7	3.9	6.8
	07/06/2005	7.0	69.0	-	685.0	15.5	42.1	20.8	0.8	117.9	9.1	2.9	2.2	0.0	0.0	0.3	1.6	-	6.6
	21/07/2005	6.5	63.6	224.0	597.0	14.7	44.0	19.6	0.7	118.4	9.0	2.9	2.3	0.0	0.0	0.3	1.6	3.7	6.6
	01/09/2005	6.9	60.2	-	605.0	14.5	41.1	18.6	0.5	114.7	10.6	2.7	2.2	0.0	0.0	0.3	1.5	-	6.5
	03/10/2005	7.0	76.7	-	600.0	-	-	-	-	-	-	-	-	-	-	-	-	-	-
	16/11/2005	6.4	69.8	-	614.0	14.6	45.4	19.6	0.5	112.3	10.0	2.6	2.2	0.1	0.0	0.3	1.6	-	6.3
	15/12/2005	-	-	-	-	15.3	43.5	19.3	0.3	113.6	10.1	2.7	2.2	0.0	0.0	0.3	1.6	-	6.4
	07/02/2006	6.7	66.2	-	612.0	14.7	44.0	19.2	0.4	113.7	10.3	2.7	2.3	0.1	0.0	0.3	1.6	-	6.4
	30/03/2006	6.7	69.6	265.8	-	15.8	44.3	21.3	0.9	114.5	10.4	2.8	2.3	0.1	0.0	0.3	1.7	4.4	6.5
	29/06/2006	6.9	65.6	-	603.0	14.7	45.9	20.2	0.6	112.8	10.2	2.7	2.2	0.1	0.0	0.3	1.6	-	6.4
	12/10/2006	6.9	64.0	256.1	591.0	14.8	44.2	22.2	0.7	111.7	9.9	3.1	4.4	0.1	0.0	0.3	1.7	4.2	6.4
Kimber Spring	22/02/2005	7.7	59.7	140.0	628.0	20.8	45.6	22.7	0.1	117.6	10.2	3.6	2.5	0.0	0.0	0.3	1.8	2.3	6.7
	19/04/2005	7.1	0.6	227.6	575.0	20.8	46.8	21.9	0.2	115.8	10.9	3.7	2.6	0.0	0.0	0.3	1.8	3.7	6.6
	07/06/2005	6.9	67.7	257.1	683.0	18.2	44.0	21.8	0.7	116.9	9.9	3.3	2.4	0.0	0.0	0.3	1.7	4.2	6.6
	21/07/2005	6.6	61.9	219.0	582.0	17.0	41.5	20.8	0.6	117.6	9.6	3.3	2.3	0.0	0.0	0.3	1.6	3.6	6.6
	01/09/2005	6.7	61.7	-	609.0	16.9	41.4	20.5	0.5	111.8	11.6	3.0	2.4	0.0	0.0	0.4	1.6	-	6.4
	03/10/2005	6.7	62.5	229.0	596.0	-	-	-	-	-	-	-	-	-	-	-	-	3.8	-
	16/11/2005	6.9	63.3	-	613.0	16.9	42.4	20.3	0.5	110.0	10.4	3.0	2.3	0.1	0.0	0.4	1.6	-	6.3
	15/12/2005	-	-	-	-	17.8	42.7	20.9	0.6	111.2	11.0	3.1	2.4	0.0	0.0	0.4	1.7	-	6.4

Table E2 – Chemical Analyses – Pang Catchment

		-	%	mg/l $HCO3^-$	$mS.cm^{-1}$	mg/l	mg/l	mg/l	mg/l	mg/l	mg/l	mg/l	mg/l	mg/l	mg/l	mg/l	meq/l	meq/l	meq/l
Name	**Date**	**pH**	**DO**	**Alk**	**Cond**	**SO_4^{2-}**	**NO_3^-**	**Cl^-**	**F^-**	**Ca**	**Na**	**Mg**	**K**	**Fe**	**Ba**	**Sr**	**Anions (excl HCO3)**	**HCO_3^-**	**Cations**
	07/02/2006	6.6	63.1	-	610.0	16.1	40.6	19.7	0.6	110.9	10.7	3.0	2.3	0.0	0.0	0.4	1.6	-	6.3
	30/03/2006	6.6	65.8	268.5	590.0	18.4	43.1	22.3	0.7	108.4	11.9	3.2	2.4	0.0	0.0	0.4	1.7	4.4	6.3
	29/06/2006	6.9	63.2	-	-	16.7	44.0	22.0	0.8	112.9	10.7	3.0	2.4	0.1	0.0	0.4	1.7	-	6.4
	12/10/2006	6.6	62.6	244.9	-	16.5	43.7	21.1	0.4	109.2	10.6	2.9	2.4	0.1	0.0	0.3	1.7	4.0	6.2
Pond South Parsonage Farm	21/07/2005	7.4	139.0	253.5	678.0	17.4	61.4	27.3	0.5	138.4	11.5	2.4	1.6	0.0	0.0	0.3	2.1	4.2	7.7
	01/09/2005	7.3	140.0	-	685.0	17.7	56.5	28.3	0.5	127.2	12.9	2.2	1.8	0.1	0.0	0.3	2.1	-	7.2
	03/10/2005	7.6	140.0	-	639.0	-	-	-	-	-	-	-	-	-	-	-	-	-	-
	16/11/2005	7.3	75.0	-	700.0	20.0	46.3	27.6	0.6	133.2	12.2	2.3	2.8	0.1	0.0	0.3	2.0	-	7.5
	15/12/2005	-	-	-	-	22.5	68.4	27.6	0.7	141.9	12.6	2.4	2.0	0.1	0.0	0.3	2.4	-	7.9
	07/02/2006	6.9	117.2	-	753.0	20.7	68.5	27.8	0.4	137.2	12.6	2.3	1.6	0.1	0.0	0.3	2.3	-	7.6
	30/03/2006	7.0	110.5	299.3	711.0	21.2	78.0	30.1	0.8	134.7	13.4	2.3	1.9	0.1	0.0	0.3	2.6	4.9	7.6
S Parsonage Farm	19/04/2005	-	-	285.6	-	23.2	78.6	29.3	0.0	153.1	11.9	2.6	1.3	0.0	0.0	0.3	2.6	4.7	8.4

Appendix F | Core Material

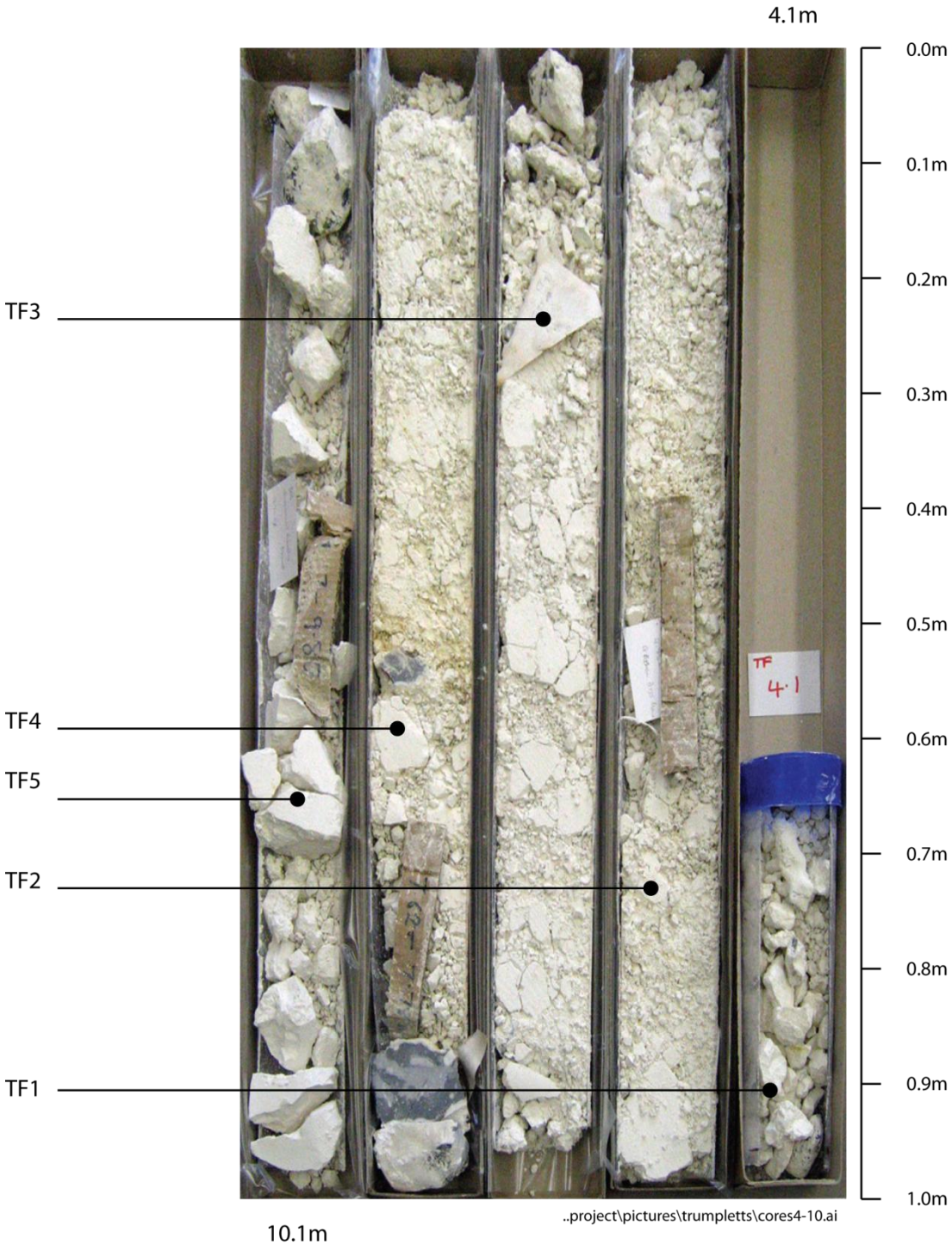

N.B Significant degree of core loss from this section, depths are approximate only.

Figure F1 Photograph of Trumpletts Farm core interval 4.1-10.1m (partial recovery).

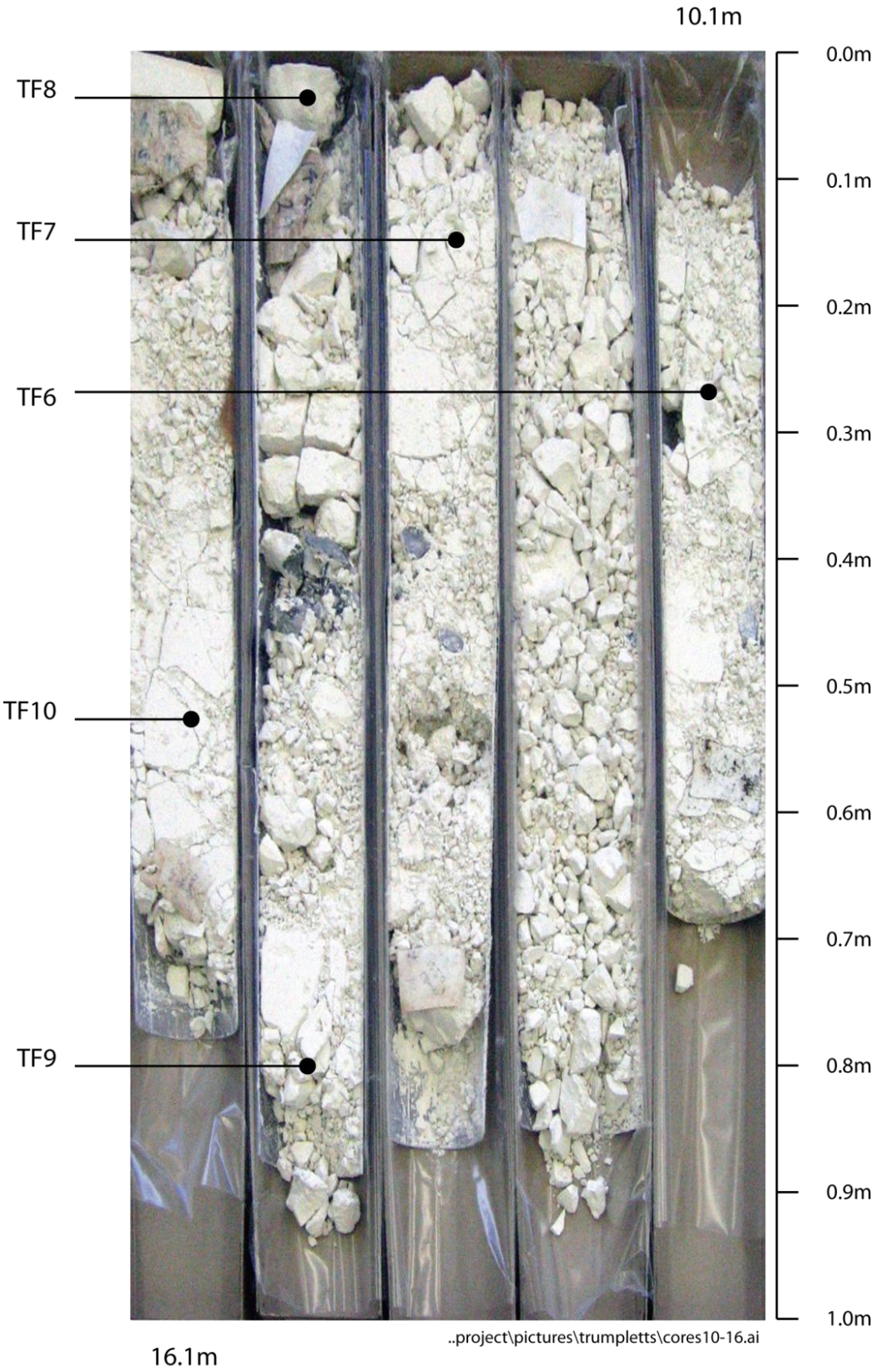

Figure F2 Photograph of Trumpletts Farm core interval 10.1-16.1m (partial recovery).

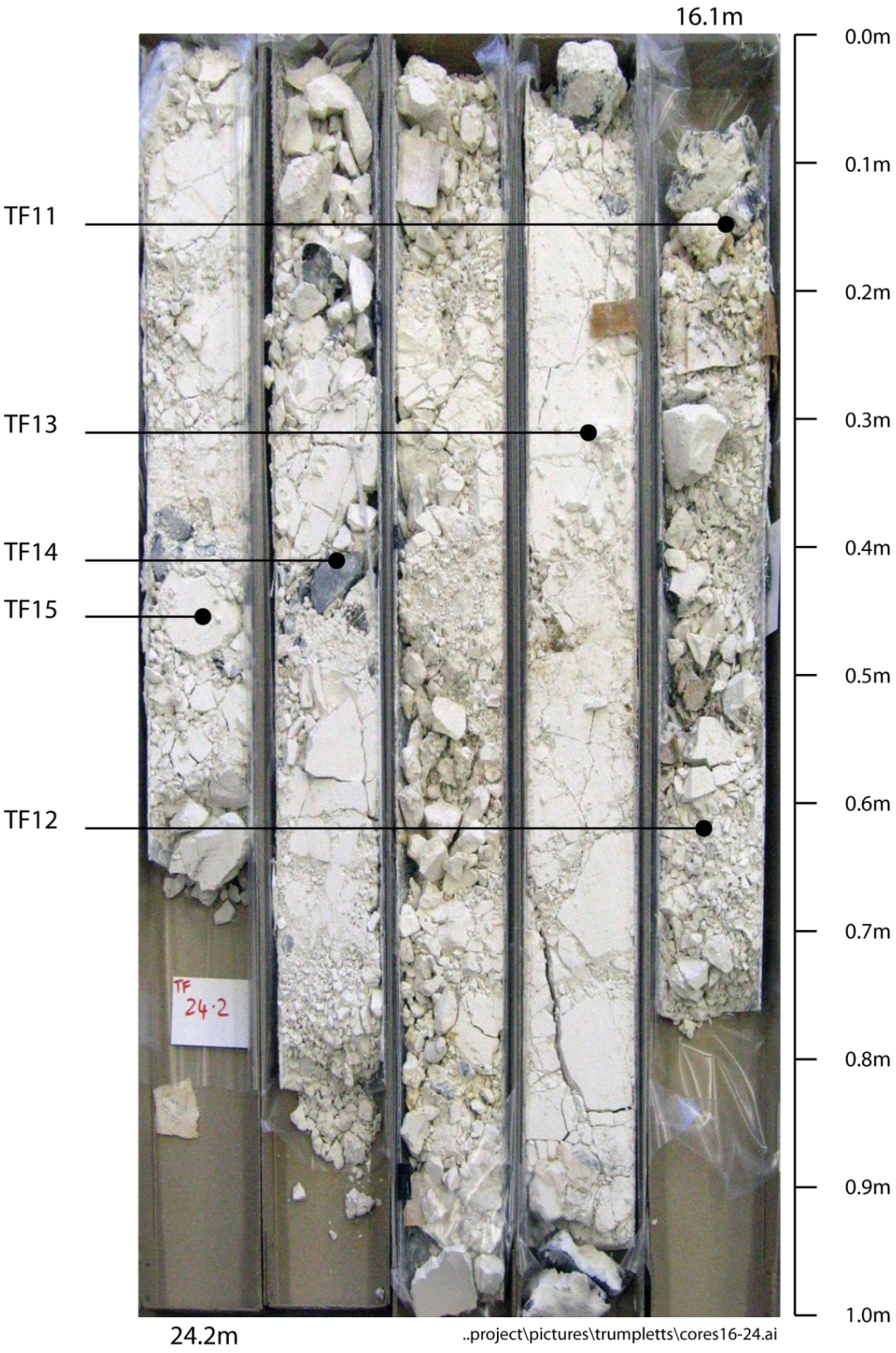

N.B Significant degree of core loss from this section, depths are approximate only.

Figure F3 Photograph of Trumpletts Farm core interval 16.1-24.2m (partial recovery).

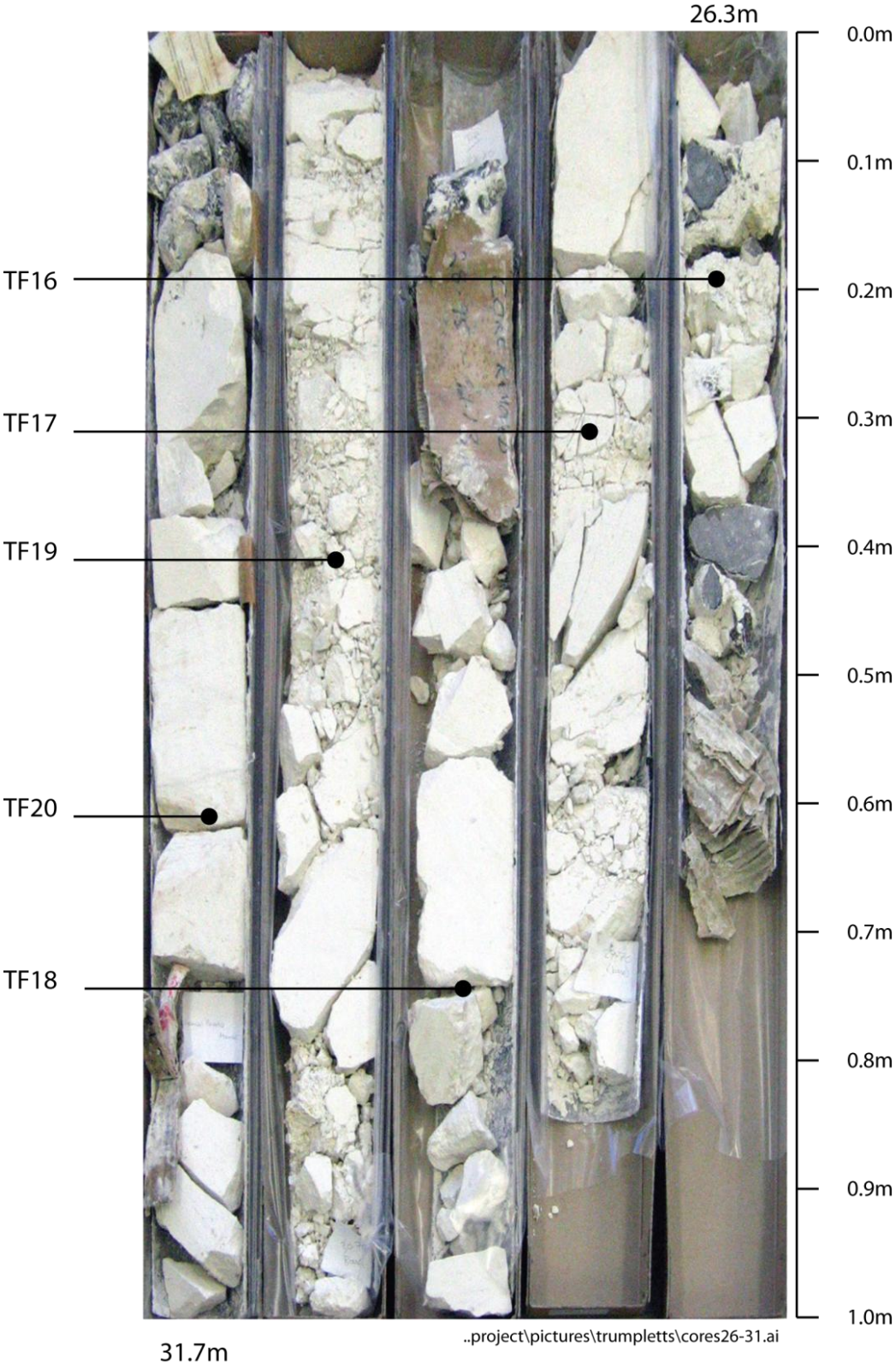

Figure F4 Photograph of Trumpletts Farm core interval 26.3-31.7m (partial recovery).

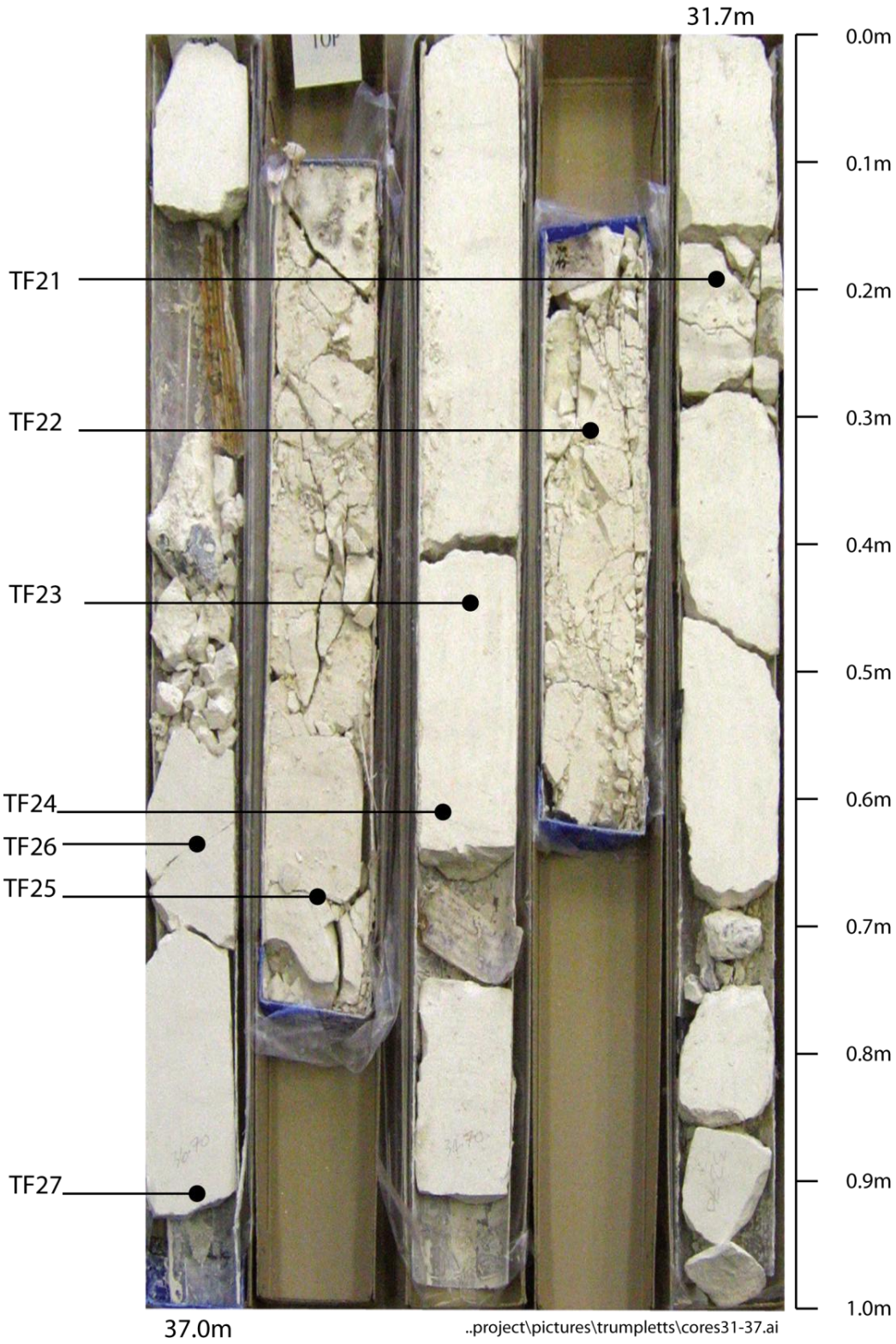

N.B Significant degree of core loss from this section, depths are approximate only.

Figure F5 Photograph of Trumpletts Farm core interval 31.7-37.0m (partial recovery).

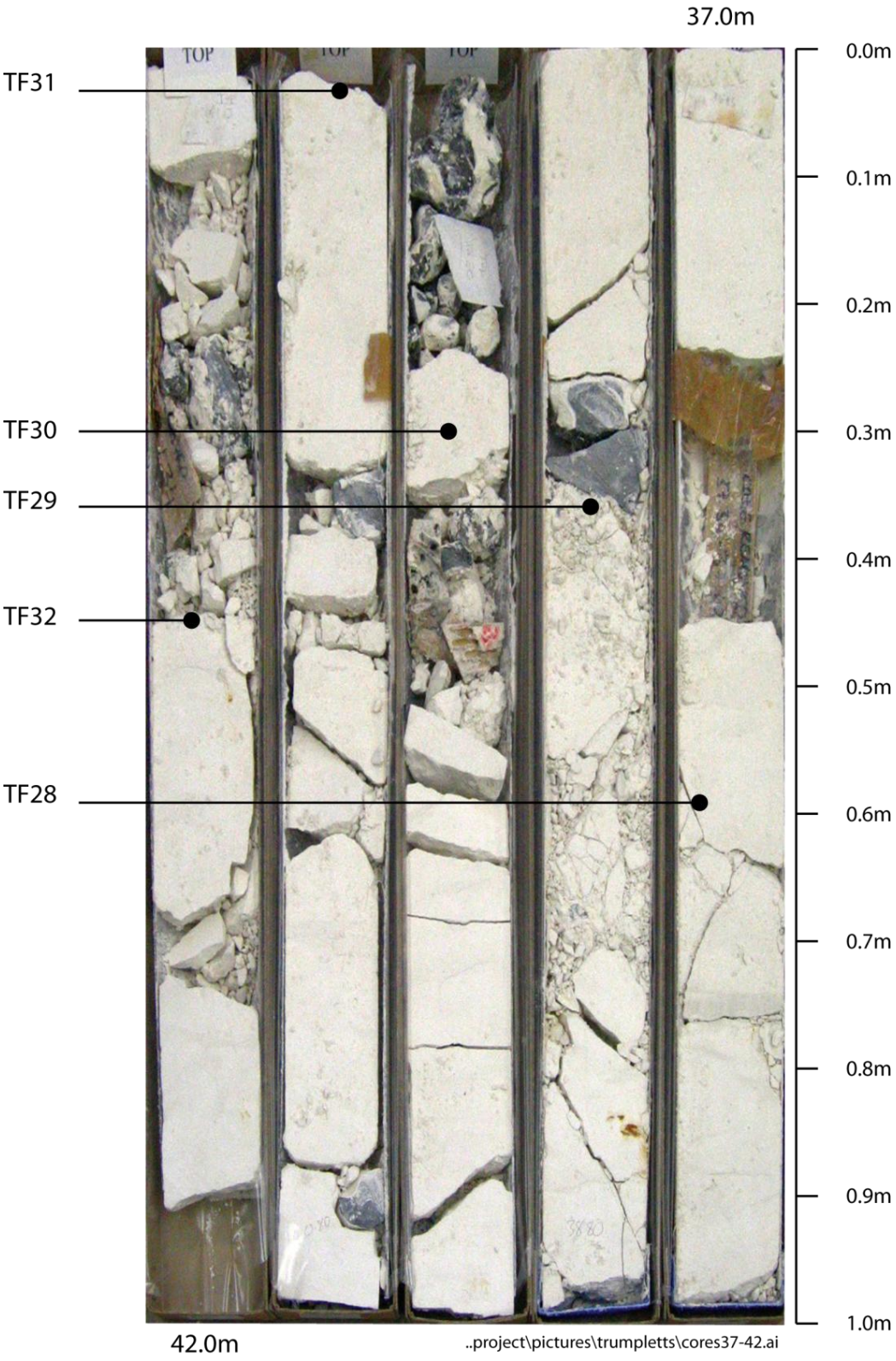

Figure F6 Photograph of Trumpletts Farm core interval 37.0-42.0m (partial recovery).

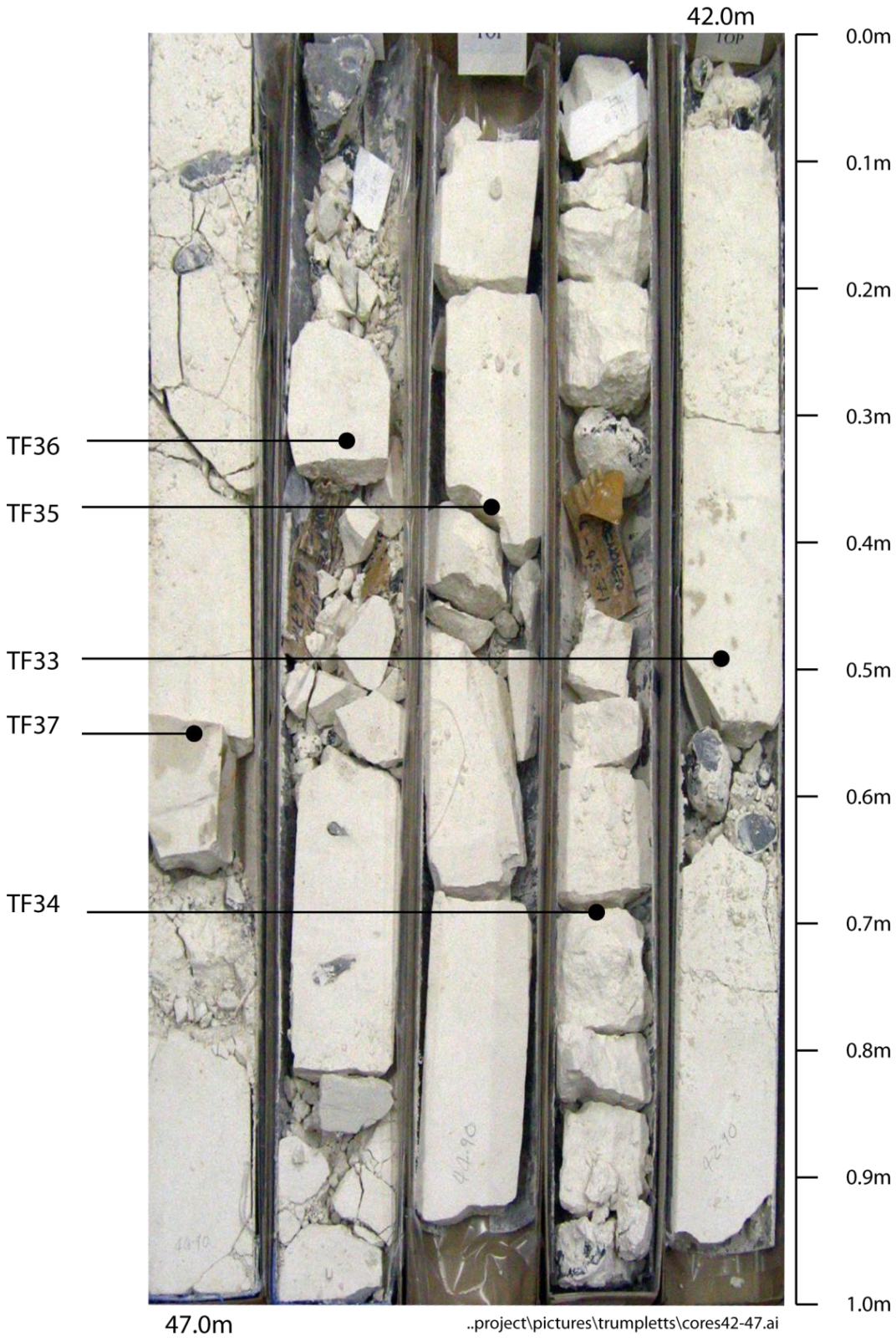

Figure F7 Photograph of Trumpletts Farm core interval 42.0-47.0m (partial recovery).

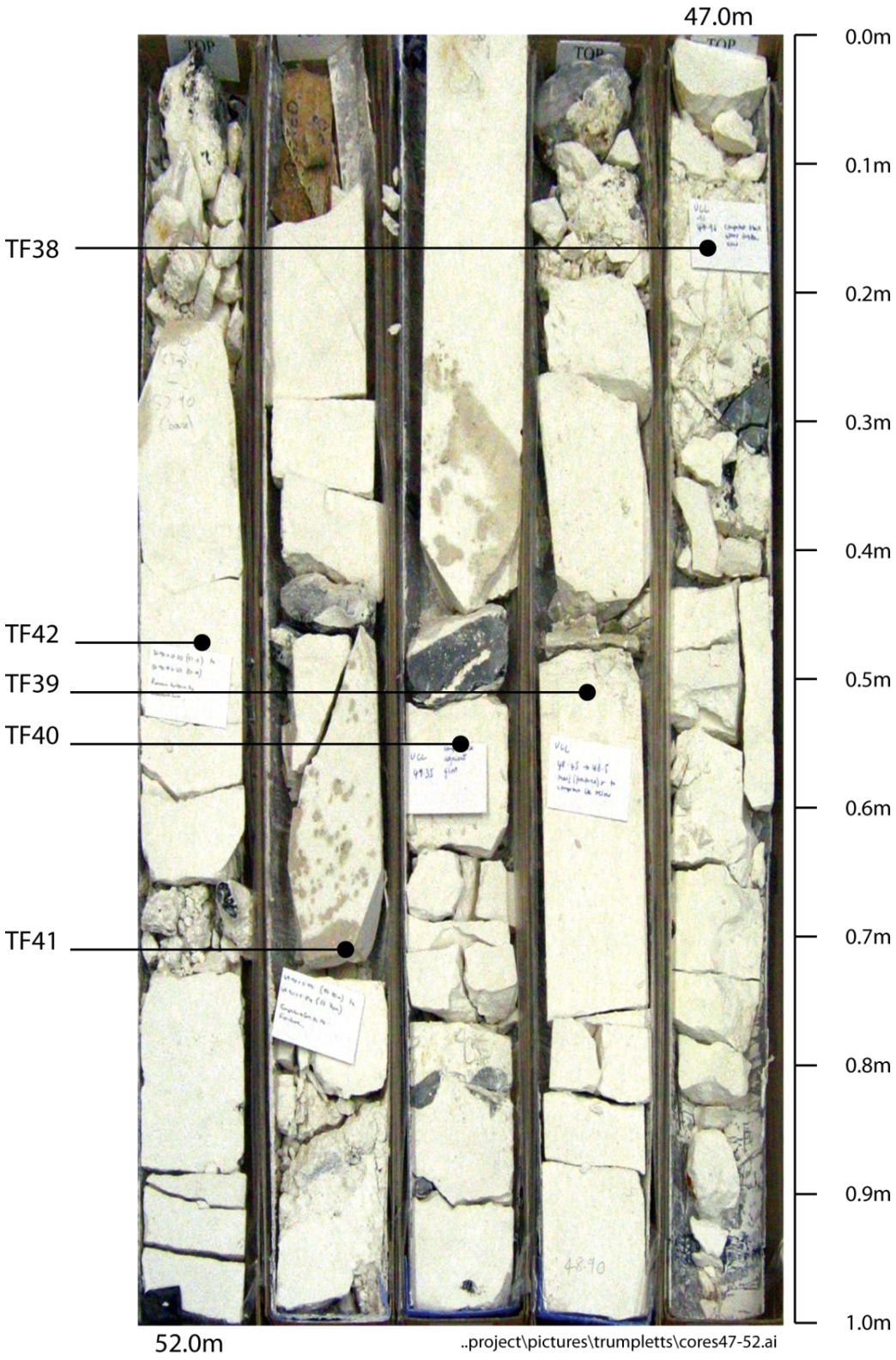

Figure F8 Photograph of Trumpletts Farm core interval 47.0-52.0m (partial recovery).

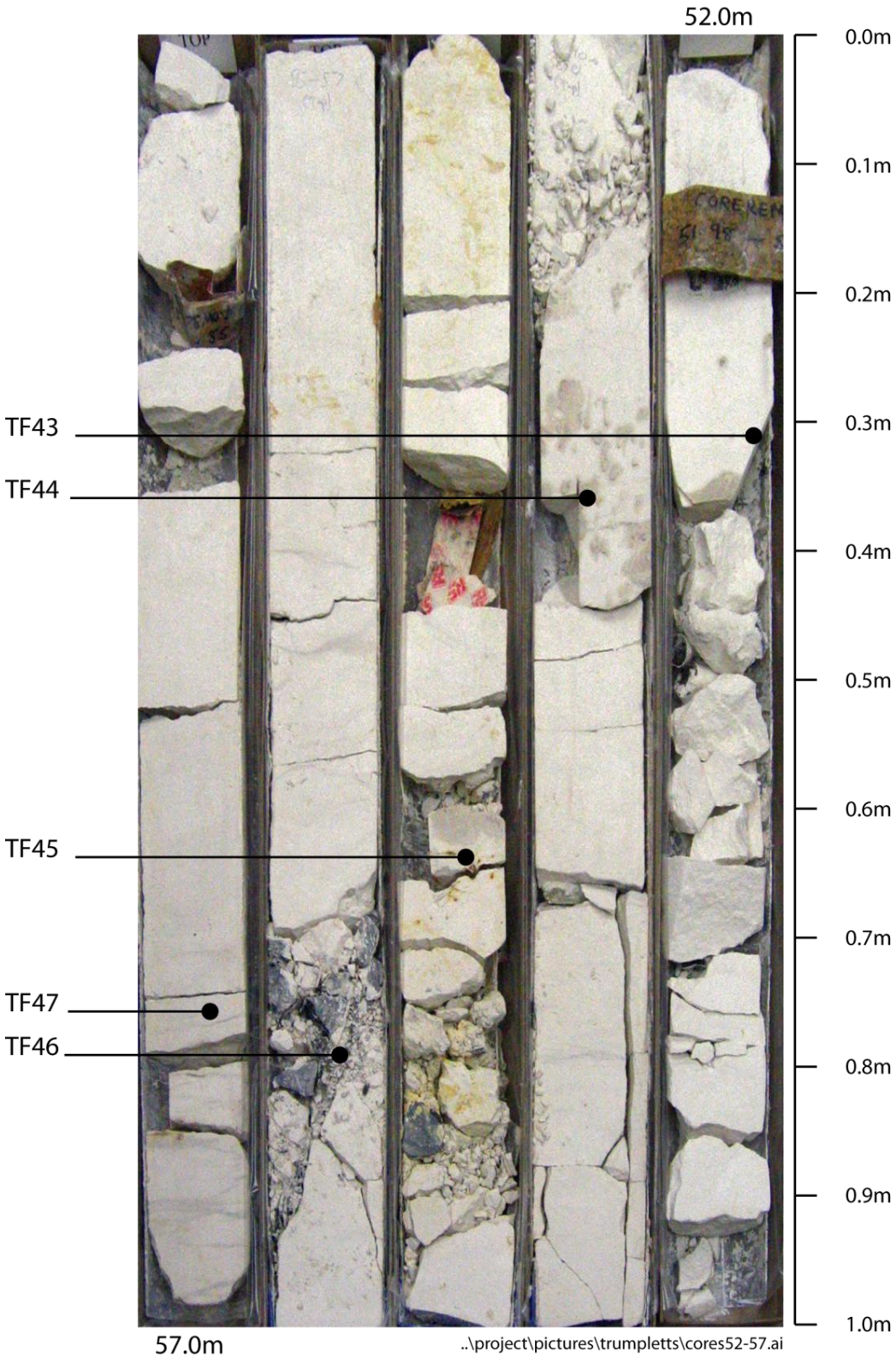

Figure F9 Photograph of Trumpletts Farm core interval 52.0-57.0m (partial recovery).

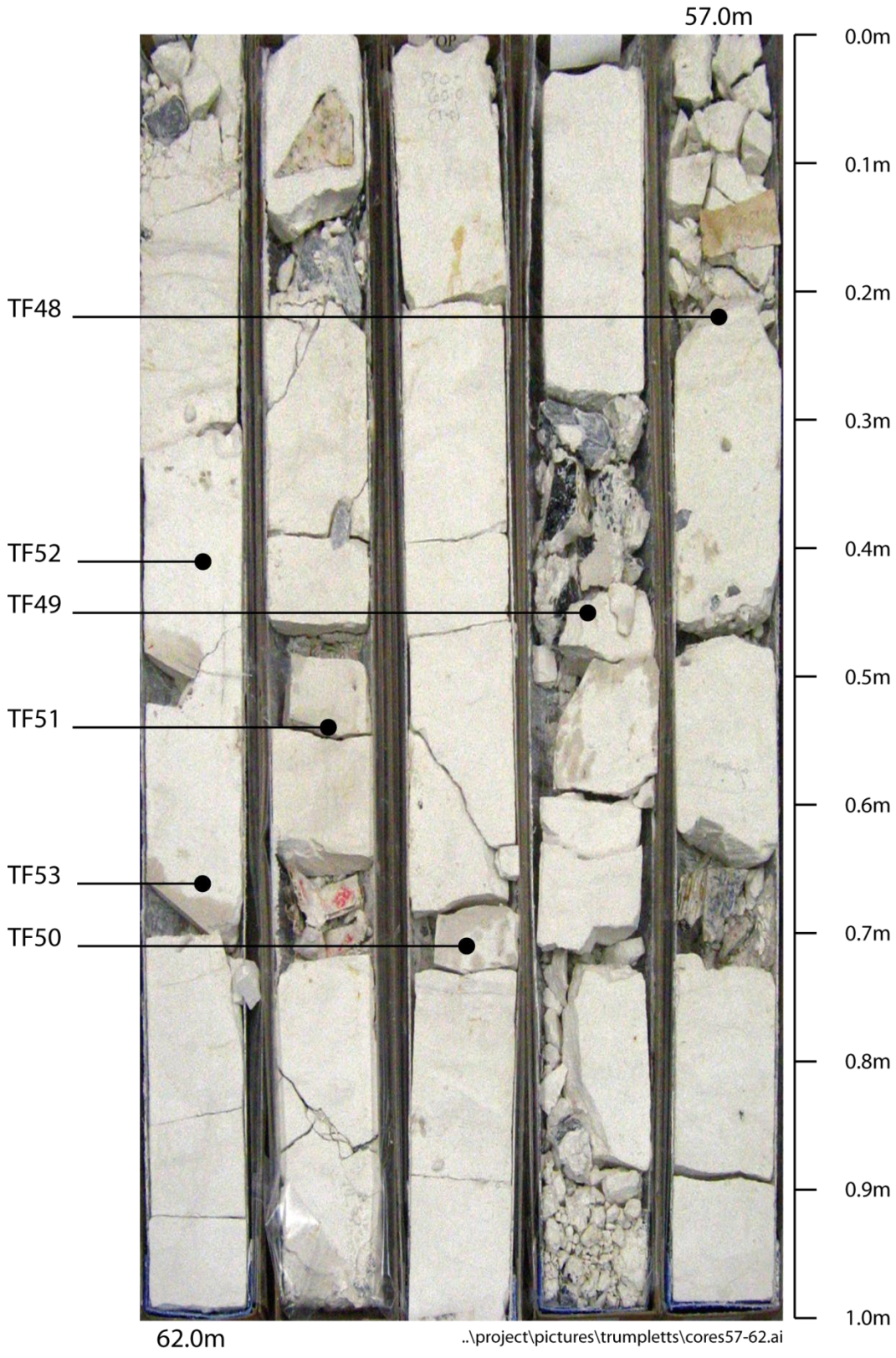

Figure F10 Photograph of Trumpletts Farm core interval 57.0-62.0m.

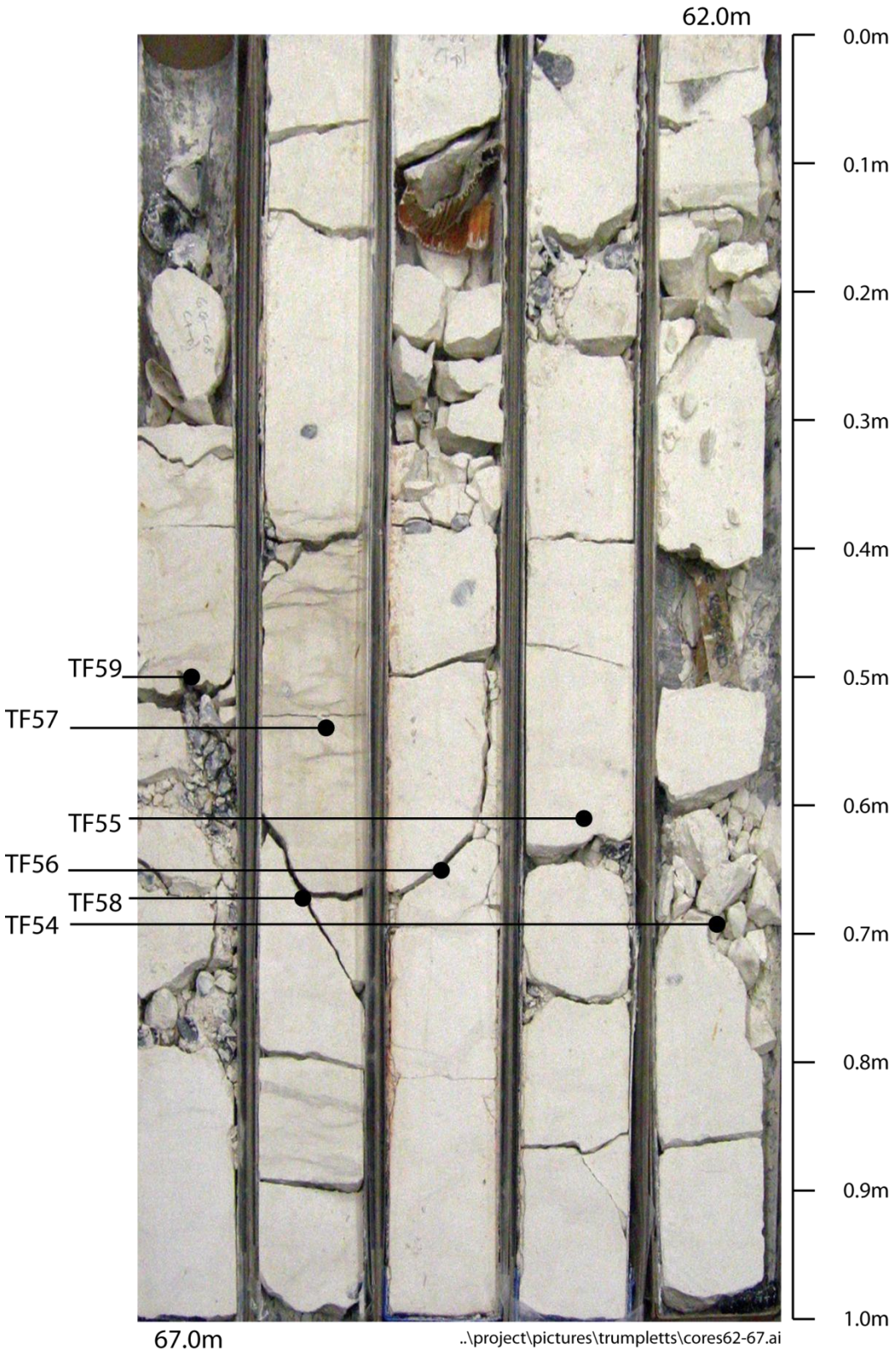

Figure F11 Photograph of Trumpletts Farm core interval 62.0-67.0m.

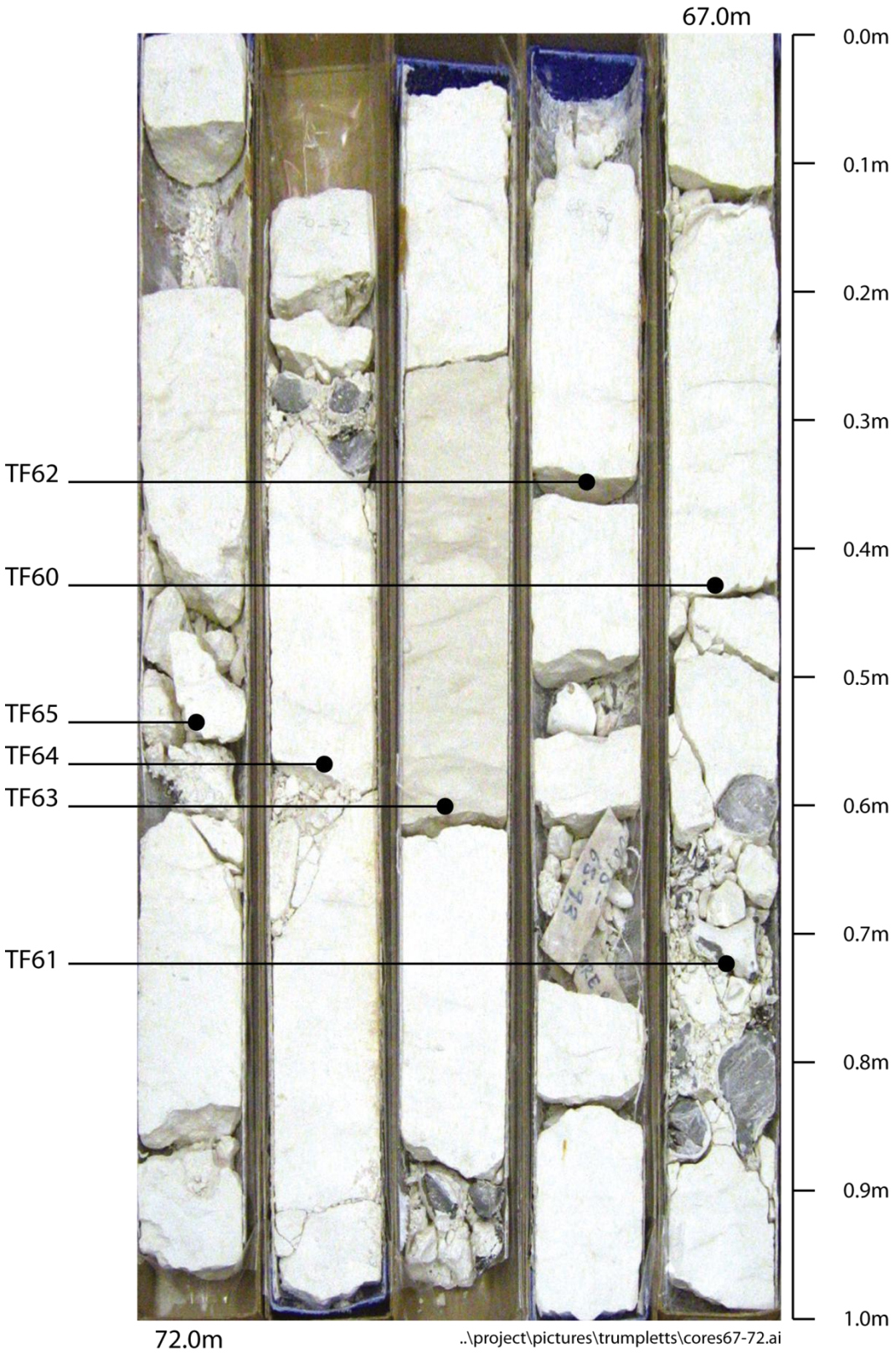

Figure F12 Photograph of Trumpletts Farm core interval 67.0-72.0m.

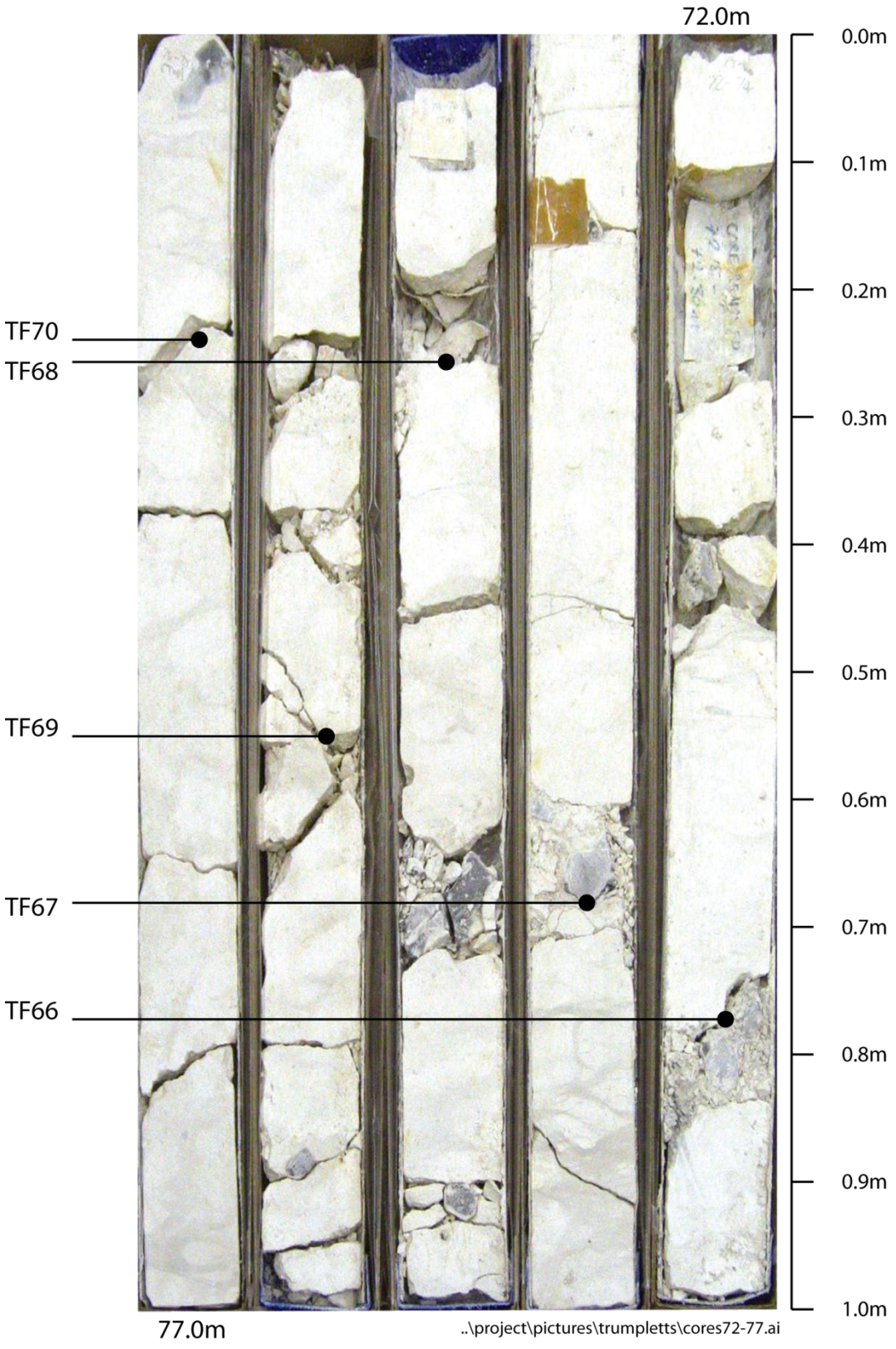

Figure F13 Photograph of Trumpletts Farm core interval 72.0-77.0m

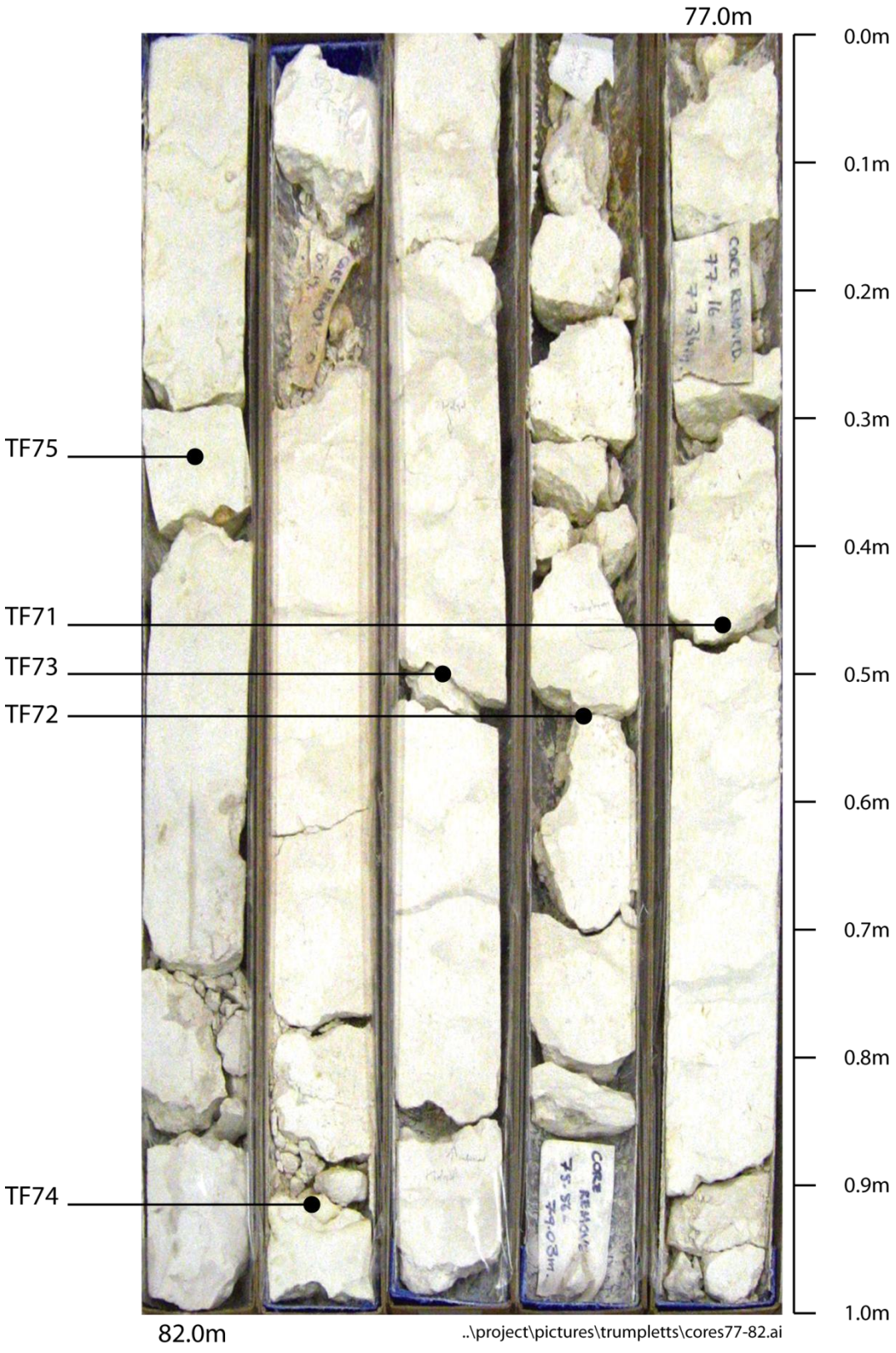

Figure F14 Photograph of Trumpletts Farm core interval 77.0-82.0m.

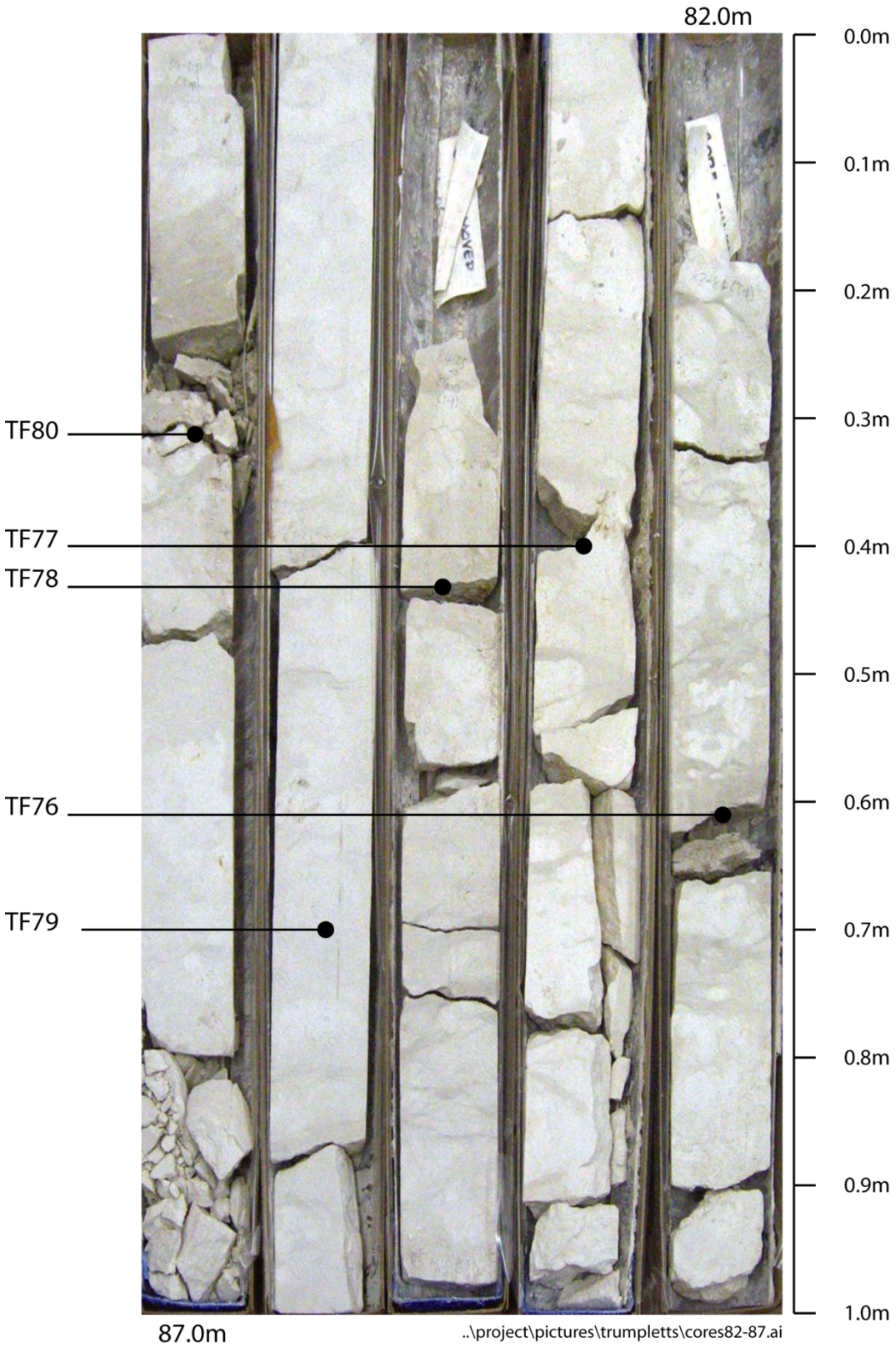

Figure F12 Photograph of Trumpletts Farm core interval 82.0-87.0m.

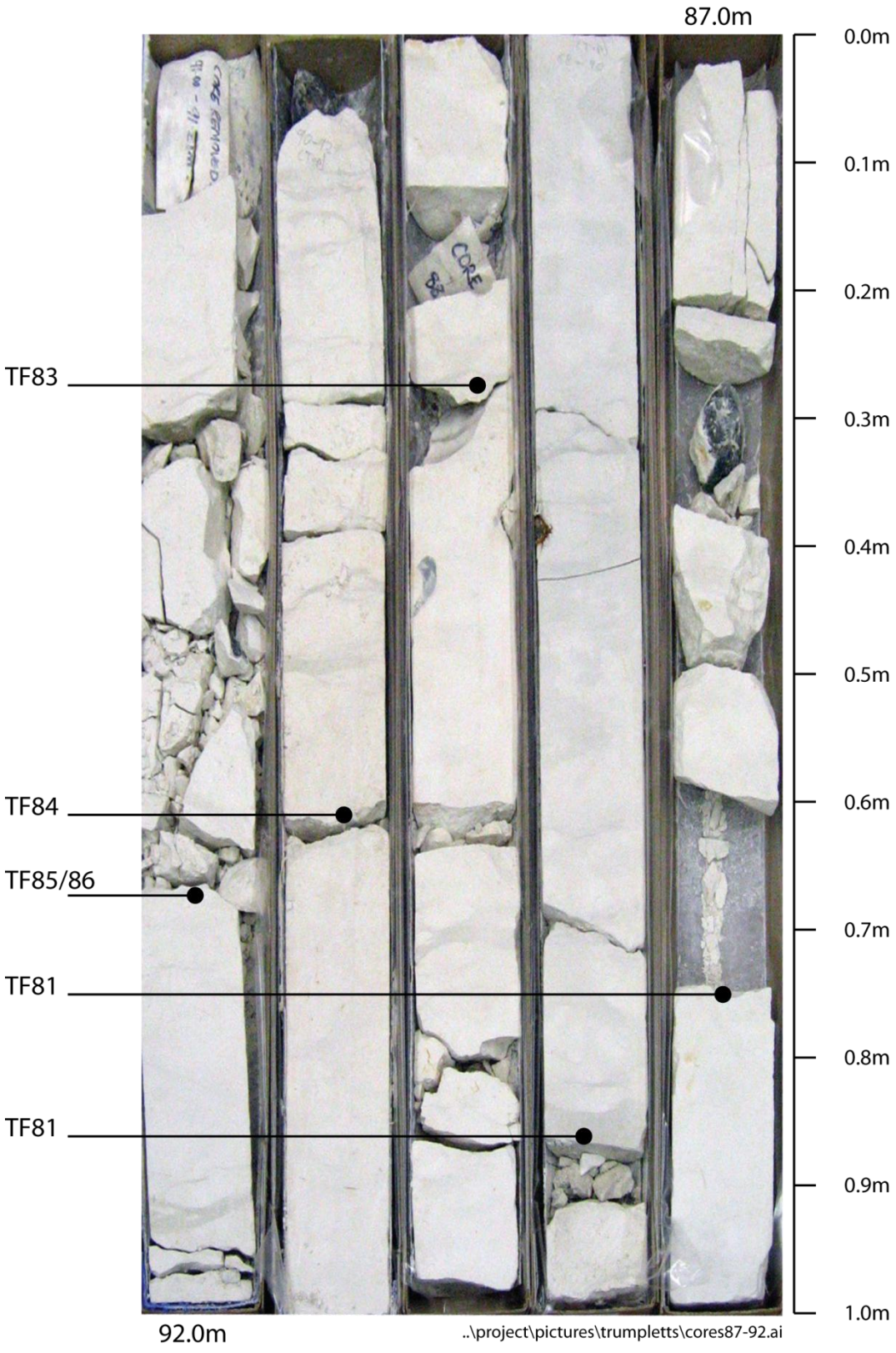

Figure F12 Photograph of Trumpletts Farm core interval 87.0-92.0m.